

Earthquake Ground Motion Models for Sri Lanka

by

Janaka Prasanna, WEPITIYA GAMAGE

A thesis submitted in total fulfillment of the requirements of the degree of Doctor of
Philosophy

August, 2015

College of Engineering and Science

Victoria University



Abstract

At present (in 2014), Sri Lanka does not have an established earthquake code of practice. Current design practice in Sri Lanka is to adopt values from other analogous codes of low to moderate seismicity. This has raised significant concerns amongst practitioners, academics and the general community. The tsunami that caused huge devastation in Sri Lanka in 2004 has also been a major driver in increasing the awareness of earthquake risks. However, to develop seismic codes of practice, an understanding of seismic hazard and wave attenuation characteristics of the region is essential. Since the hazard and attenuation are dependent on regional and local influences, many experts (Atkinson, 2004a, Chandler et al, 2001) recommend every region to develop their own attenuation and hazard models in order to provide reliable estimates of seismic hazard and risk. As far as Sri Lanka is concerned, initial work on hazard estimation has been undertaken by some researchers (Fernando and Kulasinghe, 1986; Abayakoon, 1996; Uduweriya et al, 2013). However, reliable attenuation models have not been developed. Hence the adaptation of provisions from other codes or regions may not be fully appropriate. Even the direct application of existing attenuation models in the literature needs investigation. In order to address these existing knowledge gaps and to develop reliable response spectrum models for future code of practice, a research program has been undertaken at Victoria University. In this thesis, local and regional characteristics influencing seismic hazard in the region have been systematically investigated and attenuation models have been developed. Seismological parameters derived in this process have been incorporated into stochastic modeling techniques to develop representative ground motions. These are validated based on comparisons with the recorded ground motions in the region, thus confirming the robustness of the developed models and parameters. This thesis presents an estimate of seismic hazard and response spectra (on rock) for the entire country which addresses the future needs of seismic design in the country. Further exhaustive details are provided in below:

Sri Lanka is situated around 7° degrees North of Equator (Latitude) and 81° degrees East of Greenwich (Longitude) in the northern Indian Ocean (closer to South India). Historically this region has been ascertained to be aseismic, given its location well away from major plate boundaries. However, Royer and Gordon (1997) have identified a major diffuse plate boundary, located about 300 km from the southern tip of Sri Lanka. Literature also identifies that the seismic activity in this region is comparable to that of San Andreas Fault (Stein and Okal, 1978). This situation warrants an investigation on seismic hazard for the country in addition to other potential source zones on the Western, Eastern and Northern regions of the country. On the far Eastern side around Ninety East ridge, active seismicity has been reported. On the Northern side of the country, close to South India, seismic activity can be classified as dormant as evidenced by the Indian

Earthquake Code of practice. Historical seismicity has been reported on the Western side of the country especially around Colombo, the capital city of Sri Lanka. While earthquakes exceeding magnitude 5 have regularly occurred outside the country, only minor tremors have occurred within the country's mainland (apart from some historical notes of magnitude 6 inside the country and the details have been questioned by academics). A major reason attributed to this difference in seismic activity within the country is due to the nature of underlain local geology as opposed to the tectonic setting outside the country. Therefore, in this thesis, seismogenic nature within the country is examined based on the identification of shear zones and lineaments consistent with local geological classifications of Wannu Complex, Highland Complex, Vijayan Complex, while the seismogenics outside the country are examined with respect to crustal formations and plate boundaries.

A major challenge in modelling hazard and attenuation of a region lies in the availability of strong motion data. In countries such as the United States, the availability of data has facilitated the development of well-established models. In contrast, regions like Australia that do not have sufficient recorded data have resorted to fundamental approaches such as stochastic modeling in addition to probabilistic approaches of modeling hazard. Sri Lanka presents a unique situation with three major broadband network centers deployed post 2005. This facilitated an opportunity to analyse the characteristics of a low and moderate seismic region based on data availability. Therefore a novel and judicious approach of combining established techniques developed in the aforementioned regions and the adaptation to a significantly different situation of Sri Lanka has provided useful results as explained in below.

In particular 181 archival data of 71 events recorded at the three digital broadband stations, have been analysed to estimate the crustal quality factor Q value for the region surrounding Sri Lanka. Multiple linear regression analysis of recorded vertical component Fourier acceleration amplitudes yielded a Q_0 value of about 389 ± 2.35 . Furthermore, the effect of the upper crustal amplification has been assessed using the standard H/V ratio method. The upper crustal amplification obtained from the H/V analysis was found to be insignificant. Analysis was further undertaken to investigate the far-source geometric attenuation rate and high frequency cutoff filter parameter ($Kappa$). The far-source geometric attenuation rate was estimated by fitting processed records to a predefined attenuation equation at a selected frequency range of 0.5-8.5 Hz, using the multiple linear regression method. As a novel approach, a secondary regression in the frequency domain on constants derived from the first regression, was carried out to find the frequency independent $Kappa$ (κ) and the reference distance that defines the second hinge point of the trilinear geometric attenuation function. Source characteristics – stress drop, corner frequency and Moment magnitude of the selected events were determined by applying Brune's point source model. The average far-source geometric attenuation rate was found to be $R^{-0.5}$ for the selected

frequency range, but at low frequencies (below about 2 Hz) slightly lower rates than the average were observed. Kappa value was resulted in as 0.041 ± 0.009 s. The second hinge point of the geometric attenuation function was 120 ± 30 km. The complete form, after considering the final compliance with actual records, of the far-field geometric attenuation function was collated to define the geometric attenuation of the region. The average static stress drops were found to be 9.5 MPa (95 bars) and 16.0 MPa (160 bars) for m_b 4-5 and 5-6 magnitude bands, respectively. The corner frequency approximately fell within 1.0 and 7.0 Hz for the dataset. Results were found to correlate with the literature and were further validated by a comparison of ground motions between recorded events and stochastically simulated events using estimated parameters.

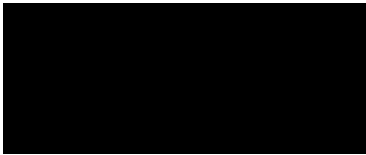
Local attenuation characteristics of the bedrock beneath Sri Lanka were investigated analysing local events reported within the country. Seismological parameters coda Q , Kappa and H/V ratio to be used in the local context were determined. The standard single scattering model that demands the decay rate of backscattered coda waves, was applied to find the local Q . A parametric study by changing coda time window as 40, 50, 60 and 70 s, was carried out to examine the significance of time dependent behavior in coda Q , if any. A clear trend of increasing Q with the length of time window at low frequencies, and a minor reversing trend at high frequencies were noted. The average variation of Q for all time window cases followed the form, $Q = (301 \pm 17)f^{(0.67 \pm 0.02)}$. Kappa was estimated by measuring the slope of displacement spectral amplitudes at frequencies below the corner frequency, and has shown to vary between 0.03 and 0.06 s for the selected locations. The average Kappa found using these local data was 0.04 ± 0.02 s, which is again comparable to that found using regional data above mentioned. The H/V ratio was estimated to be close to unity as same as that resulted in for regional data. A tri-linear geometric attenuation function to be used at local distances was also proposed based on the consistency of the spectral level between recorded and simulated events.

The above seismological parameters after satisfactory validation were then utilized in seismological models employing stochastic simulations in the preparation of two synthetic databases to be used for local and regional influences. This novel approach complemented the datasets and two attenuation models were developed. Using these attenuation models and probabilistic seismic hazard approach, maximum expected seismic hazard in terms of ground motions that are likely to exceed in selected return periods of engineering interest were determined. Hazard values show that the area around the capital city - Colombo possesses the maximum expected ground acceleration (in rock sites) which is about 0.05g for a 475 year return period. Most of other areas indicate relatively small ground motion levels. The complete work done throughout the study in terms of the attenuation models, seismological parameters and response spectra contributes to new knowledge and information that could pave the way in addressing the long term need of seismic hazard maps and future code of practice for the country.

Declaration

Doctor of Philosophy Declaration

“I, Wepitiya Gamage Janaka Prasanna, declare that the PhD thesis entitled “Earthquake Ground Motion Models for Sri Lanka” is no more than 100,000 words in length including quotes and exclusive of tables, figures, appendices, bibliography, references and footnotes. This thesis contains no material that has been submitted previously, in whole or in part, for the award of any other academic degree or diploma. Except where otherwise indicated, this thesis is my own work”.



Signature

03/09/2015

.....

Date

Acknowledgements

I would like to start by thanking the Victoria University Postgraduate Research Scholarship program for offering me this valuable opportunity of undertaking postgraduate research studies that laid the foundation for emanating my career as a researcher. By most, I shall be grateful to my principal supervisor, Dr Srikanth Venkatesan, for the continuous support and guidance given through the total period of the project. Dr Sri was always a true “mentor” with full of kindness, and was such a generous person to let me having “an open door” to discuss any matter with him whenever I needed. He guided me through the project, not only by nourishing things in the technical content, but also by enlightening essential things that I may keen on in developing a successful research career. He applauded me when there were triumphs and, particularly, encouraged me more at contretemps.

My special thanks go to the associate supervisor in Sri Lanka Prof Ranjith Dissanayake at the University of Peradeniya, for his timely help in collecting seismic data from responsible local bodies, as well as for providing essential information on previous earthquake research applications in the country, which was partly helpful in the planning of my study too by identifying the present research extent of the earthquake engineering in the country. Also, other colleagues at the University of Peradeniya, in particular, Mr Uduweriya and Mr L.R.K. Perera are appreciated for giving me previously reported earthquake information in and around the country. A detailed list of data, which is generally difficult to be found in standard archival databases, given by Mr Uduweriya, was so helpful in determining more reliable seismicity rates for the region. The kind assistance given by the former chairman of Geological Survey and Mines Bureau (GSMB) in Sri Lanka, Dr N.K. Wijayananda, and by the geologist Miss Nilmini, for facilitating important information on recent microseismic activities in the country, is heartily appreciated. Even though not by often, some stimulated discussions had at times with A/Prof Nelson Lam at the University of Melbourne and Dr Hing-Ho Tsang at Swinburne University, in turn made a critical impact on the study, hence their support is to be deeply valued. Especially, I am indebted to A/Prof Nelson Lam for letting me to use his FORTRAN routings GENQKE and ETAMAC in earthquake simulations, which were enormously useful in validating determined attenuation factors and in preparing synthetic ground motion databases.

Moreover, I want to thank Dr Zora Vrcelj at Victoria University, for being my additional supervisor, even on a short request. Her willingness for being my additional supervisor was a great relief for me, and was crucial at instances where the required smoothness of the administrative process needed to be maintained.

Last, but far away from the least, I really want to pay my sincere gratitude to my loving wife Subhashini and to my parents, for their immense patience and ultimate trust on me, till the end of the study. This work would never be possible unless their kindness and love happened to be on me, which have always energized myself towards pursuing achievements in the academic field. My siblings in the home country and my friends are also to be acknowledged for their invaluable commitments made on behalf of me, which were really influential in keeping myself merely concentrated in the research study.

Table of Contents

| | |
|--|----------|
| Title page..... | i |
| Abstract | ii |
| Declaration | v |
| Acknowledgements | vi |
| Table of Contents | viii |
| List of Figures | xi |
| List of Tables..... | xiv |
| List of Appendices | xv |
| List of symbols..... | xvi |
| List of abbreviations..... | xix |
| List of publications..... | xxi |
| 1. Introduction | 1 |
| 1.1 Background and problem statement..... | 1 |
| 1.2 Significance..... | 3 |
| 1.3 Aims, objectives and work plan | 4 |
| 1.4 Organization of the thesis..... | 4 |
| 2. Methods and applications of ground motion modelling: Literature review | 6 |
| 2.1 Introduction..... | 6 |
| 2.2 Formulation of ground motion | 7 |
| 2.3 Seismological characteristics | 10 |
| 2.3.1 Source factor [$S(f)$] | 12 |
| 2.3.2 Geometric attenuation factor (G) | 17 |
| 2.3.3 Anelastic whole path attenuation factor [$A_n(f)$] | 19 |
| 2.3.4 Upper crustal amplification factor [$V_a(f)$] | 23 |
| 2.3.5 Upper crustal attenuation factor [$P(f)$] | 25 |
| 2.3.6 Response of subsoil..... | 27 |
| 2.4 Simulation of earthquakes..... | 28 |
| 2.4.1 Deterministic procedures..... | 28 |
| 2.4.2 Stochastic procedures..... | 30 |
| 2.5 Quantification of seismic hazard..... | 32 |
| 2.5.1 Probabilistic seismic hazard analysis | 33 |
| 2.5.2 Deterministic seismic hazard analysis..... | 35 |
| 2.6 Application of seismic hazard analysis methods in Sri Lanka | 36 |
| 2.7 Summary and conclusion | 37 |

| | |
|---|-----|
| 3. Seismicity and possible seismic sources in and around Sri Lanka | 39 |
| 3.1 Introduction | 39 |
| 3.2 Seismicity within the country or local seismicity | 40 |
| 3.2.1 A summary on the general geology of Sri Lanka | 40 |
| 3.2.2 Local events reported in the country and possible seismic sources | 44 |
| 3.3 Seismicity around the country or regional seismicity | 49 |
| 3.3.1 Seismicity in the northern Indian Ocean south/southeast of Sri Lanka and southern Bay of Bengal | 49 |
| 3.3.2 Seismicity west of Sri Lanka in the Laccadive Sea and Gulf of Mannar | 55 |
| 3.3.3 Seismicity north of Sri Lanka in the southern Indian peninsula region | 56 |
| 3.4 Summary and conclusion | 58 |
| 4. Attenuation parameters for regional earthquakes in the northern Indian Ocean – Derivation of Q value and H/V ratio | 59 |
| 4.1 Introduction | 59 |
| 4.2 Database sampling and processing procedure | 60 |
| 4.2.1 Database sampling | 60 |
| 4.2.2 Processing procedure | 61 |
| 4.3 Regression analysis for Q value | 63 |
| 4.4 H/V ratio | 66 |
| 4.5 Results and discussion | 67 |
| 4.6 Summary and conclusion | 81 |
| 5. Attenuation (G and $Kappa$) and source parameters for regional earthquakes in the northern Indian Ocean | 83 |
| 5.1 Introduction | 83 |
| 5.2 Methodology | 85 |
| 5.2.1 Data processing and the main regression analysis | 85 |
| 5.2.2 The secondary regression | 87 |
| 5.2.3 Source characteristics | 90 |
| 5.3 Results and discussion | 92 |
| 5.3.1 The main regression analysis | 92 |
| 5.3.2 The secondary regression | 97 |
| 5.3.3 Apparent source parameters | 103 |
| 5.3.4 Ground motion comparison | 107 |
| 5.3.5 Ground motions for hypothesized regional events | 112 |
| 5.4 Summary and conclusion | 112 |
| 6. Seismological parameters for local earthquakes in Sri Lanka | 114 |
| 6.1 Introduction | 114 |
| 6.2 The coda Q method and Q value | 115 |

| | | |
|-----------|--|------------|
| 6.3 | Kappa (κ) value | 121 |
| 6.4 | H/V ratio..... | 124 |
| 6.5 | Results and discussion..... | 125 |
| 6.5.1 | Q , Kappa and H/V ratio..... | 125 |
| 6.5.2 | Comparison of ground motions..... | 135 |
| 6.5.3 | Source spectra | 141 |
| 6.5.4 | A scenario investigation | 143 |
| 6.6 | Summary and conclusion | 146 |
| 7. | Ground motion prediction equations for rock sites in Sri Lanka..... | 148 |
| 7.1 | Introduction..... | 148 |
| 7.2 | Methodology | 149 |
| 7.2.1 | Preparation of the database using stochastic simulation | 149 |
| 7.2.2 | Regression analysis | 151 |
| 7.3 | Results and discussion..... | 152 |
| 7.4 | Conclusion..... | 164 |
| 8. | Development of seismic hazard maps for Sri Lanka..... | 165 |
| 8.1 | Introduction..... | 165 |
| 8.2 | Methodology | 166 |
| 8.2.1 | Seismic source zones..... | 166 |
| 8.2.2 | Earthquake catalog processing..... | 170 |
| 8.2.3 | Ground motion prediction equations..... | 183 |
| 8.2.4 | Hazard computation | 183 |
| 8.3 | Results and discussion..... | 185 |
| 8.4 | Summary and conclusion | 193 |
| 9. | Results, conclusions and further research | 195 |
| 9.1 | Main results..... | 195 |
| 9.2 | Future research | 197 |
| | References..... | R-1 |

List of Figures

| | |
|---|----|
| Figure 1.1 Sri Lanka and its geographic location in the northern Indian Ocean..... | 2 |
| Figure 2.1 Some of published attenuation models to predict Peak Ground Acceleration (PGA) on rock sites..... | 9 |
| Figure 2.2 Comparison of some of widely used source spectral models available in the literature | 15 |
| Figure 2.3 Variation of the geometric attenuation factor with hypocentral distance | 19 |
| Figure 2.4 Comparison of anelastic whole path attenuations [$A_n(f)$] for selected three regions..... | 22 |
| Figure 2.5 Comparison of upper crustal effects [amplification - $V_a(f)$, attenuation - $P(f)$ and combined effects] for ENA and WNA regions | 27 |
| Figure 3.1 Typical seismotectonic features in the northern Indian Ocean surrounding Sri Lanka..... | 40 |
| Figure 3.2 General geology of Sri Lanka showing main lithotectonic units categorized according to the basement rock type and geological period of formation | 41 |
| Figure 3.3 Three broadband seismic stations presently operating in Sri Lanka..... | 45 |
| Figure 3.4 Local seismicity in Sri Lanka showing reported events within the country | 46 |
| Figure 3.5 A simple estimation of earthquake recurrence, since 1615, for Colombo area | 47 |
| Figure 3.6 Seismicity around Sri Lanka in the northern Indian Ocean and southern peninsular India | 50 |
| Figure 3.7 Large diffuse area (hatched) located amidst trisected Indo-Australian plate (Reproduced from Royer and Gordon, 1997) | 54 |
| Figure 3.8 Seismicity in the Gulf of Mannar, southern Indian peninsula and in close proximity of Sri Lanka relating to the geotectonic setup..... | 55 |
| Figure 3.9 Seismicity in the southern peninsular India..... | 56 |
| Figure 4.1 Recorded events (circles) used in the study for deriving the regional Q and assessing H/V ratio calculations | 60 |
| Figure 4.2 Distribution of the dataset in magnitude (m_b) and hypocentral distance space | 61 |
| Figure 4.3 Data processing..... | 63 |
| Figure 4.4 Comparison of recorded vertical component acceleration amplitudes with predicted ones from the attenuation relationship | 70 |
| Figure 4.5 Anelastic whole path attenuation in the Northern Indian Ocean | 71 |
| Figure 4.6 Log residual (=log observed amplitude-log predicted amplitude) variation for selected frequencies (2 and 5 Hz) | 74 |
| Figure 4.7 Average log residual variation in each magnitude band with respect to frequency... .. | 75 |
| Figure 4.8 Average log H/V ratio with 95% confidence limits on mean, calculated from equation (4.6) | 76 |
| Figure 4.9 Comparison of estimated acceleration source spectra (continuous lines) with theoretical Brune's spectra (dash lines) for typical 50, 100 and 150 bars stress drop levels | 77 |

| | |
|---|-----|
| Figure 4.10 Comparison of M_w 8.6 event with the stochastic simulation using GENQKE | 81 |
| Figure 5.1 Variation of the far-source geometric attenuation rate, b , with wave frequency | 95 |
| Figure 5.2 Comparison of recorded vertical component acceleration amplitudes with predicted ones from the applied attenuation relationship [equation (5.7)]..... | 96 |
| Figure 5.3 Log residual (= log observed amplitude-log predicted amplitude) variation for selected frequencies (4.5 and 7.0 Hz) | 97 |
| Figure 5.4 Variation of regression coefficients, C_1 , C_2 and C_T with wave frequency | 98 |
| Figure 5.5 Comparison of actual C_T resulted from the main regression with the predicted from equation (5.8) | 100 |
| Figure 5.6 Comparison of expected path attenuations for a typical shallow crustal event occurred at a hypocentral distance within a possible range of 300-1800 km in the northern Indian Ocean region | 102 |
| Figure 5.7 Comparison of source amplitudes between observed and predicted | 103 |
| Figure 5.8 Estimated source parameters by the regression of equation (5.11)..... | 106 |
| Figure 5.9 Resulted Seismic moment (M_0) vs. event magnitude m_b | 107 |
| Figure 5.10 Comparison between observed records and stochastically simulated events in terms of relative displacement for 5% critical damping ratio | 110 |
| Figure 5.11 Simulated spectral amplitudes of 3 hypothesized large magnitude events M_w 9.0, 8.5 and 8.0 occurred in the northern Indian Ocean | 112 |
| Figure 6.1 A sample seismogram band pass filtered between 1-19 Hz, indicating origin, essential phase arrivals and coda length to be used in a coda Q study..... | 118 |
| Figure 6.2 Earthquake data used in the study..... | 119 |
| Figure 6.3 Decay of coda amplitude (RMS value) with the lapse time at two random centre frequencies (4 and 14 Hz) | 121 |
| Figure 6.4 Frequency ranges used in the Kappa estimation..... | 123 |
| Figure 6.5 Kappa value estimation..... | 124 |
| Figure 6.6 Resulted Q values with standard deviations at selected centre frequencies..... | 126 |
| Figure 6.7 Variation of Q with the length of coda window used | 128 |
| Figure 6.8 Sample estimations of individual Kappa values for the selected stations..... | 130 |
| Figure 6.9 Individual Kappa variation with earthquake properties | 133 |
| Figure 6.10 H/V estimations for the selected sites in the study | 134 |
| Figure 6.11 Proposed model of geometric attenuation to be used at local distances in the country | 137 |
| Figure 6.12 Comparison between observed records with stochastically simulated events in terms of Pseudo Spectral Acceleration (PSA) for 5% critical damping ratio and acceleration time history | 139 |
| Figure 6.13 Comparison of attenuation corrected source spectra with theoretical Brune's spectra for 3 and 10 MPa (30 and 100 bars) stress drop values | 142 |
| Figure 6.14 Initial M_L vs. estimated M_w values for the selected events..... | 143 |
| Figure 6.15 A possible scenario investigation for Sri Lanka in the local context..... | 145 |

| | |
|--|-----|
| Figure 6.16 Pseudo spectral accelerations for 5% damping ratio of the M_w 6.5 scenario event occurred at 5, 10, 20 and 30 km hypocentral distances..... | 146 |
| Figure 7.1 Magnitude and hypocentral distance combinations used in the preparation of synthetic databases for deriving ground motion equations | 150 |
| Figure 7.2 Variation of residuals [log observed (in this case, simulated data) - log predicted from the derived model] for the local attenuation model..... | 156 |
| Figure 7.3 Variation of residuals [log observed (in this case, simulated data) - log predicted from the derived model] for the regional attenuation model..... | 157 |
| Figure 7.4 Comparison of the derived local attenuation model with some of published models available in the literature | 159 |
| Figure 7.5 Comparison of the derived regional attenuation model with some of published models available in the literature | 161 |
| Figure 7.6 Comparison of ground motions between actual values in recorded vertical components of events (denoted by filled squares) and predicted values (denoted by dark continuous lines) by developed attenuation models..... | 162 |
| Figure 8.1 Source zones defined in the study..... | 167 |
| Figure 8.2 Epicentral locations of earthquake catalog data used in the hazard computation in the study | 172 |
| Figure 8.3 Magnitude and hypocentral depth distributions of the selected events..... | 173 |
| Figure 8.4 Comparison of the actual earthquake distribution with the theoretical Poisson distribution | 176 |
| Figure 8.5 Stepp's plots of the completeness check..... | 179 |
| Figure 8.6 Earthquake recurrences of the defined source zones | 182 |
| Figure 8.7 Computed hazard values in terms of expected ground motions (PGA and SAs at 0.1, 0.5 and 1.0 s natural periods) at rock sites in Sri Lanka for probability of exceedance..... | 189 |
| Figure 8.8 Resulted design spectra, in terms of PSA, for selected cities in the country | 192 |
| Figure 8.9 Comparison of attenuation models used in the study | 193 |

List of Tables

| | |
|--|-----|
| Table 2.1 Examples for source spectral models available in the literature | 16 |
| Table 2.2 Some of published Q_0 and n (in $Q = Q_0 f^n$), and Kappa values for various regions .. | 22 |
| Table 3.1 Large magnitude events occurred in the diffuse area since 1900 (Source-ISC) | 51 |
| Table 4.1 Regression coefficients (C_1, C_2, C_3 and $C_4 = \pi f \log e / (Q\beta)$) of equation (4.5) | 68 |
| Table 5.1 Results of the main regression [using equation (5.5) or (5.7)] for the selected frequency range | 92 |
| Table 5.2 Results of the secondary regression by equation (5.8) | 99 |
| Table 5.3 Estimated source parameters for the dataset | 104 |
| Table 5.4 Seismological parameters used in the stochastic simulation | 109 |
| Table 6.1 List of events used in the study | 118 |
| Table 6.2 Resulted Q values from the single backscattering method | 127 |
| Table 6.3 Seismological parameters used in the stochastic simulation | 138 |
| Table 7.1 Regression coefficients of the local attenuation model developed for Sri Lanka | 152 |
| Table 7.2 Regression coefficients of the regional attenuation model developed for Sri Lanka | 153 |
| Table 8.1 Seismicity parameters of defined source zones | 178 |
| Table 8.2 Raghu Kanth and Iyengar's (2007) attenuation model for Peninsular India | 183 |
| Table 8.3 Estimated hazard values in terms of PGA and SAs (at 0.1, 0.5 and 1.0 s natural periods) with exceeding probabilities 10%, 5% and 2% in 50 years for selected major cities in Sri Lanka | 186 |

List of Appendices

| | |
|---|-----|
| Appendix A: Table A.1 Some of published attenuation models | A-1 |
| Appendix B: Table B.1 List of earthquakes used in the study | B-1 |

List of symbols

Note that, most of below symbols are also defined in the main text for convenience of the reader.

| | |
|--------------------------|--|
| a value | “ a value” of the Guttenberg-Richter recurrence law |
| $A(f,t)$ | Coda wave amplitude at time t for a given frequency f |
| a, b | Geometric attenuation rates at near-source and far-source distances |
| A, B, E | Regression coefficients in developed attenuation models |
| $A_n(f)$ | Anelastic whole path attenuation factor |
| $A_x(f)$ | Spectral (Fourier) amplitude of a frequency f seismic shear wave at the rock outcrop |
| b value | “ b value” of the Guttenberg-Richter recurrence law |
| C | Scaling factor or a regression coefficient of developed attenuation models |
| C_1 to C_s, C_T | Regression coefficients |
| D | Static slip value or Crustal thickness or a regression coefficient of developed attenuation models |
| e | Exponential value |
| f | Wave frequency |
| $f(M)$ | Probability density function for earthquake magnitude |
| $f(R)$ | Probability density function for hypocentral distance |
| f_0 | Corner frequency defined in the Brune’s model |
| f_a, f_b or f_A, f_B | Corner frequencies defined in double corner frequency source models |
| f_{max} | High frequency diminution function in Hanks (1982) |
| g | Gravitational acceleration |
| G | Geometric attenuation factor |
| H | Amplitude of the horizontal shear wave component |
| H_1, H_2 | Amplitudes of two orthogonal horizontal shear wave components |
| L_g | L_g (waves) |
| M | Magnitude of the earthquake, either m_b or M_w depending on the case |
| M_0 | Seismic moment |
| m_0 | Minimum threshold magnitude used in the hazard computation |
| m_B | Broadband body wave magnitude |
| m_b | Short period body wave magnitude |
| M_E | Energy magnitude |
| M_L | Richter (local) magnitude |
| M_{Lv} | Richter (local) magnitude measured on the vertical component |
| m_{max} | Maximum expected magnitude for the source zone |

| | |
|---------------------------------|--|
| M_N | Nuttli magnitude |
| M_s | Surface wave magnitude |
| M_w | Moment magnitude |
| M_{wp} | Moment magnitude calculated on P wave |
| n | Exponent |
| N | Number of observations or number of potential seismic sources |
| n_i | Number of earthquakes in a unit year |
| P | Compressional (waves) |
| $P(f)$ | Upper crustal attenuation factor |
| $P(\omega t)$ | Power spectral density of coda waves at time t |
| Q | Wave transmission quality factor |
| Q_0 | Q value at 1 Hz frequency |
| R or r | Hypocentral distance |
| R_0 | Reference distance equal to 1 km |
| $R_1, R_2, R_x, R_{x1}, R_{x2}$ | Reference distances (Hinge points) of G |
| R^2 | Coefficient of determination |
| S | Shear (waves) or source factor relevant to the power spectral density of coda wave |
| $S(f)$ or $A_s(f)$ | Spectral (Fourier) amplitude of a frequency f seismic shear wave at the source |
| S' | Modified source term corresponding to the coda amplitude |
| S_n | S wave bottoming in the uppermost mantle or coming from a source in the uppermost mantle |
| $SS(reg)$ | Regression sum of squares |
| $SS(Resi)$ | Residual sum of squares |
| t | Lapse time |
| T | Natural period or the selected time period in the catalog completeness |
| t_c | Time of coda wave arrival |
| t_o | Time of origin of the earthquake |
| t_p | Time of first P wave arrival |
| t_s | Time of first S or L_g wave arrival |
| V | Amplitude of the vertical shear wave component |
| $V_a(f)$ | Upper crustal amplification factor |
| V_p | Compressional wave velocity |
| V_s | Shear wave velocity |
| V_{s30} | Shear wave velocity at 30 m depth |
| W, L | Width and length of the fault |
| Y or y_{br} | Predicted ground motion parameter |

| | |
|-----------------------|---|
| α | “ <i>a</i> value” in natural logarithms in the standard Gutenberg-Richter recurrence law |
| β | Shear wave velocity or “ <i>b</i> value” in natural logarithms in the standard Gutenberg-Richter recurrence law |
| β_s, β_z | Shear wave velocity at the source and at a depth of <i>z</i> |
| $\Delta u(\xi, \tau)$ | Displacement function for position ξ at time τ at the fault |
| $\Delta\sigma$ | (Static) stress drop |
| ε | Weighting parameter |
| ε_{br} | Error term in Raghu Kanth and Iyengar’s (2007) attenuation model |
| κ | Kappa (Upper crustal/near-surface attenuation parameter) |
| λ | Mean rate of earthquake recurrence |
| λ_m | Mean annual rate of exceedance of a given (<i>m</i>) magnitude earthquake |
| λ_y | Aggregate result of the rate of exceedance of a ground motion value <i>y</i> |
| ξ | Position vector on the fault with respect to the hypocenter |
| ξ_1, ξ_2 | Component vectors of the position vector ξ |
| π | π value |
| ρ | Crustal density |
| ρ_s, ρ_z | Crustal density at the source and at a depth of <i>z</i> |
| σ | Standard error/deviation of the regression coefficient |
| $\sigma(\lambda)$ | Standard deviation of the mean rate of earthquake recurrence |
| σ_{est} | Standard error of estimate |
| τ | Time at which a $\Delta u(\xi, \tau)$ dislocation (displacement) has undergone in the fault |
| τ_n | Rise time |
| ν_i | Mean recurrence rate of source zone <i>i</i> |
| ν_r | Rupture velocity |
| ω | Circular corner frequency |

List of abbreviations

| | |
|------------|--|
| ANSS | Advanced National Seismic System |
| BHZ | Broadband High-gain Z (Vertical) component |
| CRUST2.0 | Global Crustal Model (version 2.0) developed by University of California |
| CV | Coefficient of Variation |
| EERI | Earthquake Engineering Research Institute |
| ENA | Eastern North America |
| E-W | East-West |
| exp | Exponential value |
| FAS | Fourier Acceleration Spectra |
| GBVM | Geology Based Velocity Model |
| GCMT | Global Centroid Moment Tensor (catalog) |
| GFZ-GEOFON | German Research Centre for Geosciences |
| GSMB | Geological Survey and Mines Bureau |
| H/V ratio | Horizontal to Vertical (amplitude) ratio |
| HALK | Hakmana |
| HC | Highland Complex |
| IRIS | Incorporated Research Institutions for Seismology |
| ISC | International Seismological Centre |
| KC | Kadugannawa Complex |
| Lat. | Latitude |
| ln | Logarithmic value to base-e |
| log | Logarithmic value to base-10 |
| Lon. | Longitude |
| MALK | Mahakanadarawa |
| MLTWA | Multiple Lapse Time Window Analysis |
| MMI | Modified Mercalli Intensity |
| MSK | Medvedev–Sponheuer–Karnik |
| NEHRP | National Earthquake Hazard Reduction Program |
| NEIC | National Earthquake Information Centre |
| NGA | Next Generation Attenuation (relationships) |
| NNW | North-northwest |
| N-S | North-South |
| NW-SE | Northwest-Southeast |
| PALK | Pallekelle |

| | |
|-------|--|
| PGA | Peak Ground Acceleration |
| PGD | Peak Ground Displacement |
| PGV | Peak Ground Velocity |
| PSA | Pseudo Spectral Acceleration |
| PSV | Pseudo Spectral Velocity |
| RMS | Root Mean Square |
| S/N | Signal to Noise ratio |
| SA | Spectral Acceleration |
| SCR | Stable Continental Region |
| sps | Samples per second |
| SSE | South-southeast |
| USA | United States of America |
| USGS | United States Geological Survey |
| UTC | Universal Time Coordinated |
| VC | Vijayan Complex |
| Vp/Vs | Compressional (<i>P</i>) to Shear (<i>S</i>) wave velocity ratio |
| WC | Wanni Complex |
| WNA | Western North America |
| WWSSN | World-Wide Standard Seismograph Network |

List of publications

Refereed journals

- **Gamage, P.**, and Venkatesan, S. (2015). "Attenuation and apparent source characteristics in the northern Indian Oceanic crust surrounding Sri Lanka." *Bulletin of the Seismological Society of America*, 105(4), 2041-2057, DOI 10.1785/0120140120.
- Venkatesan, S., and **Gamage, P.** (2013). "Spectral analysis of seismic waves in the northern indian ocean region." *Bulletin of the Seismological Society of America*, 103(6), 3305-3320, DOI 10.1785/0120130079.
- **Gamage, P.**, and Venkatesan, S. (under review). "Seismological parameters derived from local earthquakes reported in Sri Lanka." *Soil Dynamics and Earthquake Engineering*.
- **Gamage, P.**, and Venkatesan, S. (under review). "Seismicity and seismotectonics in and around Sri Lanka – a synoptic review." *Australian Journal of Earth Sciences*.
- **Gamage, P.**, Venkatesan, S., and Vrcelj, Z. (submitted). "A probabilistic seismic hazard analysis for Sri Lanka." *Bulletin of the Seismological Society of America*.

Refereed conference proceedings

- Venkatesan, S., and **Gamage, P.** (2015). "Development of seismic hazard maps for Sri Lanka." *11th Canadian Conference on Earthquake Engineering (CCEE)*. Victoria, British Columbia, Canada.
- **Gamage, P.**, and Venkatesan, S. (2014). "Attenuation models for expected ground motions in Sri Lanka." *23rd Australasian Conference on the Mechanics of Structures and Materials ACMSM23*. Byron Bay, Australia.
- **Gamage, P.**, Venkatesan, S., and Dissanayake, P. B. R. (2013). "Local seismicity and possible ground motion parameters for Sri Lanka." *4th International Conference on Structural Engineering & Construction Management ICSECM 2013*. Kandy, Sri Lanka.
- **Gamage, P.**, and Venkatesan, S. (2013). "Coda Q for the Sri Lankan Precambrian crust." *Australian Earthquake Engineering Society (AEES) Conference*. Hobart, Tasmania.
- **Gamage, P.**, and Venkatesan, S. (2012). "Seismic risk analysis based on historical events reported in Sri Lanka." *22nd Australasian Conference on the Mechanics of Structures and Materials ACMSM22*. Sydney, Australia.
- **Gamage, P.**, and Venkatesan, S. (2012). "Estimation of Lg-coda Q value for the Northern Indian Ocean region based on spectral analysis." *Australian Earthquake Engineering Society (AEES) Conference*. Gold Coast, Australia.
- **Gamage, P.**, Venkatesan, S., and Dissanayake, R. (2011). "Seismic drift demand on multi-storey buildings in Sri Lanka due to long-distant earthquakes." *2nd International Conference on Structural Engineering, Construction and Management ICSECM 2011*. Kandy, Sri Lanka.

1. Introduction

1.1 Background and problem statement

Global awareness on seismic hazard has increased with the occurrence of recent major disastrous earthquakes at various populous places in the world (e.g., M_w 6.3 event on 22nd February 2011 in Christchurch, New Zealand; M_w 9.0 event on 11th March 2011 in Tohoku, Japan; M_w 8.8 event on 27th February 2010 in offshore Maule, Chile; M_w 7.0 event on 12th January 2010 in Haiti; M_w 7.9 event on 12th May 2008 in Sichuan, China, etc.). The infrequent nature of such events and limitations in preparedness often result in huge devastation of infrastructure and loss of lives. Therefore, research studies on seismology and earthquake engineering should be encouraged by “relevant bodies” in any country. The degree of complexity in quantifying the hazard which is convoluted by numerous undiscovered uncertainties, should not be a valid reason to disregard the potential threat of seismicity at a place. Instead, what would really matter is the adequacy in preparation for satisfactory preparedness and response during such hazardous situations. There are many examples of places that are located at so-called “safe distances” away from major seismic sources with frequent activities (like plate boundaries, diffuse zones, shear zones, major faults and lineaments, etc.), yet they have been subjected to catastrophic events in the past; e.g., some major intraplate events such as M_w 7.7 event on 26th January 2001 in Gujarat, India; M_w 8.6 and 8.2 events on 11th April 2012 in the northern Indian Ocean; M_w 5.6 event on 28th December 1989 in Newcastle, Australia; M_w 6.4 event on 14th April 1615 in Colombo, Sri Lanka, etc. Hence, a complete negation of the seismic hazard even at a place in a stable region, has become intricate for scientists given these evidences. Damage inflicted by an earthquake in such seismically remote areas, can be significantly higher than that due to an event in an active seismotectonic region which is more “accustomed” for major and frequent seismic activities than low seismic areas. Therefore, preparedness of a place (even if it is located in an inactive region) in terms of safety of both people and physical properties for a probable event expected, is a prime requirement that should be guaranteed by people in charge of developing and enforcing national policies and guidelines.

The island of Sri Lanka, bounded by latitudes 5^oN to 10^oN and longitudes 79^oE to 82^oE (Figure 1.1), is generally identified to be in a low seismic or seismically inactive region in the northern Indian Ocean. The closest active seismogenic sources surrounding Sri Lanka are located at the boundaries of the Indo-Australian Plate, e.g., the Sunda Arc subduction zone and Great Sumatran fault towards east (at about 1100 km), northern transform faults of the Central Indian Ridge towards west (at about 1500 km) and the continental boundary of convergent at the

Himalayan suture towards north (at more than about 2000 km). The country has experienced a range of natural hazards such as landslides, flash flooding, severe droughts, etc., in the history, however, the topic of earthquakes has invited a little national attention until the disastrous tsunami happened in 2004. The tsunami that occurred in the aftermath of M_w 9.1 mega earthquake happened on 26th December 2004 in the Sunda Arc subduction zone, caused an enormous burden for the country's public community as well as for the economy. The situation prompted for a number of research studies on Tsunamis to be initiated on the spot by both the local and international scholars, yet resulted in a very little attention towards undertaking research activities on seismic hazard of the country. Overall, few earthquake research is carried out so far in Sri Lanka for characterizing the seismicity of the country (Fernando and Kulasinghe, 1986; Abayakoon, 1996; Peiris, 2007; Uduweriya et al, 2013), however, major efforts to develop design guidelines that can be adopted in future codes of practice have not been envisaged.

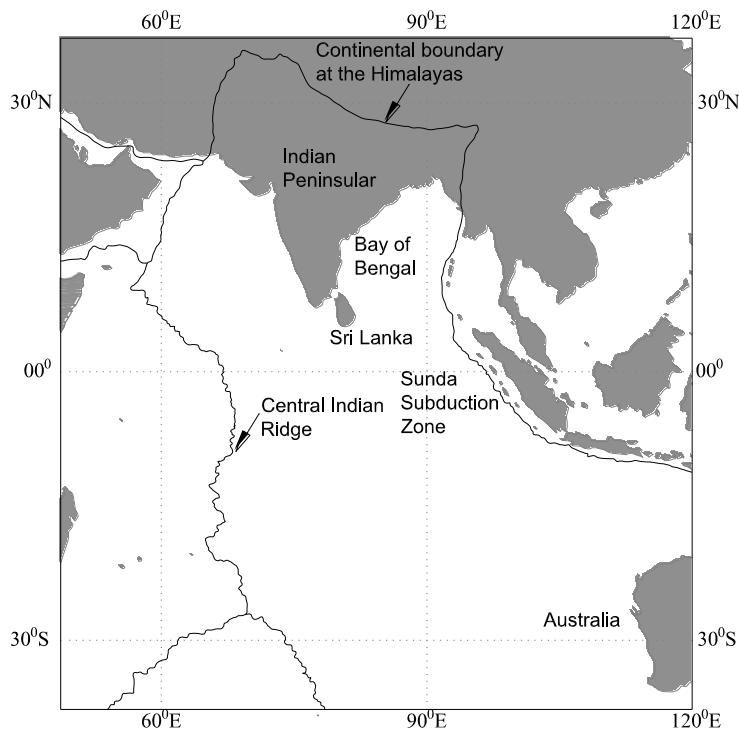


Figure 1.1 Sri Lanka and its geographic location in the northern Indian Ocean (plate boundaries are denoted by dark lines).

The amount of research studies conducted on assessing seismic hazard in Sri Lanka, would not be that sufficient to ascertain a reliable estimate of hazard levels of the country. Besides, majority of these studies are found to be short of a comprehensive hazard evaluation that may involve detailed investigations including those such as regional attenuation and source characteristics, regional seismotectonic nature, etc. The possible biases that can arise as a result

of inadequate considerations can lead to erroneous results and possible erroneous policies at the decision making levels. Therefore a comprehensive state-of-the-art modelling of seismic hazard in Sri Lanka is essential towards developing a seismic code of practice for the country. It is envisaged that a code of practice will ensure better construction and preparedness for earthquake induced hazards in the country.

1.2 Significance

Modelling ground motions to match with real records, would provide an excellent opportunity to predetermine the level of performance of structures required to safely resist earthquake loads. This is particularly useful in the present-day construction industry in Sri Lanka where a number of newly started projects are embarking on. Scale of these projects may necessitate a proper evaluation of the safety of structures for natural hazards such as earthquakes. Implementation of region-specific studies on characterizing ground motions and seismicity in low to moderate seismic regions like Sri Lanka, would be significant in the first place because it would restrict further applications of “imported” models and values from other countries, which are developed in different seismological conditions. The common practice adopted by practicing engineers is to apply design basis ground motion values simply hired from Indian and Australian codes of practice which are thought to be appropriate to represent Sri Lankan conditions. However, performing independent studies in the country per se would not only establish reliable hazard estimations to the region, which can be more confidently adopted in the seismic design criteria, but also clear any disputes on the wrong use of values taken from other codes of practice. The present study is also significant in the aspect of its investigations on distant events that could produce sufficiently strong ground motions at target sites in Sri Lanka. Being an island mostly surrounded by an oceanic crust with a sparse but uncertain seismicity, has set the country’s seismotectonic position in such a place that distant strong magnitude events are quite important in assessing the seismic risk. Furthermore, study on the seismic impact by the newly identified diffuse plate boundary in the northern Indian Oceanic crust is significant due to lacking such studies undertaken for the country. Determination of region-specific attenuation parameters that are largely dependent upon regional seismological characteristics, is important in understanding the seismotectonic nature of the region. A new regression technique, which could be of interest by the earthquake engineering and seismological community, is introduced in Chapter 5 in deriving Kappa value that characterizes upper crustal attenuation effects. Investigation of ground motions by oceanic crustal earthquakes that occur at teleseismic distances would be imperative to the earthquake engineering and seismology field. Therefore, this study may serve as a significant starting point.

1.3 Aims, objectives and work plan

The main aim of the study is to develop reliable ground motion estimates for the use in engineering and other applications in Sri Lanka. Key objectives to be achieved in the fulfillment of this aim, can be set as follows;

- Understanding the seismotectonic behavior in the region and identification of possible local and regional seismogenic sources in and around Sri Lanka.
- Determination of region-specific key seismological parameters using recorded data analysis.
- Development of own attenuation models for reliable application in the region.
- Computation of seismic hazard for engineering applications.

Depending on differences in the geospatial arrangement (being an island surrounded by the ocean) and other physical properties (thickness, ability to propagate different wave phases, etc.) between continental and oceanic crusts, these attenuation characteristics are to consider at two separate contexts; i.e., 1. “Local”, under which attenuation effects of events that occurred at local distances (events within the country’s close proximity) are examined 2. “Regional”, in which attenuation characteristics of distant events at teleseismic distances are explored. Estimated attenuation parameters are to be validated based on comparisons between actual recorded ground motion data and stochastic simulations (based on application of the seismological model). Preparation of a reliable dataset by stochastic simulations based on the above validated attenuation parameters has to be done for the purpose of deriving attenuation models. A synthetic database in this manner has to be built in the absence of enough actual data recorded at the country’s seismic network. Development of twin sets of attenuation models for separate applications in above mentioned two contexts (local and regional) by regression analysis of synthetic data, can be then performed. Finally, a probabilistic based seismic hazard analysis will be carried out for developing seismic hazard maps for the country. The hazard values are to be mapped in terms of some of chosen key ground motion parameters that are likely to exceed in the selected time periods of engineering importance.

1.4 Organization of the thesis

The work described in the thesis systematically fulfills the need for earthquake provisions for Sri Lanka. Chapter 2 presents a general description of seismological modeling concepts (source effects, wave path modification effects) often utilized in the ground motion modeling approaches in the present seismology and earthquake engineering practice. The Chapter also includes reviews on some basic ground motion simulation techniques (stochastic and deterministic), and hazard quantification methods (probabilistic and deterministic) commonly used in the field. Previous risk analysis studies carried out in quantifying the apparent seismic

hazard in Sri Lanka, are discussed at the end of the Chapter. In Chapter 3, seismicity and possible seismogenic sources within and around Sri Lanka are identified based on a comprehensive evaluation of the regional tectonic setting that includes continental Sri Lanka, surrounding oceanic crust and peninsular India. Efforts have been undertaken to identify possible seismogenic sources within the country based on observed coherence between the country's geotectonic characteristics that are well-investigated by both local and foreign scholars, and historical seismicity reported over many centuries. Tectonic features that are important in the regional context are rather easy to ascertain from previous studies already undertaken in the region. Chapters 4 and 5 describe spectral analysis techniques undertaken for a set of actual teleseismic data (of shallow crustal distant events occurred in the oceanic crust) recorded at the country's broadband seismic network in determining regional seismological parameters (Q value, geometric attenuation factor, upper crustal amplification and attenuation factors) including earthquake source characteristics. Estimations are validated by a comparison of recorded data with stochastic simulations. In Chapter 6, local seismological characteristics (Q value, Kappa and geometric attenuation factor) are determined based on an analysis of a smaller dataset given the lack of local events within the country. Q value is determined based on the Coda wave analysis method. A source spectral analysis is also carried out to discover apparent earthquake source characteristics within Sri Lanka. Estimations are again validated by a comparison with stochastic simulations. Chapter 7 demonstrates the derivation of attenuation models by using synthetic databases prepared based on estimated seismological parameters described in previous Chapters. Chapter 8 is about an application of the probabilistic seismic hazard analysis method for the development of hazard maps for the country. Chapter 9 provides conclusions of the study and possible recommendations in future research applications in seismology in Sri Lanka.

2. Methods and applications of ground motion modeling: Literature review

2.1 Introduction

Earthquake ground motion models commonly referred to as attenuation models are used in estimation of ground motions expected in a region due to any selected combination of earthquake magnitude and site-source distance. Estimated ground motion can be expressed as either a direct amplitude measure of the ground movement (e.g., Peak Ground Acceleration/Velocity/Displacement – PGA/PGV/PGD) or a frequency content measure of the generated seismic waves (e.g., Fourier Spectral parameters, Power Spectral parameters, Responses Spectral parameters at selected frequencies, etc.) or even a measure of the damage incurred at the site of interest (e.g., intensity). Reliable estimations of ground motion are primarily used in quantifying “the hazard level” of a region in the engineering seismic risk analysis. Concepts and initial forms of ground motion models were first introduced to the field of seismology and earthquake engineering in early and mid of the 20th century (e.g., Nakano, 1923; Richter, 1935; Guttenberg, 1936; Guttenberg and Richter, 1956; Kanai, 1957), and since then many scholars have devoted their time in the development of various advanced attenuation models. The final purpose of any attenuation model is to maintain the adequate reliability/accuracy in predictions. The first detailed models appeared in “the strong motion” streams were developed in the late 1960s and early 1970s by the work of USA, Canadian and Mexican researchers (e.g., Milne and Davenport, 1969; Esteva, 1970; Johnson, 1973). Most of the attenuation models available today are originally invented in the areas where active seismicity persists (e.g., plate boundary areas such as California, Japan, New Zealand, Indonesia, etc.), by analyzing many recorded data. If a model has been derived using recorded earthquake data of a particular region, then there is a greater chance of the model being characterized by native seismo-tectonic features of that region. Therefore, the application of the model to outside regions needs to be done with care, or can lead to erroneous judgments. “Effective application” (the term “effective” signifies that any uncertainty in the model application is accounted for) of an attenuation model in a region within an engineering framework is mostly done as a key step in the seismic hazard assessment process. Both the correct use of attenuation models and a proper application of the hazard assessment can produce reliable estimations in the final hazard level for the given region (commonly interpreted as a ground motion parameter with a certain probability of exceedance in a selected time period), which can then be confidently adopted as “design basis ground motions” in seismic design applications of the region.

The following is a general yet concise discussion on concepts and methods of ground motion modeling and seismological characteristics, simulation of earthquakes and seismic hazard assessment techniques, used in the seismology and earthquake engineering practice.

2.2 Formulation of ground motion

Empirical development of ground motion models for predicting strong ground motion parameters, in particular, in active seismic regions, has become a standard practice which majority of seismologists and engineers rely upon. Determination of model coefficients are undertaken through a statistical process of regression analysis of recorded data available in the region. Therefore, a good quality set of data to be used as “raw material” is a priority. The quality of data is to ensure that the data are free from background noise contaminations (should have a higher signal to noise ratio), that records are generated by instruments which have properly functioned at the moment of recording (without false triggering, correctly equipped to transfer data to the database, etc.), and that data possess a rational distribution unbiased in any of independent properties, i.e., magnitude, hypocentral distance and frequency. The amount of data should also be statistically adequate so that the use of regression models in deriving ground motion prediction equations, seems sound more logical. Application of regression models by various techniques for developing predictive attenuation models in active tectonic regions, became a kind of convention among scientists. Adapting the least-squares technique in the multiple linear regression, Joyner and Boore (1981) have performed “the two-stage regression analysis” that effectively takes both magnitude and distance into account for characterizing the ground motion in Californian earthquakes. Building a realistic format of the regression equation, in which independent variables essentially comply with the actual forms of attenuations in the region, should be done with careful attention to regional seismological characteristics. Higher the number of independent variables included in the equation, may result in a higher unbiasedness of final predictions, which in turn would increase the accuracy of the model’s generic applicability in various other possible regions. However, including variables for which scientists have not yet come to clear grips, can eventually cause misleading conclusions. Hence, when working on complicated areas such as directivity effects, basin effects and asymmetric ground motions (the hanging wall versus the footwall of thrust faults), additional care must be taken for proper characterization of ground motions (Atkinson, 2004a). Brillinger and Preisler (1984; 1985) have introduced “the random effects model”, in which explicit earthquake to earthquake component variance and record to record component variance are incorporated by the application of one-stage maximum likelihood method. Joyner and Boore (1993) have proposed a two-stage method with the same application of maximum likelihood method, and have shown that the both one-stage and two-stage methods are, properly applied, unbiased though the latter can be computationally more efficient. Many have later followed their method

of regression for modeling region-specific attenuation models in other regions (e.g., Atkinson, 2004b; Motazedian, 2006; Munson and Thurber, 1997). Validity and usability of a final attenuation equation, which is developed by any empirical modeling method, for generic application of a region, need to be always assessed based on a statistical evaluation of the model that clearly describes the fitness of the model with actual data (e.g., evaluation of statistical parameters such as standard deviation, correlation coefficient, residuals, etc.), as well as using results of any “elemental” approach (e.g., comparing with real records). Empirical modeling using regression analysis of actual data is probable as long as data are sufficiently available in the region. However, regions lacking such actual data shall not be treated in the same way as the regions that are rich in actual records. In the development of predictive attenuation models for low seismic or seismically inactive regions where the amount of available actual data does not guarantee an accurate empirical characterization of regional seismological features, ground motion simulation techniques (stochastic and/or deterministic, e.g., Green’s function method) can be used with the aid of effective application of the seismological model. The applied seismological model, however, needs to be complete if not at least reasonably accurate representation of attenuation or seismological properties of the subject region. Synthetic ground motion data produced based on above said simulation techniques have been successfully applied in the development of regional attenuation models in seismically low/sparse regions (Atkinson and Boore, 2006; 1995; Raghukanth and Iyengar, 2007). Satisfactory results are even obtained in developing more generalized versions of attenuation models using stochastic simulations, which are possible to apply in many low and moderate seismic intraplate regions (Lam et al, 2000a; Chandler and Lam, 2004).

The knowledge of regional seismological properties, which establishes the important link between geo-tectonic features and earthquake characteristics both at the origin and during the wave propagation through the rock, is advantageous for accurate formulation of ground motions for the given region (Boore, 2003). This knowledge becomes essential and provides a prime interface for assessing seismic risk when the region is lacking actual event data to be used in the empirical modeling (Chandler et al, 2001). Identification of seismological properties in a region can also be helpful to expand research studies on other relevant areas such as source parameter estimation, tectonic stresses and seismic structure investigation, etc. Additionally, the knowledge of seismological characteristics would be important at instances such as when comparing seismotectonic features of a region with others, so that “an overall evaluation” of the region’s attenuation behavior in the global context can be ascertained. Such a comparison would partly be helpful when choosing ground motion predicting equations from other regions in the absence of an own derived model for the region, in which case the best suited model that has

been originally developed in an analogous region with similar seismological conditions, can be selected without much difficulty.

Some of published attenuation models that predict PGA on rock sites are shown in Figure 2.1. Newly published models are chosen for the comparison, in which most of them are originally developed in both interplate as well as intraplate regions using regression analysis of moderate and strong magnitude shallow crustal earthquake data recorded in those regions. Attenuation models depicted in Figure 2.1 are given in Appendix A.

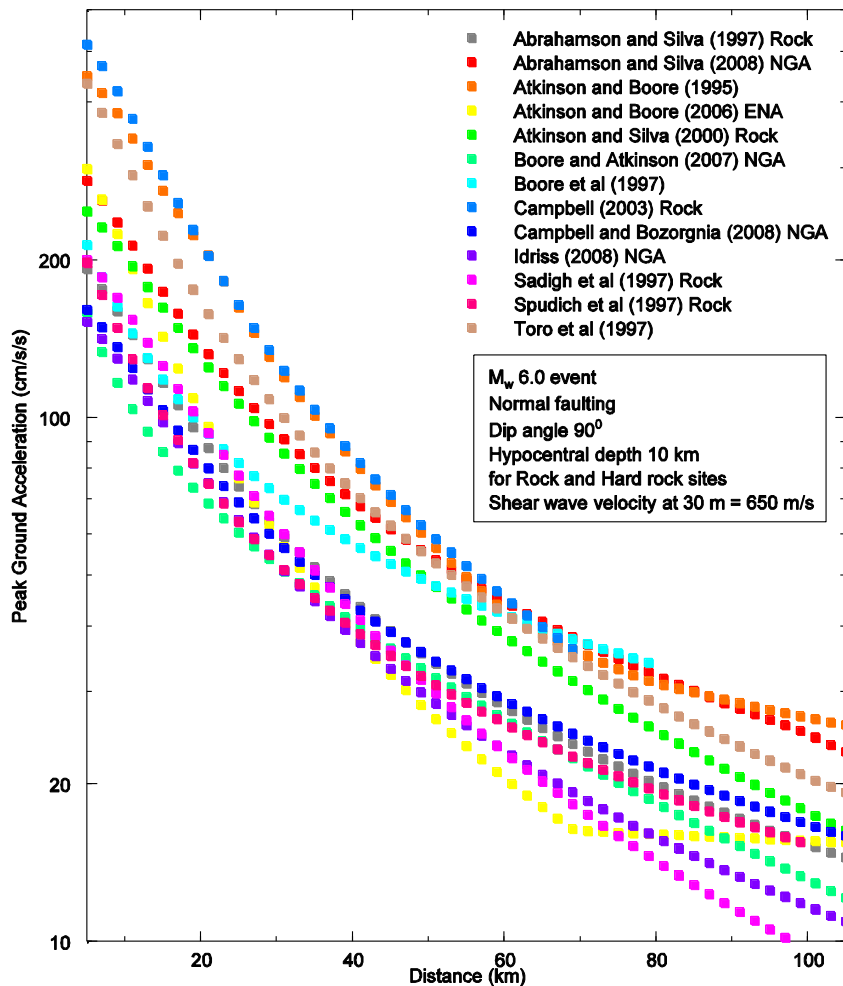


Figure 2.1 Some of published attenuation models to predict Peak Ground Acceleration (PGA) on rock sites. Newly published models are chosen for the comparison, in which most of them are originally developed based on moderate to strong magnitude shallow crustal earthquakes occurred at both interplate and intraplate regions. Predictions are for a selected M_w 6.0 shallow crustal event. Chosen attenuation modes are presented in Table A.1 in Appendix A.

2.3 Seismological characteristics

Seismological properties are generally characterized at two different stages in the process of an earthquake event; at the source where the earthquake has originated and during the wave transmission through the medium. Characteristics of seismic waves at the source (fault) are defined by the source factor, whereas modifications that the waves would undergo during the propagation through the medium are acquired as path effects (Lam et al, 2000b). Hence, the ground motion intensity at a site due to an event is a measure of the combined impact of both these source and path effects. Therefore, amplitude spectrum [$A_x(f)$] of seismic shear waves reaching rock outcrop at a site, can be denoted by a single equation that encapsulates source properties of the origin and relevant path modifications (attenuations and amplifications) during the transmission through the medium (Lam et al, 2000b);

$$A_x(f) = S(f).G.A_n(f).V_a(f).P(f) \quad (2.1)$$

$S(f)$ is the source factor that characterizes shape of the amplitude spectrum at the source, and is generally identified to be dependent of frequency f . G is the geometric attenuation factor that accounts for attenuations of waves by geometrical spreading (wave scattering). $A_n(f)$ is the anelastic whole path attenuation factor that may include both intrinsic and scattering attenuation effects, through the total path of wave travel. $A_n(f)$ also depends on wave frequency. $V_a(f)$ and $P(f)$ are the upper crustal amplification and upper crustal attenuation factors, respectively. These two modification factors are also dependent of wave frequency, and are normally accentuated at high frequencies than at low frequencies.

In equation (2.1), $S(f)$ solely represents source effects, whilst other factors typify path specific wave modification effects (attenuations and amplifications) encountering during the wave propagation. Researchers have sometimes used to segregate wave modifications at the upper crustal level [$V_a(f)$ and $P(f)$] from the rest of other “path modifications” [i.e., $A_n(f)$ and G], and have used to caption them more under site specific local effects in the studies (Atkinson and Boore, 1995, Boore, 2003). Expected net wave modification by the combined action of $V_a(f)$ and $P(f)$ is found to be typically higher than that by other path modifications for near-field earthquakes. Consequently, these upper crustal wave modifications for a given upper crust appear to be approximately remained constant irrespective to the site-source distance of the event (i.e., whether the event is a near-source or a distant event) (Lam et al, 2000b). Therefore, effects by $V_a(f)$ and $P(f)$ can be considered reasonable to be categorized as distance independent scenario in which case as “site effects”. It may be noteworthy that the spectral amplitude $A_x(f)$ (most of the times Fourier amplitude) at a given frequency in the model

[equation (2.1)] is equal to the source amplitude $[S(f)]$ at the frequency times a set of modification factors each of which represents the respective portion of wave modification. These modification factors become greater than one if they involve in wave amplification, or can be less than one for wave attenuation. Although, the net wave modification at a given frequency is simply a single value, accurate estimation of this value which is composed of the above mentioned individual modifications, can be a challenging task that may require to follow a set of proper methodologies with correct assumptions (respective methods of determining modification factors are separately discussed in the section). Spectral characteristics of seismic waves of an earthquake at the source prior to the propagation are formulated with certain ideal conditions, e.g., homogeneous medium, uniform rupture process without any intermittent slips, constant rupture velocity and finite (or sometimes infinite) rise time, unidirectional rupture propagation, etc. Sometimes these uncertainties are accounted for by introducing separate parameters to the main equation, or are compensated by using wave path modification factors already in the equation; e.g., use of a two-corner source spectrum (Atkinson and Silva, 2000) or allowing the geometrical spreading to be magnitude dependent (Silva et al, 2003).

The basic form of equation (2.1) to represent the amplitude spectrum of seismic waves is initially introduced to the field by one of the renowned seismologists Aki (1967). He has assumed the form of the autocorrelation function of slip as a function of space and time to derive an “ ω^2 model” (ω is the circular corner frequency) of the spectrum, in which he named this model as “ ω^2 model”. He has further derived a source-scaling law that the spectral amplitude at the corner frequency goes as the inverse-cube power of the corner frequency, which behaves almost as a constant-stress-drop model. Since then many fellow researchers have worked toward for further developing the model and scaling relations of amplitude spectra in strong and moderate magnitude earthquakes; valuable contributions such as by Brune (1970; 1971), Hanks (1979), Hanks and McGuire (1981), Boore (1983), Joyner (1984), Anderson and Hough (1984), Boore and Atkinson (1987), etc. are worthy of mention. McGuire and Hanks, and Hanks and McGuire, respectively, in 1980 and 1981 have successfully employed a fundamental form of the seismological model [given in equation (2.1)] with Brune’s (1970; 1971) single corner frequency source spectrum in a stochastic process to generate artificial ground motions. Boore’s (1983) study is an extended version of the original work by Hanks and McGuire’s (1981), to generalize the model into more complex forms with many ground motion measures. Joyner (1984) proposes a modified model of spectral scaling relations for large magnitude earthquakes which have relatively large rupture areas, probably running across the entire seismogenic zone, where “similarity” principles do not apply. The spectrum of the proposed scaling law in his study, is controlled by two corner frequencies each being inversely proportionate to the rupture length and rupture width, respectively. Anderson and Hough’s

(1984) findings on a frequency filter function characterized by a frequency independent parameter “Kappa” to cutoff high frequency spectral amplitudes, lay the basis for near-surface attenuation parameterization. Similar to the format as that of Aki’s (1967) model, yet with different ω variations of the amplitude models have later been proposed by some researchers (e.g., $\omega^{-1.5}$ model by Hartzell and Heaton, 1985; ω^{-1} model by Boatwright and Choy, 1992).

Equation (2.1) is a derivation of the amplitude spectrum of seismic waves at a site of crustal rock. If one may interest on deriving the spectrum at a soil site, an additional factor (site amplification factor) needs to be considered to take soil amplification effects into the account. Seismic waves experience large amplifications during travel through subsoil in which the wave amplification increases as a result of the decrease in the propagation velocity as to obey with the law of conservation of energy (Kramer, 1996). This effect can be modeled by considering an upward propagating shear wave front travelling within a horizontally layered soil column which rests on the rock half space (Schnabel et al, 1972). Determining the site amplification factor is a separate process that necessitates individual assessment of each and every site of interest based on the respective local subsoil profile (data can be obtained from borehole logs) at the site. Final amplifications by subsoil effects can be immensely varied even within the same region owing to significant variation of soil properties (soil type, thickness, composition of layers, etc.) in the region. Therefore, engineers and seismologists often consider ground motions at rock sites separately from soil sites, and combine both these motions if needed to estimate say the final ground motion level at a particular soil site. In the present study, ground motions at soil sites are not considered, and hence individual site amplification factors at local sites of the country are not estimated.

Seismological factors defined in equation (2.1) are briefly discussed in following paragraphs.

2.3.1 Source factor [$S(f)$]

First known efforts to develop a source model were given by a Japanese scientist Nakano (1923). It has then been taken around 40 years of time to develop an appropriate model based on a validated theory for widespread application; e.g., the double couple model (Maruyama, 1963; Burridge and Knopoff, 1964). Successful efforts on developing finite source models were also undertaken at the same time and were continued until the next decade or more by both Californian and Japanese seismologists (e.g., Ben Menahem, 1961; 1962; Maruyama, 1963; Burridge and Knopoff, 1964; Haskell, 1964; 1966; Brune, 1970; 1971). In the Haskell’s (1964, 1966) famous dislocation model (known as “ ω^3 model”), a uniform displacement discontinuity spreads at a constant rupture velocity inside a rectangular shaped fault. The model has shown incompatibilities at high frequencies, and can only be considered as a rough low-frequency

approximation of fault slip (Madariaga, 1978). In comparison to source models that are based on dislocation theories, models derived based on the crack theory known as “crack models”, are sometimes considered to be more precise in characterizing large earthquake sources in near-field (Madariaga, 2007); e.g., self-similar circular crack model (Kostrov, 1964), simple circular crack model (Madariaga, 1976), quasi-dynamic circular crack model (Sato and Hirasawa, 1973). One of the first notable contributions toward accurately formulating of earthquake source characteristics as a circular finite source, has been made by Brune (1970; 1971). In his landmark paper in 1970, the source spectral model is derived by relating the effective stress available to accelerate the sides of the fault. The model takes account of effects of the fractional stress drop, and describes the near- and far-field displacement time functions and spectra. In short form, the model postulates that the source spectra of an event can be simply characterized by only two independent scalar parameters; seismic moment and corner frequency. The model successfully predicts near- and far-field spectra for observed earthquake spectra and indicates that the effective stresses are generally of the order of 100 bars for moderate magnitude events. Development of the model was primarily based on the assumption that earthquake source ruptures can be approximated as circular fault sources. Other parallel hypotheses may include ω^2 variation of spectral amplitude with frequency, uniform rupture process with constant velocity, a single corner frequency which features stress drop and seismic moment of the event, uniform energy release in all directions without any intermittent slipping and/or any directivity effect, etc. Brune’s model is given in equation (2.2);

$$S(f) = \frac{CM_0}{1 + \left[\frac{f}{f_0} \right]^2} \quad (2.2)$$

Where, $C = 0.78 / (4\pi\rho\beta^3)$

C is called “scaling factor”. M_0 is the seismic moment, which is related to $\log M_0 = 1.5M_w + 10.7$ (Hanks and Kanamoori, 1979). f_0 is the corner frequency. ρ and β are the crustal density and shear wave velocity of the source region, respectively. A deduced relationship for the corner frequency is given by, $f_0 = 4.9 \times 10^6 \beta (\Delta\sigma / M_0)^{1/3}$ (Boore, 1983). Here, $\Delta\sigma$ is the static stress drop value in the event. Note that the relationship given for corner frequency f_0 is valid when β , $\Delta\sigma$ and M_0 are in km/s, bars and dyne centimeters, respectively. Generally, intraplate regions can exhibit higher static stress drops than for typical interplate regions. For instance, intraplate Eastern North America (ENA) is associated with a higher average stress drop value of the order of 15 MPa (150 bars) for moderate to large magnitude events (Atkinson, 1993a), while the value of interplate Western North America (WNA) can be

as small as about 5 MPa (50 bars) for larger events (Atkinson and Silva, 1997). Similar observations have been made by Kanamori and Anderson (1975) in a global study of earthquake source characteristics, in which they have noted that stress drops in areas of intraplate events can be about 10 MPa (100 bars) on average, while observing a lower value of about 3 MPa (30 bars) for interplate areas. Surprisingly, relatively small stress drops are also rarely noted in some intraplate regions; e.g., an average of 3 MPa (30 bars) for the intraplate region of the Central European continental crust (Malagnini et al, 2000a). The stress drop value of a region is generally found to be an independent of the earthquake magnitude, however, there are cases in which a certain increase of the stress drop with the magnitude (in smaller events) has been reported (Atkinson, 2004b). Overall, a parameter like the stress drop would be uncertain to identify always as a constant value for a given region, and hence variations can be expected even event wise due to trade-offs which may be rather difficult to be ascertained within the limits of current knowledge, i.e., fault geometry, rupture properties, tectonic setting and crustal structure, as an artifact of the modeling method followed, etc.

Brune's model has shown departing from actual source characteristics for large magnitude events for which the single corner frequency representation may be unrealistic (Atkinson and Silva, 1997). Large magnitude events have shown lower spectral amplitudes at long periods than that of small and moderate events, and thus may cause a little "sag" in the source spectrum forming two corner frequencies (Figure 2.2) in comparison to the single corner frequency Brune's model (Atkinson, 1993a). Strong events with large magnitudes are recognized to be different than to small and moderate events; rectangular rupture areas (as opposed to circular), partial stress drop, asperities and barriers, large directivity effects, etc. Therefore, for sources of large magnitude events of which the site-source distance is small (i.e., for near-field observations), the finite source double corner frequency models that take the geometry of the source and propagation of the rupture across the fault into account appears to be more appropriate (Lam et al, 2000b). More sophisticated double corner frequency source models, which are explicitly capable of modeling source spectral characteristics of large magnitude events, were introduced since 1990s (Boatwright and Choy, 1992; Atkinson, 1993a; Joyner, 1997). Boatwright and Choy's (1992) model has been derived by analyzing teleseismic records of 16 large intraplate earthquakes occurred in Canada and Australia, which are selected on the basis of tectonic setting, compressive focal mechanism and shallow focal depth as to comply with conditions in ENA. The model has sometimes evidenced on underestimating and overestimating short period amplitudes and intermediate to long period amplitudes for ENA events, respectively (Atkinson and Boore, 1998). Atkinson (1993a) has developed a two corner frequency source model to cover a range of magnitudes between 3.0 and 7.0 in Moment magnitude (M_w) scale, based on an analysis of many ENA earthquake records. Efforts are also

made to develop a similar model for interplate regions based on approximately 1000 WNA records (Atkinson and Silva, 1997). The ENA model has proven to be successfully applicable in the ground motion modeling, especially in the stochastic simulation, in low to moderate seismic intraplate regions (such as Australia, Hong Kong, Singapore, Iran) at many instances (Lam et al, 2000b; 2009; Balendra et al, 2002; Yaghmaei-Sabegh and Lam, 2010). The use of the ENA source spectrum as a “generic source spectrum” in other intraplate seismic regions outside the USA, is justified by the fact that the final wave frequency content at the rock outcrop is little affected by changes in source spectrum characteristics for a particular magnitude of earthquake. In other words, the final shape of the spectrum is mainly governed by due modifications happening during the wave travel through the medium, i.e., as attenuations and amplifications.

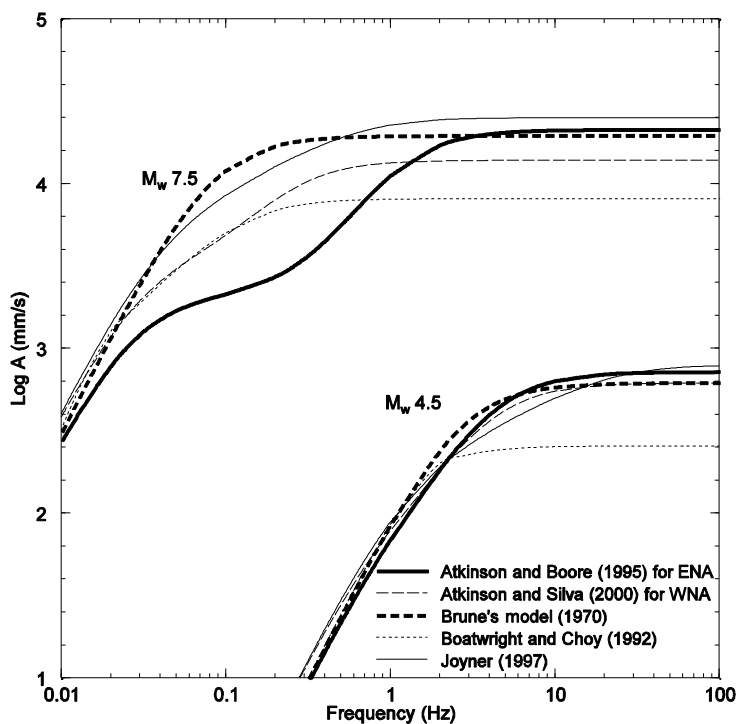


Figure 2.2 Comparison of some of widely used source spectral models available in the literature. Comparisons are in terms of acceleration amplitude of Fourier spectra (in logarithmic form) for two sample magnitudes (M_w 4.5 and 7.5). It is evident that for smaller magnitude events single corner frequency Brune’s (1970; 1971) model, is generally in a good agreement with selected double corner frequency models, however, for larger events the model clearly shows overestimating low frequency amplitudes. The reason is explained by the point source assumption of Brune’s (1970; 1971) model, which is less effective in capturing finite-fault effects in large magnitude events. Two corner frequencies for the selected large magnitude event are clearly visible in Atkinson and Boore’s (1995) and Atkinson and Silva’s (2000) source models. Boatwright and Choy’s (1992) model seems predicting relatively low amplitudes for high frequencies than that do other models. Note that, any high frequency diminution function (like “Kappa” or “ f_{max} ”) has not been applied to shape the spectra at high frequencies.

$$S(f) = CM_0 \left[\frac{1}{\left[1 + \left(\frac{f}{f_a} \right)^8 \right]^{1/8}} \right] \left[\frac{1}{\left[1 + \left(\frac{f}{f_b} \right)^8 \right]^{1/8}} \right]$$

moment, f_a and f_b are corner frequencies.
 $\log f_a = 2.3 - 0.5M$
 $\log f_b = 3.4 - 0.5M$
 M is the Magnitude in Moment magnitude scale.

2.3.2 Geometric attenuation factor (G)

The term G in equation (2.1) represents the geometrical attenuation factor which accounts for attenuations resulted by scattering effects of seismic waves (wave reflections and refractions) taking place when elastic waves travel through a layered medium. G is not usually referred to any form of attenuation happening in the intrinsic nature. The geometric attenuation is commonly identified to be a parameter that is independent of both frequency and magnitude (Atkinson and Boore, 1995; Atkinson and Mereu, 1992; Herrmann and Kijko, 1983). However, the rate of attenuation is dependent of the type of wave being dominant at the respective distance range; for example, within the near-source range [hypocentral distance (R) is less than about 70 or 60 km] where direct S (shear) waves are leading the wave front, G exhibits higher rates of attenuation such as R^{-1} and $R^{-1.3}$, yet when furthering away from the hypocenter towards the peripheral region at the far-source distance range (R is greater than about 120, 130 km), the rate of attenuation changes to a lower value of $R^{-0.5}$ due to the dominance of surface waves such as L_g formed by multiple reflections and refractions of body waves. Based on these key observations, two generic forms of G are formulated using recorded event data, which are given in below (Atkinson and Boore, 1995; Herrmann and Kijko, 1983);

$$G = R^{-1} \quad \text{for } R \leq R_x$$

$$= (RR_x)^{-0.5} \quad \text{for } R > R_x$$

Bilinear form (2.3)

$$G = R^{-1} \quad \text{for } R \leq 70 \text{ km}$$

$$= 70^{-1} \quad \text{for } 70 \text{ km} < R \leq 130 \text{ km}$$

$$= 70^{-1} \left(\frac{130}{R} \right)^{0.5} \quad \text{for } R > 130 \text{ km}$$

Trilinear form (2.4)

R_x in equation (2.3) denotes a reference distance that parts the near-source and far-source attenuations in respective to the dominant wave type in the case as explained above to form a bilinear variation in G , and is estimated to be around 100 km for a continental crust of typical thickness about 40-50 km (Herrmann and Kijko, 1983). Equation (2.4) also follows the same form as which in equation (2.3), but additionally includes a separate attenuation rate for

“medium” distance range (R between about 70 and 130 km). This newly introduced rate of attenuation at the medium distance range is given as a constant (that implies, there is “no attenuation” within the medium distance range), which is explained by the phenomenon that compensatory actions resulted by post-critical reflections of seismic waves happening at Moho and Conrad discontinuities in the crust. Two reference distances (70 and 130 km) in comparison to one (R_x) in equation (2.3), can also be observed in equation (2.4). Note that, the form of relationship tagged as “linear” (bilinear and trilinear) in each of the equations, means that the variation of G with respect to R compares in the logarithmic scale, and not in the linear scale. Indicated attenuation rates by the above relationships could be subject to vary depending on seismo-geological features in the region; e.g., much higher near-source geometric attenuation rate of $R^{-1.3}$ (instead of R^{-1}) for southeastern Canada and northeastern United States (Atkinson, 2004b; Sonley, 2004), a higher far-source attenuation of $R^{-1.6}$ for Australia (Allen et al, 2007) and even negative attenuation of about $R^{+0.2}$ (in real sense an amplification) in the medium distance range for southeastern Canada (Atkinson, 2004b), etc. The rate of geometric attenuation not only depends on the region, but it can also be dependent of the frequency of wave considered [e.g., frequency dependent attenuation rates for crustal, in-slab and offshore events in southwestern British Columbia and northwestern Washington (Atkinson, 2005)] and of the magnitude of the event (Campbell and Bozorgnia, 2012). The reference distances have shown as varying with the average thickness of the crust in accordance with the norm that higher the crustal thickness higher the reference distances and vice versa (Lam et al, 2000a; Herrmann and Kijko, 1983). Therefore, for a region of a higher average crustal thickness, the norm suggests higher geometric attenuations to be expected during the wave propagation through the crust, whilst for a much thinner form of crust such as the ones beneath the oceans are susceptible for lesser geometric attenuations. Lam et al (2000a; 2000b; 2006; 2009) have strongly followed this norm for simulating strong ground motions by applying the stochastic approach. In the trilinear shape, they use $1.5D$ and $2.5D$, respectively, as the first (70 km) and second (130 km) reference distances, where D represents the average crustal thickness (in kilometers) in the region. This adaptation in G has successfully been validated for different intraplate crustal regions (Australia, Iran, Hong Kong, Singapore) with the use of real records. Notwithstanding, the researchers who rely more on empirical modeling methods, still prefer to investigate the actual shape of G based on regression analysis of actual waveform data in the region of interest.

The geometric attenuation can be a prevalent case than other modes of attenuation (such as the anelastic and upper crustal attenuations) in “local events” (events at smaller hypocentral distances) occurred in the regions of hard rock crustal conditions. G would also govern “the amplitude level” of the spectrum of teleseismic events occurred at thousands of kilometers away

from the site (evidence supports in the present study), in case where the anelastic attenuation has not been a dominant. Variation of the geometric attenuation factor with the hypocentral distance for above discussed models are indicated in Figure 2.3.

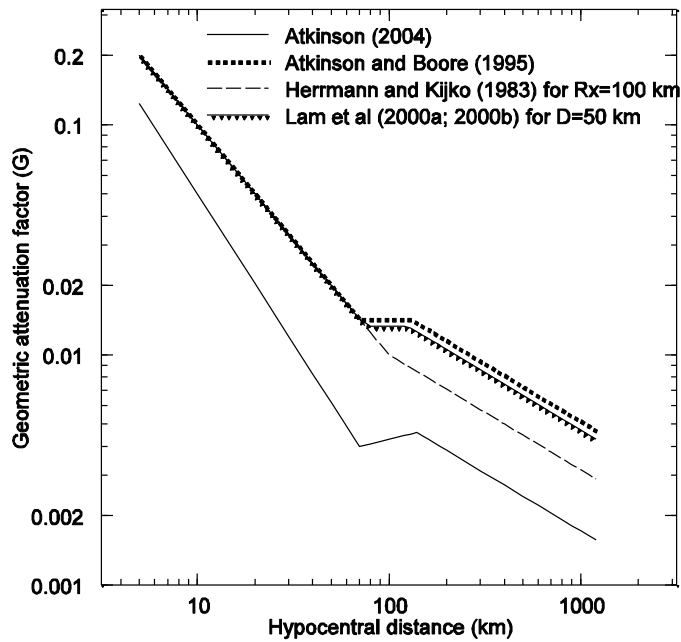


Figure 2.3 Variation of the geometric attenuation factor (G) with hypocentral distance. Both of the frequency independent trilinear (Atkinson, 2004b; Atkinson and Boore, 1995, Lam et al, 2000a; 2000b) and bilinear (Herrmann and Kijko, 1983) forms are considered in the comparison. Proposed models by Herrmann and Kijko (1983) and Lam et al (2000a; 2000b) are for a typical crust of about 50 km thickness, so that the comparison with models by Atkinson (2004b), and Atkinson and Boore (1995), which are empirically derived for the ENA crust (which also has an average thickness of around 50 km), is credible. Atkinson (2004b) model exhibits higher geometrical attenuations than the others due to rapid near-source attenuations. The other three models coincide each other, except Herrmann and Kijko's (1983) bilinear model which deviates towards higher attenuations at far-source distances.

2.3.3 Anelastic whole path attenuation factor [$A_n(f)$]

The anelastic attenuation is described as a wave path effect that explicitly incorporates attenuations of intrinsic nature such as which due to energy dissipation happening along the wave travel path. This energy dissipation may include heating of the heterogeneous medium as a result of frictional forces applied between particles, dislocation or rearrangement of the medium's particles during the vibration, elastic energy transformation into the sound and any other energy losses that are not counted in G . Unlike the geometric attenuation, the anelastic attenuation is identified as significantly depending on the wave frequency, and this frequency

dependence is commonly expressed by an exponential variation (the basic form was introduced by Aki and Chouet, 1975);

$$A_n(f) = \exp(-\pi fR / Q\beta) \quad [\text{Here, } Q = Q_0 f^n \text{ (Mitchell, 1981)}] \quad (2.5)$$

where, f is the wave frequency, R is the length of the wave travel path (approximately taken as the hypocentral distance), β is the shear wave velocity around the source region, Q is the wave transmission quality factor and n is called the exponent. One may note that, the amount of attenuation is not only a factor of the wave frequency, but it also a reliant of the hypocentral distance, the wave transmission quality factor and the shear wave velocity of the source. For a selected event of a region, it is evident from the equation that high frequency waves diminish more rapidly than that do low frequency waves, and the reason for this is sometimes explained by taking the analogy with an ideal situation that is frequency dependent amplitude decaying nature of the wave motion in an elastic medium due to viscous damping (Lam et al, 2000b) in which the rate of decay also gradually increases with the number of wave cycles in a unit length (frequency). Importantly, the regional wave transmission quality factor parameterized by Q_0 (equals to Q at 1 Hz frequency), can be critically influential on the amount of attenuation undergone during wave transmission. The quality factor Q (or Q_0) of a region is a kind of “seismological measure” that assesses the quality of the regional crust in terms of being how good at transmitting waves through the medium (this “quality” may infer some physical properties of the crust such as hardness, density, cavity content, amount of fractures, etc.). The wave propagation would possess improved characteristics (with lesser attenuations) in a medium of higher Q values than in a medium of smaller Q values. Density, hardness and other physical features of a regional crust generally increase with the age of the medium, and thus, older crustal forms would be associated with higher Q values than much younger crustal structures. For instance, ENA crustal rocks that belonged to the Precambrian era are associated with higher Q_0 values such as 680 (Atkinson and Mereu, 1992) and 893 (Atkinson, 2004b), whereas younger Californian bedrocks are associated with a lower Q_0 value of about 204 (Atkinson and Silva, 1997). Another clear example can be found in the continental crust in Australia, in which much older southwestern and western Australia has exhibited a higher $Q_0=457$ (Allen et al, 2006) than that of the state of Victoria located in younger southeastern Australia, which is about 100 (Wilkie and Gibson, 1995).

The relationship between Q and f can be either linear (in the logarithmic scale) as introduced by Mitchell (1981) or sometimes can be a polynomial form of several degrees. With the increasing use of advanced regression techniques in spectral analysis, researchers tend to examine the complete shape of regional Q values in the frequency domain. One of common observations in most of these regression analyses, is higher Q values resulted even at lower frequencies ($f < 1.0$

Hz), which in turn produces an overall “U-shape” variation (due to higher Q values on either side of Q_0) of Q in the frequency domain for the region (e.g., Atkinson, 2004b; Allen et al, 2006; Motazedian, 2006).

Region-specific Q_0 and n are determined using recorded instrumental data by means of standard methods such as the coda Q method, the Multiple Lapse Time Window Analysis (MLTWA) method, the spectral analysis method, etc. The coda Q method which is widely being referred to its technical name “the single backscattering method”, proposed by Aki (1969) and Aki and Chouet (1975), is based on the exponential variation of Root-Mean-Square (RMS) values of amplitudes of coda waves – the waves which are recorded at the tail part of a seismogram. In the method, both scattering effects due to the heterogeneity and intrinsic attenuations due to the anelasticity can be accounted for in the derivation of Q . However, the effect of scattering on the decay rate would depend on the amount of scattering taking place within the medium; when the scattering is weak the decay rate depends on both of the attenuation modes (intrinsic and scattering), while when it is strong (as in a defuse medium) the rate would depend only on the intrinsic attenuation (Wu and Aki, 1988). Some studies have shown that the results of the coda Q method can be significantly dependent of the lapse time which is related to the size of the volume sampled during wave propagation in the crust (Pulli, 1984; Gusev, 1995). Considering a possible variation of Q_0 with distance, Mak et al (2004) have proposed to interpret Q_0 by distance dependent contours as opposing to sticking to a constant Q_0 value for a given region. The MLTWA method (Zeng et al, 1991) adapts the stationary energy transport theory, by assuming random isotropic scattering effects and non-collocated source-receiver conditions. The method is advantageous in the sense which taking all possible multiple scattering contributions into the consideration. The spectral analysis methods by using regression analysis have become popular in the seismology and earthquake engineering field because of more accurate estimation of attenuation characteristics than by other methods for a given region (Atkinson and Mereu, 1992). Because of most of the spectral analysis methods use the strong motion part of a seismogram, the attenuation parameters obtained through the analysis would reflect actual strong motion characteristics in the region. However, one must be careful to apply an appropriate attenuation relationship (regression equation) that encompasses all possible means of attenuation likely to undergo in the subject region. Comparison of the anelastic whole path attenuation factors for three geologically different regions (ENA hard rock, WNA rock and younger rock forms in Victoria in Australia) is shown in Figure 2.4. Comparisons are given in both of the frequency and hypocentral distance domains. Some of published Q_0 and n (in $Q = Q_0 f^n$), and Kappa values (discussed in section 2.3.5) for various regions are given in Table 2.2.

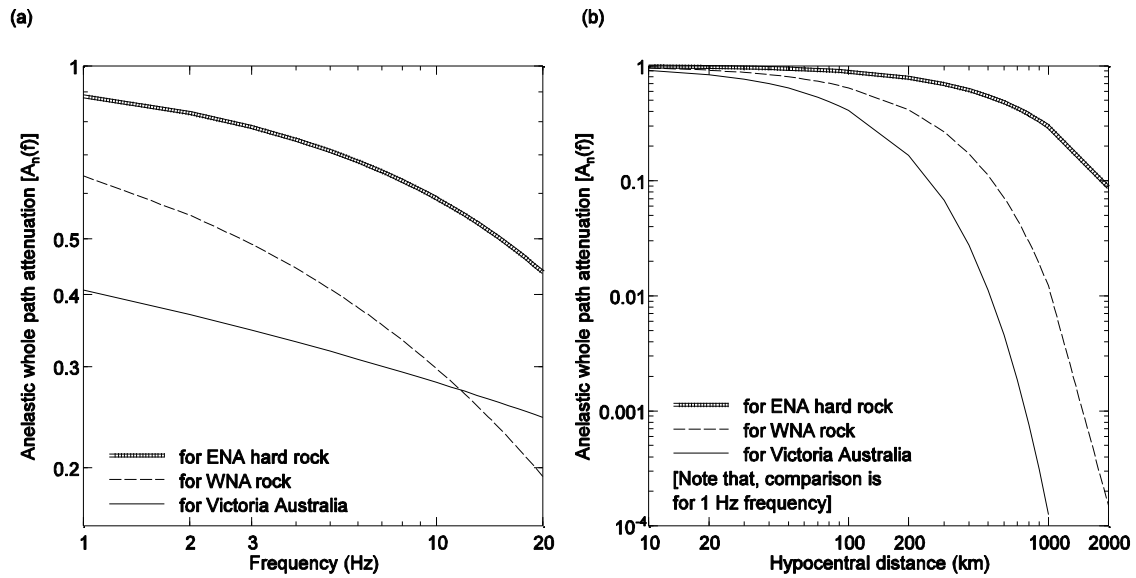


Figure 2.4 Comparison of anelastic whole path attenuations $[A_n(f)]$ for selected three regions; ENA hard rock [$Q=893f^{0.32}$ (Atkinson, 2004b)], WNA rock [$Q=204f^{0.56}$ (Atkinson and Silva, 1997)] and Victoria in Australia [$Q=100f^{0.85}$ (Wilkie and Gibson, 1995)]. (a) Comparison of the frequency domain. (b) Comparison of the hypocentral distance domain. Note that, the variation in the hypocentral distance domain is considered only for a sample (1 Hz) wave frequency. Figures indicate that $A_n(f)$ is dominant at high frequencies for distant events. It is also evident that $A_n(f)$ varies with “the quality” of the regional crust in a manner which higher attenuations being associated with low quality younger crusts, with lower attenuations in high quality older crustal formations.

Table 2.2 Some of published Q_0 and n (in $Q=Q_0f^n$), and Kappa values for various regions

| Region | Q_0 | n | κ (Kappa) |
|---------------------|-------|---------------------------------|--|
| California | 204 | 0.56 (Atkinson and Silva, 1997) | 0.035-0.050 s for M_w 5.5-7.5, respectively (Atkinson and Silva, 1997) |
| Southeastern Canada | 680 | 0.36 (Atkinson and Mereu, 1992) | |
| Scandinavia | 438 | 0.71 (Kvamme et al, 1995) | |
| Victoria, Australia | 100 | 0.85 (Wilkie and Gibson, 1995) | |
| New Brunswick | 500 | 0.65 (Shin and Herrmann, 1987) | |
| Northeastern Italy | 480 | 0.43 (Woodgold, 1990) | |
| Northeastern Italy | 260 | 0.55 (Malagnini et al, 2002) | 0.045 s (Malagnini et al, 2002) |
| Central Europe | 400 | 0.42 (Malagnini et al, 2000a) | 0.05 s (Malagnini et al, 2000a) |
| British Columbia | | | 0.011±0.002 s (Atkinson, 1996) |
| Apennines, Italy | 130 | 0.10 (Malagnini et al, 2000b) | 0.04 s (Malagnini et al, 2000b) |
| Northern Iran | 87 | 1.46 (Motazedian, 2006) | 0.03 and 0.05 s for vertical |

| | | | | |
|--|-----|------------------------------------|--|---|
| Southeastern Canada and northeastern United States | 893 | 0.32 (Atkinson, 2004b) | and horizontal components, respectively (Motazedian, 2006) | |
| New England | 460 | 0.40 (Pulli, 1984) | | |
| Washington | 63 | 0.97 (Havskov et al, 1989) | | |
| Indian shield | 800 | 0.42 (Singh et al, 2004) | | |
| Southwestern western Australia | 457 | 0.37 (Allen et al, 2006) | | |
| Northeastern India (Indo-Burma tectonic domain) | 431 | 0.70 (Raghukanth and Somala, 2009) | | Overall Kappa for the whole region; 0.013 and 0.033 for vertical and horizontal components in soft rocks, respectively |
| Northeastern India (Bengal basin-Shillong plateau) | 224 | 0.93 (Raghukanth and Somala, 2009) | | |
| Hong Kong | 256 | 0.70 (Mak et al, 2004) | | 0.025 and 0.041 for vertical and horizontal components in firm grounds, respectively ((Raghukanth and Somala, 2009) |
| Guangdong, China | 482 | 0.31 (Wong et al, 2002) | | |

2.3.4 Upper crustal amplification factor [$V_a(f)$]

Amplification of seismic waves in rocks has never been an interested topic among scholars in the field up until 80s, and it has been about a decade since its well-known applications in the soil by Schnabel et al (1972). The amplification in rock was first introduced to the ground motion simulation by Boore (1986) in his seismological model that is used in the stochastic method. The theory which the computational procedure of rock amplification was based on in his paper, was the same as that applied in the theory of soil amplification, which is the law of conservation of energy. In the theory, upward propagating shear waves are subject to amplifications as to compensate loss of energy taken place as a result of reduction of the propagating velocity. The propagation velocity at the point of origin (source), which can globally vary between about 2.5 and 4.0 km/s for S waves of Crystalline rocks (CRUST2.0), continuously depletes by due attenuation effects while during the wave propagation in the rock. Since intrinsic attenuation effects (such as the anelastic attenuation) are generally more intense at the upper crustal level than at the mid and deeper levels of the crust owing to poor quality of the upper crustal rock, corresponding amplifications can also be more enhanced at the upper crustal level than at the other levels beneath. The evolution of a typical crust makes denser and older materials to be always stacked at the deeper levels of the crust and the sedimentation of newer and lighter forms (which ultimately can result to originate younger sedimentary rocks) to

be taken place at the upper level. Therefore, the upper crustal level of a typical crust of rock and even hard rock can be easily impaired by poorer physical characteristics than in a mid or deeper parts of the crust. Thus, reduction of the propagation velocity at the upper crustal level (can be even less than 1.0 km/s for S waves, CRUST2.0) can be significant.

Boore and Joyner (1997) have successfully applied a methodology which is initially proposed by Joyner et al (1981), called “the quarter wavelength approximation method” for determining upper crustal amplifications in WNA regions where younger upper crustal forms are in abundance. In the method, the shear wave velocity travel times along the depth of the upper crust are averaged over one quarter wavelengths of shear waves to obtain the expected amplification of the wave and the corresponding frequency (or period). The expected amplification $V_a(f)$ at the frequency f is defined by the following equation (Boore and Joyner, 1997);

$$V_a(f) = \sqrt{\rho_s \beta_s / \rho_z \beta_z} \quad (2.6)$$

Here, ρ and β are the crustal density and shear wave velocity, respectively. Subscript “s” is to denote the parameters are relevant to the source region, and “z” indicates the values are averaged at the corresponding depth z , so that the amplification is always expressed as a relative measure of the properties at the source. A reliable estimation of the regional shear wave velocity profile is a prerequisite for accurate modeling of the upper crustal amplification in a region. Real-time measurements of wave travel-time data in borehole records provide essential information to derive an accurate shear wave velocity profile. However, such instrumental measurements may be unavailable in regions where sufficient resources on earthquake and seismological research activities are limited. Particularly, regions of low to moderate seismicity (or seismically stable regions) would be less keen on carrying out such experimental works. Chandler et al (2005) have developed power law relationships as a complementary solution to this absence of empirical data for deriving the regional shear wave velocity profile in such regions. They use “Geology Based Velocity Model (GBVM)”, initially proposed by Faust (1951) and further developed by Magistrale et al (1996), to form a tri-linear P wave velocity model with the aid of CRUST2.0 (The University of California, 2001) information, which is then applied to derive respective S wave velocities by using Poisson’s ratio values to develop the complete shear wave velocity profile of the region.

The upper crustal amplification is sometimes approximated as a crude value of “H/V ratio” defined by the amplitude ratio between the horizontal and vertical components (Lermo and Chavez-Garcia, 1993; Nakamura, 1989; Atkinson and Cassidy, 2000; Siddiqqi and Atkinson, 2002). While the horizontal component is continuously subject to the amplification due to the

above discussed energy loss happening during the propagation from a high impedance medium to a low impedance medium, the vertical component almost remains the same as that at the source as a result of counteraction of wave refractions directing toward the vertical direction (Atkinson, 2004b). Hence, the H/V ratio (generally calculated as the ratio of the geometric mean of the two horizontal components to the vertical component) is a useful approximation to represent the site amplification expected at rock sites in regions those have no shear wave velocity information.

The upper crustal amplification as evidenced from the equation, is a frequency dependent parameter and the amplification has shown increasing with the wave frequency. For WNA Californian rocks, the upper crustal amplification has given to be between around 1 and 4 for the frequency range 0.1-60 Hz, whereas for ENA hard rock conditions the value has indicated close to almost unity implying a negligible upper crustal amplification (Boore and Joyner, 1997).

2.3.5 Upper crustal attenuation factor [$P(f)$]

Depletion of the wave amplitude due to above explained low quality bedrock conditions at the upper crustal level is parameterized by the upper crustal attenuation factor. The mode of attenuation is identified to be virtually similar to that of the anelastic attenuation (i.e., in the form of intrinsic attenuation), however the distance dependency as in $A_n(f)$, is neglected in $P(f)$. Unlike in the whole path attenuation, attenuation effects considered in $P(f)$ take place in a relatively small portion of the crust, i.e., in the uppermost part of the crust (mostly, the topmost part within of 3-4 km depth). Therefore, any distance dependency within such a small area would be of not that practical importance to include as a separate parameter in $P(f)$. Moreover, comparing with other attenuation types (such as geometric, anelastic whole path and upper crustal) for a typical shallow crustal earthquake occurred at the local distance range, yields that attenuation effects at the upper crustal level are significantly dominant that they appear to be more like independent of the distance (Lam et al, 2000b). Studies have found regions having younger upper crustal formations can pose up to about 90% of the total anelastic attenuation just within the topmost 3 km (Abercrombie, 1997). The equation for parameterizing upper crustal attenuation effects, is also in the exponential form as similar to the anelastic attenuation factor (Anderson and Hough, 1984);

$$P(f) = \exp(-\pi f \kappa) \quad (2.7)$$

Here, κ (Kappa) is termed as the near-surface attenuation parameter in the given region, which is determined by analyzing recorded waveforms in the region. The exponential decay of the

wave amplitude, given in equation (2.7), shows increasing with the wave frequency, which may result in a rapid amplitude cutoff (roll-off) of high frequency wave amplitudes. Many researchers, who pursue studies in the streams such as ground motion simulations, utilize this effect of “high frequency roll-off” for scaling the synthetic seismogram by cutting-off additional high frequency amplitudes (Atkinson and Boore, 1995; Boore, 1983, Lam et al, 2000b). However, a correct κ value that parameterizes actual near-surface attenuations in the region, is a pre-requirement for such simulations. While some studies point out this high frequency wave diminution is merely as a source effect (Papageorgiou and Aki, 1983), others tend to attribute more as a site specific attenuation effect taking place at the near-surface level (Anderson and Hough, 1984; Hanks, 1982). In the practice, κ estimation requires to follow the spectral analysis methods of recorded waveform data in the region where κ to be estimated. Slope of an attenuation corrected Fourier amplitude spectrum (either acceleration or displacement), can be used to determine the corresponding κ for that record. The slope is only measured in the less steep part (margined by the corner frequency) of a typical bilinear shaped spectrum. κ generally takes values greater than zero, and associates with lesser values for harder and older upper crusts, e.g., for ENA crusts about 0.005 s (Atkinson and Boore, 2006). On the other hand, κ is noted giving higher values for softer and younger sedimentary upper crusts, e.g., for WNA crusts 0.04-0.07 s (Atkinson and Silva, 1997). In WNA regions, a little magnitude dependency of κ , varying from about 0.05 s for M_w 5.5 to about 0.07 s for M_w 7.5 has also been observed (Atkinson and Silva, 1997).

A comparison of upper crustal effects (amplification, attenuation and combined effects) for ENA and WNA regions is demonstrated in Figure 2.5. WNA has more pronounced upper crustal modifications than ENA regions which consists much older and harder forms at the upper crustal level. Shear wave velocity profiles at the upper crustal level in each region are also shown. It is clear by the shear wave velocity profiles (Figure 2.5c) that ENA is characterized by much quality upper crustal forms than of WNA, as it shows higher velocities with a much steeper gradient for ENA than for WNA regions.

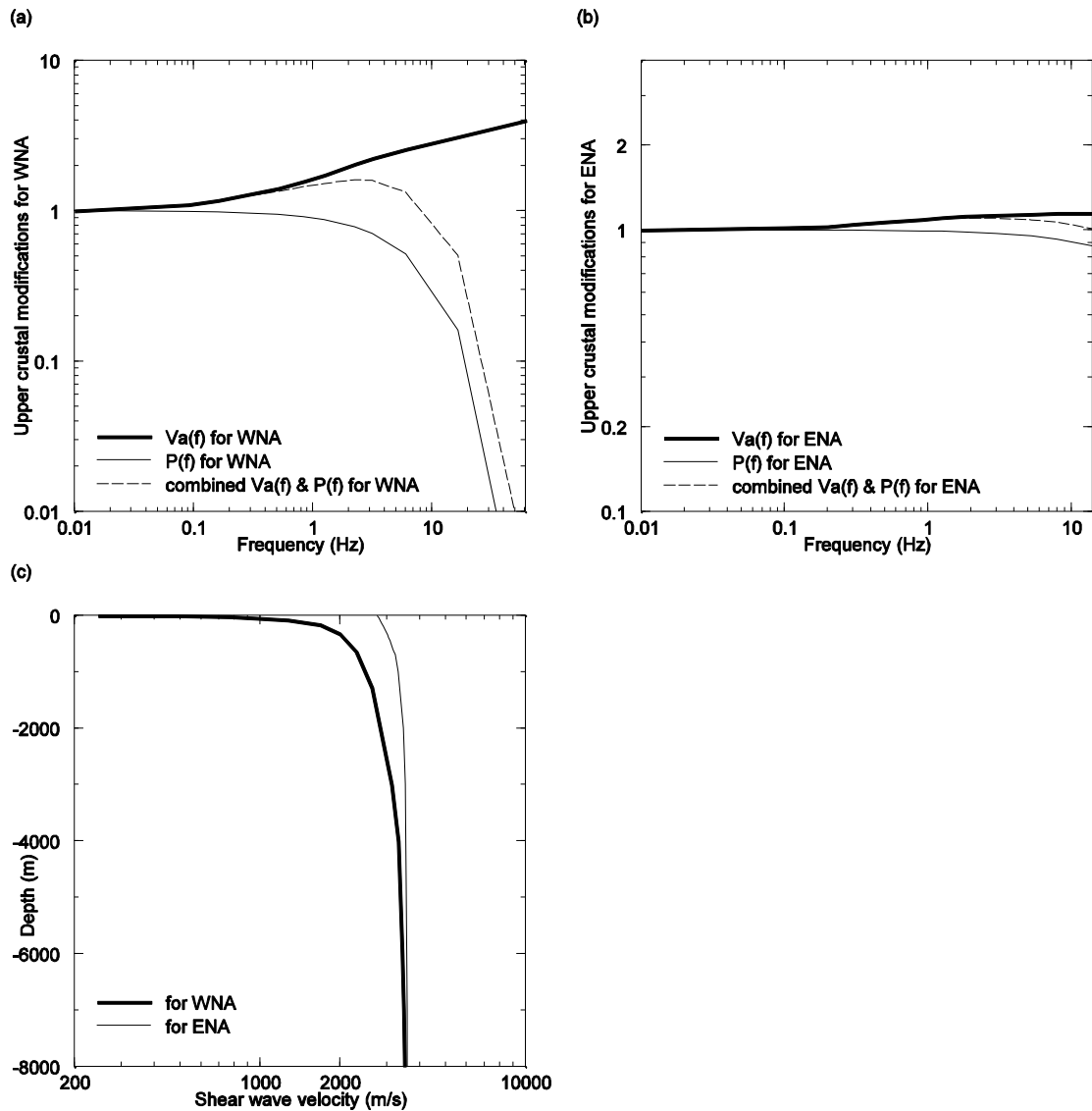


Figure 2.5 Comparison of upper crustal effects [amplification - $V_a(f)$, attenuation - $P(f)$ and combined effects] for ENA and WNA regions. Figures 5a and 5b, respectively, indicate comparably higher upper crustal modifications for WNA regions and negligible upper crustal effects (close to unity) for ENA regions. The reason as described in the text is low quality younger sedimentary formations in WNA upper crustal rocks in comparison to much harder and older formations inherited in the ENA upper crust. This is evidenced by the shear wave velocity profiles in two regions (Figure 5c), in which WNA is associated with “a slower upper crust” (low propagation velocities), while the upper crust in ENA poses higher velocities even at the surface/outcropping level. Figures are produced based on information provided in Boore and Joyner (1997).

2.3.6 Response of subsoil

Seismic waves travelling in the subsoil, which is directly lying on the bedrock, can be subject to extensive amplifications as a result of decreasing the propagation velocity due to poor wave propagation characteristics of the medium (i.e., in accordance with the law of conservation of

energy, as explained in section 2.3.4). This effect is mostly modeled considering an upward propagating shear wave front starting from the top of the bedrock underlain using a method called “one dimensional equivalent linear method” given that the soil structure is essentially horizontal (infinitely) and each soil layer is assumed to be homogenous and isotropic (Schnabel et al, 1972). The program SHAKE, originally developed by Schnabel et al (1972), later upgraded into SHAKE91 by Idriss and Sun (1992), has the virtue of modeling soil amplification effects based on the above method essentially considering soil non-linear properties. SHAKE91 has been the most widely used program among earthquake engineers to compute seismic response for horizontally layered soil strata, and has proven to be accurate as much as other advanced methods such as two-dimensional (Hudson et al, 1994) and Finite Element methods (Krahn, 2004). In the seismic micro-zonation studies, in which sites are individually categorized in accordance with available subsoil characteristics, the equivalent linear method along with SHAKE91 play a vital role in determining site specific “site amplification factor” which is defined as the ratio of the maximum spectral ordinate of soil to the corresponding spectral ordinate of the rock. This site amplification factor has been one of the major concerns to adopt in the site classification specified in worldwide seismic codes of practice (IBC 2006 and AS1170.4, 2007).

2.4 Simulation of earthquakes

Simulation of ground motions for application in the seismic hazard studies has become a versatile technique, particularly, for regions with a limited number of recorded data to be used in the empirical modeling. Matching simulated ground motions with actual recorded data in both time and frequency domains, is one of the accepted ways of validating the procedure followed in the simulation (Lam et al, 2009). Application of attenuation parameters (those described in section 2.3) appropriately determined for the region of interest, in a theoretical background which qualifies in modeling the vibration theory for simulation of motions in that region, is the key norm that needs to be followed in any simulation process. Two such simulation processes widely being used in the practice, are deterministic and stochastic procedures.

2.4.1 Deterministic procedures

Most of deterministic procedures involve in the process of earthquake generation and wave propagation primarily on subjective basis. Source and path characteristics of an identified seismogenic element (i.e., active fault, lineament, subduction zone, etc.) are separately and independently evaluated in detail, until that an accurate modeling of earthquake ground motion from that seismogenic element becomes possible. In the terminology, sometimes these modeling

approaches are called as “geophysical modeling” in which the name (by meaning) implies that the procedures following in the modeling approach involve deep investigations of seismo and geophysical features in the specific area of interest. Thus, most of the times, deterministic modeling procedures offer “site-specific simulations” than allowing to perform any generic application of the model in different areas such as done by the stochastic approach.

Kinematic modeling, one of geophysical modeling approaches, considers the dislocation time history along the causative fault’s surface (which should be known at the outset) for deriving ground motions at the target site. The earliest kinematic models such as of Aki (1968) and Haskell (1969), consider a simple and uniform dislocation traveling at a constant rupture velocity on a rectangular fault in an infinite and homogeneous medium. The model by Aki (1968), which is based on the point shear dislocation theory, characterizes source effects by both the seismic moment and an assumed fault-slip function, and path effects by applying wave theory in a homogeneous medium. The model, however, is incapable of modeling random irregularities in the rupture process, and does not account for all possible path effects in the wave scattering associated with an actual heterogeneous medium. Deterministic models based on the empirical Green’s function, are subject to the serious attention by many scholars due to the model’s excellent ability of modeling strong motions of actual large magnitude events (Irikura, 1983; 1986; Irikura and Kamae, 1994; Beresnev and Atkinson, 1997). In the method, the relevant empirical Green's function derived using a smaller event to define the wave propagation in an elastic medium due to a small impulse, is superimposed with short time lags to generate accelerograms of much larger events based on the available scaling laws. In the Irikura’s (1986) paper, he has given attempts to model large earthquakes using the aftershocks of them dividing the mainshock’s fault plane into sub-fault planes as to satisfy with the scaling law of the source spectrum. Here, size of the mainshock’s fault plane and that of an aftershock’s sub-fault plane correspond to the rupture areas of the main event and a smaller event, respectively. Irikura et al (1997) use a modified exponential slip function in order to match the frequency content of a smaller event with that of the target larger event by enhancing low frequency energy in the simulation. It was Hartzell (1978), who first proposed the use of smaller earthquake records in a way that they are summed with short time lags to produce rupture propagations of much larger earthquakes. The method is advantageous in senses of modeling large magnitude events with finite source effects and simplicity, but its potential can be sometimes limited by the fact that representative real seismic events and hence the suitable empirical Green's functions are not always available (Lam et al, 2000b). Another derivative approach of the Green’s function method, which is also in the kinematic modeling stream, is “the ray-theory method”. In the method, ground motions are synthesized by convolving an empirical source function derived based on a past event, with the use of theoretical Green’s

function for a specific crustal model (Atkinson and Somerville, 1994). In here, the estimated Green's function is utilized for describing effects of wave propagation from the source to the site, which depend on the regional crustal structure and focal depth of the event. Hence, the ray theory method based on the Green's function modeling approach, is capable of synthesizing reliable ground motion estimations for a well-studied crustal structure in which the fault layout and crustal properties are exactly known in detail, but may be difficult to apply for low to moderate seismic intraplate regions where much of such information is unavailable. One of the deterministic methods naming "the composite source model" (Zeng et al, 1994) uses synthetic Green's functions convolved with the composite source time functions, in which the source is modeled as a superposition of circular sub-events having a constant stress drop. However, the model requires accurate information on the crustal structure underneath, in terms of wave propagation velocity, Q and stress drop.

In essence, aforementioned deterministic based simulation methods would be quite suitable for modeling ground motions in "well-identified" regions where necessary information on seismotectonic properties (e.g., faults/sources and source characteristics, crustal thickness, crustal quality – Q , shear wave velocity information, etc.) are adequately available. Therefore, these approaches may not that befit for direct and generic application in seismic hazard studies in other regions (particularly, in stable intraplate regions) where such information is lacking. However, "hybrid models" combining both deterministic and stochastic procedures at low and high frequencies, respectively, have shown to be more successful than the application of each method alone (Graves and Pitarka, 2004; Frankel, 2009).

2.4.2 Stochastic procedures

Ground motion simulation based on stochastic procedures has established a new yet a firm working platform for both engineers and seismologists towards working on seismic hazard assessment studies in many parts of the world. In particular, regions of low to moderate seismic activities like "stable continentals" with mild intraplate seismicity, are much benefitted by stochastic based ground motion modeling methods for characterizing the expected hazard level. Application of the stochastic method in simulating synthetic accelerograms is first tested in early 1980s by Hanks (1979). He along with McGuire in their corporative works (McGuire and Hanks, 1980; Hanks and McGuire, 1981) develop a simple relationship to predict peak acceleration of an earthquake, with the assumptions that the far-field accelerations on an elastic half space are band-limited, finite-duration and can be represented by white Gaussian noise. They have applied Brune's (1970; 1971) source spectral model with a single corner frequency, and have used Parseval's theorem to predict the RMS acceleration by the integral of the squared acceleration spectrum. They (in their 1981 paper) equip a simple windowing function, in which

the effective duration of the earthquake is directly given by the inverse of the corner frequency defined by Brune's source model. The methodology has been successfully validated for about 16 different events in their papers. Boore (1983) extends this work towards producing simulations of time series, peak ground velocities (along with Wood-Anderson response) and elastic response spectra even in arbitrary complex cases. The method described in the Boore's paper (1983) can be summarized along these lines; first, the band-limited white Gaussian noise is generated; second, a windowing function, which is derived by Saragoni and Hart (1973) based on a number of recorded motions, is applied to shape into a real accelerogram; third, the windowed noise is transformed into a Fourier amplitude spectrum in the frequency domain, which is then normalized by the square-root of the mean square amplitude spectrum; next, the normalized amplitude spectrum is multiplied by the target amplitude spectrum defined by the seismological model [given in equation (2.1)] to characterize the frequency content; finally, the resulted amplitude spectrum is transformed back into the time domain as a time history. Safak and Boore (1988) show that the windowing is always preceded before the filtering done by using the seismological model, otherwise, some long period level of the motion can be distorted. Lam et al (2000b) have used a functional form developed in the Shinozuka-Sato form (Vanmarcke, 1977) for use in the windowing of white noise. They further use a set of random phase angles (to account for different phase arrivals) for simulating many time histories at a time, yet whose ensemble average is set to be closely matched with the target spectrum.

The most important part of any stochastic simulation procedure is the seismological model that characterizes region-specific source and attenuation features, to specify the frequency content of the target time history. Higher the accuracy in estimated seismological parameters (seismological parameters are discussed in section 2.3), higher the precision in fit between the simulations and actual records. Some of early models developed for the stochastic simulation (e.g., Hanks and McGuire, 1981; Boore, 1983) have indicated that the resulted simulations are more consistent with small and moderate magnitude events than with actual larger events. The inconsistency with larger events has mainly resulted because of the use of point source models such as that by Brune (1970; 1971), which are not yet good enough in modeling finite-fault effects (e.g., heterogeneity in the process of slip, directivity effects, large fault and rupture areas, etc.) in actual large events. It is an established way to model such finite-fault effects as a sum of all contributions coming from sub-faults created by dividing the fault into small zones as commonly do in the empirical Green's function method (Hartzell, 1978; Irikura, 1986; Beresnev and Atkinson, 1998). When modeling finite-faults in the stochastic simulation, these sub-faults are treated as small point sources, therefore, the ground motion contribution from each of the sub-faults can be modeled by employing a point source spectrum in the stochastic process. Then, these contributions are summed at the observation point, with a proper time delay, to

obtain the ground motion from the entire fault. Boore (2009) has incorporated finite-fault effects in the stochastic simulation, and has shown that the Fourier and response spectra for point source and finite-fault models are similar to one another even for an earthquake as large as about M_w 7.0. There are some critics on the dependence of final ground motions over the sub-fault size chosen in the finite-fault simulation (Beresnev and Atkinson, 2002). Motazedian and Atkinson (2005) have proposed to use a dynamic corner frequency to avoid such size dependencies in the final results.

Stochastic based ground motion simulations also suffer from some identified drawbacks which may sometimes have a contextual influence upon the final values. As explained by Boore (2003) some of which are; the method does not include any phase effects due to the propagating rupture and to the wave propagation enroute to the site (including local site response), the method ignores the type of wave component (whether horizontal or vertical) and the type of wave dominant at the motion (e.g., whether S or S_n). Stochastic methods also assume that the frequency content of waves would remain constant with time, however this is not the case for events that occur in deep sedimentary basins where long-period surface waves are generated (Joyner, 2000). However, the method is still a powerful yet a simple set of tools for simulating mean ground motions (ground motions in average/generic terms, and not site-specific ground motion simulations as done in deterministic methods) expected in a region for a selected magnitude and site-source distance, and is particularly useful for obtaining ground motions at a range of frequencies which most of earthquake engineers are interested (Boore, 2003).

Given the acknowledged limitations in both of the main methods (deterministic and stochastic), some researchers argue that the hybrid methods developed by combining both the deterministic and stochastic approaches, would be the most effective approach in simulating broadband ground motions (Hartzell et al, 1999; Pitarka et al, 2000; 2002).

2.5 Quantification of seismic hazard

As both engineers and seismologists, the ultimate purpose of implementing numerous research studies in related areas of the seismology and earthquake engineering field, is to quantify the final hazard level expected at the place of interest due to a possible scenario case which is selected as being “the most conservative” among a range of magnitude – distance combinations. Such final hazard levels, commonly described by a ground motion parameter expected to exceed in a selected period of time, can be used as design specifications/guidelines in seismic design of various structures in the region. Selection of the worst case scenario which the structure can be subject to during the expected lifetime, is often carried out with an engineering notion mostly in a probabilistic framework, or rarely as an intuitive selection of the most severe magnitude –

distance combination in a deterministic framework based on the historical seismicity and source layout of the region. Depending on the basis of the framework and core principles used (either probabilistic or deterministic) in the estimation of hazard, seismic hazard analysis methods are generally categorized into two main streams; probabilistic risk analysis methods and deterministic risk analysis methods.

2.5.1 Probabilistic seismic hazard analysis

Seismic hazard of a region is mostly assessed using probabilistic concepts which allow for explicit modeling of uncertainties in the earthquake size, location, recurrence rate and variation of the predictive attenuation relationship used in the hazard estimation (Kramer, 1996). Pioneering works in the method were established by Cornell in his outstanding paper published in 1968 which was later coded into a program by McGuire (1976). The paper describes a theoretical development on the use of a probabilistic approach to analyze the seismic hazard at a particular site in terms of ground motion parameters and return period. Geographical relationships between the site and source, defined by considering the source as a line or area, are finally incorporated with historical data (fault's average annual number of earthquakes) and a minimum magnitude of interest to produce expected site intensities and return periods for the particular site. Event recurrences are assumed to comply with the well-known Gutenberg-Richter recurrence law (1944) and are treated following a Poissonian arrival process in main events (without dependent events). The main assumptions taken in the original development of the method, which may introduce some biases on the final results are; equal likelihood of event occurrences in a particular line/area fault, negligence of naturally existing random irregularities along the fault line/area, the sequence of main event occurrence is considered following a Poissonian arrival process which may not be the case as always. Especially, the use of Gutenberg-Richter recurrence law for determining the mean annual rate of recurrence has been questioned at many instances (Aki, 1987; Pacheco et al, 1992; Speidel and Mattson, 1997). The relationship is found to be sometimes incompatible with recorded large earthquakes (change of b value), and is difficult to apply in regions with small amount of recorded data since it requires a sufficient amount of previous data for a particular source for accurate derivation of the relationship. Schwartz and Coppersmith (1984) have proposed a concept of "the characteristic earthquake" which is the maximum earthquake repeatedly occurs more times than that predicted through b value projections generated from the historical and/or instrumental record of seismicity on a particular fault segment. McGuire and Arabasz (1990) derive alternative bounded forms for the original Gutenberg-Richter law by avoiding extreme magnitudes in either end (both of low and high ends), to ensure more realistic behavior of event recurrence. Lomnitz-Adler and Lomnitz (1979) develop a modified version of the Gutenberg-Richter law on the basis that the lognormal distribution of earthquake energy (or seismic moment) released

at the source. Apart from further modifications to the Gutenberg-Richter recurrence law, some new recurrence relationships have also been introduced to the field (e.g., Merz and Cornell, 1973; Shah et al, 1975). Application of the Poisson model to represent the temporal variation of event recurrence is also contested by both engineers and seismologists (Esteva, 1970; Coppersmith, 1981). Poisson event arrival demands that a succession of events occurred at a fault in a given period of time in a given region, is independent in every sense, i.e., in magnitude, location, energy release, etc. Nevertheless, it is well affirmed by researchers that the occurrence of an event is significantly dependent of the predecessors in the region (in terms of magnitude, location, time of occurrence, etc.). Occurrence of a single event (even if it is a so-called “independent event”) is just a part of the whole process of continuous stress accumulation happening due to the plate motion. Releasing accumulated stresses as an earthquake, once reached to the maximum stress capacity that the plates can hold, would temporarily stabilize the stress field to an extent which is primarily compensated with the released amount of energy (or seismic moment) in the event, but certainly “schedule” the next event (in size, location and time) depending on the residual stress level and rate of plate motion. Therefore, the Poisson model that certifies independent event arrivals would be unrealistic to represent the actual nature of event recurrence. A number of models that account for this dependent behavior of event arrivals have been proposed (Vere-Jones and Ozaki, 1982; Esteva, 1970; Kiremidjian and Anagnos, 1984; Coppersmith, 1981). However, Cornell and Winterstein (1986) have shown that the Poisson model is sufficiently accurate for practical seismic hazard analysis, except in cases where a single source dominates the hazard level. Woo (1996) has developed a new approach called “Kernel estimation method” for probabilistic risk analysis, in which the method does not require to abide with source zones that are defined based on actual seismotectonic or geological characteristics in the region, instead that defines a grid of point sources for each site of interest with the activity rate of each point being determined according to the earthquake catalog for the region.

Probabilistic risk analysis methods have been developed over the years as a powerful tool to quantify the actual hazard level of a region. In engineering perspective, the methodology’s better capability in handling various uncertainties (in earthquake size, location, temporal distribution of events, ground motion predicting equations, etc.) in respect to other methods such as the deterministic, offers a suite of calculations for a more realistic estimate of the hazard in the region. Further developments in the peripheral aspects of the method like ascertaining “an independent dataset” by removing dependent shocks (e.g., methods proposed by Gardner and Knopoff, 1974; Reasenber, 1985), obtaining reliable completeness periods to avoid any data miscount [such as by Stepp’s method (1972)], and even application of more sophisticated approaches such as a logic tree to account for uncertainties (Kulkarni et al, 1984; McGuire and

Shedlock, 1981), have overall made the probabilistic risk analysis technique as the most reliable risk analysis method to use in developing seismic hazard maps for the engineering purpose.

2.5.2 Deterministic seismic hazard analysis

Deterministic methods of risk analysis are not as popular as probabilistic methods in the field. One of the main reasons for less popularity of the method would be its less competency of capturing possible uncertainties in the calculation process. The methodology is simple and can be easily implemented in regions where potential seismic sources are well identified. Reiter (1990) extracts the complete process of deterministic risk analysis into four simple steps; identification of seismic sources in the region, selection of the site-source distance in each of the identified sources (in most cases, the shortest distance is chosen to account for the highest hazard), selection of “the controlling earthquake” which is likely to produce the highest ground motion at the target site, estimation of the expected ground motions by applying a proper attenuation model. Since, the methodology does not appropriately count uncertainties associated with these fundamental steps, the final predictions can be overly conservative and be far from realistic predictions. Furthermore, the method presumes a hundred percent likelihood on the selected scenario event being taken place. For instance, the method essentially occupies the hypothesis that the probability of occurring the largest possible event at the shortest site-source distance as being one. In contrary, in the probabilistic approaches, each of magnitude and site-source distance combinations is assigned a certain probability value (less than one) estimated based on the probability density functions of the event magnitude and site-source distance. The largest possible event used in the deterministic methods is sometimes called as “the maximum credible earthquake” or as “the maximum probable earthquake”, in which the former is chosen as the largest event likely to occur in the given tectonic framework, whilst the latter is defined as the maximum historical event occurred in the region (generally about in 100 years) (Kramer, 1996). However, a little consensus among scientists on what to choose as the maximum event for the final hazard evaluation, has led to discourage further applications of either term by “EERI (Earthquake Engineering Research Institute) committee on seismic risk” in 1984.

Despite its limited potential of capturing obvious uncertainties, the deterministic based risk analysis methods are still given attention. As claimed by Menon et al (2010), zoning maps depicted in IS 1893 –seismic code provisions for India, are produced based on a deterministic approach; seismic zonation is based on known earthquake magnitudes, epicentral locations, tectonics, lithology, and macro-seismic intensity data up to 1993 and not probabilistic in the hazard computation. McGuire (2001) concludes that both of the deterministic and probabilistic seismic hazard analyses should be complementary, and that the strength of one approach over

the other method depends on the earthquake mitigation decisions to be made, on the seismic environment, and on the scope of the project.

2.6 Application of seismic hazard analysis methods in Sri Lanka

Seismic hazard in Sri Lanka has been assessed by some local experts; Fernando and Kulasinghe, 1986; Abayakoon, 1996; Peiris, 2007; Uduweriya et al, 2013. Fernando and Kulasinghe's (1986) study, does not apply any of the above discussed methods to quantify the possible seismic hazard in the country, albeit it provides some validated inferences obtained using correlations made between the apparent micro-seismicity and identified geological features in the country's central highland part. Abayakoon (1996) has derived expected ground motion levels for selected local cities based upon both probabilistic and deterministic methods using historical events reported in Sri Lanka and the surroundings. In the deterministic approach, the maximum horizontal PGA in the capital city – Colombo, is predicted to be about 150 gals (0.15g) which is based on modeling a M_s 5.7 historical event occurred in Colombo. In the probabilistic method, the maximum PGA (again in Colombo) is estimated to around 35 gals (0.036g) for a 300 year return period. He has further produced hazard maps showing seismic hazard contours of maximum PGA for different return periods. As the first ever effort on quantifying the seismic hazard in Sri Lanka, the work presented in his paper shall be admired, however, because of both the use of a little amount of reported data in the region and application of unverified ground motion models which are originally developed in elsewhere, the reliability of the resulted final hazard levels can be questioned. He has later given efforts (Abayakoon, 1998) to find site response effects in Colombo suburb by estimating site amplification factors using SHAKE91 (Idriss and Sun, 1992) for five broadly identified soil sub-series. Peiris (2007) applies a probabilistic hazard assessment technique to determine the level of seismic hazard in the country. The assessment has been carried out based on a catalogue, compiled by using data since 1819 AD extracted from various sources for an area bounded by latitudes $0^{\circ}N$ to $15^{\circ}N$ and longitudes $75^{\circ}E$ to $85^{\circ}E$. Results show that the horizontal PGA at rock sites for a 10% probability of exceedance in 50 years (or for a 475 year return period) is around 0.026g. The author proposes Sri Lanka to be categorized into a seismic zone that is equivalent to “Zone 1” delineated in UBC 1997 (PGA less than 0.075g for a 475 year return period). The results have also been compared with UBC 1997, IBC 2003 and Eurocode 8. Uniform Hazard Response Spectra for 5% damping have shown a maximum of 0.15g and 0.06g at 0.1s for 2475 year and 475 year return periods, respectively. The study particularly warns on buildings with shallow foundations which are founded on soft soil sites, as they are susceptible for much higher ground shakings during an event. One of the main issues in the study is the absence of a detailed evaluation of source zone characterization in and around the country. The study has not examined possibilities to identify different local and regional source zones in the region, instead

considers a single large rectangular area source zone that encloses the whole country for the hazard analysis. Uduweriya et al (2013) have estimated the design PGA at Colombo rock sites for a 475 year return period as 0.1g. The study compiles a comprehensive event catalog consisting both instrumental and historical data since from 1063 AD. Source zones defined in the study basically follow the same as that in Menon et al (2010), which have originally been defined for assessing the seismic hazard in Tamil Nadu in southern India. However, the study does not seem to characterize local and regional seismic sources prevalent in Sri Lanka and the surroundings. Apart from seismic hazard analysis studies, Vitanage (1994; 1995) has investigated the seismotectonic nature of the island. In these studies, he describes that the tectonic movement of the country in both macro (as the whole continental movement with the Indian plate towards north northwest directions) and micro (individual movement of the Sri Lankan mini-plate towards south southeast directions) contexts, has resulted to create the local seismicity in Sri Lanka. In these studies, he also attempts to identify active lineaments, local faults and bedrock fractures which are closely linked with microseismic activities reported in the country, especially in central upland areas.

2.7 Summary and conclusion

Ground motion modeling techniques have been well developed over many decades. Empirical regression analysis methods using actual recorded data, have become “de-facto” approaches, particularly, in active seismic areas due to their reliability in capturing inherent seismological characteristics of the region. The classification and theoretical definitions of seismological characteristics are established based on the understanding of the mechanism of earthquake occurrence and the theory of elastic wave propagation. Therefore, these established relationships of seismological characteristics attribute potential for generic use in any desired place in seismological studies, and would allow for estimating seismological parameters that are specific to the region. The seismological parameters are separately determined to account for “source” and “path effects” in which path effects are commonly ascertained as wave attenuations and amplifications during the propagation through the medium. Various standard methods are proposed in determining these region-specific seismological parameters, and most of them involve direct analysis of recorded data in the region of interest. Ground motion simulation techniques have offered a new dimension for the seismology and earthquake engineering field, and have become popular in seismic hazard assessment studies especially in low to moderate seismic regions. Depending on the basic theory followed in each case, these ground motion simulation methods can be categorized as stochastic methods and deterministic methods. Stochastic methods along with the seismological model are shown to be advantageous over the latter methods mainly due to their ability of successful application in different tectonic regions where detailed information of geotectonic features is not much available. Nevertheless,

the accurate estimation of seismological model parameters is essential for reliable simulations. On the other hand, deterministic methods such as Green's function method, ray theory method, etc. are evidenced to be more successful in regions where such geotectonic information is abundant. However, hybrid methods developed based on both stochastic and empirical deterministic methods have shown sometimes more reliable than independent application of either method. Seismic hazard at a given place is mostly estimated using probabilistic based approaches because of the requirement of proper quantification of uncertainties. In contrast, deterministic based methods are not that popular among the scientists due to its limited potential on capturing uncertainties. Seismic hazard evaluation of Sri Lanka has implemented at few times by local scientists, though a comprehensive effort that may cover identification of both local and regional seismogenic sources, estimation of region-specific seismological parameters, derivation of region-specific attenuation models, is not undertaken.

3. Seismicity and possible seismic sources in and around Sri Lanka

3.1 Introduction

Sri Lanka has long been recognized as an aseismic or a Stable Continental Region (SCR), given its proximity away from major plate boundaries such as Sunda Arc subduction zone and Sumatran fault to the east, and transform faults of the northern extension of Central Indian Ridge to the west (Figure 3.1). The risk of striking an interplate earthquake in the country can therefore be treated impassable, although, secondary effects such as a mega tsunami can be possible by a large magnitude earthquake triggering at above plate boundaries. In spite of clear evidence of regional intraplate activities, little concern has been given in the remit of local academia on them, and this turns to result in a few local studies to be undertaken so far in the field (Abayakoon, 1996; Fernando and Kulasinghe, 1986; Peiris, 2007; Uduwariya et al, 2013). Subsequently, rigorous efforts to implement a proper seismic hazard assessment for the country have not been envisaged. Nevertheless, a number of studies have been carried out in the international context by many researchers (e.g., Stein and Okal, 1978; Sykes, 1970; Royer and Gordon, 1997; Wiens, 1986) to investigate the seismicity and seismotectonic nature in oceanic regions surrounding Sri Lanka (discussed in section 3.3). These studies play a vital role in evaluating the impact of identified seismogenic zones and their inherent hazardous nature, for assessing the seismic risk of the country. Perhaps, the studies may challenge the existing conclusions made upon the level of seismicity of Sri Lanka, which have been previously drawn by omitting surrounding seismotectonic behaviour of the oceanic crust.

Seismicity of the Sri Lankan region can be studied by separating into local and regional seismicity. This classification would reflect difference of the seismicity in between Sri Lanka and the surrounding oceanic crust, and would be effective in accounting for their separate influence on the seismic hazard evaluation for the country. Whilst events occurred within the country are sparsely recorded, those reported outside the country have been properly recorded in international archival databases such as ISC (International Seismological Centre-UK), ANSS (Advanced National Seismic System-USA), etc. Hence, the latter provides essential primary information for identifying the associated intraplate seismicity around Sri Lanka. This chapter discusses the seismotectonic nature of Sri Lanka in both local and regional contexts along with potential seismic sources observed in and around the country. Identification of seismic sources within the country is accomplished with a limited number of historical records available in local catalogues. The underlying geotectonic setup has also been considered in advance to study a correlation, if any, between the reported events and local tectonic features. Regional seismicity surrounding the

country in northern Indian Ocean and in southern peninsular India has been assessed with active tectonic structures located within these regions, considering their proximity to the country and the level of intensity of the sources. The work described in the chapter is organized as first seismicity within the country or local seismicity, second seismicity outside the country or regional seismicity, followed by summary and conclusion, respectively.

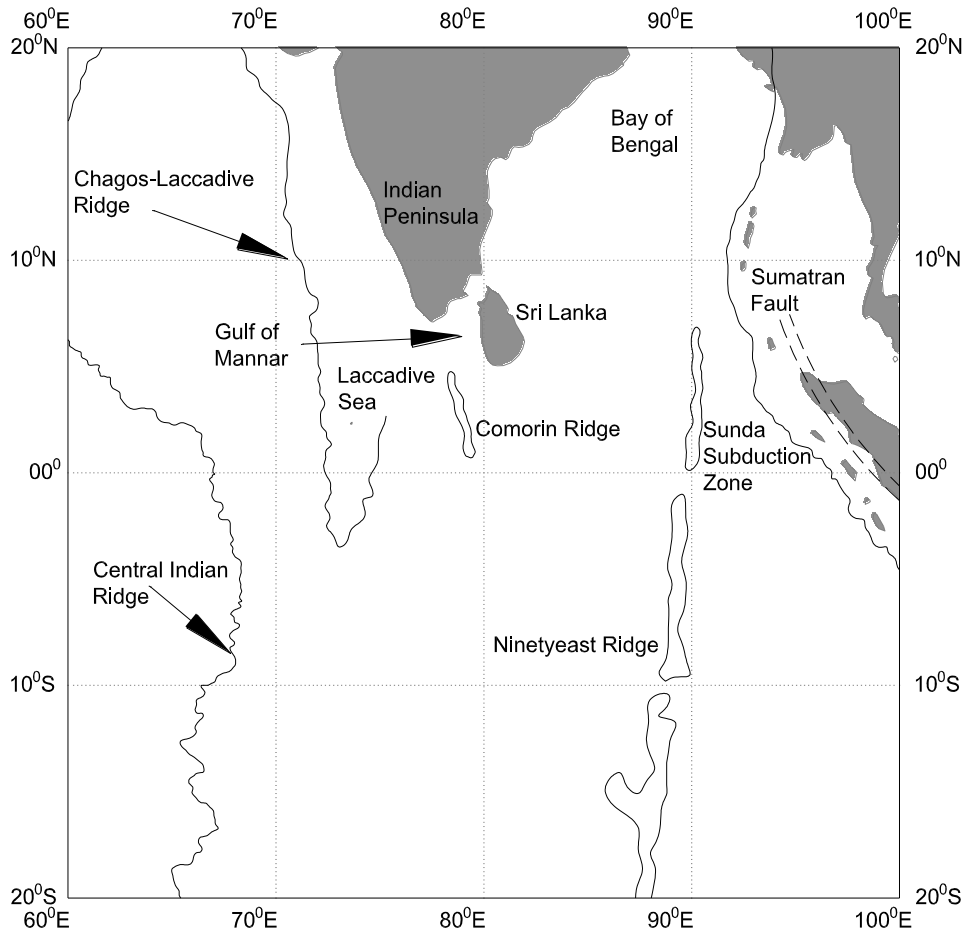


Figure 3.1 Typical seismotectonic features in the northern Indian Ocean surrounding Sri Lanka.

3.2 Seismicity within the country or local seismicity

3.2.1 A summary on the general geology of Sri Lanka

The geology of Sri Lanka has well been documented since the early 20th century through the work of many local and international geologists and geophysicists. Most of the matters related to the origin, geological age, lithotectonic classification, etc., of the basement crust underlain, have already been resolved after much effort. Sri Lanka is generally divided into three main lithotectonic unites based on the type of basement rock and the geological period of formation (Figure 3.2), under which, the crust is considered to be originated in the Precambrian period (Mesoproterozoic and Paleoproterozoic eras) and is composed of non-fossiliferous crystalline

rocks (Cooray, 1994); the Highland Complex (HC), the Vijayan Complex (VC) and the Wannu Complex (WC). The Kadugannawa Complex (KC), a minor unit located between the WC and the HC, in the central highland area, has been categorised as a separate geological unit after noting some anomalous characteristics of the basement rock from surrounding lithotectonic complexes.

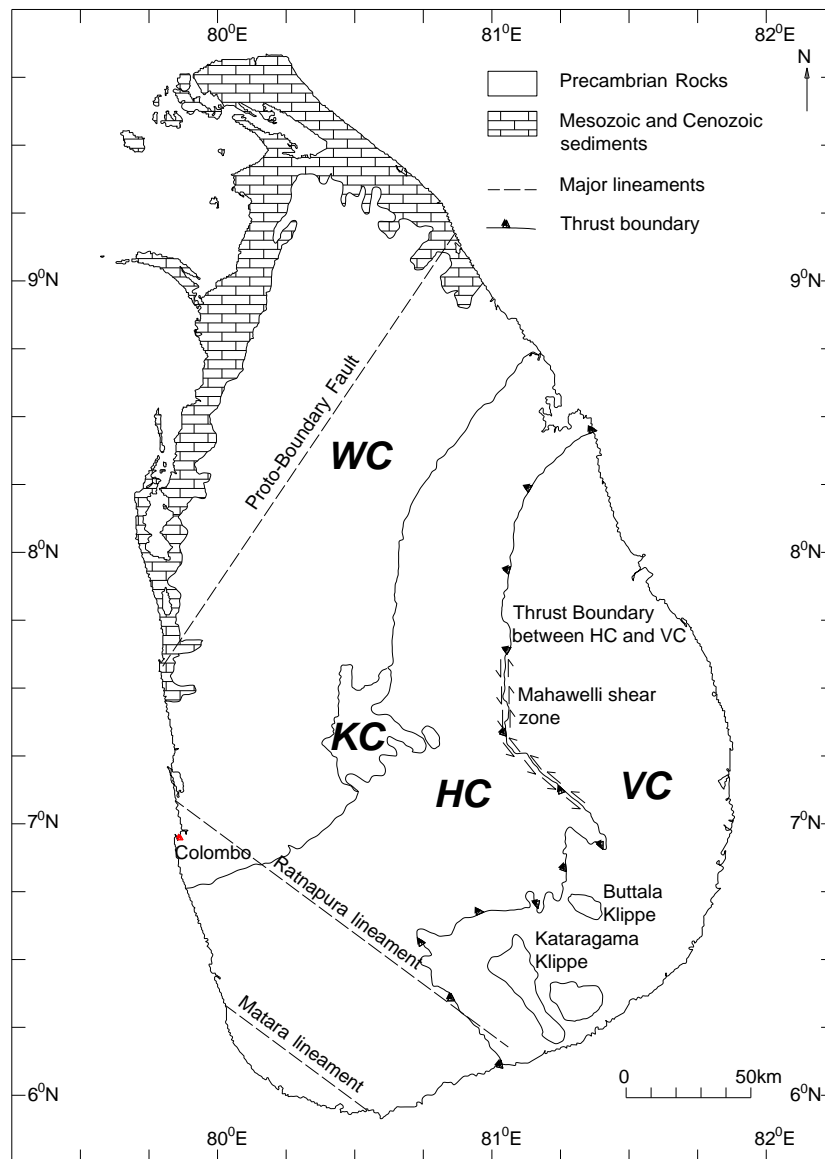


Figure 3.2 General geology of Sri Lanka showing main lithotectonic units categorized according to the basement rock type and geological period of formation. More than 90% of the country's rock geology consists with Crystalline rocks of the Precambrian age. Precambrian basement has basically been divided into three lithotectonic units; the Highland Complex (HC), the Vijayan Complex (VC) and the Wannu Complex (WC). The Kadugannawa Complex (KC) is a minor unit located again in the WC. The boundary between the HC and the VC is proven to be tectonically a thrust zone (Vitanage, 1985; Pathirana, 1980; Kroner, 1986), of which the direction of the collision has been identified as E-W (Kehelpannala, 2004). Approximated boundaries between other lithotectonic units and identified major lineaments are also shown.

The HC largely consists with high grade inter-banded metamorphic rocks of granulite facies, and runs across the central part of the country from southwest to northeast. Geochronological studies confirm that the deposition of supra-crustal rocks of the HC has been completed about 2 Ga ago during the Palaeoproterozoic era (Barber, 2000; Mathavan et al., 1999). The crust probably would represent the oldest formation in the region. Granulite facies metamorphism has taken place on regional basis within the HC during the Neoproterozoic era at about 610-560 Ma ago (Baur et al., 1991). The common rock types include Granitoid (Charnockitic to Enderbitic) gneisses, Marble, Quartzite and Quartzofeldspathic gneisses. Barber (2000), and Dissanayake and Munasinghe (1984) have noticed a resemblance of thick shelf like sedimentation of metasediments such as Quartzites, Carbonates and Calcsilicate gneisses in the HC, with that of Grenville province in Canadian Shield region. However, unlike in typical shield regions (Canadian, western Australian, Indian, etc.), flat or levelled topography cannot be seen in the HC, instead, rapid variations in elevation over the whole area of the unit, are quite abundant. Moreover, this steep form of terrain configurations may be attributed to the folds and deformations undergone due to local tectonic activities such as thrusting of the HC over the VC during their relative movements in underlying mini-plates (Pathirana, 1980).

The VC, located in the southeastern part of the island, has a younger, yet more complicated geological structure than that in the HC. Most of the rocks were metamorphosed under amphibolite facies conditions at comparably low pressure and temperature (Barber, 2000), and show some evidence of granulite facies metamorphism as which happened in the adjacent HC (Kröner et al, 2013). Crustal deposition and regional metamorphism of rocks apparently completed about 1100 Ma and 465-558 Ma ago, respectively (Kröner and Williams, 1993), and which in turn assure on late formation of the crust in the region. Rock types include Calc-Alkaline Granitoid gneisses, Augen-gneisses, with minor amphibolite layers (derived from mafic Dykes) and sedimentary Xenoliths such as Metaquartzite and Calc-Silicate rocks (Kroner and Brown, 2005). Some studies point out that the origin of VC rocks was happened in a subduction related tectonic environment (Milisenda, 1991), and that VC rocks have a link to a Mesoproterozoic island arc setting (Kröner et al, 2013). In contrary to the HC, a flat/levelled topography seems dominating in the entire VC, except few HC rock klippens preserved (such as Katharagama and Buttala) towards the southern part of the unit.

The WC, virtually the largest lithotectonic unit, lies next to the HC in the north and northwestern parts of the country. Sources indicate the crustal deposition has taken place in a similar geological period as such happened in the VC, i.e., about 1100 Ma ago (Kröner and Williams, 1993; Kröner and Brown, 2005). Common rock types include Hornblende bearing gneisses, Pink Granite, Granitoid, Gabbroic, Charnockitic and Enderbitic gneisses, Migmatites, etc. The estimated metamorphic grade indicates widely varying from upper amphibolite to granulite facies, and

which appears to be a unique characteristic of the WC. Metamorphism can be dated back to 600-550 Ma ago (Mathavan et al., 1999). Structural dissimilarities within the WC suggest further subdivision of the unit into a western and an eastern WC. The macroscopic structure of the former mainly consists of non-uniform and non-linear folds, whilst the latter is featured by well-developed linear folds quite similar to that in the HC (Tani, 1997). The KC, a smaller sub-unit, is also located in the WC and is basically composed of Calc-Alkaline hornblende biotite gneisses (Barber, 2000). The structural boundary between the WC and the HC is yet to be clearly defined, although, assertions can be found sometimes referring to a tectonic boundary (Kehelpannala, 1991) of which the WC thrusts over the HC towards southeast direction. Some recent works (Kehelpannala and Ranaweera, 2007; Ranaweera, 2008) demonstrate that this boundary is a crustal-scale ductile shear zone along which the WC and HC have collided during the amalgamation of the Gondwana around Sri Lanka. However, studies have not so far indicated a significant relative movement between two units involving a higher rate of stress release, which may also be evidenced by apparent nullified seismicity reported within the boundary.

The uppermost north and northwestern strip like part (juxtaposed with the WC), that represents about 10% of the country's geology, is mostly composed of sediments of upper Mesozoic and Cenozoic periods (hatched in Figure 3.2). These sedimentary rocks are significantly younger than crystalline rocks found in the Precambrian geological units.

The structural boundary between the HC and the VC is well defined due to explicit difference in geological features (metamorphic grade, origin and sedimentation, etc.). The boundary is said to be tectonically a thrust zone (Vitanage, 1985; Pathirana, 1980; Kröner, 1986), of which the direction of the collision has been identified as E-W (Kehelpannala, 2004). Directions of the relative movement of the two units (HC and VC) are established by the orientation of lineations located along the boundary. Stretching lineations are oriented in N-S and NNW-SSE directions mainly in northeastern and southwestern parts of the HC, respectively (Kleinschrodt, 1994). The same author shows that several open and gentle folds have been formed during the thrusting process along the contact boundary of two units with fold axes parallel to these lineations. Pathirana (1980), argues that the Highland-Vijayan boundary can be a Paleo plate boundary of subduction, where the crust of the VC and adjacent continental-Ocean boundary, has been sinking itself downward into the mantle as a result of collision with the continental crust of the WC. The conclusion has primarily been based on the presence of paired metamorphic belts (granulite and amphibolite facies) and existence of hard rocks (basic and ultrabasic) with Igneous and Copper-Magnetite related mineralised origin found along the contact boundary. A number of hot springs confined close to the boundary area also reinforces the above conclusion. The subduction process may date back to the Precambrian time and as speculated this convergent type boundary has been formed during the collision of East and West Gondwana (Büchel, 1994). However, recent studies

claim to avoid this idea of a possible subduction zone, instead identify the boundary of HC-VC as a ductile shear zone formed at lower crustal levels (Kleinschrodt, 1994; 1996; Kehelpannala, 2004; Kröner et al, 2013).

Although Sri Lanka is a small landmass separating from other countries by the surrounding sea, its geological and tectonic anomalies, as discussed above, could “outweigh” its physical shape and size when assessing the seismic hazard. Local seismic sources characterized by these geotectonic features within the island can be more critical than active regional or external sources, in respect of the site-source distance considered (this is clearly evidenced from the final hazard levels computed in Chapter 8). Hence, a separate identification of potential local seismic sources other than regional sources, is of paramount importance in obtaining reliable hazard estimates to the country.

Efforts are given in the next section to identify possible local seismic sources which are correlated with certain tectonic features aforementioned.

3.2.2 Local events reported in the country and possible seismic sources

Local seismicity within the country has rarely been assessed due to scarcity in instrumental records. Lack of resources in terms of allocated funding and expertise, are the key impediments to be overcome by Sri Lanka for such a comprehensive task. Most of early seismic records in the country were lost or were badly recorded with a very high signal to noise ratio at local networks due to improper maintenance. Sudden power failures, bad site selection, incorrect triggering of equipment and poor or abrupt means of data transferring systems from sub-stations to the base station, are the common drawbacks observed in these networks. Besides, the country’s “aseismic” location of that being away from major plate boundaries, has resulted a very little or no strong motion records available at local networks for further studies. However, seismic stations established under permanent networks maintained by well-known global institutions, are currently operating more effectively in the country. For instance, there are three broadband stations presently operating at Pallekelle (PALK), Hakmana (HALK) and Mahakanadarawa (MALK), maintained by United States Geological Survey (USGS) and by German Research Centre for Geosciences (GEOFON) (Figure 3.3). These broadband stations are beneficial in numerous ways to carry out seismological studies far better than previously possible.

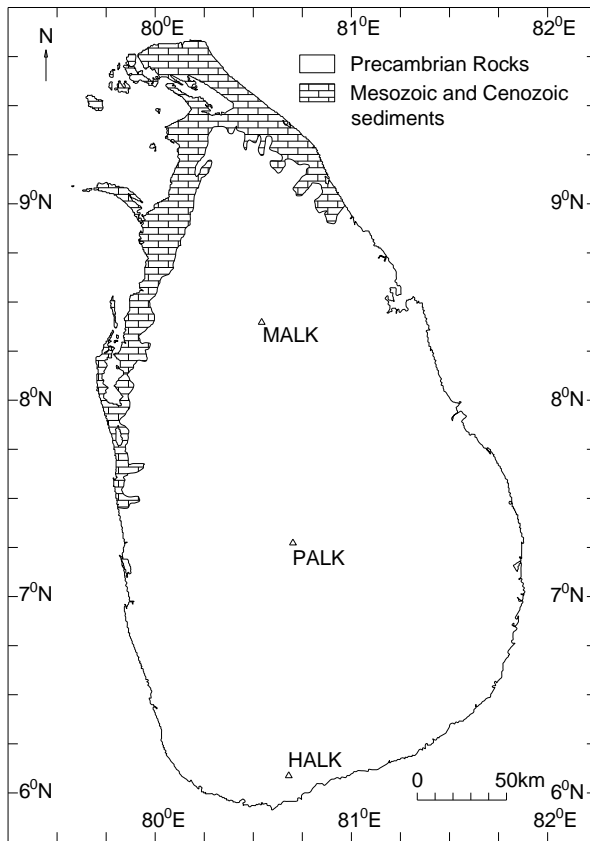


Figure 3.3 Three broadband seismic stations (denoted by triangles) presently operating in Sri Lanka; PALK (Pallekelle), HALK (Hakmana) and MALK (Mahakanadarawa).

A few authors have reported some local events, magnitude ranging from small microtremor to strong magnitude, occurred in the country (Abayakoon, 1996; Fernando and Kulasinghe, 1986; Kehelpannala, 2007). Abayakoon (1996), based on USGS archival data, reports around 12 number of small and strong earthquakes ($M_w \geq 3$) within inland (Figure 3.4). The study presents historical evidence of the most disastrous earthquake ever known to occur in the country, which was happened on 14th of April 1615 in Colombo with an estimated magnitude about M_w 6.4. The event incurred a damage of 200 houses and caused over 2000 casualties (Wimalaratne, 1993). Other structural collapses including a portion of the masonry city wall and a total collapse of a stone bridge, would rank the intensity of the event at least as VIII in Modified Mercalli Intensity (MMI) scale. Gamage and Venkatesan (2012a), based on a conversion of reported MMI to PGV, deduce the PGV of the event could be even higher than 60 cm/s at rock sites in Colombo. Sources further report an emission of sulphurous fumes from fissures opened up on the ground surface during the rupture (Peiris, 1920). This seems a bit sceptical in the viewpoint of current tectonic setting of Sri Lanka, where no active volcanism can be found, though, the plausible reason may be sometimes associated with some attributes on volcanic activities in Gulf of Mannar region (Rana et al, 2008). A total of 10 small to strong earthquakes, magnitude from M_w 3.0 to 6.4, were reported within about 20 km of Colombo, out of which at least 3 were greater than M_w 5.0 and

about 9 occurred during the last 200 years (Gamage and Venkatesan, 2012a). Many of these eruptions are likely to link with local lineaments and fractures of the bedrock in the area.

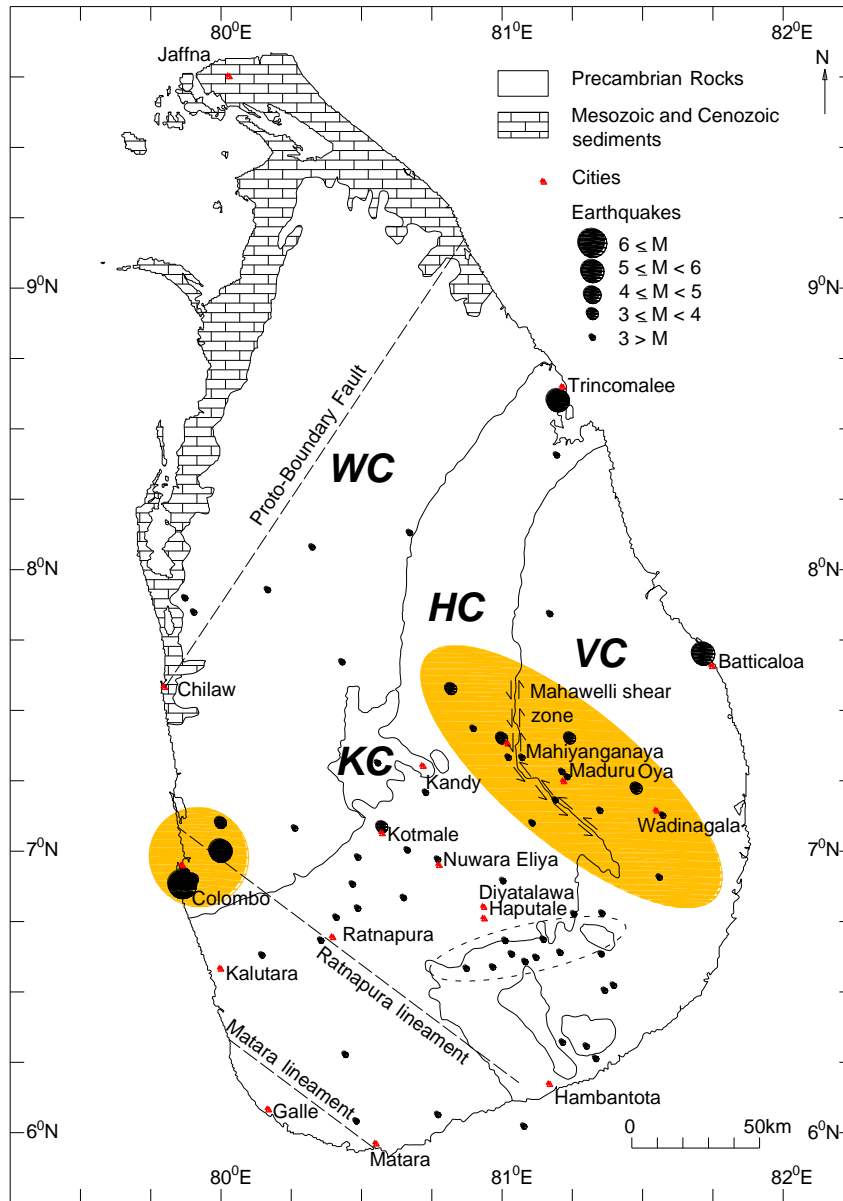


Figure 3.4 Local seismicity in Sri Lanka showing reported events within the country (from 1500 to 2012) (sources: Abayakoon, 1996; Fernando and Kulasinghe, 1986; Gamage and Venkatesan, 2012a; Geological Survey and Mines Bureau (GSMB) for newer events). Past evidence enables to formulate two possible seismic zones within the country (darkened areas); 1. Area around the capital city - Colombo 2. Area enclosing Mahawelli shear zone and NW-SE oriented thrust zone closed to Mahiyanganaya. Microseismicity is mainly concentrated in the HC, especially along E-W trending Haputale escarpment area (enclosed in dash line).

A simple estimation of earthquake recurrence, since 1615, for Colombo area is shown in Figure 3.5, in which λ_m represents the mean annual rate of exceedance of a given magnitude earthquake.

The Figure evidences actual observations are following approximately two linear trends, with the hinge point around M_w 3.5. The common reason is the catalogue incompleteness, and is arisen mainly due to negligence of smaller magnitude events that occurred before the instrumental period. Hence, a lower threshold of M_w 3.5 is set, above which the catalogue is considered remain complete. The original Gutenberg-Richter law and its bounded version, taking M_w 3.5 and 7.5, respectively, as lower and upper limits, are applied for estimation of recurrence periods. Estimations yield an event exceeding M_w 5 would be possible in Colombo in about 150 years. A strong event greater than M_w 6 has return periods of 340 years and 450 years in accordance with the original and the bounded Gutenberg-Richter laws, respectively. Inferred return periods for events of this size, are lower than that typically specified in seismic code of practices for “Design basis ground motion”. The risk in striking a moderate magnitude earthquake at Colombo thus could be high. The vulnerability of such an event may also be the highest in Colombo, since it holds the largest population density and the most congested city arrangement in the country.

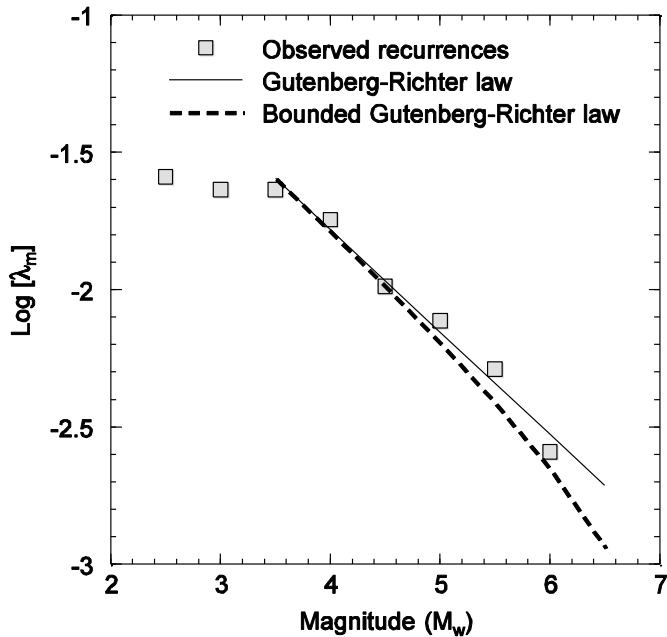


Figure 3.5 A simple estimation of earthquake recurrence, since 1615, for Colombo area. The Figure evidences actual observations following approximately two linear trends, with the hinge point around M_w 3.5. The original Gutenberg-Richter law and its bounded version, taking M_w 3.5 and 7.5, respectively, as lower and upper limits, are applied for estimation of recurrence periods. Estimations yield an event exceeding M_w 5 would be possible in Colombo in about 150 years. A strong event greater than M_w 6 has return periods of 340 years and 450 years in accordance with the original and the bounded Gutenberg-Richter laws, respectively. λ_m represents the mean annual rate of exceedance of a given magnitude earthquake

On the eastern coast, two significant events, one in Trincomalee (in 1882) and the other in Batticaloa (in 1814), were reported. The event in Trincomalee had a magnitude estimated around M_w 5.9 and located about 5 km northwestwards from Trincomalee city. The probable reason of the event was undiscovered, though may be attributed to the action of a local fault. The Batticaloa event, occurred in June 1814, by the sea as clued in historical reports, could be of at least around M_w 5.5, given its major property damage.

Fernando and Kulasinghe (1986) in their local seismic study, analyse a number of micro-earthquakes ($M_L \leq 2.5$) recorded during the period February 1983 - August 1984 at the microseismic network installed as part of the Kotmale hydropower project. They conclude the local seismicity within Sri Lanka has primarily concentrated in the central Highland and Upland areas associating mega lineaments and escarpments, more precisely along the N-S trending Mahawelli lineament where the river Mahawelli takes a straight course, and the E-W oriented Haputale escarpment (Figure 3.4). Vitanage (1994; 1995; 1983) relates these occurrences of local earthquakes in the island, to sudden reactivation of lineaments when releasing stresses that accumulated by the local movement of the Sri Lankan mini-plate about 1-2 mm annually in a SSE direction away from India. He also claims the above “micro-movement” of the Sri Lankan mini-plate, along with the regional “macro-movement” of the Indian plate in an opposite direction (i.e., NW direction), created the central highland uplift.

It may be noteworthy, recently reported small magnitude events that occurred in the eastern part of the country in the VC and HC. A couple of smaller events, between M_L 2.0-3.6, at Maduru Oya area close to the HC-VC boundary around the Mahawelli shear zone, are notable. Events were well recorded at seismic stations indicating a PGA of about 6 mm/s^2 at PALK for the largest event M_L 3.6. This event felt at many places, and caused even little cracks to be formed of the loadbearing walls of several masonry dwellings. Any reactivation of the local fault system in the boundary of two geological lithotectonic units (HC-VC) due to imposed thrust is susceptible for these eruptions. Vitanage (1985) and Hatherton et al (1972) identify the Mahawelli lineament as a well-defined mega lineament located in a Precambrian thrust zone (Mahawelli shear zone) that is formed by the collision between the VC and HC (discussed in section 3.2.1). In Figure 3.4, the dark area, other than Colombo area, roughly encloses the events that are possible to be induced by reactivated faults in this region. There is also evidence that the Precambrian basement of Sri Lanka contains an abundance of brittle fractures (Kehelpannal et al, 2006; Vitanage, 1985). In particular, the area of the VC where these events have occurred is identified to have a crust with a large number of younger brittle faults and fracture lineaments (Kehelpannala, 1987; Kehelpannala et al, 2006). Vitanage (1983; 1995) argues these bedrock fractures and faults have potential to induce seismic activities when they were subject to an inexorable thrust as a result of which he relates the relative movement of the Sri Lankan mini-plate away from the Indian plate.

Therefore, any of these cases (i.e., reactivation of the thrust boundary and the subsequent fault system or reactivation of bedrock fractures) can be possible to link with the recent seismic activities in the area.

A cluster of small events (more than 10) struck very recently at Wadinagala in the eastern part of the VC. The events were reported within close time intervals, with magnitude varying from M_L 2.0 to 3.0, and showed a higher rate of recurrence with the epicentral locations confined to a narrow area in the VC.

In summary, at least two seismic zones can possibly be formulated within the country: (1) The area around the capital Colombo; (2) Mahawelli shear zone enclosing geological thrust boundary close to Mahiyanganaya (Figure 3.4). The former poses more adverse effects than the latter because of both uncertainty in the geological structure and higher recurrence rate of moderate/strong events. Despite of apparent aseismic behaviour at present, Colombo can still be subjected to a strong earthquake, magnitude of the order of M_w 6.5, as such earlier happened in 1615. Gamage and Venkatesan (2012a) show the Pseudo Spectral Acceleration (PSA) of M_w 6.5 event at Colombo rock sites can be around 50 m/s^2 (5g). A value like 5g of PSA is quite unusual in engineering seismology, though, such a ground motion may not be unexpected as it evidences recently in Christchurch-New Zealand in 2011. The Mahawelli shear zone, which is located at the thrust boundary between the HC and VC near Mahiyanganaya, would also be a probable source of active seismicity. Historical seismicity of the area would suggest a maximum probable event of about M_w 4.0 would be reasonable for hazard assessments. Apart from these two zones, the Haputale escarpment area which shows a scatter of microseismic events oriented along the E-W direction at the boundary of HC-VC, also warrants attention.

3.3 Seismicity around the country or regional seismicity

Intraplate seismicity surrounding Sri Lanka can be discussed under following headings (named features are shown in Figure 3.1):

1. Seismicity in the northern Indian Ocean south/southeast of Sri Lanka and in the Bay of Bengal
2. Seismicity west of Sri Lanka in the Laccadive sea and in the Gulf of Mannar
3. Seismicity north of Sri Lanka in the southern Indian peninsula region

3.3.1 Seismicity in the northern Indian Ocean south/southeast of Sri Lanka and southern Bay of Bengal

The northern Indian Ocean region has been identified as a prominent example of intraplate activities prone area (Figure 3.6). The equatorial region between Central Indian ridge to the west and Sumatra trench to the east is recognized as a unique region that undergoes extensive intraplate

deformation in the oceanic lithosphere. The occurrence of a considerable number of strong earthquakes greater than M_w 6-7 during last two centuries, assures its exceptional intraplate seismicity which is uncommon to observe in other typical oceanic crusts (Wiens et al., 1986).

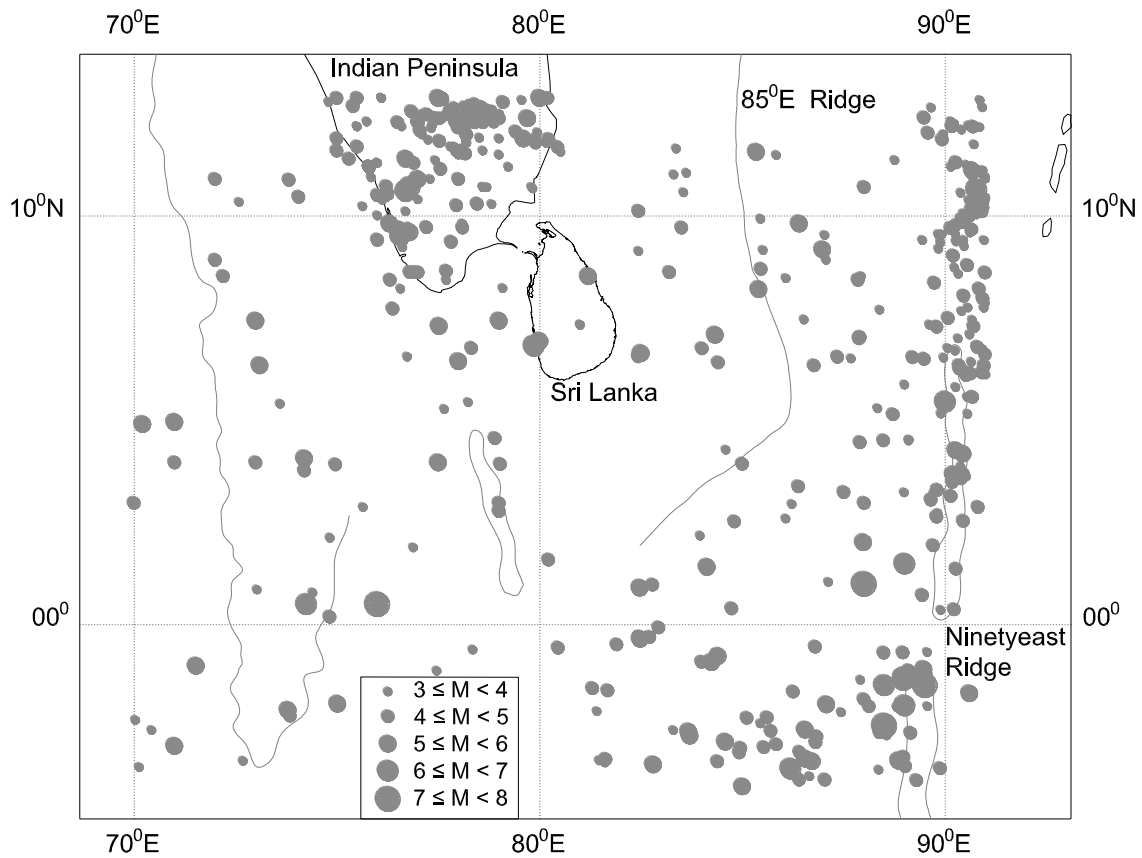


Figure 3.6 Seismicity around Sri Lanka in the northern Indian Ocean and southern peninsular India. Reported intraplate earthquakes between 1500-2012 are denoted by filled circles with size varying with the magnitude. A considerable number of events indicate their epicentral locations towards east and southeast directions closed to the Ninetyeast ridge. Sources-ISC, ANSS, local catalogues in India and Sri Lanka.

A list of large magnitude events occurred in the region since 1900 is given in Table 3.1. The intensity of the seismicity of the subject region is still under investigation, however, some authors (Stein and Okal, 1978) have mentioned the rate of seismic moment release of the region is comparable to that of the San Andreas Fault in California. This strong seismicity concentrated amidst the large Indo-Australian plate has been studied by various authors since the 1950s (Gutenberg and Richter, 1954; Sykes, 1970; Stein and Okal, 1978; Wiens et al., 1986; Royer and Gordon, 1997). Previous tectonic models proposed for the region were based on the conventional theory of rigid plate motion, in which the seismicity is assumed to be confined to narrow margins. The higher rate of seismicity associated with particularly the northern Ninetyeast ridge in southern Bay of Bengal, was able to explain to a certain extent with the rigid plate assumption. The studies on focal mechanisms of historical earthquakes leading the above assumption, reveal a left lateral

strike-slip movement of two rigid parts (eastern and western) of Indo-Australian plate due to splitting the plate along the Ninetyeast ridge (Stein and Okal, 1978; Minster and Jordan, 1978). Wiens (1986), deviating from the rigid plate assumption, proposes a model which represents a large diffuse area thousand kilometres in size covering the whole region between Central Indian ridge and Sumatra trench in the northern Indian Ocean. The area, that extends as far north as Sri Lanka, is characterized undergoing significant vertical thickening and crustal shortening owing to E-W striking long-wavelength lithospheric undulations indicated in marine seismic profiles (Wiens et al., 1986). In the model, they further postulate a rotation of northern and southern parts of the Indian plate about a pole located just east of the Chagos Bank, forming tensional and compressional stresses near the Chagos-Laccadive ridge and the Ninetyeast ridge, respectively. Cloetingh and Wortel (1986) show large compressional stresses of several kilobars near the Ninetyeast ridge, and conclude this can be attributed to large scale continental collisions of the Indian plate at the Himalayan suture and to the ongoing subduction taken place at the Sunda arc.

Table 3.1 Large magnitude events occurred in the diffuse area since 1900 (Source-ISC)

| Date | Time (UTC) | Lat. | Lon. | Depth (km) | Magn. Type | Magnitude |
|-------------|------------|-------|-------|------------|----------------|-----------|
| 11/5/1912 | 17:26:24 | -9 | 72 | 35 | M _S | 6.8 |
| *19/01/1913 | 17:05:06 | 2 | 86 | NA | M _S | 7 |
| 9/5/1916 | 14:33:42 | 1.5 | 89 | 35 | M _S | 6.3 |
| 13/04/1918 | 0:51:15 | -8 | 85 | 35 | M _S | 6.5 |
| 28/05/1923 | 1:25:53 | -1.5 | 88.5 | 35 | M _S | 6.5 |
| 18/01/1926 | 21:07:23 | -2 | 89 | 35 | M _S | 6.8 |
| 7/2/1928 | 0:01:43 | -2.5 | 88.5 | 35 | M _S | 6.8 |
| 9/3/1928 | 18:05:27 | -2.5 | 88.5 | 35 | M _S | 7.7 |
| 24/04/1935 | 15:52:18 | 0.5 | 74.25 | 35 | M _S | 6 |
| 30/11/1937 | 0:40:27 | 5.5 | 90 | 35 | M _S | 6.5 |
| 21/03/1939 | 1:11:09 | -1.5 | 89.5 | 35 | M _S | 7.2 |
| 29/02/1944 | 16:28:07 | 0.5 | 76 | 35 | M _S | 7.2 |
| *23/01/1949 | 6:31:04 | -11.6 | 92.8 | NA | M _S | 6.8 |
| 1/9/1950 | 2:46:55 | -4.5 | 89.25 | 35 | M _S | 6 |
| 22/03/1955 | 14:05:06 | -8.7 | 91.6 | NA | M _W | 7 |
| *25/05/1964 | 19:44:07 | -9.1 | 88.9 | NA | M _S | 6 |
| 12/9/1965 | 22:02:38 | -6.46 | 70.76 | 62 | m _b | 6.1 |
| 10/10/1970 | 8:53:05 | -3.56 | 86.19 | 32 | M _S | 6.3 |
| 30/08/1973 | 19:50:04 | 7.15 | 84.33 | 43 | M _W | 6.1 |
| 30/11/1983 | 17:46:01 | -6.85 | 72.04 | 10 | m _b | 6.5 |
| 1/12/1983 | 5:45:38 | -6.61 | 71.41 | 33 | m _b | 6 |
| 3/12/1983 | 17:43:18 | -6.5 | 71.4 | 34 | M _S | 6.2 |
| 26/04/1984 | 10:11:12 | -6.79 | 71.49 | 21 | m _b | 6 |

| | | | | | | |
|------------|----------|--------|-------|----|-----------------|-----|
| 19/09/1984 | 0:21:50 | -6.95 | 72.76 | 10 | M _S | 6 |
| 10/6/1988 | 11:31:55 | -6.89 | 72.26 | 34 | m _b | 6.2 |
| 6/1/1990 | 21:44:56 | -10.64 | 92.97 | 15 | m _b | 6.1 |
| 15/10/1990 | 1:35:41 | -2.22 | 92.23 | 9 | M _S | 6.6 |
| 13/01/1991 | 11:54:37 | -2.9 | 84.58 | 10 | m _b | 6.1 |
| 13/05/1991 | 16:28:14 | -3.46 | 82.8 | 10 | M _W | 6 |
| 16/08/1992 | 14:49:08 | -3.05 | 84.95 | 33 | m _b | 6.1 |
| 27/07/1995 | 5:51:20 | -12.58 | 79.23 | 24 | m _b | 6 |
| 15/11/1999 | 5:42:43 | -1.37 | 88.97 | 10 | m _b | 6.2 |
| 28/11/1999 | 10:17:19 | -1.29 | 88.92 | 10 | M _L | 6.3 |
| 29/11/1999 | 3:46:30 | -1.3 | 89.01 | 10 | M _S | 6.4 |
| 2/9/2001 | 2:25:55 | 0.91 | 82.47 | 13 | M _W | 6.1 |
| 31/12/2004 | 12:07:47 | 10.75 | 90.77 | 33 | M _S | 6 |
| 22/03/2007 | 6:10:45 | -3.38 | 86.72 | 29 | M _E | 6.1 |
| 7/1/2011 | 3:09:59 | 4.25 | 90.35 | 18 | M _S | 6.4 |
| 18/06/2011 | 23:22:26 | -14.54 | 89.65 | 10 | m _B | 6.2 |
| 17/10/2011 | 9:51:31 | 6.13 | 83.13 | 27 | m _B | 6.1 |
| 24/10/2011 | 1:38:29 | -1.23 | 93.71 | 10 | M _{wp} | 6.6 |
| 10/1/2012 | 19:57:28 | -0.77 | 89.66 | 10 | m _B | 7.5 |
| 10/2/2012 | 4:08:15 | -8.36 | 88.71 | 10 | m _B | 6.3 |
| 11/4/2012 | 8:38:37 | 2.31 | 93.06 | 23 | M _W | 8.6 |
| 11/4/2012 | 9:51:42 | 2.51 | 90.32 | 20 | m _B | 6 |
| 11/4/2012 | 10:08:30 | 2.65 | 90.08 | 16 | M _W | 6.1 |
| 11/4/2012 | 10:43:09 | 0.79 | 92.44 | 16 | M _W | 8.2 |
| 11/4/2012 | 11:04:45 | 0.6 | 92.48 | 10 | M _W | 6.1 |
| 11/4/2012 | 11:34:14 | 0.73 | 93.67 | 10 | M _W | 6.1 |
| 11/4/2012 | 11:53:37 | 2.93 | 89.53 | 15 | m _b | 6 |
| 11/4/2012 | 13:58:05 | 1.49 | 90.75 | 6 | M _W | 6.1 |
| 11/4/2012 | 14:34:19 | 1.5 | 90.89 | 14 | m _B | 6.2 |
| 11/4/2012 | 15:41:38 | 0.91 | 92.37 | 21 | m _B | 6 |
| 11/4/2012 | 16:58:12 | 2.56 | 90.22 | 10 | m _B | 6.1 |
| 11/4/2012 | 22:15:26 | 0.51 | 92.44 | 14 | M _{wp} | 6.4 |
| 11/4/2012 | 22:51:59 | 2.9 | 89.6 | 15 | M _{Lv} | 6.1 |
| 11/4/2012 | 23:56:34 | 1.8 | 89.67 | 14 | m _B | 6.1 |
| 12/4/2012 | 7:34:57 | 3.4 | 89.82 | 16 | M _{wp} | 6.1 |
| 12/4/2012 | 9:44:18 | 0.53 | 92.38 | NA | m _B | 6.6 |
| 15/04/2012 | 5:57:39 | 2.55 | 90.28 | 15 | m _b | 6.3 |
| 16/04/2012 | 9:46:24 | 0.83 | 92.43 | NA | m _b | 6.1 |
| 19/04/2012 | 1:20:07 | 0.54 | 92.39 | NA | m _B | 6.2 |
| 30/04/2012 | 8:00:10 | 1.76 | 89.6 | 10 | m _B | 6 |
| 2/5/2012 | 20:39:57 | -0.27 | 91.88 | NA | M _{wp} | 7.1 |
| 4/5/2012 | 16:23:44 | 2.01 | 89.68 | 15 | M _{Lv} | 6 |

| | | | | | | |
|------------|----------|-------|-------|----|-----------------|-----|
| 5/5/2012 | 12:08:44 | 4.81 | 87.91 | 10 | M _{wp} | 6 |
| 9/5/2012 | 5:09:13 | 4.92 | 87.77 | 10 | m _B | 6 |
| 9/5/2012 | 7:31:20 | 6.21 | 90.75 | 10 | m _B | 6.5 |
| 13/05/2012 | 1:19:10 | -3.35 | 89.42 | 12 | M _{wp} | 7.2 |
| 23/06/2012 | 21:27:30 | 2.63 | 90.51 | 16 | M _{Lv} | 6.3 |
| 28/10/2012 | 1:27:53 | 0.61 | 87.33 | 10 | m _B | 6 |

*from Stein and Okal (1978)

Royer and Gordon (1997) develop a further enhanced mechanism for understanding the intraplate tectonic behaviour of the subject region based on a comprehensive study of focal mechanisms of recorded events in the area (Figure 3.7-reproduced from Royer and Gordon, 1997). The study concludes the original single Indo-Australian plate has been trisected into individual rigid plates (Indian, Australian and Capricorn) forming three diffuse areas that act as plate boundaries between these component plates. Two of them, which are unconnected with each other, undergo horizontal stretching, while the remaining larger zone is subject to shortening, by accommodating plate divergence and convergence, respectively. The latter diffuse deformation that accommodates horizontal convergence due to thrust imposed by surrounding plates, induces active seismicity near the Ninetyeast ridge area. The diffuse convergence and the individual motions of component plates are estimated to have been since 11 Ma ago.

The identified diffuse area is located approximately 350-400 km away from the southern coast of the country, and therefore, needs to be emphasized in seismic hazard studies for Sri Lanka. The possible source area may be located much closer to the country than that specified in Figure 3.7, since several events with magnitude M_w 4.0-5.5 have occurred within about 300 km southeast of the coast. The largest oceanic intraplate earthquake ever recorded in the previous century, M_L 7.7, was reported on 9th March in 1928 about 875 km southeastwards of the country. On 11th April 2012, M_w 8.6 horizontal strike-slip event, which is the largest oceanic intraplate event ever recorded to date, struck again in the same region about 1340 km away from the country. On the same day, about 2 hours later, the next largest one M_w 8.2 erupted 185 km further southeast from the first one. Both of these events produced noticeable ground shakings at several places in the country including Colombo, and caused minor structural damages as well in some places. Two other strong events, M_L 7.0 in 1913 and M_L 7.2 in 1944, occurred in eastern side of the Chagos-Laccadive Ridge and western side of the Ninetyeast Ridge, respectively, tremorred many places of the country including both coastal (Colombo, Galle, Matara) and upland areas (Nuwara Eilya and Ratnapura). The most notable earthquake recently reported in the closest vicinity of the country is M_w 6.1 event on 2nd September 2001, which had the epicentre in the diffuse area just 600 km off the southern coast. Tremors were felt along the southeastern coastline and in some inland areas.

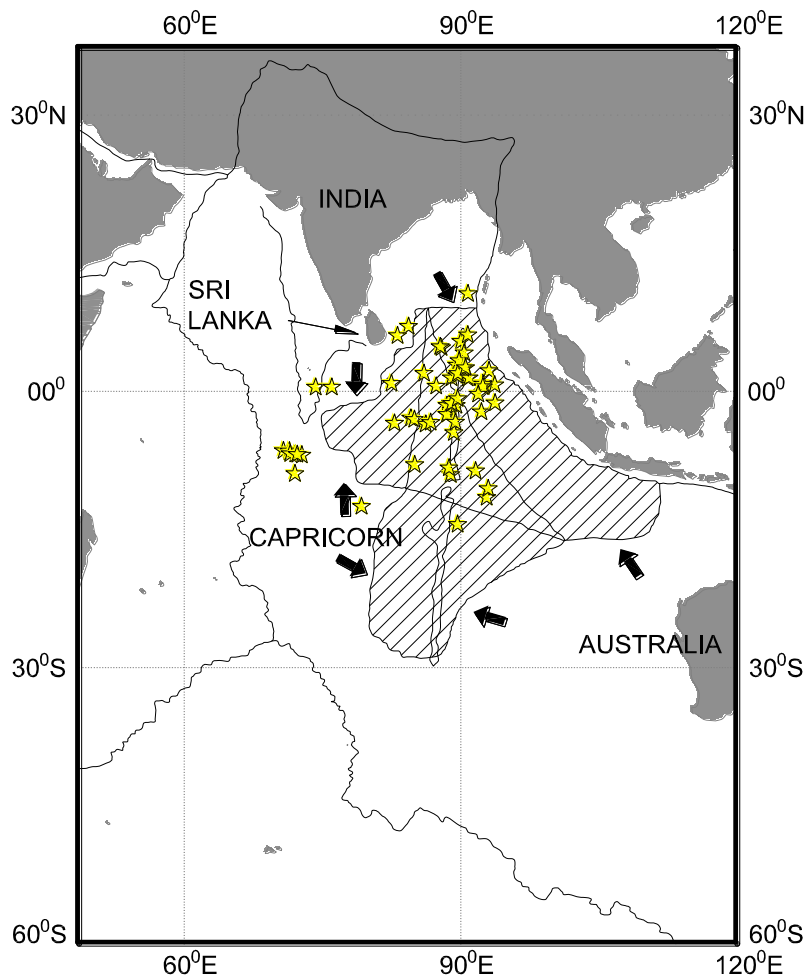


Figure 3.7 Large diffuse area (hatched) located amidst trisected Indo-Australian plate (Reproduced from Royer and Gordon, 1997). The diffuse deformation that accommodated horizontal convergence due to thrust imposed by surrounding plates, induces the active seismicity near the Ninetyeast ridge area. Stars denote epicentral locations of strong events given in Table 3.1. Areas undergoing horizontal stretching are not shown for clarity.

International archival data evidence on a number of events located around the 85°E Ridge in southern Bay of Bengal in the previous century. These events gave rise to minor and strong tremors in several parts of the country. Majority of the literature refers the 85°E Ridge to as an aseismic formation of having volcanic features in younger lithosphere that undergoes N-S oriented compression during the diffuse deformation (Bergman and Solomon, 1985; Liu et al., 1982). Nevertheless, a sufficient number of moderate and strong events have been generated along the ridge close to Sri Lanka, and have made major tremors especially in southeastern and central parts of the country (e.g., M_L 5.8 in 1973, M_L 6.5 in 1918).

Thus, given plenty of major seismic activities inherited, the possibility of occurrence of a large magnitude earthquake anywhere within the source area would be uncertain. For the purpose of hazard assessment, it is therefore appropriate to consider a uniform seismicity over the entire area

of source. Dissanayake (2005) for the first time cautions the local community about this newly identified broad seismic zone, and advise responsible authorities to take stringent measures which need to face any future seismic threat. Gamage et al (2011) implement the stochastic approach with estimated and approximated seismological factors for the region to simulate ground motions at Colombo and at Hambantota due to four hypothesized events (M_w 6.0, 7.0, 7.5 and 8.0) generated in the diffuse area. The study shows a PGV of about 22 and 14 cm/s, respectively, at Hambantota and Colombo due to a M_w 8.0 event simulated at about 350 km off the southern coast of Sri Lanka.

3.3.2 Seismicity west of Sri Lanka in the Laccadive Sea and Gulf of Mannar

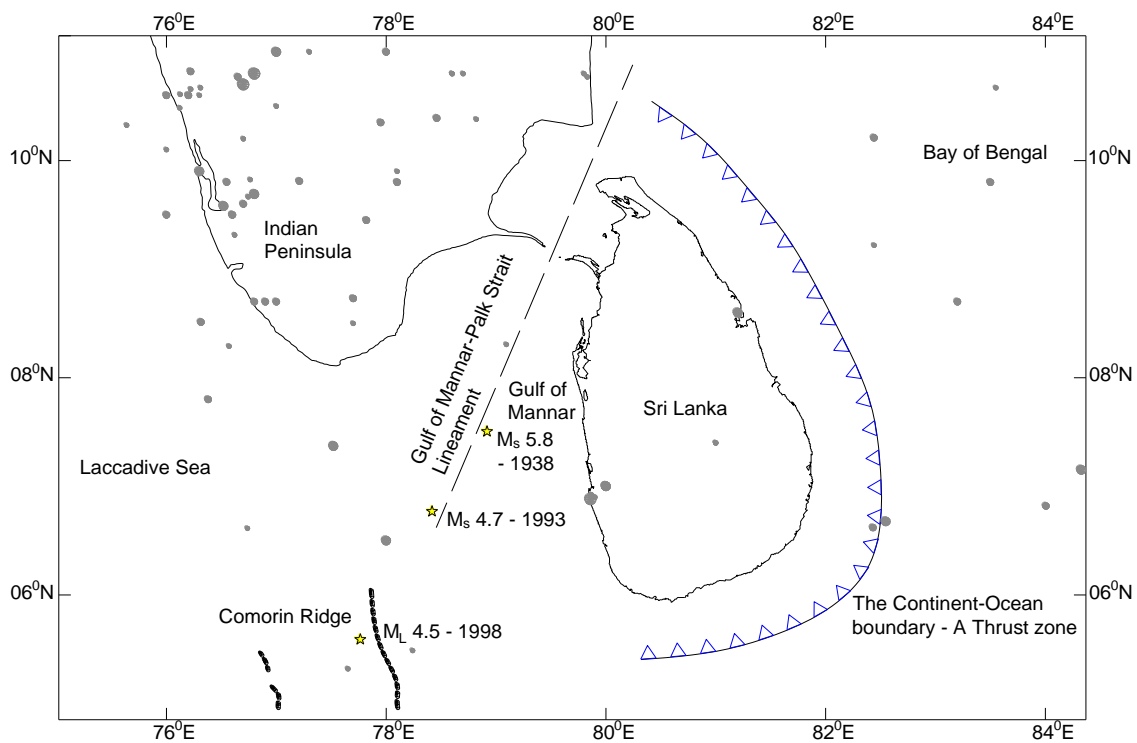


Figure 3.8 Seismicity in the Gulf of Mannar, southern Indian peninsula and in close proximity of Sri Lanka relating to the geotectonic setup. Some noticeable events are shown by stars.

The seismotectonic nature in the western Indian Ocean region (Figure 3.8) spanning between the western coastal line of Sri Lanka and the eastern banks of Chagos-Laccadive Ridge including the Laccadive Sea and the Gulf of Mannar, poses a moderate level of seismicity. The seismotectonic nature in the area would be important to take into account in seismological studies of Sri Lanka as well as of southern India. Evidence of past events in the region is worthy of mention; two moderate earthquakes M_s 4.7 in 1993 and M_s 5.8 in 1938 occurred in the Gulf of Mannar region at 170 and at 85 km away from the western coastline of the country, respectively. The events were felt in both coastal and inland areas, whilst, the second event caused significant shakings along the western coastline at places such as Colombo, Galle and Matara, and induced tremors as far as

central Kandy and Trincomalee (Martin and Szeliga, 2010). Non-structural damages including an injury were reported due to this event. The epicentral locations of the events are speculated to be aligned with the Gulf of Mannar-Palk Strait lineament (Vitanage, 1995). Two other recent events M_L 4.5 in 1998 and M_L 4.7 in 2011, reported along the Comorin Ridge, producing tremors again in the western and southwestern coastline. The active tectonic structures of the source area are obscure, but, Vestal and Lowrie (1982) identify two submarine slumps, namely “The Eastern Comorin” and “The Colombo”, in the southern sea bed of Gulf of Mannar region. Past evidence on the existence of large-scale landslides associated with these slumps, urges their capacity of producing some pronounced seismic activities in the region. Other tectonic features including volcanic eruptions, strong linear gravity lows and transform ridges can be correlated with seismic activities in the region, especially, towards the Comorin ridge and continent-ocean boundaries of India and Sri Lanka (Rana et al., 2008; Desa et al., 2006). In here, the continent-ocean boundary, which lies about a 250 km away from the southwest coast of Sri Lanka (Sreejith et al, 2008), is identified to be a possible source of seismic activities (Wijesundara, personal communication).

3.3.3 Seismicity north of Sri Lanka in the southern Indian peninsula region

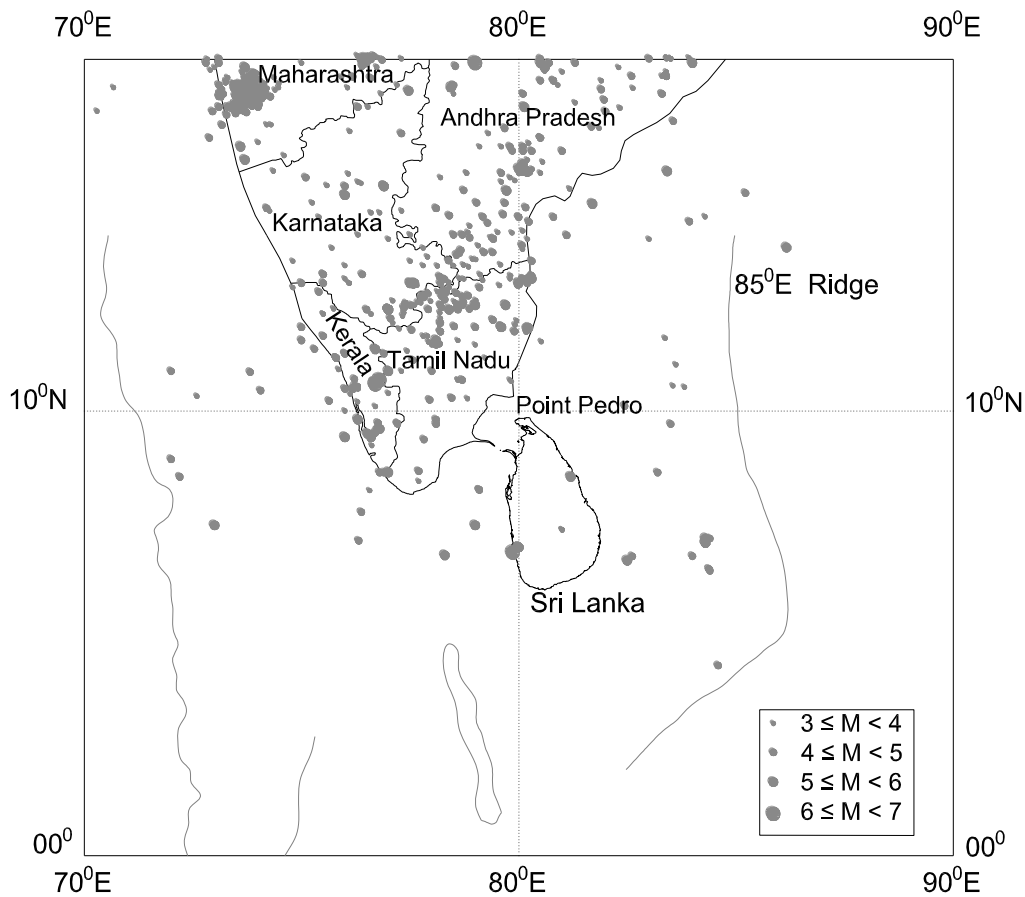


Figure 3.9 Seismicity in the southern peninsular India (most of the reported events in the surrounding oceanic crusts are not shown for clarity).

Seismicity in the Southern Indian peninsula region has rigorously been documented. The region covering Tamil Nadu, Kerala, Karnataka and Andhra Pradesh features small to moderate seismicity in the local context, yet, has not made any noticeable impact on Sri Lanka (Figure 3.9). The closest southern Indian territory-Tamil Nadu, separated by less than 30 km from Sri Lanka at Palk Strait, is generally considered aseismic with respect to the neighbouring territories. Nevertheless, some densely populated areas within the state such as Chennai and places at the border between Andhra Pradesh, have been classified into Zone III in the Indian Standard IS 1893 (Part 1-2002) to comply with a ground shaking intensity of VII in MSK (Medvedev–Sponheuer–Karnik) scale. Most of other places are categorized under Zone II. The adjoining state Kerala, which is exposed to the northern Laccadive Sea on its western side, is assigned into Zone III. Reported events in Tamil Nadu are confined to boundary areas with other territories such as Karnataka and Andhra Pradesh, and most of them are attributed to activities of local faults and lineaments (Gangrade and Arora, 2000). The recent major event M_w 5.5 occurred at Pondicherry in 2001, about 230 km northward of Point Pedro, did not exert any reported shaking in Sri Lanka. By referring to the regional geology and to the proximity, one would argue, Sri Lanka may also lie in a similar level of seismicity as such in the southern Indian peninsula region – more likely Tamil Nadu. However, the final seismicity of a particular place would depend on several factors including local geological variations (lineaments, faults), degree of exposure to surrounding seismic sources, adherence to seismic code of practices, etc.

When assessing the seismic risk for Sri Lanka, the northern Indian Ocean would be far more important to take into account than the peninsular India, though the proximity matters southern India the most. The difference in tectonic settings would be important to consider as the reason here. In the first place, Northern Indian Ocean is a thinner lithospheric crustal form of about 10 km in maximum thickness (CRUST2.0), that undergoes continuous internal deformations (as discussed in section 3.3.1), would result in a lesser wave attenuation in geometric spreading than that happens in a typical thicker continental crust such as the one of India. In the second place, the presence of some special tectonic features (such as discontinuities and barriers of the crust, younger sedimentary formations) between Sri Lanka and southern India, can be effective in such a way which leads rapid diminishing of generated seismic waves. Accordingly, a shallow earthquake occurred in the northern Indian Oceanic crust at a long distance would be more perceivable than a similar event that occurs in the continental Indian crust in close proximity. Furthermore, other distinctivenesses such as the higher rate of seismic release and the rapid recurrence of events, would emphasize the Indian Oceanic crust to be dominant in the regional context for seismic hazard investigations in Sri Lanka.

3.4 Summary and conclusion

A study in generic terms has been undertaken to identify possible seismic sources for Sri Lanka considering the country in the local context and in the regional context at teleseismic distances in the northern Indian Ocean. Seismic sources within the country are inferred based on a correlation of historical seismic activities reported within the country with the local geotectonic setup. The geological studies indicate the majority of Sri Lanka's basement crust consists with Crystalline rocks that were originated in the late Precambrian stage. The geological boundary between the HC and VC can be a potential tectonic boundary of convergence, where the HC thrusts over the VC in south and southeastern directions. This, along with reported seismic activities, motive Mahawelli shear zone enclosing the thrust zone near Mahiyanganaya at the boundary between the HC and VC, to be formulated as one of possible seismic zones within the country. As evidenced clearly by the historical seismicity, the area close to the capital city-Colombo would pursue to be the most critical zone in the local context. Seismicity in the regional context is studied separating the surrounding region into sub-areas, i.e., northern Indian Ocean south of Sri Lanka and Bay of Bengal, Laccadive sea and Gulf of Mannar region, and the southern Indian peninsula region. The northern Indian Ocean south of Sri Lanka and southern Bay of Bengal would be far more important than other two owing to higher rate of seismic activities and distinctive seismotectonic nature. This oceanic crust towards south and southeast directions close to the Ninetyeast ridge, is identified as one of the most active intraplate oceanic crusts on the globe, and hails a prime concern in the regional context, to be taken into account in hazard assessments for Sri Lanka.

4. Attenuation parameters for regional earthquakes in the northern Indian Ocean – Derivation of Q value and H/V ratio

4.1 Introduction

Attenuation of ground motion amplitudes away from the seismic source (i.e., at far-field) is recognised as a significant issue by researchers. Of particular interest is the attenuation of seismic waves propagating from long distant sources. Regions like Sri Lanka have experienced noticeable tremors even from events as far as 1500 km, e.g., accelerograms recorded at Palkeleke rock broadband station produce horizontal PGA of the order of about 15 and 3 mm/s² for recent (11th April 2012) M_w 8.6 and 8.2 distant events, respectively. Although these values appear to be low, ground motions recorded on rock can further be accentuated several times by subsoil strata seated on the rock crust. A recently identified diffuse plate boundary just around 350-400 km away from the southern tip of Sri Lanka (discussed in Chapter 3) emerges as a considerable seismic risk to the country. There are significant amounts of moderate and strong shallow focus intraplate earthquakes generated due to internal deformations of the subject region especially in the oceanic crust towards southeastern direction close to Ninety and Eighty-five east ridges (Figures 3.5 and 3.6). This indicates that the seismic hazard studies related to Sri Lanka, must include both the effects of large magnitude - distant earthquakes as well as the intraplate activities of moderate earthquakes with distance considerations of about 300 km in addition to possible local intraplate earthquakes within the mainland. However, a comprehensive study of the region with respect to the propagation or attenuation of seismic waves has generally been lacking. Recognising the need to understand the attenuation characteristics of the region, in this Chapter (and also in the next Chapter) an effort to study the wave transmission characteristics is undertaken as it is an important step towards quantifying the potential seismic hazard from distant earthquakes.

This Chapter involves a data analysis to estimate the Q value of the northern Indian Oceanic crust surrounding Sri Lanka by analysing 181 digital broadband vertical component records of 71 intraplate earthquakes. The average effect of the upper crustal amplification of Sri Lanka has been assessed using the standard H/V ratio method. Preliminary estimations of average source spectra of events have also been done and compared with theoretical Brune's spectra for a selected stress drop value. The findings have further been verified by matching real records of M_w 8.6 mega event occurred on 11th April 2012, with stochastically simulated seismograms using parameters derived from the analysis. The study is oriented mainly on deriving a reliable

Q value for characterizing anelastic attenuations of the regional events of the northern Indian Ocean region. Q known as the wave transmission quality factor (described in section 2.3.3 in Chapter 2), which is a measure of the quality of the crust in terms of wave propagation characteristics, is an important seismological parameter of distant events since attenuations of those distant events are primarily governed by anelastic (or intrinsic) effects along the wave travelling paths.

4.2 Database sampling and processing procedure

4.2.1 Database sampling

Geological Survey and Mines Bureau in Sri Lanka, in collaboration with USGS and German Research Centre for Geosciences (also known as GFZ-GEOFON), is responsible for maintaining 3 broadband seismic stations located at Pallekele (PALK), Hakmana (HALK) and Mahakanadarawa (MALK) rock sites. While PALK station (with USGS) has been operating since 2000, the other two had been established in 2011 under GEOFON permanent network. Digital waveforms of recorded events at the above stations are available to download from their respective data management system, i.e., IRIS (Incorporated Research Institutions for Seismology) data management centre for PALK and GFZ seismological data archive for HALK and MALK. 181 such records of 71 shallow crustal earthquakes magnitude ranging from 4.0 to 5.9 in short period body wave magnitude scale (m_b), have been downloaded and processed for further analysis (Refer Figure 4.1 and for a detailed list of events refer Appendix B).

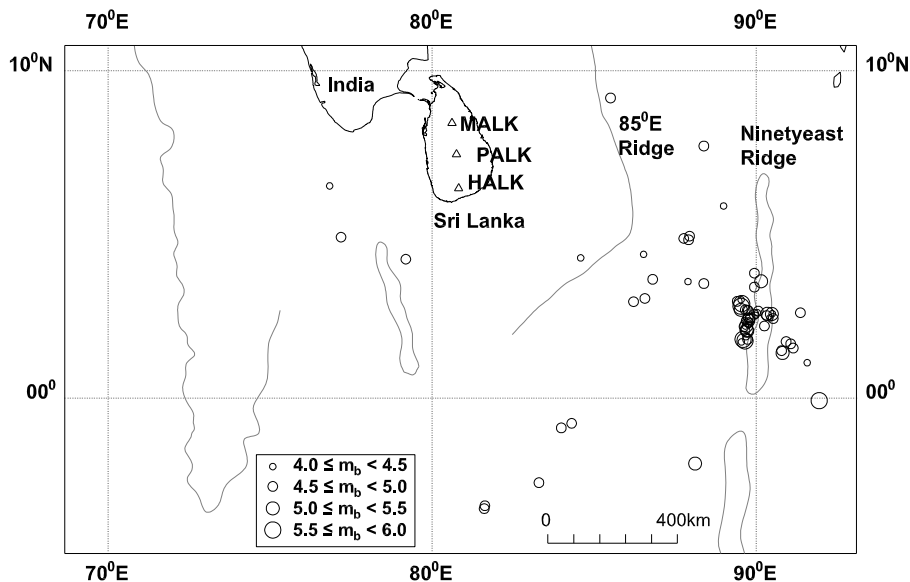


Figure 4.1 Recorded events (circles) used in the study for deriving the regional Q and assessing H/V ratio calculations (Sources; ISC-UK, GEOFON-Germany and ANSS-USA). Triangles denote broadband stations at Pallekele (PALK), Hakmana (HALK) and Mahakanadarawa (MALK).

Distribution of data in magnitude-hypocentral distance is presented as a dot plot in Figure 4.2. Location and magnitude data of older events (events before 2010) which represent about 17% of the total are directly obtained from “Reviewed ISC bulletin”, whereas those of newer events (about 83% of the total) are taken from GEOFON and ANSS data archives depending on the availability of the event in the respective data archive. The data archives assign short period body wave magnitude as the common scale. Therefore this magnitude parameter is chosen for regression analysis to ensure consistency. Epicentral distance varies from 2.3^0 (260 km) to 14.1^0 (1578 km) for the whole dataset. The database consists of a large number of records from aftershocks of the aforementioned M_w 8.6 earthquake, and this in turn strengthen the dataset by increasing the original sample size. Magnitude and location uncertainties, if any, are omitted in all newer records even though it is presumed that an uncertainty associated with the distance alone may not produce any notable deviations in the final results in the case of long-distant earthquakes. After removing random outliers (discussed under “4.5 Results and discussion”) identified in the database, original records and events dropped down to 162 and 62, respectively. Thus the quality of data sampling has been ensured.

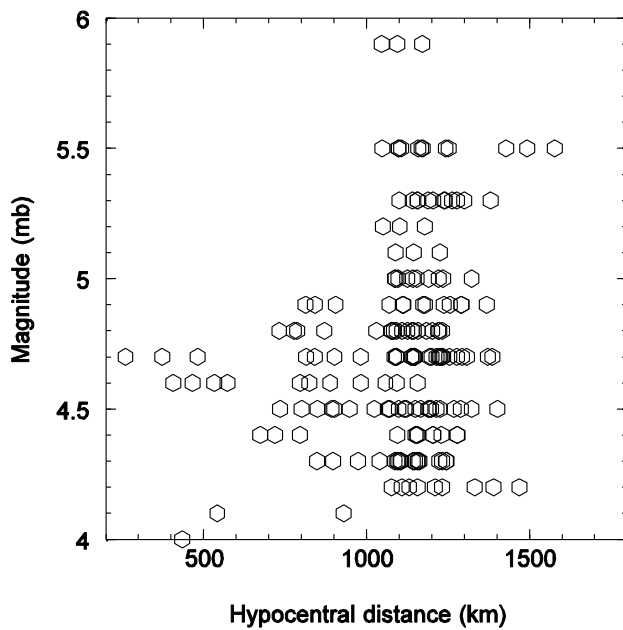


Figure 4.2 Distribution of the dataset in magnitude (m_b) and hypocentral distance space. Magnitude ranges from m_b 4.0 to 5.9, whereas hypocentral distance varies between 260 and 1578 km.

4.2.2 Processing procedure

Broadband High-Gain vertical component data (BHZ) are selected in each of the waveform record. At PALK rock site, since there are two seismometers installed at two different depths (one at 1 m and the other at 90 m depth), vertical components corresponding to upper one (at 1

m depth) are selected to be compatible with records at other two sites. Horizontal components are not considered in the regression analysis as they would be susceptible to inherent local site amplifications that can be quite significant (sometimes) at high frequencies and may result in extensive spatial variations. However, the horizontal motion has been taken into account in the H/V calculations as described in section 4.4 of the Chapter. Vertical motion is said to be less affected by near-source upper crustal modifications (in terms of attenuation and amplification) offsetting any decay in wave propagation velocity with refracted waves travelling in the vertical direction (Atkinson, 2004b). Selected vertical components are bandpass filtered between 0.1 – 9.0 Hz frequencies after applying tapering of 10% at both ends of the each trace. This also covers the range of natural periods of engineering significance (between 0.1 sec and 10 sec). The maximum frequency 9.0 Hz is selected in such a way that the maximum frequency limit should be less than half of the sample rate of the instrument (Havskov and Ottemoller, 2012). In the current case they are 40, 20 and 20 sps (samples per second) for seismometers at PALK, HALK and MALK, respectively. Next, filtered traces are corrected for instrument effects to produce acceleration time histories. Fourier Acceleration Spectra (FAS) of each processed record are obtained by selecting the “shear/strong window” containing the multiple reflected and refracted *S* phases. FAS are visually inspected for signal strength relative to the background noise spectra and amplitudes of frequencies at 0.1, 0.2 and 0.3 Hz are left out owing to low frequency noise amplifications. FAS are smoothed for the selected whole frequency range at 0.1 log frequency bins by introducing a box/rectangular weighting function and thus taking the geometric average of amplitudes in each frequency bin. This frequency dependent smoothing (due to constant width in log frequency) allows uniform smoothing of amplitudes over the entire frequency range in the log frequency scale and is considered to be more desirable for regression analysis due to reductions in noise. Box weighting smoothing has been shown to produce little scatter at low frequencies with respect to other smoothing options (such as triangular weighting) although Boore (2012) notes the effect can be negligible in the final results. Acceleration amplitudes of smoothed spectra in each vertical record are then tabulated in 0.1 frequency increments for the selected frequency range. A processed sample accelerogram with respective FAS are shown in Figure 4.3.

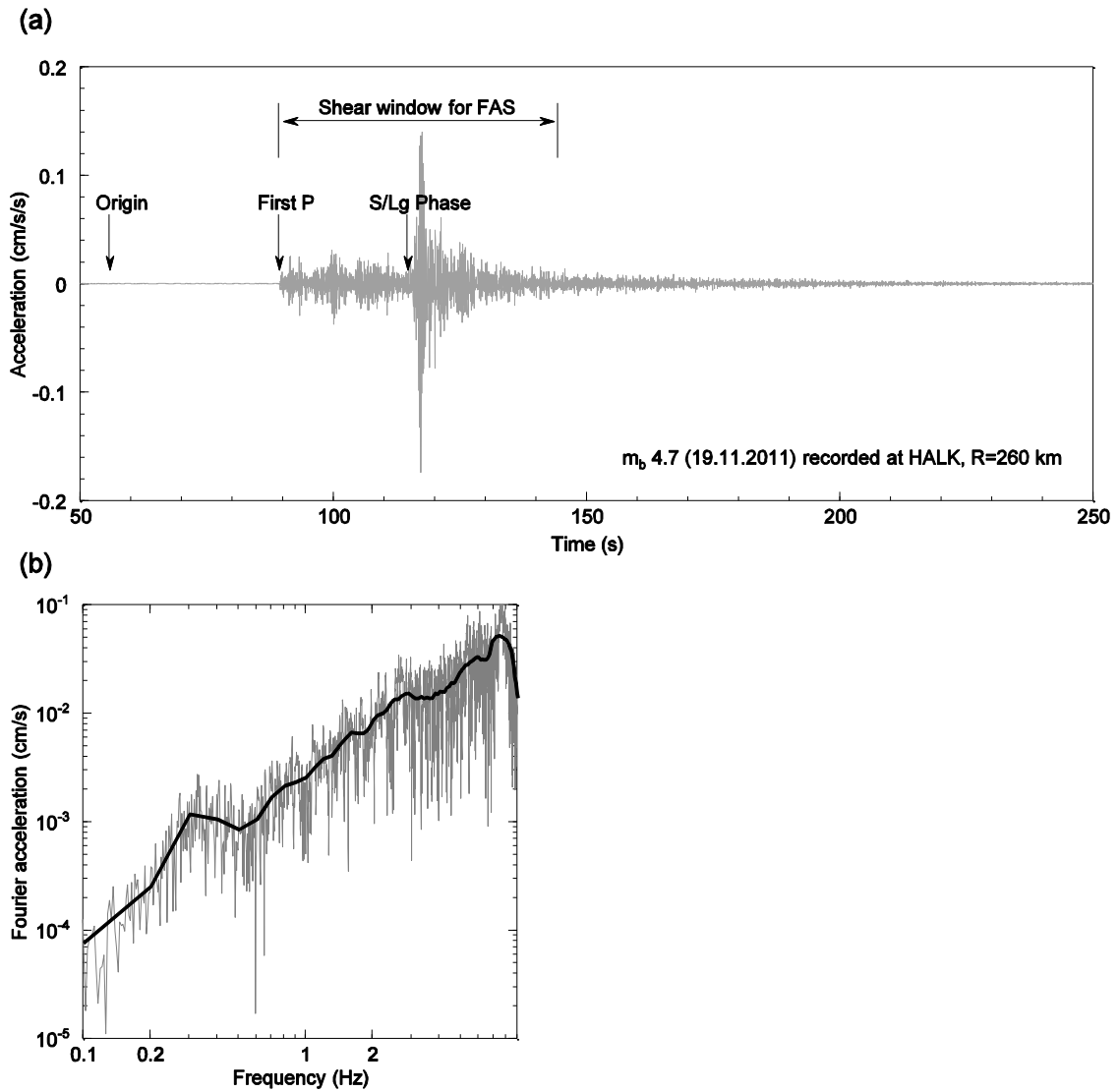


Figure 4.3 Data processing: (a) A sample acceleration time history produced after filtering (between 0.1-9.0 Hz), tapering (10% at both ends) and correcting for instrument. Main phases along with the shear/strong window to be used for Fourier Acceleration Spectra (FAS) are also shown. (b) FAS of the record in (a). Dark line represents the smoothed spectrum (smoothing method is described in the text).

4.3 Regression analysis for Q value

The following well-established attenuation model (Atkinson and Mereu, 1992) is fitted with observed Fourier amplitudes by using the multiple linear regression technique. Regression analysis was undertaken in MS Excel. Note that, local site amplification term has been omitted since all recordings are on rock sites.

$$[A_x(f)]_{ij} = [S(f)]_i \cdot G \cdot A_n(f) \quad (4.1)$$

Where, $[A_x(f)]_{ij}$ is the acceleration amplitude of Fourier spectra at j^{th} station due to i^{th} event for a given frequency f . $[S(f)]_i$ is the acceleration amplitude of Fourier spectra of i^{th} event at the source for a given frequency f . G and $A_n(f)$ are, respectively, geometric attenuation factor and anelastic whole path attenuation factor, having with following relations;

$$\begin{aligned}
 G &= \frac{R_0}{R} && \text{for } R \leq 1.5D \\
 G &= \frac{R_0}{1.5D} && \text{for } 1.5D < R \leq 2.5D \\
 G &= \frac{R_0}{1.5D} \sqrt{\frac{2.5D}{R}} && \text{for } R > 2.5D
 \end{aligned} \tag{4.2}$$

$$A_n(f) = \exp[-\pi fR/Q\beta] \tag{4.3}$$

Here, D , R , f , Q and β are crustal thickness, epicentral distance, wave frequency, wave transmission quality factor, and shear wave velocity at the source region, respectively. R_0 , the reference distance, is equal to 1 km. Geometric damping or spreading parameter given in equation (4.2) for distant earthquakes accounts for attenuation of seismic waves at R^{-1} rate up to $1.5D$ distance due to spherical spreading of direct waves near the source area, zero attenuation between $1.5D$ and $2.5D$ due to compensatory effect of post-critical reflections and refractions from Moho and Conrad discontinuities and $R^{-0.5}$ rate cylindrical attenuation after $2.5D$ due to multiple reflection and refraction of body waves dominating L_g phase in the shear window of the trace (Lam et al, 2000a; 2000b; 2000c). However, there is a general agreement that, unlike in continental crusts, L_g is not effective or totally absent to traverse in a thinner oceanic crust due to incompatibility associated with the wave field and seismic structure which governs physical features such as thickness and composition, i.e., presence of sediments (Knopoff et al, 1979; Kennett, 1985; 1986; Zhang and Lay, 1995). In light of this argument, it is refrained to relate the estimated Q value in this study as $L_g Q$, since all the dominant wave paths in the region are through a thinner oceanic crust spanning thousands of kilometres in size. Empirical studies based on recorded data analysis generally indicate fixed distance ranges for the geometric attenuation function, rather than distance ranges based on crustal thickness as denoted above. For instance, Atkinson (2004b) derives 70 and 140 km as best fitting hinge points for the geometric attenuation of southeastern Canadian region. Perhaps the values may show a reasonable consistency with the average crustal thickness of the region (40-50 km) especially for shallow crustal earthquakes. However, the applicability of equation (4.2) to account for geometric damping has been verified in numerous intraplate crustal regions (Lam et al, 2000b; 2009; Wilson and Lam, 2003). In some cases more rapid attenuation instead of R^{-1} near the source region (Atkinson, 2004b; Sonley and Atkinson, 2006) and negative attenuation instead of

zero attenuation (Atkinson, 2004b) have been reported for stable intraplate regions such as southeastern Canada. In the present study, spreading parameters are retained the same as denoted in equation (4.2) to be consistent with other typical stable regions like Australia, Hong Kong and Singapore. Furthermore, uncertainties exist about the exact spreading rate of near-source attenuation for the subject region owing to lack of near-field records and thereby the rate accounted in equation (4.2) is more relied for the study. However, please note that a more reliable form of G for the northern Indian Ocean region is later derived using a separate spectral analysis which is described in Chapter 5. Crustal thicknesses, D values, near the source areas in the oceanic crust in the subject region are determined using the global crustal model called CRUST2.0 in which average crustal thicknesses all over the world are compiled to represent in $2^0 \times 2^0$ tiles. A value of 10 km is inferred for most of the parts in northern Indian Oceanic crust by referring to the data from CRUST2.0 and this value is also consistent with the hypocentral depth values given in catalogues in the database.

Equation (4.3) denotes attenuation of waves as a result of energy dissipation along the whole travel path during wave propagation through the rock medium. This energy dissipation entails heating of the heterogeneous medium and rearrangement/dislocation of particles during vibration of the medium, which are considered as permanent losses of energy. Moreover, whole path attenuation or seismic absorption depends on wave frequency in a manner in which high frequency waves are diminishing more rapidly than low frequency waves and hence the decaying has an exponential form, as noted in equation (4.3). The reason may be explained by comparing the situation with frequency dependent amplitude decaying nature of wave motion in an elastic medium due to viscous damping, in which decaying rate increases with the number of wave cycles in a unit length (frequency). Importantly, whole path attenuation can be dominant in distance earthquakes in which the amount of attenuation largely depends on the crustal quality of the travelled medium. If quality of the rock is high, the wave propagation is good and vice versa. Hence, the wave transmission quality of the rock, parameterized as Q (or, Q_0 equals to Q at 1 Hz frequency), is a key parameter to be estimated correctly for long-distant events i.e., for regions like Sri Lanka.

$[S(f)]_i$, which denotes FAS at the source for a given frequency, depends significantly on the energy release i.e., seismic moment/magnitude of the event and the typical stress drop level ($\Delta\sigma$) of the subject region which can generally be considered to remain independent of the magnitude of the event, except for smaller magnitudes ($M_w < 4.3$) in which $\Delta\sigma$ has shown an increasing trend with the magnitude (Atkinson, 2004b). Furthermore, stable continental regions have shown comparably higher stress drop values associated with hard rock conditions, than that of active regions located close to plate boundaries or subduction zones (Chen and Atkinson,

2002; Castro et al, 1990). During the regression analysis the magnitude dependency (which comes through the source term) of observed FAS at the recorded station has been nullified by employing an assumed second order polynomial relationship between the source term and the magnitude which is shown in equation (4.4).

$$\log[S(f)]_i = C_1(M - 4)^2 + C_2(M - 4) + C_3 \quad (4.4)$$

where M is the magnitude in m_b and C_1 to C_3 are constants to be determined from the regression. Equation (4.4) decouples magnitude dependency of the regression equation and hence enables to perform the analysis for the whole dataset simultaneously over the entire magnitude range without the need to calculate for each magnitude separately (Joyner and Boore, 1981; Atkinson, 2004b). Besides, this decoupling technique is advantageous, since it minimizes errors in regression coefficients which can arise due to magnitude uncertainties associated especially with newer events, and it also curtails the total number of analysis steps of the regression process. Substituting terms of equations (4.2), (4.3) and (4.4) in (4.1) and taking logarithms give the following attenuation equation for regressions;

$$\log[A_x(f)]_{ij} = C_1(M - 4)^2 + C_2(M - 4) + C_3 - \log[1.5D] - 0.5 \log\left[\frac{R}{2.5D}\right] - \left[\frac{\pi f \log e}{Q\beta}\right]R \quad (4.5)$$

4.4 H/V ratio

In the above attenuation model, wave modifications at the upper crustal level in terms of attenuations and amplifications have been neglected. The reason is collated based on the consideration of the underlying rock stratigraphy in the region. A number of sources indicate, as discussed in Chapter 3, that more than 90% of Sri Lanka's upper crustal rock layer consists of Crystalline rocks of Precambrian age in which the age can be as old as about 2000 Ma (Kroner and Brown, 2005; Cooray, 1994). Therefore, wave propagation in the upper 3-4 km would be less affected by modifications caused due to poor rock quality characteristics as in the case of younger Sedimentary rocks. This can further be explored by using the standard H/V ratio method. H/V ratio, for a given site, is termed as a measure of the net amplification of seismic waves which arises due to poor quality rock characteristics that exist mostly at the upper crustal level during wave travel. Horizontal wave component gets modified during wave propagation whereas the vertical component is considered to remain almost the same as that at the source where it originated (as aforementioned). Further, both of these components are treated to have the same amplitude at the source, so that the H/V ratio would give the net amplification of the horizontal wave component incurred due to loss of propagation velocity throughout its entire journey from source to rock/soil outcrop (Lermo and Chavez-Garcia, 1993). In many cases, the effect is critical only at upper crustal levels and can be neglected at mid and deeper levels of the

crust at places where good quality much older rocks exist. Therefore, the H/V ratio denotes a local or a near-surface effect which would represent the wave propagation quality of the underlying rock at upper 3-4 km. The ratio should initially enclose the combined effect of the upper crustal amplification plus the attenuation which is parameterized by “Kappa (K)”, though the latter attenuation can be cancelled each other in the equation [see equation (4.6)] for horizontal and vertical motions given a constant Kappa in either case. Nevertheless, studies have also shown that the anelastic wave attenuation can be significant at upper crustal levels associated especially with relatively young rocks i.e., places such as California-USA (Abercrombie, 1997) and Victoria-Australia (Wilkie and Gibson, 1995). However, the H/V ratio in the study would be assumed to merely represent the “amplification effect” of seismic waves at the upper crustal level due to the constant “Kappa” assumed in each case. Following relationship is used in calculating the frequency dependent H/V values;

$$\log(H / V) = \log \frac{\sqrt{H_1 H_2}}{V} \quad (4.6)$$

Here, H_1 and H_2 are recorded horizontal amplitudes at two orthogonal directions and V is the amplitude recorded in vertical direction. During the current study, H/V is estimated using a total 125 records that are averaged at each station to find the average site effect, and finally are averaged for all stations to find the overall effect as well. The average shear wave velocity of source regions within the oceanic crust is taken as 3.9 km/s based on CRUST2.0 data.

Results of the multiple linear regressions, estimated Q values and H/V ratio are discussed in the next section.

4.5 Results and discussion

Coefficients C_1 through to C_3 and Q values at each 0.1 frequency increment for the whole frequency range of 0.4 to 9.0 Hz have been determined by regression analysis. Estimated regression coefficients have further been refined by removing random outliers identified in the original sample. This lead to increase conformity of the regression analysis resulting in lower standard errors and higher correlations. The outliers are believed to exist as a result of epistemic uncertainties such as poor and/or too strong recordings or may be due to noise amplification (particularly at high and low frequencies), technical defects and/or due to any other unknown reason. Outliers are identified on the basis of standardized residual value of log amplitudes (between actual and predicted) being greater than 3.0. This in turn help to improve coefficients of determination (R^2) at least as close to 70% and to keep residual sum of squares [SS(Resi)] less than 10. However a numerically distant observation cannot always be classified as an outlier unless extenuating reasons exist. Estimated values for certain selected frequencies along

with their respective coefficients of determination and Standard Error of Estimates (σ_{est}) are tabulated in Table 4.1.

Table 4.1 Regression coefficients (C_1, C_2, C_3 and $C_4 = \pi f \log e / (Q\beta)$) of equation (4.5)

| Frequency (Hz) | Regression coefficients | | | | R^2 | σ_{est} | SS(Resi) | Q^* |
|-------------------|-------------------------|--------|--------|---------|-------|----------------|----------|-------|
| | C_1 | C_2 | C_3 | C_4 | | | | |
| 0.4 | 0.580 | -0.261 | -0.848 | -0.0006 | 0.64 | 0.25 | 9.69 | 234 |
| 0.5 | 0.545 | -0.121 | -0.890 | -0.0007 | 0.72 | 0.22 | 7.87 | 269 |
| 0.6 | 0.496 | 0.012 | -0.863 | -0.0007 | 0.77 | 0.20 | 6.50 | 298 |
| 0.7 | 0.407 | 0.167 | -0.865 | -0.0007 | 0.73 | 0.23 | 8.05 | 346 |
| 0.8 | 0.350 | 0.305 | -0.765 | -0.0008 | 0.75 | 0.22 | 7.60 | 347 |
| 0.9 | 0.363 | 0.293 | -0.627 | -0.0009 | 0.77 | 0.21 | 7.13 | 350 |
| 1 | 0.369 | 0.250 | -0.540 | -0.0009 | 0.75 | 0.22 | 7.62 | 373 |
| 1.1 | 0.360 | 0.226 | -0.504 | -0.0009 | 0.73 | 0.23 | 8.00 | 418 |
| 1.2 | 0.358 | 0.188 | -0.456 | -0.0009 | 0.70 | 0.23 | 8.47 | 461 |
| 1.3 | 0.334 | 0.209 | -0.411 | -0.0009 | 0.69 | 0.23 | 8.39 | 487 |
| 1.4 | 0.320 | 0.223 | -0.365 | -0.0010 | 0.70 | 0.23 | 8.12 | 511 |
| 1.5 | 0.329 | 0.225 | -0.305 | -0.0010 | 0.72 | 0.22 | 7.92 | 523 |
| 1.6 | 0.342 | 0.209 | -0.245 | -0.0010 | 0.73 | 0.22 | 7.44 | 552 |
| 1.7 | 0.334 | 0.225 | -0.184 | -0.0010 | 0.74 | 0.22 | 7.34 | 572 |
| 1.8 | 0.324 | 0.234 | -0.127 | -0.0011 | 0.75 | 0.21 | 7.11 | 580 |
| 1.9 | 0.292 | 0.276 | -0.108 | -0.0011 | 0.74 | 0.21 | 7.08 | 603 |
| 2 | 0.279 | 0.289 | -0.075 | -0.0011 | 0.75 | 0.21 | 6.78 | 611 |
| 2.1 | 0.295 | 0.250 | -0.052 | -0.0012 | 0.76 | 0.20 | 6.47 | 627 |
| 2.2 | 0.301 | 0.240 | -0.044 | -0.0012 | 0.76 | 0.20 | 6.50 | 647 |
| 2.3 | 0.296 | 0.236 | -0.043 | -0.0012 | 0.75 | 0.21 | 6.77 | 676 |
| 2.4 | 0.283 | 0.255 | -0.022 | -0.0012 | 0.74 | 0.21 | 7.02 | 692 |
| 2.5 | 0.262 | 0.278 | -0.016 | -0.0012 | 0.73 | 0.21 | 7.26 | 723 |
| 2.6 | 0.252 | 0.273 | 0.004 | -0.0012 | 0.72 | 0.22 | 7.31 | 754 |
| 2.7 | 0.253 | 0.255 | 0.038 | -0.0012 | 0.72 | 0.21 | 7.30 | 780 |
| 2.8 | 0.259 | 0.234 | 0.061 | -0.0012 | 0.72 | 0.21 | 7.08 | 801 |
| 2.9 | 0.269 | 0.209 | 0.072 | -0.0012 | 0.73 | 0.21 | 6.92 | 828 |
| 3 | 0.278 | 0.179 | 0.101 | -0.0012 | 0.73 | 0.21 | 6.70 | 847 |
| 3.1 | 0.300 | 0.130 | 0.133 | -0.0013 | 0.73 | 0.20 | 6.61 | 866 |
| 3.2 | 0.317 | 0.096 | 0.157 | -0.0013 | 0.73 | 0.21 | 6.69 | 884 |
| 3.3 | 0.315 | 0.094 | 0.189 | -0.0013 | 0.73 | 0.21 | 6.91 | 890 |
| 3.4 | 0.321 | 0.081 | 0.212 | -0.0013 | 0.72 | 0.21 | 7.16 | 904 |
| 3.5 | 0.318 | 0.078 | 0.239 | -0.0013 | 0.72 | 0.22 | 7.36 | 915 |
| 3.6 | 0.329 | 0.044 | 0.272 | -0.0014 | 0.71 | 0.22 | 7.54 | 932 |
| 3.7 | 0.334 | 0.025 | 0.277 | -0.0013 | 0.71 | 0.22 | 7.70 | 961 |
| 3.8 | 0.345 | -0.004 | 0.298 | -0.0014 | 0.71 | 0.22 | 7.63 | 982 |
| 3.9 | 0.351 | -0.016 | 0.314 | -0.0014 | 0.71 | 0.22 | 7.76 | 999 |
| 4 | 0.356 | -0.031 | 0.333 | -0.0014 | 0.71 | 0.22 | 7.78 | 1015 |
| 4.1 | 0.357 | -0.043 | 0.330 | -0.0014 | 0.71 | 0.22 | 7.59 | 1046 |
| 4.2 | 0.377 | -0.089 | 0.345 | -0.0014 | 0.70 | 0.22 | 7.64 | 1073 |

| | | | | | | | | |
|-----|-------|--------|-------|---------|------|------|------|------|
| 4.3 | 0.390 | -0.122 | 0.360 | -0.0014 | 0.71 | 0.22 | 7.38 | 1098 |
| 4.4 | 0.401 | -0.150 | 0.371 | -0.0014 | 0.71 | 0.22 | 7.42 | 1123 |
| 4.5 | 0.399 | -0.154 | 0.378 | -0.0014 | 0.70 | 0.22 | 7.43 | 1148 |
| 4.6 | 0.413 | -0.182 | 0.405 | -0.0014 | 0.70 | 0.22 | 7.52 | 1161 |
| 4.7 | 0.417 | -0.186 | 0.427 | -0.0014 | 0.71 | 0.22 | 7.57 | 1171 |
| 4.8 | 0.419 | -0.192 | 0.441 | -0.0014 | 0.71 | 0.22 | 7.56 | 1188 |
| 4.9 | 0.426 | -0.212 | 0.452 | -0.0014 | 0.71 | 0.22 | 7.57 | 1214 |
| 5 | 0.427 | -0.217 | 0.464 | -0.0014 | 0.71 | 0.22 | 7.53 | 1231 |
| 5.1 | 0.431 | -0.220 | 0.486 | -0.0014 | 0.72 | 0.22 | 7.49 | 1239 |
| 5.2 | 0.432 | -0.219 | 0.504 | -0.0015 | 0.72 | 0.22 | 7.34 | 1248 |
| 5.3 | 0.429 | -0.213 | 0.512 | -0.0015 | 0.73 | 0.21 | 7.26 | 1263 |
| 5.4 | 0.421 | -0.200 | 0.530 | -0.0015 | 0.73 | 0.22 | 7.39 | 1270 |
| 5.5 | 0.415 | -0.192 | 0.539 | -0.0015 | 0.73 | 0.22 | 7.38 | 1286 |
| 5.6 | 0.410 | -0.179 | 0.549 | -0.0015 | 0.73 | 0.21 | 7.28 | 1298 |
| 5.7 | 0.401 | -0.159 | 0.552 | -0.0015 | 0.74 | 0.21 | 7.18 | 1312 |
| 5.8 | 0.390 | -0.139 | 0.561 | -0.0015 | 0.74 | 0.21 | 6.98 | 1324 |
| 5.9 | 0.390 | -0.141 | 0.578 | -0.0015 | 0.75 | 0.21 | 6.80 | 1336 |
| 6 | 0.396 | -0.154 | 0.598 | -0.0016 | 0.75 | 0.21 | 6.74 | 1349 |
| 6.1 | 0.385 | -0.137 | 0.600 | -0.0016 | 0.76 | 0.20 | 6.62 | 1365 |
| 6.2 | 0.384 | -0.130 | 0.616 | -0.0016 | 0.77 | 0.20 | 6.49 | 1372 |
| 6.3 | 0.383 | -0.130 | 0.630 | -0.0016 | 0.77 | 0.20 | 6.47 | 1385 |
| 6.4 | 0.386 | -0.138 | 0.645 | -0.0016 | 0.77 | 0.20 | 6.44 | 1399 |
| 6.5 | 0.388 | -0.143 | 0.656 | -0.0016 | 0.77 | 0.20 | 6.51 | 1415 |
| 6.6 | 0.387 | -0.142 | 0.668 | -0.0016 | 0.77 | 0.20 | 6.48 | 1427 |
| 6.7 | 0.387 | -0.139 | 0.673 | -0.0016 | 0.77 | 0.20 | 6.39 | 1444 |
| 6.8 | 0.387 | -0.135 | 0.685 | -0.0016 | 0.78 | 0.20 | 6.27 | 1453 |
| 6.9 | 0.393 | -0.147 | 0.704 | -0.0016 | 0.78 | 0.20 | 6.24 | 1463 |
| 7 | 0.401 | -0.161 | 0.717 | -0.0017 | 0.78 | 0.20 | 6.25 | 1478 |
| 7.1 | 0.409 | -0.177 | 0.727 | -0.0017 | 0.79 | 0.20 | 6.24 | 1496 |
| 7.2 | 0.420 | -0.195 | 0.737 | -0.0017 | 0.79 | 0.20 | 6.21 | 1513 |
| 7.3 | 0.429 | -0.212 | 0.750 | -0.0017 | 0.79 | 0.20 | 6.24 | 1524 |
| 7.4 | 0.438 | -0.228 | 0.756 | -0.0017 | 0.79 | 0.20 | 6.29 | 1542 |
| 7.5 | 0.446 | -0.244 | 0.752 | -0.0017 | 0.79 | 0.20 | 6.26 | 1566 |
| 7.6 | 0.458 | -0.266 | 0.763 | -0.0017 | 0.79 | 0.20 | 6.22 | 1579 |
| 7.7 | 0.464 | -0.278 | 0.761 | -0.0017 | 0.79 | 0.20 | 6.22 | 1598 |
| 7.8 | 0.476 | -0.302 | 0.760 | -0.0017 | 0.79 | 0.20 | 6.15 | 1619 |
| 7.9 | 0.481 | -0.313 | 0.755 | -0.0017 | 0.80 | 0.20 | 6.08 | 1636 |
| 8 | 0.491 | -0.331 | 0.750 | -0.0017 | 0.80 | 0.20 | 6.01 | 1653 |
| 8.1 | 0.495 | -0.341 | 0.731 | -0.0017 | 0.80 | 0.19 | 5.89 | 1677 |
| 8.2 | 0.504 | -0.361 | 0.723 | -0.0017 | 0.80 | 0.19 | 5.89 | 1694 |
| 8.3 | 0.516 | -0.385 | 0.715 | -0.0017 | 0.80 | 0.19 | 5.98 | 1710 |
| 8.4 | 0.525 | -0.404 | 0.699 | -0.0017 | 0.80 | 0.20 | 6.08 | 1728 |
| 8.5 | 0.534 | -0.425 | 0.681 | -0.0017 | 0.79 | 0.20 | 6.24 | 1748 |
| 8.6 | 0.545 | -0.447 | 0.655 | -0.0017 | 0.78 | 0.20 | 6.53 | 1774 |
| 8.7 | 0.552 | -0.463 | 0.625 | -0.0017 | 0.77 | 0.21 | 7.02 | 1798 |
| 8.8 | 0.559 | -0.476 | 0.599 | -0.0017 | 0.76 | 0.22 | 7.64 | 1815 |

| | | | | | | | | |
|-----|-------|--------|-------|---------|------|------|------|------|
| 8.9 | 0.572 | -0.500 | 0.569 | -0.0017 | 0.74 | 0.23 | 8.51 | 1836 |
| 9 | 0.580 | -0.521 | 0.549 | -0.0017 | 0.72 | 0.24 | 9.22 | 1859 |

* Q values are derived from C_4 and expressed as a function of frequency

The regression has resulted in a good match as indicated in Figure 4.4 which shows a comparison of recorded vertical component Fourier amplitudes with predicted ones by the attenuation equation (4.5) at two selected frequencies (2 and 5 Hz) for the magnitude range of m_b 4.5-5.0.

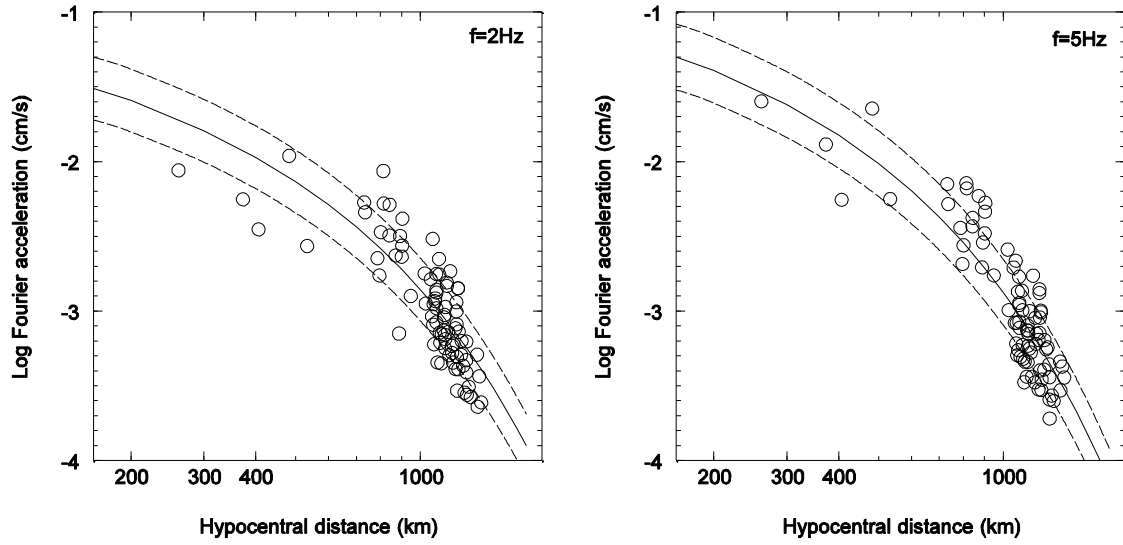


Figure 4.4 Comparison of recorded vertical component acceleration amplitudes with predicted ones from the attenuation relationship [equation (4.5)] at two selected frequencies (2 and 5 Hz) for the magnitude range of m_b 4.5-5.0. Solid line represents the predicted amplitudes and circles represent recorded amplitudes.

Frequency dependent Q values are estimated from the regression coefficient which is relevant to the anelastic attenuation term (C_4 in Table 4.1), and then these values are fit to the following logarithmic relationship using method of least squares for frequencies greater than 1 Hz. Here, Q_0 equals to Q at 1 Hz frequency and n is the “exponent”. Both these parameters are related with the wave transmission quality of the underlying rock of the region in terms of intrinsic attenuation (as discussed above) and/or the amount of scattering due to wave reflection and refraction occurring in the medium (Wu and Aki, 1988). Frequency dependent Q values with the line of best fit to equation (4.7) have resulted in a Q value at 1 Hz (Q_0) as $= 389 \pm 2.35$ and the exponent (n) as $= 0.70 \pm 0.004$. These values are shown in Figure 4.5a.

$$\log Q = n \log f + \log Q_0 \quad (4.7)$$

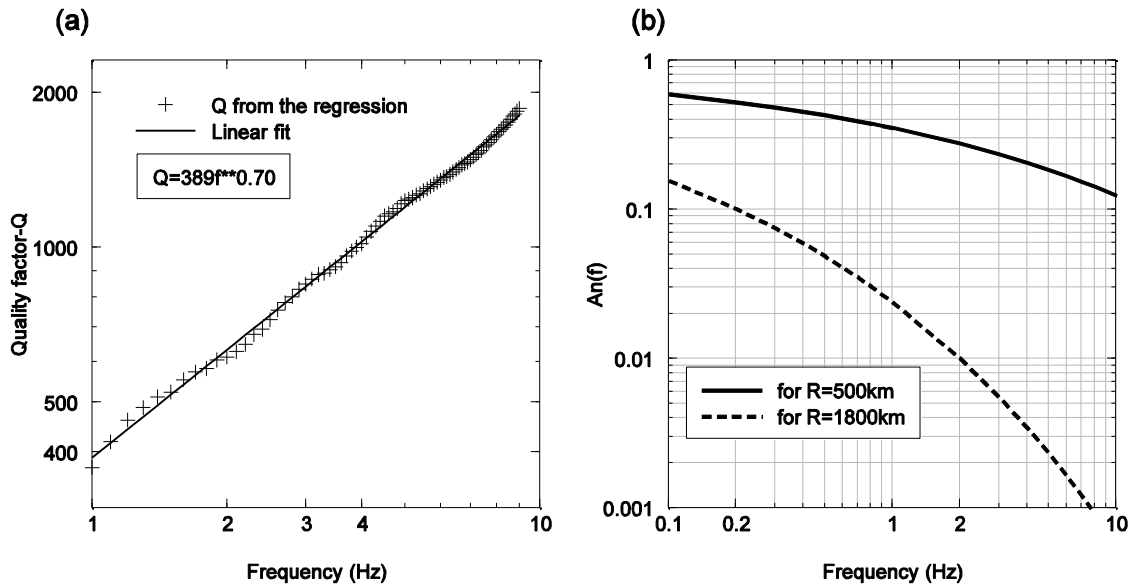


Figure 4.5 Anelastic whole path attenuation in the Northern Indian Ocean: (a) Estimated frequency dependent Q values and the line of best fit (for $f \geq 1$), which results the Q value at 1 Hz (Q_0) as 389 ± 2.35 and the exponent (n) as 0.70 ± 0.004 . (b) Shape of anelastic attenuation with the frequency for two random epicentral distances (500 and 1800 km) selected by considering possible upper and lower site-source distances.

Frequency dependent Q values from the regression, has resulted in a typical linear variation in the log frequency scale for the subject region. Though this is the more common shape of Q variation with the frequency, in some cases special “U-shape” forms, which resulted from higher Q values on either side of 1 Hz, have also been noted (Motazedian, 2006; Allen et al, 2006). A relatively higher Q_0 value has been determined for the region under consideration, even though the area consists largely of a thin oceanic crust with younger formations. This higher Q_0 value does not imply a straight forward comparison with other typical older continental crustal regions such as Western Australia and Central Europe, due to the difference in their tectonic settings and level of seismicities. In other words, a simple comparison of the resulted Q_0 value with similar Q_0 values estimated in typical intraplate continental regions [such as Central Europe, $Q_0=400$ and $n=0.42$ (Malagnini et al, 2000a); Western Australia, $Q_0=457$ and $n=0.37$ (Allen et al, 2006); New England, $Q_0=460$ and $n=0.40$ (Pulli, 1984); Guangdong-China, $Q_0=370$ and $n=0.40$ (Jin and Aki, 1988)], may not be adequate to reflect some distinctive characteristics of the oceanic crust in the region, which are uncommon in typical continental crust. Many studies have shown the regional seismic wavefield in an oceanic crust can be significantly different from that in a continental crust and in a transition boundary at oceanic-continental crusts (Knopoff et al, 1979; Kennett, 1985; Campillo, 1990; Walker, 1977). Discrepancies in physical characteristics such as thickness, lateral heterogeneity and composition can govern the final shape of the crustal structure and thus would influence on

various wave modes which can be guided through the medium. Especially thinner oceanic crusts are said to be less effective for some dominant phases such as L_g in teleseismic range (Zhang and Lay, 1995; Knopoff et al, 1979), and may pose higher energy dissipation from the crust as converting to mantle phases due to pre-critical wave incidence at crust-mantle boundary (Kennett, 1986). Therefore, the wave traverse pattern and the final content of waves which travel through a thinner oceanic crust such as the northern Indian Ocean can be considerably different to that of a typical thicker continental crust. Moreover, in the recurrence rate of events viewpoint, it is obvious that the subject region is not comparable with above mentioned stable intraplate continental areas, despite similarity in Q_0 values. Few studies are available in the literature on Q investigation in oceanic and/or oceanic-continental boundary regions; $Q_0=498$ for a plate-margin area around Korea and Japan (Hong, 2010), $Q_0=224$ for Hispaniola Island Region of the Caribbean Sea close to a plate margin (McNamara et al, 2012). Jin et al (1985) have shown that the variation in scattering Q across different oceanic crusts can be smaller than that across continental crusts, implying continental crusts are more probable to have higher Q values than oceanic crusts, despite possible dissimilarities in seismicity between two crusts. Singh et al (2004) have estimated a much higher L_g coda Q value of about 800 for the neighbouring Indian Shield region based on FAS analysis, which suggests an even older continental crust in the region. This significant Q difference may be associated mainly with the dissimilarities of the crust of the two regions as discussed above (i.e., difference of being older/thicker continental and younger/thinner oceanic), with other possible trade-offs associated with the rupture properties, fault geometry, etc. The inferred Q_0 in this study, should be represented not in the local context but in a regional context which includes both the continental crust lying under the Sri Lanka and the oceanic crust surrounding the country. It may be contested that the inevitable deviations caused due to the assumed geometric attenuation function from the actual attenuation which defines hinge points, would have sometimes led a higher Q_0 value. However, the resulted Q_0 and n values would not be subject to any alteration in the regression analysis as long as “the change in G ” is a constant for the total dataset. Since all of the events used in the present study are from distant sources ($R \gg$ about $2.5D$), G should be always given by the distant form of the G function [i.e., either by equation (4.2) as in this study or the relevant distant form of any other empirical equation with different hinge points, such as given in section 2.3.2 in Chapter 2]. Therefore, the change in G due to possible change in hinge points would be considered as nearly constant for the whole dataset (given also G is frequency independent), and thus would be assumed to be no any harm for the estimated Q_0 and n values in the anelastic attenuation function. However, the change in the amount of geometric attenuation can offset the final source spectral level of events [through regression coefficient C_3 in equation (4.5)] determined by after correcting for path attenuations. Our analysis has already shown that the geometric attenuation resulted in a lower attenuation [due to lower crustal

thickness of about 10 km and a lower near-source spreading coefficient of negative “1”- see equation (4.2)], and therefore, would have a counterbalancing effect on the apparent source spectral level of data. Nevertheless, this would not result in any compensatory effect on the anelastic attenuation to yield a higher Q_0 value than estimated herein. However, it should also be noted that the anelastic attenuation and its parameters (i.e., Q_0 and n) can be markedly subject to change in the regression analysis if the change in G (the difference between the adopted G and actual G) varies with respect to the hypocentral distance and frequency values in the dataset. Perhaps this could be one of the explanations to Singh et. al. (2004)’s observations of higher Q_0 value in the neighbouring region. Furthermore, the geometric attenuation is almost a frequency independent parameter which causes to reduce amplitudes by constant amount in each frequency whereas “ n - exponent” [in equation (4.7)] depends on the slope of the line and hence frequency dependent. Shape of the anelastic attenuation with the frequency for the subject region is shown in Figure 4.5b, in which two random epicentral distances (500 and 1800 km) are selected to demonstrate possible lower and upper limits for the region considered.

Residual analysis for regression results based on Log residuals (=log observed amplitude-log predicted amplitude) are plotted against hypocentral distance and earthquake magnitude to see whether any trends exist (Figure 4.6) with these parameters. Plots clearly show no apparent trend for selected frequencies. In both cases (with respect to epicentral distance and magnitude), residuals are well within 0.3 log margins. Figure 4.7 shows average log residual variation in each magnitude band with respect to frequency. Plot shows a negligible frequency dependency (within about 0.1 log margin) in each magnitude range, however the average of all magnitudes does not further indicate any trend associated with the frequency. Hypocentral depth dependency is not inspected as all the events are shallow-focus earthquakes with depth less than or equal to 10 km.

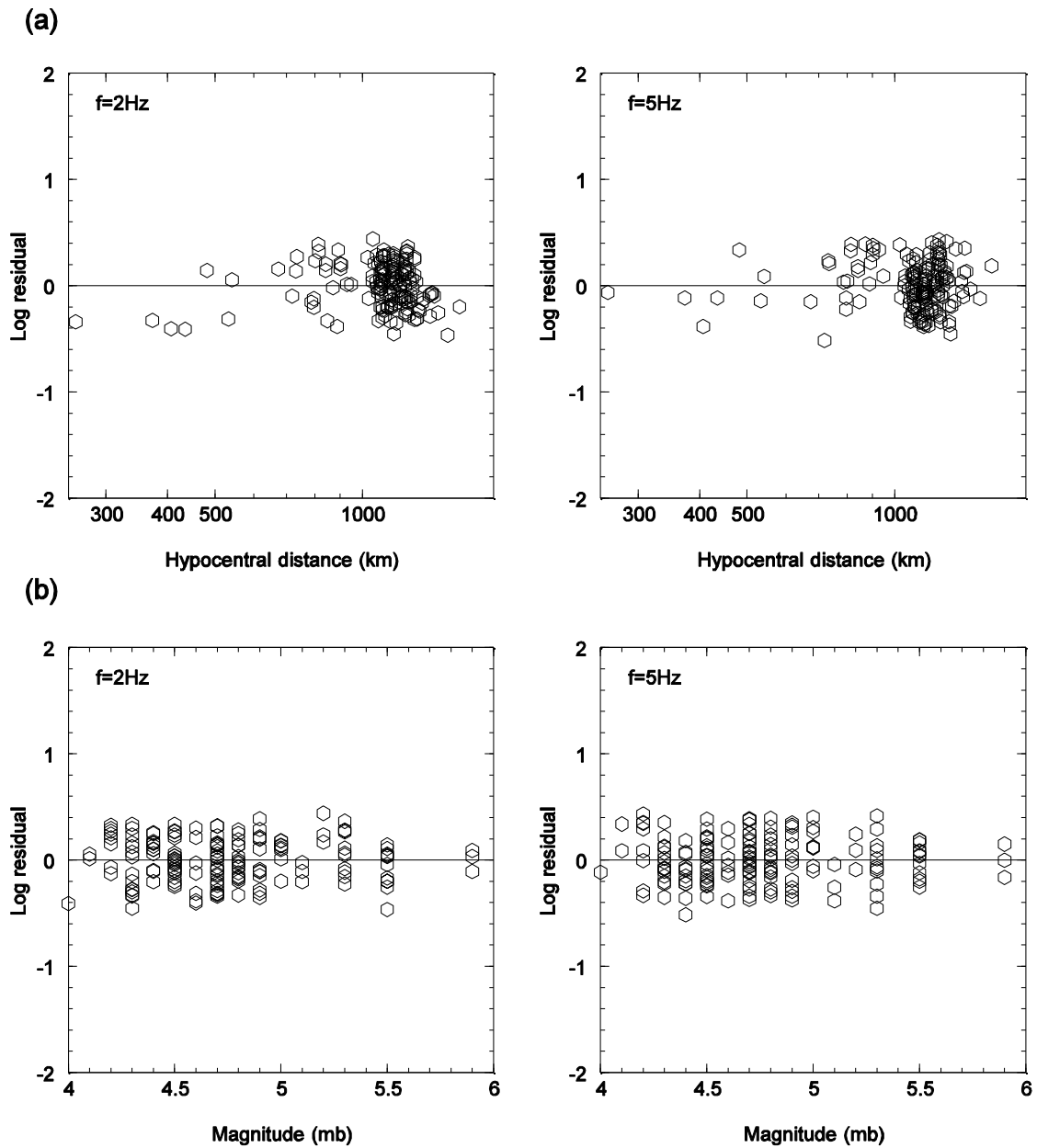


Figure 4.6 Log residual (=log observed amplitude-log predicted amplitude) variation for selected frequencies (2 and 5 Hz). (a) Log residual vs. hypocentral distance. (b) Log residual vs. magnitude (m_b).

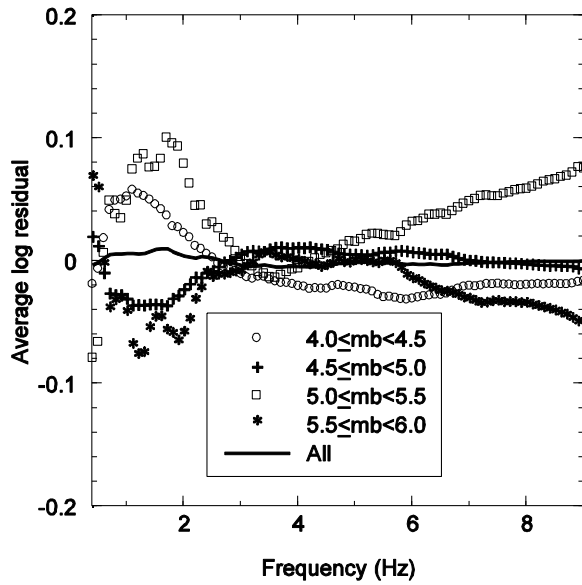


Figure 4.7 Average log residual variation in each magnitude band with respect to frequency. Plot poses a negligible frequency dependency (within about 0.1 log margin) in each magnitude range, however the average of all magnitudes does not further indicate any trend with the frequency.

H/V ratios are calculated from equation (4.6) and are plotted in Figure 4.8 in which average H/V ratio (of log values) at each station with 95% confidence limits on mean are shown. Note that, for PALK station (Figure 4.8a), discernible spikes and comparably higher confidence intervals from the mean are indicated owing to its lower sample size of about 7, because many of horizontal records are only available in a single channel out of two horizontal channels and hence are omitted for the analysis. For other two stations, ratio shows almost a flat shape for the whole frequency range and remains as close to zero. This is even true for the overall average (Figure 4.8d) taken considering all stations. A negative amplification at low frequencies can also be noted, may be due to higher attenuation, for long period waves for which periods higher than say 1.5 seconds (especially in Figures 4.8c and 4.8d). It shows clear evidences about insignificant upper crustal modifications in terms of amplifications and attenuations for the Sri Lankan region, which confirms the validity of the regression equation [equation (4.5)] used. Moreover, this supports the existing literature available on an older crustal rock staitighaphy of Precambrian age underlying Sri Lanka (discussed earlier).

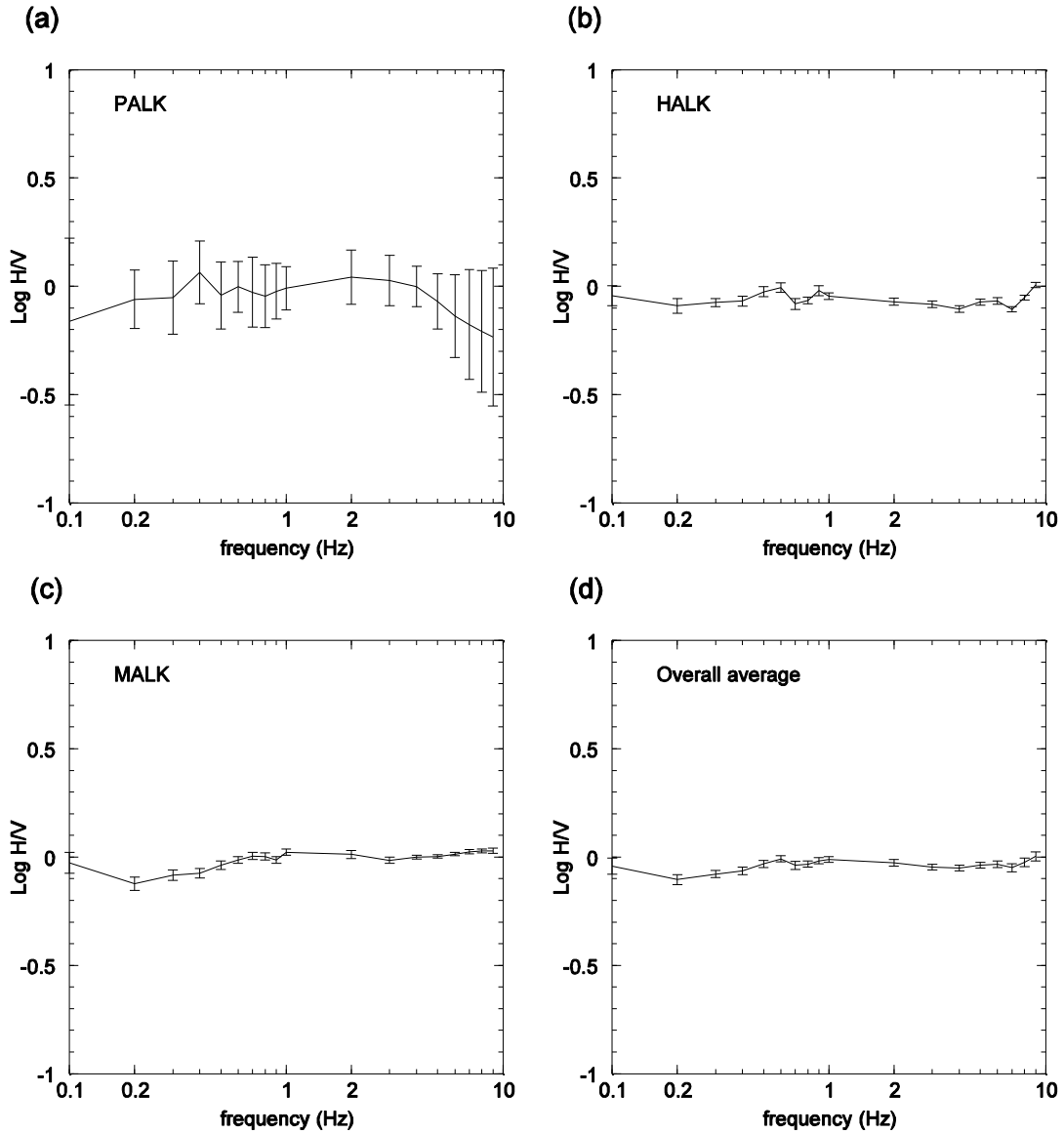


Figure 4.8 Average log H/V ratio with 95% confidence limits on mean, calculated from equation (4.6). (a) Average log H/V ratio at PALK (discernible spikes and comparably higher confidence intervals upon mean are indicated owing to its lower sample size). (b) Average log H/V ratio at HALK. (c) Average log H/V ratio at MALK. (d) Average log H/V ratio for all stations.

The source spectra associated with recorded events can be examined by correcting the observed amplitude for geometric and anelastic attenuation as to satisfy the following equation;

$$\log[A_s(f)] = \log[A_x(f)] + \log[1.5D] + 0.5 \log\left[\frac{R}{2.5D}\right] + \left[\frac{\pi f \log e}{Q\beta}\right]R \quad (4.8)$$

Here, the subscript “s” in the log amplitude term is to denote amplitude at “the source” and all other terms have their same definitions as noted earlier. This method of estimating source spectra may create bias sometimes especially when the amplitude correction has been carried

out for just 3 localized stations. However, considering a range of similar magnitudes and thus estimating source spectra for a range of similar events, would give a preliminary estimate about source characteristics of the region. Estimated source spectra have been compared with Brune's theoretical source spectra (1970; 1971) with an average stress drop ($\Delta\sigma$) value of about 50 bars. This value is selected in a way to comply with corner frequencies of estimated source spectra. Generally, higher stress drop results in slightly higher corner frequencies (see the equation given for corner frequency (f_0) in next paragraph), in which the value again depends on the seismo-tectonic nature of the region. For instance, intraplate Eastern North America (ENA) is associated with higher stress drop values of the order of about 150 bars (Atkinson, 1993a), whereas for interplate Western North America (WNA), the stress drop can be as low as about 50 bars (Atkinson and Silva, 1997). Kanamori and Anderson (1975) have concluded that the stress drops in areas of intraplate events can be about 100 bars on average, while that for interplate events can be relatively a lower value of about 30 bars. On the other hand, Malagnini et al (2000a) have indicated an average of about 30 bars as a reasonable stress drop value for Central European continental crust lying in an intraplate region which also shows a similar Q_0 value with this study. In the present study, although the subject region is termed as an intraplate area, 50 bars is considered as reasonable with comparably lower corner frequencies for small to moderate magnitude events as can be seen in Figure 4.9 which compares estimated average acceleration source spectra of recorded events for two magnitude bands (m_b 4.0-5.0 and 5.0-6.0) with Brune's model source spectra for typical 50, 100 and 150 bars stress drop levels.

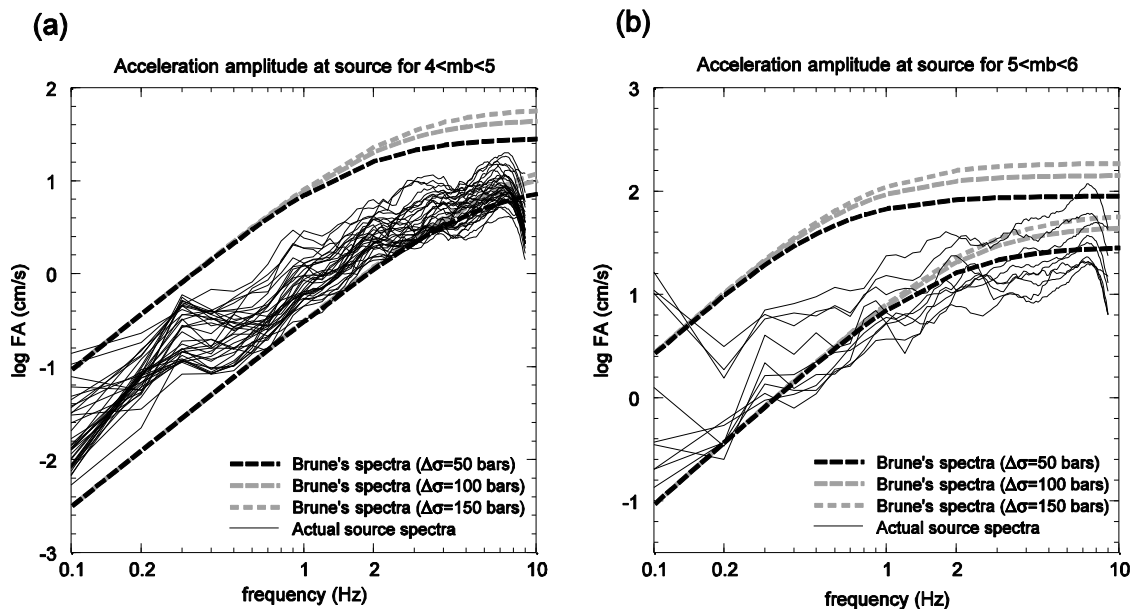


Figure 4.9 Comparison of estimated acceleration source spectra (continuous lines) with theoretical Brune's spectra (dash lines) for typical 50, 100 and 150 bars stress drop levels. (a) Source spectra for $4 < m_b < 5$. (b) Source spectra for $5 < m_b < 6$.

Note that, a sudden amplitude descent pronounced at high frequencies (after about 8 Hz) is not related with the corner frequency but should be linked with bandwidth issue. A number of studies undertaken on seismo-tectonic nature of intraplate earthquakes that (especially) occurred in Oceanic lithosphere, have shown comparably higher stress drop values associated with moderate earthquakes generated in oceanic transform faults (Allmann, 2008; Choy and Boatwright, 1995; Abercrombie et al, 2003). Furthermore, Allmann (2008) shows a slightly lower average stress drop value of about 28 bars for Oceanic ridge events, though the study particularly indicates higher stress drops more than 100 bars for intraplate events occurred in the northern Indian Ocean region close to Wharton basin (a sub-area in the northern Indian Ocean located around the diffuse plate boundary). The same study evidences the northern Indian Ocean region as one of possible intraplate regions governed by apparent high stress drops for large magnitude events. Abercrombie et al (2003) also confirm relatively higher stress drop levels between 50-100 bars for large magnitude events in Wharton basin based on a study of M_w 7.9 event occurred in the region. The higher stress drops associated with oceanic crusts as seen in above studies may be attributed with higher apparent stresses as noted by Choy and McGarr (2002) in mainly shallow-focus earthquakes occurred in younger lithospheric oceanic crusts which are undergoing extensive intraplate deformations such as the case of our study. However, a parameter like stress drop is ascertained to vary even within the same region and may result in considerable variations due to trade-offs that may not be quantified in generic terms, i.e., fault geometry, rupture properties, tectonic setting and crustal structure, etc. Furthermore the deficiency can be anticipated as an artefact of the modeling method followed; for instance two different average stress drops (125 and 68 bars) have shown to be consistent for the same region (northern Iran), estimated from the same set of data (Motazedian, 2006). For this study, a reasonable stress drop value has been assigned in Brune's spectra for the purpose of comparison with actual source spectra as to comply with the corner frequencies. Brune's source model is given in equation (4.9);

$$[A_s(f)] = CM_0(2\pi f)^2 / [1 + (f / f_0)^2] \quad (4.9)$$

Where, $C = 0.78 / (4\pi\rho\beta^3 R)$ in which ρ and β are density (taken as 2800 kg/m³) and shear wave velocity (taken as 3.9 km/s) of the source region, respectively. M_0 is the seismic moment. The corner frequency, $f_0 = 4.9 \times 10^6 \beta(\Delta\sigma / M_0)^{1/3}$, when β , $\Delta\sigma$ and M_0 are in km/s, bars and dyne centimetres, respectively. The seismic moment of each event is estimated first by converting available body wave magnitude (m_b) to moment magnitude (M_w) using the relationship proposed by Atkinson (1993a) and then converting M_w to seismic moment, M_0 , using the original relationship proposed by Hanks and Kanamori (1979).

$$M_w = 0.98M_N - 0.39 \quad \text{and} \quad M_w = \frac{\log M_0}{1.5} - 10.7 \quad (4.10)$$

In the above equation, M_N is referred to as “Nuttli magnitude” which has been considered to be equivalent to m_b estimated for tectonically “stable” regions (such as ENA) where attenuations of primary (body) waves are relatively less (Nuttli, 1973) as of which the data are available in the current case. Discrepancies if any, available between M_N and m_b have been omitted in this case although it can cause some obvious anomalies in estimated Brune’s acceleration amplitudes. On the other hand, magnitude scaling has to be related with a local scale derived based on events reported in the regional context. However this has not yet been developed for the region. Source spectra lie within the limits of Brune’s spectra for the selected range of magnitudes noting the average closes to the lower bounds (Figure 4.9). Moreover, high frequency source spectral amplitudes of recorded events between $4 < m_b < 5$ are in better conformity with Brune’s source spectra than that of moderate events between $5 < m_b < 6$. The reason may be associated with the magnitude conversion reconciling two dissimilar regions as identical regions for the applicability of conversion equations. Despite this high frequency amplitude unconformity of moderate events ($5 < m_b < 6$), estimated source spectra show a good match with Brune’s source spectra for typical 50 bars stress drop value. Hence, the frequency content and the general “shape” of the source spectrum in the subject region are consistent with the “theoretical source spectrum” developed in the global context. Subsequently, the final wave frequency content at the rock outcrop is little affected by changes in source spectrum characteristics for a particular magnitude of earthquake, since the final shape of the spectrum is governed mainly by modifications during the wave travel through the rock medium in terms of attenuations and amplifications as described previously. The apparent source spectra are compared with Atkinson’s two corner frequency source spectra models. No discernible differences are observed in the low frequency range; Atkinson’s source spectra over estimate amplitudes in the high frequency range. Of significant interest is the observation of two corner periods with higher magnitudes which is not evident in Brune’s source spectra models (see Figure 2.2 in Chapter 2).

Finally, ground motion on rock sites due to a recent M_w 8.6 event is modelled using a theoretical approach commonly known as “Stochastic method” (a synoptic description of the method is given in Chapter 2) by employing the “seismological model” formulated in equation (4.1) with the estimated Q_0 value (389). Atkinson’s typical double corner frequency ENA source spectrum is used herein (Atkinson and Boore, 1995), since Brune’s model over estimates long period amplitudes in large magnitude events (Chen and Atkinson, 2002). Lam et al (2000b) have combined the seismological model with the stochastic process to simulate seismograms to fit with the frequency contents defined by the model [a detailed description of the process is given in Lam et al (2000b)]. These stochastic simulations provide enormous opportunity to estimate

seismic hazard especially in low to moderate seismic regions, over other conventional approaches. Therefore, once the seismological parameters for a given region are readily available, the stochastic method can be employed to simulate earthquakes. FORTRAN based GENQKE (Lam, 1999) is used to simulate ground motions. During the modeling, it has been omitted upper crustal modifications owing to higher wave propagation characteristics of the country's underlying near-surface basement rocks of Precambrian age, as demonstrated earlier using the estimated H/V ratio. The shear wave velocity near rock outcrops for typical Sri Lankan Precambrian rocks is considered as about 2.5 km/s (Jayawardena, 2001). The value shows consistency with shallow reference shear wave velocities of other Precambrian regions found in the world such as Western Australia, Canadian Shield, etc. (Chandler, 2006). However, presence of Sedimentary deposits and other localised variations in geology can cause possible higher attenuations at high frequencies, albeit of being a so-called "Precambrian crust". Such attenuations are characterized by the upper crustal attenuation parameter Kappa which will be examined in next two Chapters for the Sri Lankan upper crust. Hence, for the present sample modeling, the upper crustal modifications are assumed to be minimal in effect and are safely neglected. Pseudo Spectral Velocities (PSVs) of modelled ground motions along with recorded components (two horizontal and a vertical) at each station are shown in Figure 4.10. Comparison of acceleration time histories between simulated and recorded at PALK, is also indicated for demonstration purpose.

Dash and continuous lines represent horizontal and vertical components recorded at each station, respectively, whereas circles represent PSVs of simulated ground motions. Interesting consistency between modelled and recorded values can be seen from Figure 4.10, which in turn validates the estimated Q_0 value for the subject region in the northern Indian Ocean. Apparent little overestimation of modeled PSVs than the actuals at higher frequencies (about $f > 1$ Hz), may be related with not taking possible upper crustal attenuations in to the account.

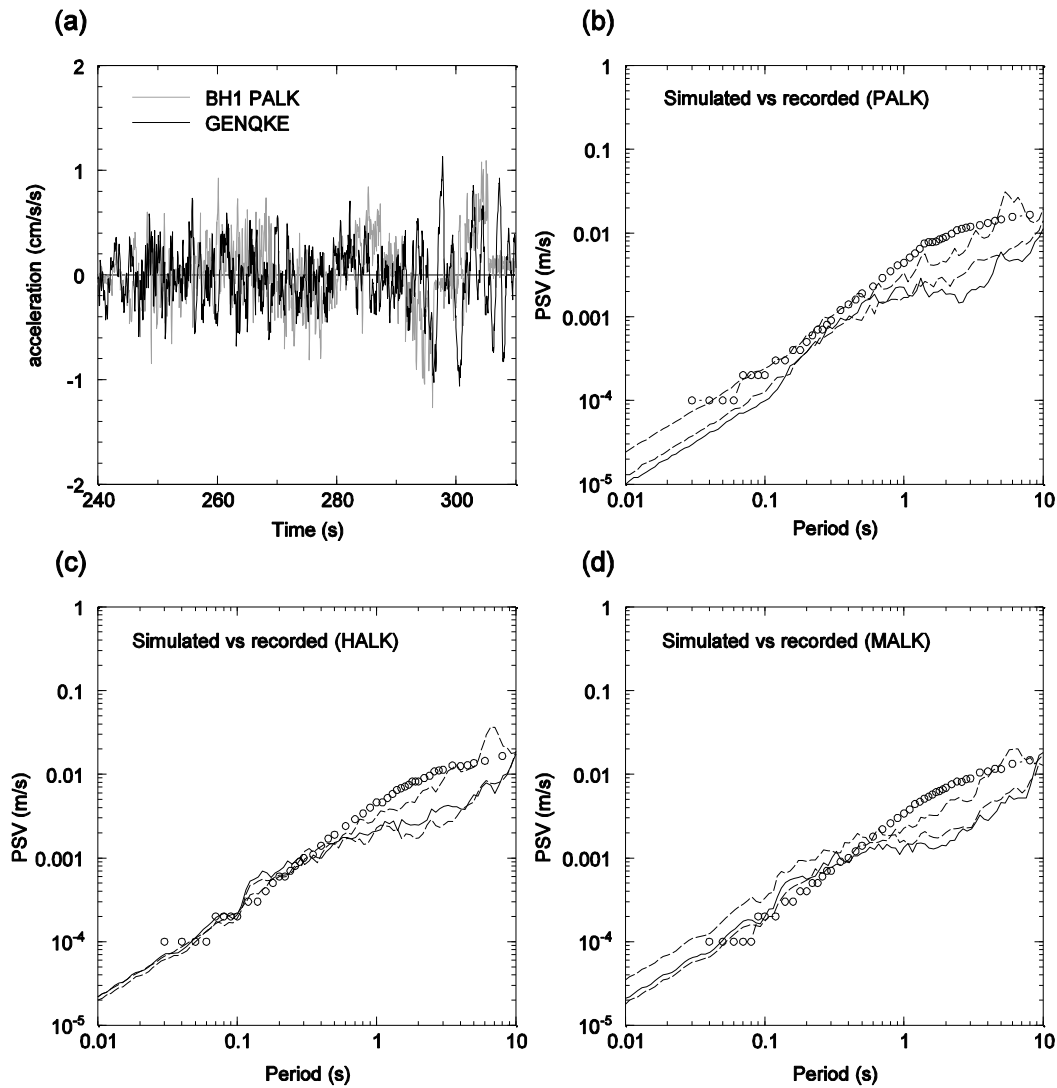


Figure 4.10 Comparison of M_w 8.6 event with the stochastic simulation using GENQKE. (a) Comparison of acceleration time history between recorded (BH1-horizontal) at PALK and simulated from GENQKE. (b), (c) and (d). Pseudo Spectral Velocity (PSV) comparison between simulated and recorded at PALK, HALK and MALK, respectively. Dash and continuous lines represent horizontal and vertical components recorded at each station, respectively. Circles represent PSVs of simulated ground motions.

4.6 Summary and conclusion

Seismic wave transmission quality factor Q_0 for the Sri Lankan region surrounding northern Indian Ocean has been determined by using multiple linear regression analysis of FAS of 181 intraplate records. Analysis of vertical component FAS recorded at three broadband stations has resulted in a higher Q_0 value of about 389 ± 2.35 which suggests a unique correlation with the identified younger oceanic lithospheric crust in the region which is undergoing intense deformations. Estimated Q_0 implies improved wave propagation features, in contrast to the lithospheric age and the abnormal intraplate seismicity of the region. However it should be

noted the wave transmission quality factor represents a very complex wave travel mechanism and should be used in the analysis with expert advice.

Upper crustal modifications in terms of amplification during wave travel through the near-surface rock have been estimated using the standard H/V ratio method. Results show negligible upper crustal modification, supporting the contention that the country's underlying basement rock consists of crystalline rock of Precambrian age. This urges upper crustal effects not to be taken in to account during both regression analysis and the stochastic modeling. Source spectra estimated by correcting the observed amplitude for geometric and anelastic attenuation show a good match with Brune's source spectra for a typical stress drop value of the order of about 50 bars. It is important to note that studies elsewhere have shown that the stress drop level associated with the region can be as high as 2 or more times in order as the preliminary value used in this study. Such values are trialled and it has found that higher stress drops are incompatible with the records, and have resulted in overestimation of source amplitudes at high frequencies (Figure 4.9). However, it should be worthy of pointing out that until a detailed study, which is based on an analysis of source spectra, is carried out, the actual stress drop level in the subject region would be hard to reveal, and such an analysis that is predominantly based on source spectral amplitudes in the region is discussed in Chapter 5. It is acknowledged further that the use of different conversion scales between body wave magnitudes and moment magnitude scales will lead to differences in observed values. Despite these, the stochastically modelled M_w 8.6 event using the estimated Q_0 value exhibits a reliable match with the actual records. This matching suggests that the value of Q_0 estimated herein and other results from this research can provide useful estimates of the possible design scenarios to be considered for the country. Further validation of these scenarios and modeling inland seismicity would be later undertaken as part of estimating seismic hazard for Sri Lanka.

5. Attenuation (*G* and *Kappa*) and source parameters for regional earthquakes in the northern Indian Ocean

5.1 Introduction

The previous Chapter examined anelastic attenuation characteristics of the northern Indian Ocean region and H/V ratio estimations for average upper crustal amplification effects in the Sri Lankan region. In the present Chapter, two other important attenuation modes, namely the geometric attenuation and high frequency cutoff filter (otherwise known as the upper crustal attenuation) are investigated for regional earthquakes in the region. Apparent source spectral parameters of the selected intraplate events are also determined for attenuation corrected amplitudes with Brune's point source model. Main findings of these studies accompanied by some other extended studies on possible ground motions expected in Sri Lanka due to large magnitude events of the subject region (the northern Indian Ocean), are also published in separate articles (Gamage and Venkatesan, 2012b; Venkatesan and Gamage, 2013; Gamage et al, 2011).

Proper evaluation of path attenuation characteristics of a region is of primary importance in any seismic hazard/risk analysis. These attenuations are largely influenced by crustal properties of the region (e.g., age, density and composition of the crust, degree of heterogeneity, amount of asperities and irregularities, etc.), and therefore, are commonly referred to as "region-specific attenuation characteristics" in the field of seismology and earthquake engineering. Region-specific attenuation properties can be easily studied by explicit analysis of recorded data using various techniques. The anelastic attenuation characterized by *Q*-wave transmission quality factor, is one of the dominant attenuation types in distant earthquakes (hypocentral distance greater than about 200 km), in which a major portion of total attenuation takes place as seismic absorption (or intrinsic attenuation) along the whole path of wave travel. Hence, a reliable estimation of *Q* is essential to continue with further hazard studies. Knowing the value of *Q* in a region also helps to establish a proper understanding on the type of the underlain crust and its various geotectonic features that "regulate" the seismic wave propagation in the medium. As shown in Chapter 4, the regional *Q* value for the northern Indian Ocean can be modeled using the form $Q = 389f^{0.70}$ at high frequencies ($f \geq 1$ Hz).

The geometric attenuation (*G*) accounts for diminution of wave amplitudes as a result of wave scattering (reflections and refractions) during the propagation, and is typically identified as independent of both of wave frequency and earthquake magnitude (Atkinson and Boore, 1995;

Atkinson and Mereu, 1992; Herrmann and Kijko, 1983). Out of various relations proposed in the literature for formulating the geometric attenuation of a region, the following two, frequency independent bilinear form (Herrmann and Kijko, 1983) and frequency independent trilinear form (Atkinson and Boore, 1995; Atkinson and Mereu, 1992), have become widely popular among seismologists and earthquake engineers (note that, these equations are also presented in Chapter 2, however they are reproduced in this Chapter for reference);

$$\begin{aligned}
 G &= R^{-1} && \text{for } R \leq R_x \\
 &= (RR_x)^{-0.5} && \text{for } R > R_x
 \end{aligned}
 \quad \text{Bilinear form} \quad (5.1)$$

$$\begin{aligned}
 G &= R^{-1} && \text{for } R \leq 70 \text{ km} \\
 &= 70^{-1} && \text{for } 70 \text{ km} < R \leq 130 \text{ km} \\
 &= 70^{-1} \left(\frac{130}{R} \right)^{0.5} && \text{for } R > 130 \text{ km}
 \end{aligned}
 \quad \text{Trilinear form} \quad (5.2)$$

Here, R and R_x , respectively, are the hypocentral distance and a constant reference distance usually expressed as a multiple of notional crustal thickness. In equation (5.2), two fixed reference distances (70 and 130 km) are used instead of a single distance as in equation (5.1). These reference distances are commonly referred to as “the hinge points”, which may vary with spatial/geometric properties of the regional crust. A rapid attenuation of R^{-1} at near-source distances and a lower rate of $R^{-0.5}$ at the far-source distance range are clear observations in both of the relationships. This is to comply with the dominant wave type in respective case; direct S -waves attenuate much more rapidly at near-source distances (R^{-1}) than surface waves such as L_g (formed by multiple reflections and refractions of body waves) do at far-source distances ($R^{-0.5}$). In equation (5.2), at the medium distance range (between 70 and 130 km), a negligible or zero attenuation is indicated, and is explained as a compensatory effect resulting from post-critical reflections incidental at Moho and Conrad discontinuities. In some cases, a higher near-source geometric attenuation than that given in the above equations (Atkinson, 2004b) and even frequency dependent attenuation rates (Atkinson, 2005) are also noted.

In the study described in this Chapter, the far-source geometric attenuation rates of the northern Indian Ocean region are estimated at frequencies between 0.5-8.5 Hz, by again using a Fourier spectral analysis of moderate magnitude intraplate earthquake records. Further analysis to estimate the average high frequency filter function parameter, Kappa (κ), has also been undertaken. Apparent source characteristics – such as stress drop, corner frequency and Moment magnitude of the selected events are determined by applying Brune’s point source model. Finally, a ground motion comparison of spectral amplitudes between recorded and stochastically

simulated, is carried out as a credence to estimated seismological parameters (in both Chapters 4 and 5) for the region.

5.2 Methodology

5.2.1 Data processing and the main regression analysis

Data and method of data processing in the main regression analysis are basically similar to that adopted in Chapter 4, which is also available as a published material by Venkatesan and Gamage (2013). A database of 171 Broadband High-Gain vertical component (BHZ) data of 71 shallow crustal intraplate events recorded at the country's seismic network, is used in the analysis (Chapter 4 - Figure 4.1 and Appendix B). Vertical components are selected since they are little affected by near-surface wave modifications (such as amplifications and attenuations) in comparison to horizontal components. Event magnitude varied from 4.0 to 5.9 in the short period body wave magnitude scale, and the hypocentral distance ranged between 2.3° (260 km) and 14.1° (1578 km) for the dataset (Chapter 4 - Figure 4.2).

A quick summary of the main steps followed in the data processing is presented here. Original waveform file in each vertical component is tapered (10% at both ends), is instrument corrected and is band-pass filtered between 0.1 and 9.0 Hz, in the first place. Then, the corresponding acceleration time history in each record is obtained. The maximum frequency 9.0 Hz is selected to accommodate the norm that the upper limit should be less than half the sampling rate of the recording instrument (Havskov and Ottemo"ller, 2012). Next, FAS are produced for "strong motion part" in each processed time history. FAS are visually inspected for signal strength relative to background noise, and this resulted in the elimination of low frequency amplitudes (frequencies lower than or equal to 0.4 Hz) owing to higher noise amplification. Subsequently, the upper frequency limit is dropped to 8.5 Hz after noting some bandwidth issues which can be associated with the instrument's sampling rate. A more reliable frequency range, which is narrower than that used in the previous study (Chapter 4), has chosen as the final effective frequency range in the present study. FAS are then smoothed for the final frequency range (i.e., 0.5 to 8.5 Hz) at 0.1 log frequency bins by introducing a box/rectangular weighting function in each of the log frequency bins. This frequency dependent smoothing (due to constant width in log frequency) allows a uniform smoothing of amplitudes for the selected frequency range, and is considered to be more desirable in the regression analysis especially that requires minimal noise amplifications (Boore, 2012). Acceleration amplitudes of smoothed spectra in each record are finally tabulated at 0.1 frequency increments for the purpose of regression. The procedure followed in the data processing is graphically indicated in Figure 4.3 of Chapter 4, and is also explained in section 4.2.2 in the same Chapter.

The attenuation model proposed by Atkinson and Mereu (1992) is refitted with observed FAS by the multiple linear regression method, yet this time with known anelastic attenuation contributions which are determined by the Q values estimated in Chapter 4. The local site amplifications possible at soil sites are not accounted since all the recordings are on rock sites. The same basic attenuation equation as in Chapter 4 is used in here with the same definitions of terms [equation (4.1) - Chapter 4];

$$[A_x(f)]_{ij} = [S(f)]_i \cdot G \cdot A_n(f) \quad (5.3)$$

$A_n(f)$ is modeled by equation (4.3) in Chapter 4 taking $Q = 389f^{0.70}$ for the selected frequency range. Here, the variation of Q at low frequencies ($f < 1.0$) is assumed to be the same as that at high frequencies ($f \geq 1$), despite the original derivation of the form which is based on high frequency Q values ($f \geq 1$). G is modeled following the format proposed in equation (5.2), considering the trilinear (in log scale) hinged shape form is more applicable for the region. Equation (5.1), in the bilinear form, approximates the rate of attenuation at medium distances as similar to that at near-source region, and offers a simpler form of modeling. Nevertheless, the trilinear form which additionally includes a negligible reduction or sometimes even a smaller increment in wave amplitudes at medium distance range (within about 70-130, 140 km), possibly due to post-critical reflections from Moho and Conrad discontinuities, has been well recognized in seismological studies conducted in continental America (Atkinson, 2004b; Atkinson and Boore, 1995; Atkinson and Mereu, 1992). Moreover, the trilinear form has successfully been utilized in ground motion simulations in Eastern and Western North America (ENA and WNA) by the above authors. Therefore, the basic form defined in the trilinear shape is chosen for the geometric attenuation in the subject region, and the complete shape of the function is derived by estimated and collated reference distances and attenuation rates. G adopted in the previous study (Chapter 4), is based on the assumption that the regional geometric spreading or damping of seismic waves at long distances complies with the generic functional form [equation (4.2)] proposed by Lam et al (2000a; 2000b; 2000c), in which the functional form defines the amount of geometric attenuation of an event in the region as a direct measure of the average regional crustal thickness [see equation (4.2)]. In the present study, however, efforts are undertaken in characterizing a more empirical form of G for the region based on the spectral analysis.

Far-source attenuation rates at each frequency in the trilinear form are estimated by the main regression. One of the reference distances, which defines the second hinge point [R_{x2} in equation (5.5)], is determined by results of the main regression as described in section 5.2.2 (“The secondary regression”). Since, the actual attenuation rates corresponding to near- and medium-source distances in the region are difficult to ascertain due to unavailability of near-field records

in the current dataset, these values are taken from the literatures mentioned before. The reference distance of the first hinge point (R_{x1}) is also impossible for a direct derivation due to the same reason, so that the value is inferred based on a spectral matching of recorded and simulated ground motions. The source factor $S(f)$, which significantly depends on seismic energy release (or magnitude), is formulated using the same relationship [equation (4.4)] as given in Chapter 4;

$$\log[S(f)]_i = C_1(M-4)^2 + C_2(M-4) + C_3 \quad (5.4)$$

M represents magnitude of the earthquake, which is the short-period body wave magnitude (m_b) in the current case. m_b is chosen due to its common use in reporting small and medium size earthquakes in many archival databases. C_1 through to C_3 are frequency dependent coefficients to characterize regional source properties. Substituting equations (5.2), (4.3) and (5.4) into the logarithmic form of equation (5.3) and rearranging terms would yield;

$$\log[A_x(f)]_{ij} + \left[\frac{\pi f \log[\exp]}{Q\beta} \right] R = C_1(M-4)^2 + C_2(M-4) + C_3 + a \log R_{x1} + b \log \left[\frac{R}{R_{x2}} \right] \quad (5.5)$$

In the above equation, the geometric attenuation rates given in equation (5.2) are taken as a (instead of -1) and b (instead of -0.5) for near-source and far-source distance ranges, respectively. b is to be directly found from the multiple linear regression. The two reference distances 70 and 130 km in equation (5.2), are defined as R_{x1} and R_{x2} , respectively. The dependent variable is obtained by correcting recorded $\log[A_x(f)]_{ij}$ for the anelastic attenuation with $Q = 389f^{0.70}$. The shear wave velocity of the region is taken as 3.9 km/s based on CRUST2.0 information. Regressions are undertaken using the least squares method by setting line of best-fits between the dependent variable and independent variables; $(M-4)^2$, $(M-4)$ and $\log R$. Regression coefficients thus resulted are refined further by removing random outliers, which are believed to exist due to epistemic uncertainties such as poor and/or too strong recordings, background noise amplification (particularly at very high and at very low frequencies), technical defects and/or due to any other unknown reason. Outliers are defined on the basis of standardized residual value of log amplitudes (between actual and predicted) being greater than 3.0 as similar to that in Chapter 4. The overall purpose of this is enhancing the regression conformity with higher coefficients of determinations (R^2) at least as close to 60% and lower residual sum of squares [SS(Resi)] less than to about 20.

5.2.2 The secondary regression

In equation (5.5), the regression constant is composed of C_3 and $[a \log R_{x1} - b \log R_{x2}]$. This constant is susceptible for an amalgamation with the high frequency diminution filter that causes rapid amplitude cutoff of high frequency waves. Some studies have pointed out, the high frequency diminution is merely a source effect (Papageorgiou and Aki, 1983), while others still

attribute as a site specific attenuation effect taking place at the near-surface level (Anderson and Hough, 1984; Hanks, 1982). The latter identification is often titled as “the upper crustal attenuation $P(f)$, which is parameterized by a factor called “Kappa (κ)” (see section 2.3.5 in Chapter 2). The upper crustal attenuation is described as a rapid depletion of high frequency wave amplitude happening in the intrinsic nature due to a mechanism similar to which in the anelastic attenuation. These intrinsic attenuation effects can be significant at the upper level of the crust than at mid and deeper levels because of poorer wave propagation characteristics associated with the upper crustal bedrock. Stratified variation of rock quality is generally found to be substantial at shallow depths due to the presence of younger rock formations. Usually rocks that are at shallow depths closer to the surface/out cropping layer, are composed of younger sedimentary formations than those are at deeper depths such as older crystalline formations. This may lead significant attenuations are to be undergone at the upper level of the crust than at mid/deeper levels. Studies indicate regions having such younger formations can pose up to about 90% of the total anelastic attenuation within the topmost 3 km (Abercrombie, 1997). Therefore, in practice, the amount of attenuation at the upper part of the crust is considered separately from other path attenuations. Consequently, the upper crustal attenuation is formulated irrespective to the hypocentral distance, given the dominance (mainly in near-field events) over other attenuation modes (Anderson and Hough, 1984);

$$P(f) = \exp[-\pi f \kappa] \quad (5.6)$$

In equation (5.6), Kappa is formulated as a frequency independent parameter. However, slight magnitude dependence has been identified for moderate and large magnitude earthquakes in WNA regions (Atkinson and Silva, 1997). Kappa typically exhibits lower values for regions with older and harder rocks such as of Precambrian, but indicates higher values for areas of younger upper crustal formations. Even in regions like Sri Lanka where the local geology is ascertained as being composed of non-fossiliferous crystalline rocks of Precambrian (Cooray, 1994; Kroner and Brown, 2005), “localized effects” of such high frequency roll-offs due to above discussed upper crustal attenuation, would be possible. Inconsistency in the composition and presence of Sedimentary strata, asperities and other similar variations can affect the apparent inhomogeneity of the crust. In particular, a thinner sedimentary lining seating on some or most parts of the country’s crust is susceptible. Data given in CRUST2.0 also clue on such occurrence, indicating a soft sedimentary layer of half a kilometer thickness in central and southern parts of the country. Therefore, despite geological assertions which identify the country’s crust as a Precambrian craton, effects of the high frequency cutoff filter on the spectral shape of regional earthquakes are examined. Note that, although, there are other functional forms such as f_{max} (Hanks, 1982) proposed to account for the high frequency rolling-off effect, the Kappa function [equation (5.6)]

is used in the study. The main reason for this selection is the Kappa function's generic application in the field, which would facilitate for an easy comparison of the upper crustal characteristics in Sri Lanka with other regions.

In view of the above argument, the regression constant in equation (5.5) may additionally include the high frequency cutoff filter. Therefore, the total constant is taken to be the sum of C_3 , $[a \log R_{x1} - b \log R_{x2}]$ and $(-\pi f \kappa) \log[\exp]$, so that equation (5.5) can be rewritten as,

$$\log[A_x(f)]_{ij} + \left[\frac{\pi f \log[\exp]}{Q\beta} \right] R = C_1(M-4)^2 + C_2(M-4) + b \log R + C_T \quad (5.7)$$

$$\text{Where, } C_T = -\pi \kappa \log[\exp] f - \log[R_{x2}] b + C_3 + a \log R_{x1} \quad (5.8)$$

Upon completion the main regression [using either equation (5.5) or (5.7)], the secondary regression is planned to be performed using equation (5.8) to estimate the reference distance of the second hinge point (R_{x2}) in the trilinear geometric attenuation form, and Kappa of the high frequency diminution filter function given in equation (5.6). This time, C_T is kept as the dependent variable while f and b (already found from the main regression) turn into the independent variables. For effective application of equation (5.8) in the regression, C_3 [the constant coming from the source factor-equation (5.4)] should be independent of wave frequency. However, it is difficult to anticipate a constant variation of C_3 for the selected frequency range, as the source amplitude of a given event normally varies with frequency. If the actual source spectra agree with Brune's (1970; 1971) classical point source model (ω^2 -model), Fourier amplitude at the source would follow a bilinear variation (in log scale), in which the displacement Fourier spectra of a given magnitude event would approximately remain constant at frequencies below the corner frequency. Accordingly, following the assumption that the actual source spectra of the region to concur with theoretical Brune's model, the regression is carried out by equation (5.8) at frequencies below a possible average corner frequency. Since, the events are of moderate sizes in magnitude and are having larger hypocentral distances of hundreds kilometers, it would be reasonable to approximate their rupture areas as point sources. Therefore, first, the constant- C_T of the main regression is transferred into the corresponding displacement amplitude by adding $-\log[2\pi f]^2$ at each frequency. The secondary regression is then undertaken for a selected lower frequency range, for which the displacement source amplitude would remain nearly constant. A lower frequency range of 0.5-5.5 Hz is assigned considering both the average magnitude of the dataset that is about m_b 4.7, and retaining a sufficient frequency range for stable results. The upper frequency limit 5.5 Hz is selected as a compromise between assigning a reasonable corner frequency value for such an average magnitude event of a region with higher average static stress

drop, and the requirement to maintain an adequate length in the frequency for consistent results in the regression.

5.2.3 Source characteristics

Source spectra of the recorded events are obtained by correcting the observed amplitude for geometric, anelastic and upper crustal attenuations as necessary with satisfying the following equation;

$$\log[S(f)]_i = \log[A_x(f)]_{ij} - a \log R_{x1} - b \log \left[\frac{R}{R_{x2}} \right] + \left[\frac{\pi f \log[\exp]}{Q\beta} \right] R + \pi\kappa \log[\exp]f \quad (5.9)$$

$[S(f)]_i$ denotes Fourier acceleration amplitude at the source of the event i as defined in equation (5.3). One may note that, equation (5.9) can be easily derived using equations (5.4), (5.7) and (5.8). Source amplitudes of each individual event are averaged over all the stations at which the event has recorded, so that any localized site effect which can be pronounced at high frequencies, is essentially negated. Source parameters such as corner frequency, stress drop and Moment magnitude are simply determined by the least squares regression between the observed source spectra given in equation (5.9) and Brune's point source model (1970; 1971). The Brune's model is defined in equation (5.10);

$$S(f) = CM_0(2\pi f)^2 / \left[1 + \left(\frac{f}{f_0} \right)^2 \right] \quad (5.10)$$

Where, $C = 0.78 / (4\pi\rho\beta^3 R)$ in which ρ and β are the crustal density (taken as 2800 kg/m³) and the shear wave velocity (taken as 3.9 km/s) of the source region, respectively (values are taken from CRUST2.0 model and are similar to that in Chapter 4). M_0 is the seismic moment. The corner frequency, $f_0 = 4.9 \times 10^6 \beta (\Delta\sigma/M_0)^{1/3}$ when β , $\Delta\sigma$ and M_0 are in km/s, bars and dyne centimeters, respectively (Boore, 1983). Rearranging terms in equation (5.10) gives the following relation to be fitted in the regression;

$$\frac{1}{S(f)} = \frac{1}{CM_0 4\pi^2 f^2} + \frac{1}{CM_0 4\pi^2 f_0^2} \quad (5.11)$$

M_0 and f_0 are estimated by the line of best-fits between the dependent variable (reciprocal of source amplitude) and the independent variable, i.e., $1/f^2$. Regression is undertaken event wise, since M_0 and f_0 remain constant for a given event. A lower frequency range of 0.5-4.0 Hz is considered herein as more stable for the regression. Although, the equation form offers an idyllic linear variation between two variables, a lower frequency range is chosen to minimize effects

which may arise due to parametric uncertainties, if any, in the estimated anelastic and upper crustal attenuations. The estimated attenuations and thereby uncertainties associated with them, increase with the frequency [see equation (4.3) in Chapter 4 and equation (5.6)]. The stress drop ($\Delta\sigma$) is deduced from the equation given in the preceding paragraph using estimated M_0 and f_0 by the direct regression. Finding source characteristics this way by fitting theoretical Brune's model implies that the actual sources are compatible with fundamental assumptions associated with the model; ω^2 variation of spectral amplitude with frequency (here, $\omega = 2\pi f$), being a circular point source with a constant rupture velocity and a single corner frequency, uniform energy release in all directions without any intermittent slipping and/or any directivity effect, are noteworthy among them. Point source assumption seems logical to a certain point, since the events have arisen at distant sources, and are of moderate sizes in magnitude. However, other assumptions related with the rupture process and energy release are not assured, since deviations can always be expected due to the actual crustal inhomogeneity. It may also be expected, some alterations in final results by actual finite-fault effects especially in strong magnitude events (m_b greater than about 5.5), which do not explicitly take into the consideration in Brune's point source model.

Source parameters such as static stress drop and corner frequency are helpful in identifying numerous key characteristics of a regional crust. Both of these are directly related to the rupture time and stress release of a given earthquake, and are sometimes used as "initial or surface measures" of seismological properties pertaining to "the quality" of the crust. Stress drop, which is interrelated with the amount of strain or with the energy released during the rupture, is a common parameter used in the comparison of different crustal types. Harder and older crusts generally exhibit higher stress drops than younger and softer crusts do. For instance, ENA's crust built with Precambrian hard rocks is associated with an average stress drop of about 15 MPa (150 bars) for moderate and large magnitude earthquakes (Atkinson, 1993a). On the other hand, in WNA, which is of much younger formations, the value can be as low as about 5 MPa (50 bars) even for large magnitude events (Atkinson and Silva, 1997). Higher stress drops can accentuate high frequency acceleration amplitudes, since the acceleration spectrum is governed by the average stress drop in addition to the Moment magnitude of the event. For a given event of interest, the higher the stress drop value the higher the corner frequency (from $f_0 = 4.9 \times 10^6 \beta (\Delta\sigma / M_0)^{1/3}$). Since, the corner frequency and rupture time are inversely related (Beresnev and Atkinson, 1997), the rupture times of events in older/harder crusts can be a bit lower than that of similar events in younger/softer crusts. In other words, crustal earthquakes in older/harder crusts can be "quicker" than those in much younger/softer crusts. In engineering perspective, the degree of impact by both the stress drop and corner frequency on the final shape and frequency content of a spectrum, is of significance in hazard studies. Higher stress drop leading higher corner frequency causes the response spectrum to be dominated by high frequency

waves, which can be a concern for spectral acceleration and base shear demand in low-rise structures with smaller natural periods. On the contrary, the frequency content of events that occur in lower stress drop regions can be dominated by long period waves. In such instances, the displacement or drift demand in long period structures (e.g., high-rise buildings, dams and other structures with flexible forms) needs to be critically assessed.

During the last few decades, there have been various other empirical relations suggested to scale actual source spectral characteristics (discussed in section 2.3.1 in Chapter 2). Many of these relations follow the same fundamental shape as that proposed by Brune (1970; 1971) based on magnitude independent stress drop approximation; e.g., a much sharper single corner frequency model by Boatwright (1980), a two corner frequency model for large intraplate events by Boatwright and Choy (1992), a more elaborative double corner frequency model by Atkinson (1993a), etc. However, for the present study, the original Brune’s model is applied for source parameter estimation, mainly, because of the simplicity of the model for general application in different regions outside the model is derived. Moreover, the model’s wider application in the field is also advantageous when comparing final results with other regions.

5.3 Results and discussion

5.3.1 The main regression analysis

Results of the main regression are presented in Table 5.1. The far-source geometric attenuation rate b has resulted in negative values for the selected frequency range. Values are approximately between -0.1 and -0.6, and the average is close to -0.5.

Table 5.1 Results of the main regression [using equation (5.5) or (5.7)] for the selected frequency range (see end of the table for definitions of terms)

| f (Hz) | Regression coefficients for equation (5.7) | | | | | | | | | σ_{est} | R^2 | SS(reg) | SS(resi) |
|----------|--|----------|--------|----------|------|----------|--------|----------|------|----------------|-------|---------|----------|
| | C_1 | σ | C_2 | σ | b | σ | C_T | σ | | | | | |
| 0.5 | 0.577 | 0.10 | -0.196 | 0.18 | -0.1 | 0.19 | -2.474 | 0.56 | 0.22 | 0.72 | 18.81 | 7.17 | |
| 0.6 | 0.529 | 0.09 | -0.069 | 0.17 | -0.2 | 0.17 | -2.264 | 0.50 | 0.20 | 0.78 | 19.96 | 5.76 | |
| 0.7 | 0.443 | 0.10 | 0.078 | 0.18 | -0.1 | 0.19 | -2.353 | 0.56 | 0.22 | 0.73 | 19.08 | 7.19 | |
| 0.8 | 0.381 | 0.09 | 0.223 | 0.18 | -0.2 | 0.18 | -1.970 | 0.55 | 0.22 | 0.74 | 19.94 | 6.88 | |
| 0.9 | 0.375 | 0.09 | 0.253 | 0.17 | -0.3 | 0.17 | -1.621 | 0.53 | 0.21 | 0.76 | 20.54 | 6.38 | |
| 1 | 0.375 | 0.09 | 0.223 | 0.18 | -0.3 | 0.18 | -1.547 | 0.55 | 0.22 | 0.74 | 19.29 | 6.80 | |
| 1.1 | 0.378 | 0.10 | 0.169 | 0.18 | -0.2 | 0.18 | -1.719 | 0.56 | 0.22 | 0.71 | 17.51 | 7.16 | |
| 1.2 | 0.383 | 0.10 | 0.116 | 0.19 | -0.2 | 0.19 | -1.889 | 0.58 | 0.23 | 0.67 | 15.90 | 7.72 | |
| 1.3 | 0.352 | 0.10 | 0.152 | 0.19 | -0.2 | 0.19 | -1.817 | 0.58 | 0.23 | 0.66 | 15.04 | 7.64 | |
| 1.4 | 0.337 | 0.10 | 0.172 | 0.18 | -0.2 | 0.19 | -1.753 | 0.56 | 0.23 | 0.67 | 14.70 | 7.23 | |
| 1.5 | 0.335 | 0.10 | 0.202 | 0.18 | -0.3 | 0.18 | -1.424 | 0.56 | 0.22 | 0.69 | 15.52 | 7.07 | |
| 1.6 | 0.348 | 0.09 | 0.187 | 0.18 | -0.3 | 0.18 | -1.419 | 0.54 | 0.22 | 0.71 | 15.90 | 6.63 | |
| 1.7 | 0.332 | 0.09 | 0.220 | 0.18 | -0.3 | 0.18 | -1.406 | 0.54 | 0.22 | 0.71 | 16.03 | 6.64 | |
| 1.8 | 0.312 | 0.09 | 0.250 | 0.18 | -0.3 | 0.18 | -1.202 | 0.53 | 0.21 | 0.71 | 15.63 | 6.48 | |

| | | | | | | | | | | | | |
|-----|-------|------|--------|------|------|------|--------|------|------|------|-------|------|
| 1.9 | 0.285 | 0.09 | 0.280 | 0.17 | -0.3 | 0.17 | -1.198 | 0.53 | 0.21 | 0.70 | 14.87 | 6.35 |
| 2 | 0.266 | 0.09 | 0.307 | 0.17 | -0.4 | 0.17 | -1.005 | 0.51 | 0.21 | 0.71 | 14.43 | 6.03 |
| 2.1 | 0.273 | 0.09 | 0.286 | 0.16 | -0.4 | 0.16 | -0.828 | 0.50 | 0.20 | 0.71 | 14.17 | 5.66 |
| 2.2 | 0.282 | 0.08 | 0.274 | 0.16 | -0.4 | 0.16 | -0.759 | 0.49 | 0.20 | 0.72 | 14.29 | 5.47 |
| 2.3 | 0.275 | 0.09 | 0.277 | 0.16 | -0.5 | 0.16 | -0.728 | 0.50 | 0.20 | 0.71 | 13.95 | 5.68 |
| 2.4 | 0.250 | 0.09 | 0.325 | 0.17 | -0.5 | 0.17 | -0.560 | 0.51 | 0.20 | 0.70 | 13.94 | 5.86 |
| 2.5 | 0.227 | 0.09 | 0.352 | 0.17 | -0.5 | 0.17 | -0.560 | 0.51 | 0.20 | 0.69 | 13.41 | 5.91 |
| 2.6 | 0.219 | 0.09 | 0.345 | 0.17 | -0.5 | 0.17 | -0.654 | 0.50 | 0.20 | 0.69 | 12.63 | 5.77 |
| 2.7 | 0.225 | 0.09 | 0.318 | 0.16 | -0.5 | 0.16 | -0.631 | 0.50 | 0.20 | 0.68 | 12.14 | 5.64 |
| 2.8 | 0.224 | 0.08 | 0.312 | 0.16 | -0.5 | 0.16 | -0.578 | 0.49 | 0.19 | 0.69 | 11.86 | 5.38 |
| 2.9 | 0.239 | 0.08 | 0.276 | 0.16 | -0.4 | 0.16 | -0.658 | 0.48 | 0.19 | 0.69 | 11.63 | 5.22 |
| 3 | 0.248 | 0.08 | 0.247 | 0.15 | -0.4 | 0.15 | -0.623 | 0.46 | 0.19 | 0.70 | 11.25 | 4.90 |
| 3.1 | 0.268 | 0.08 | 0.201 | 0.15 | -0.4 | 0.15 | -0.593 | 0.46 | 0.18 | 0.70 | 11.03 | 4.73 |
| 3.2 | 0.286 | 0.08 | 0.166 | 0.15 | -0.4 | 0.15 | -0.520 | 0.46 | 0.18 | 0.70 | 11.02 | 4.83 |
| 3.3 | 0.283 | 0.08 | 0.166 | 0.15 | -0.5 | 0.15 | -0.397 | 0.47 | 0.19 | 0.69 | 10.88 | 5.00 |
| 3.4 | 0.288 | 0.08 | 0.154 | 0.16 | -0.5 | 0.16 | -0.351 | 0.48 | 0.19 | 0.67 | 10.81 | 5.25 |
| 3.5 | 0.289 | 0.08 | 0.144 | 0.16 | -0.5 | 0.16 | -0.236 | 0.49 | 0.20 | 0.66 | 10.53 | 5.48 |
| 3.6 | 0.296 | 0.09 | 0.119 | 0.16 | -0.5 | 0.16 | -0.177 | 0.50 | 0.20 | 0.65 | 10.24 | 5.59 |
| 3.7 | 0.292 | 0.09 | 0.120 | 0.16 | -0.5 | 0.17 | -0.196 | 0.50 | 0.20 | 0.64 | 10.03 | 5.72 |
| 3.8 | 0.297 | 0.09 | 0.106 | 0.16 | -0.5 | 0.16 | -0.216 | 0.50 | 0.20 | 0.64 | 9.89 | 5.67 |
| 3.9 | 0.305 | 0.09 | 0.091 | 0.16 | -0.5 | 0.17 | -0.194 | 0.50 | 0.20 | 0.63 | 9.89 | 5.72 |
| 4 | 0.301 | 0.09 | 0.095 | 0.16 | -0.5 | 0.17 | -0.199 | 0.50 | 0.20 | 0.63 | 9.80 | 5.73 |
| 4.1 | 0.295 | 0.09 | 0.099 | 0.16 | -0.5 | 0.16 | -0.275 | 0.50 | 0.20 | 0.63 | 9.56 | 5.60 |
| 4.2 | 0.311 | 0.09 | 0.060 | 0.16 | -0.5 | 0.17 | -0.295 | 0.50 | 0.20 | 0.62 | 9.39 | 5.70 |
| 4.3 | 0.321 | 0.08 | 0.035 | 0.16 | -0.5 | 0.16 | -0.283 | 0.49 | 0.20 | 0.63 | 9.22 | 5.46 |
| 4.4 | 0.327 | 0.08 | 0.017 | 0.16 | -0.5 | 0.16 | -0.293 | 0.49 | 0.20 | 0.63 | 9.06 | 5.40 |
| 4.5 | 0.318 | 0.08 | 0.028 | 0.16 | -0.4 | 0.16 | -0.311 | 0.49 | 0.20 | 0.62 | 8.89 | 5.40 |
| 4.6 | 0.330 | 0.08 | 0.004 | 0.16 | -0.5 | 0.16 | -0.273 | 0.49 | 0.20 | 0.62 | 8.87 | 5.42 |
| 4.7 | 0.338 | 0.08 | -0.009 | 0.16 | -0.5 | 0.16 | -0.173 | 0.49 | 0.20 | 0.62 | 8.95 | 5.43 |
| 4.8 | 0.343 | 0.08 | -0.021 | 0.16 | -0.5 | 0.16 | -0.102 | 0.49 | 0.20 | 0.62 | 8.88 | 5.42 |
| 4.9 | 0.349 | 0.08 | -0.041 | 0.16 | -0.5 | 0.16 | -0.093 | 0.49 | 0.20 | 0.61 | 8.70 | 5.48 |
| 5 | 0.353 | 0.08 | -0.049 | 0.16 | -0.5 | 0.16 | -0.086 | 0.49 | 0.19 | 0.62 | 8.66 | 5.38 |
| 5.1 | 0.361 | 0.08 | -0.062 | 0.16 | -0.5 | 0.16 | 0.001 | 0.48 | 0.19 | 0.62 | 8.74 | 5.28 |
| 5.2 | 0.362 | 0.08 | -0.061 | 0.16 | -0.5 | 0.16 | 0.060 | 0.48 | 0.19 | 0.63 | 8.85 | 5.19 |
| 5.3 | 0.358 | 0.08 | -0.053 | 0.16 | -0.5 | 0.16 | 0.074 | 0.47 | 0.19 | 0.63 | 8.83 | 5.10 |
| 5.4 | 0.351 | 0.08 | -0.042 | 0.16 | -0.6 | 0.16 | 0.150 | 0.48 | 0.19 | 0.63 | 8.76 | 5.18 |
| 5.5 | 0.348 | 0.08 | -0.040 | 0.16 | -0.5 | 0.16 | 0.127 | 0.47 | 0.19 | 0.63 | 8.66 | 5.15 |
| 5.6 | 0.346 | 0.08 | -0.036 | 0.15 | -0.5 | 0.16 | 0.132 | 0.47 | 0.19 | 0.63 | 8.67 | 5.03 |
| 5.7 | 0.336 | 0.08 | -0.015 | 0.15 | -0.5 | 0.15 | 0.124 | 0.47 | 0.19 | 0.64 | 8.71 | 4.95 |
| 5.8 | 0.321 | 0.08 | 0.014 | 0.15 | -0.5 | 0.15 | 0.101 | 0.46 | 0.18 | 0.64 | 8.67 | 4.82 |
| 5.9 | 0.316 | 0.08 | 0.021 | 0.15 | -0.5 | 0.15 | 0.117 | 0.45 | 0.18 | 0.65 | 8.59 | 4.68 |
| 6 | 0.317 | 0.08 | 0.019 | 0.15 | -0.5 | 0.15 | 0.118 | 0.45 | 0.18 | 0.65 | 8.59 | 4.59 |
| 6.1 | 0.306 | 0.08 | 0.037 | 0.15 | -0.5 | 0.15 | 0.101 | 0.44 | 0.18 | 0.65 | 8.50 | 4.50 |
| 6.2 | 0.302 | 0.08 | 0.047 | 0.14 | -0.5 | 0.14 | 0.131 | 0.44 | 0.18 | 0.66 | 8.57 | 4.37 |
| 6.3 | 0.295 | 0.07 | 0.060 | 0.14 | -0.5 | 0.14 | 0.150 | 0.44 | 0.17 | 0.66 | 8.56 | 4.32 |
| 6.4 | 0.297 | 0.07 | 0.057 | 0.14 | -0.5 | 0.14 | 0.166 | 0.43 | 0.17 | 0.67 | 8.55 | 4.31 |
| 6.5 | 0.293 | 0.08 | 0.062 | 0.14 | -0.5 | 0.14 | 0.177 | 0.44 | 0.18 | 0.66 | 8.51 | 4.35 |
| 6.6 | 0.290 | 0.07 | 0.069 | 0.14 | -0.5 | 0.14 | 0.188 | 0.43 | 0.17 | 0.66 | 8.52 | 4.30 |
| 6.7 | 0.290 | 0.07 | 0.071 | 0.14 | -0.5 | 0.14 | 0.191 | 0.43 | 0.17 | 0.67 | 8.56 | 4.22 |
| 6.8 | 0.289 | 0.07 | 0.077 | 0.14 | -0.6 | 0.14 | 0.259 | 0.42 | 0.17 | 0.68 | 8.70 | 4.11 |
| 6.9 | 0.292 | 0.07 | 0.072 | 0.14 | -0.6 | 0.14 | 0.349 | 0.42 | 0.17 | 0.68 | 8.73 | 4.07 |
| 7 | 0.291 | 0.07 | 0.077 | 0.14 | -0.6 | 0.14 | 0.377 | 0.42 | 0.17 | 0.69 | 8.78 | 4.03 |
| 7.1 | 0.297 | 0.07 | 0.065 | 0.14 | -0.6 | 0.14 | 0.373 | 0.42 | 0.17 | 0.69 | 8.80 | 4.00 |

| | | | | | | | | | | | | |
|------------|-------|------|--------|------|------|------|-------|------|------|------|------|------|
| 7.2 | 0.306 | 0.07 | 0.050 | 0.14 | -0.6 | 0.14 | 0.381 | 0.41 | 0.17 | 0.69 | 8.84 | 3.92 |
| 7.3 | 0.312 | 0.07 | 0.041 | 0.14 | -0.6 | 0.14 | 0.410 | 0.41 | 0.17 | 0.70 | 8.93 | 3.87 |
| 7.4 | 0.319 | 0.07 | 0.028 | 0.14 | -0.6 | 0.14 | 0.404 | 0.41 | 0.16 | 0.70 | 8.97 | 3.85 |
| 7.5 | 0.325 | 0.07 | 0.016 | 0.13 | -0.6 | 0.14 | 0.357 | 0.41 | 0.16 | 0.70 | 8.97 | 3.82 |
| 7.6 | 0.333 | 0.07 | 0.002 | 0.13 | -0.6 | 0.13 | 0.383 | 0.40 | 0.16 | 0.71 | 9.02 | 3.69 |
| 7.7 | 0.336 | 0.07 | -0.002 | 0.13 | -0.6 | 0.13 | 0.354 | 0.40 | 0.16 | 0.71 | 9.04 | 3.62 |
| 7.8 | 0.346 | 0.07 | -0.022 | 0.13 | -0.6 | 0.13 | 0.337 | 0.39 | 0.16 | 0.72 | 9.04 | 3.51 |
| 7.9 | 0.350 | 0.07 | -0.031 | 0.13 | -0.6 | 0.13 | 0.333 | 0.38 | 0.15 | 0.73 | 9.03 | 3.38 |
| 8 | 0.356 | 0.06 | -0.041 | 0.12 | -0.6 | 0.12 | 0.329 | 0.38 | 0.15 | 0.74 | 9.05 | 3.24 |
| 8.1 | 0.357 | 0.06 | -0.047 | 0.12 | -0.6 | 0.12 | 0.255 | 0.37 | 0.15 | 0.75 | 8.99 | 3.07 |
| 8.2 | 0.362 | 0.06 | -0.057 | 0.12 | -0.5 | 0.12 | 0.239 | 0.36 | 0.14 | 0.75 | 8.97 | 2.94 |
| 8.3 | 0.368 | 0.06 | -0.067 | 0.12 | -0.6 | 0.12 | 0.237 | 0.36 | 0.14 | 0.76 | 8.98 | 2.88 |
| 8.4 | 0.373 | 0.06 | -0.079 | 0.12 | -0.5 | 0.12 | 0.197 | 0.36 | 0.14 | 0.76 | 8.96 | 2.88 |
| 8.5 | 0.377 | 0.06 | -0.090 | 0.12 | -0.5 | 0.12 | 0.142 | 0.36 | 0.14 | 0.75 | 8.88 | 2.96 |

σ - Standard error of the coefficient

σ_{est} - Standard error of the estimate

R^2 - Coefficient of determination

SS(reg)-Regression Sum of Squares

SS(res)-Residual Sum of Squares

The variation of b with the wave frequency is graphically indicated in Figure 5.1, in which it shows slightly lower attenuation rates (less than $R^{-0.5}$) scattered between $R^{-0.1}$ and $R^{-0.5}$ are given for low frequencies (below about 2 Hz). At high frequencies, attenuations follow the common form $R^{-0.5}$ which has been previously established by many researchers based on the studies of regional seismic phases such as L_g (Herrmann and Kijko, 1983; Kennett, 1986; Shin and Herrmann, 1987). Although, the resulted average far-source attenuation rate coincides with previous studies, the explanatory reason may need to be placed in a different context. The attenuation rate $R^{-0.5}$, found in the above studies, is generally based on earthquake data of continental crusts, whereas the data in the present study are originally from a thinner oceanic crust. Studies have shown that regionally dominant phases like L_g is not effective or totally absent to traverse through a thinner oceanic crust due to inconsistency in the wave field and crustal structure, which may be attributed with physical features like thickness and composition (presence of sediments) (Kennett, 1986; Knopoff et al, 1979). Hence, oceanic crusts such as in the northern Indian Ocean could be less effective in transmitting L_g waves through the medium, in which case a direct comparison of the far-source attenuation rate obtained in the present study with that in the aforementioned studies on continental crusts, is a little intricate. However, despite the difference in the regional wave field and physical attributes between the two crustal types, a similar far-source geometric attenuation rate as of a continental crust has resulted for the northern Indian Oceanic region. This would imply that the attenuation rate is more independent of both the type of the crust (whether continental or oceanic) and regional seismic wave field associated with the medium. Consequently, multiple reflections and refractions of seismic waves taking place at far-source distances, appear insensitive to the dominant wave type in the particular case (e.g., L_g for continental crusts and may be S_n for oceanic crusts).

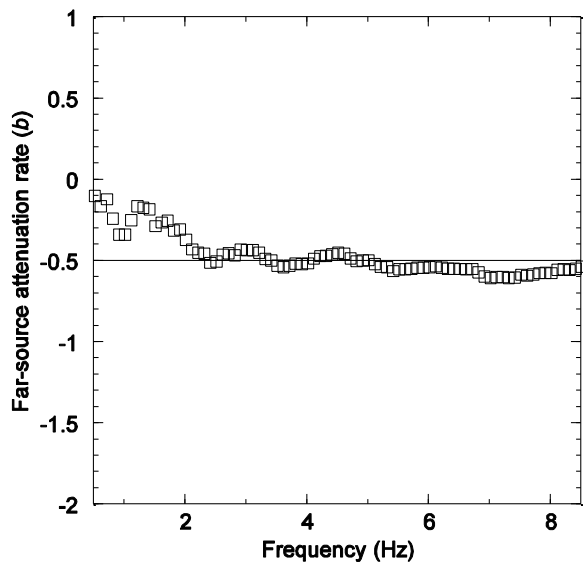


Figure 5.1 Variation of the far-source geometric attenuation rate, b , with wave frequency. Values are approximately within -0.1 and -0.6, while being the average close to -0.5. Slightly lower attenuation rates especially scattered at low frequencies up to about 2 Hz are noticeable. At high frequencies, attenuations show generally following -0.5 rate as indicated previously by many others based on studies of regional seismic phases such as L_g (Herrmann and Kijko, 1983; Kennett, 1986; Shin and Herrmann, 1987)

Figure 5.2 shows a comparison of recorded and predicted [from equation (5.7)] acceleration amplitudes for two sample frequencies 4.5 and 7.0 Hz. Two magnitude bands (m_b 4.0-4.5 and 4.5-5.0) are selected for the comparison. The predicted amplitudes are based on the median magnitude in each selected magnitude band, i.e., m_b 4.25 and 4.75, respectively, for m_b 4.0-4.5 and 4.5-5.0. Recorded amplitudes show a good comparison with the predicted ones for the chosen magnitude-distance combinations.

A residual analysis is carried out to see whether any unforeseen tradeoff exists between the results and regression variables. This partly validates the selected independent variables and their coherence to the regression equation. Residuals are defined as the difference between log observed amplitudes and log predicted amplitudes. Figure 5.3 shows the variation of residuals with the earthquake magnitude (m_b) and with the logarithmic value of the hypocentral distance ($\log R$). The figures do not show any apparent trend in residuals with the selected variables, and thus ensure the reliability of the selected attenuation equation for defining the actual dataset. Hypocentral depth dependency on the regression is not considered since all the selected events are shallow crustal with depths around 10 km maximum.

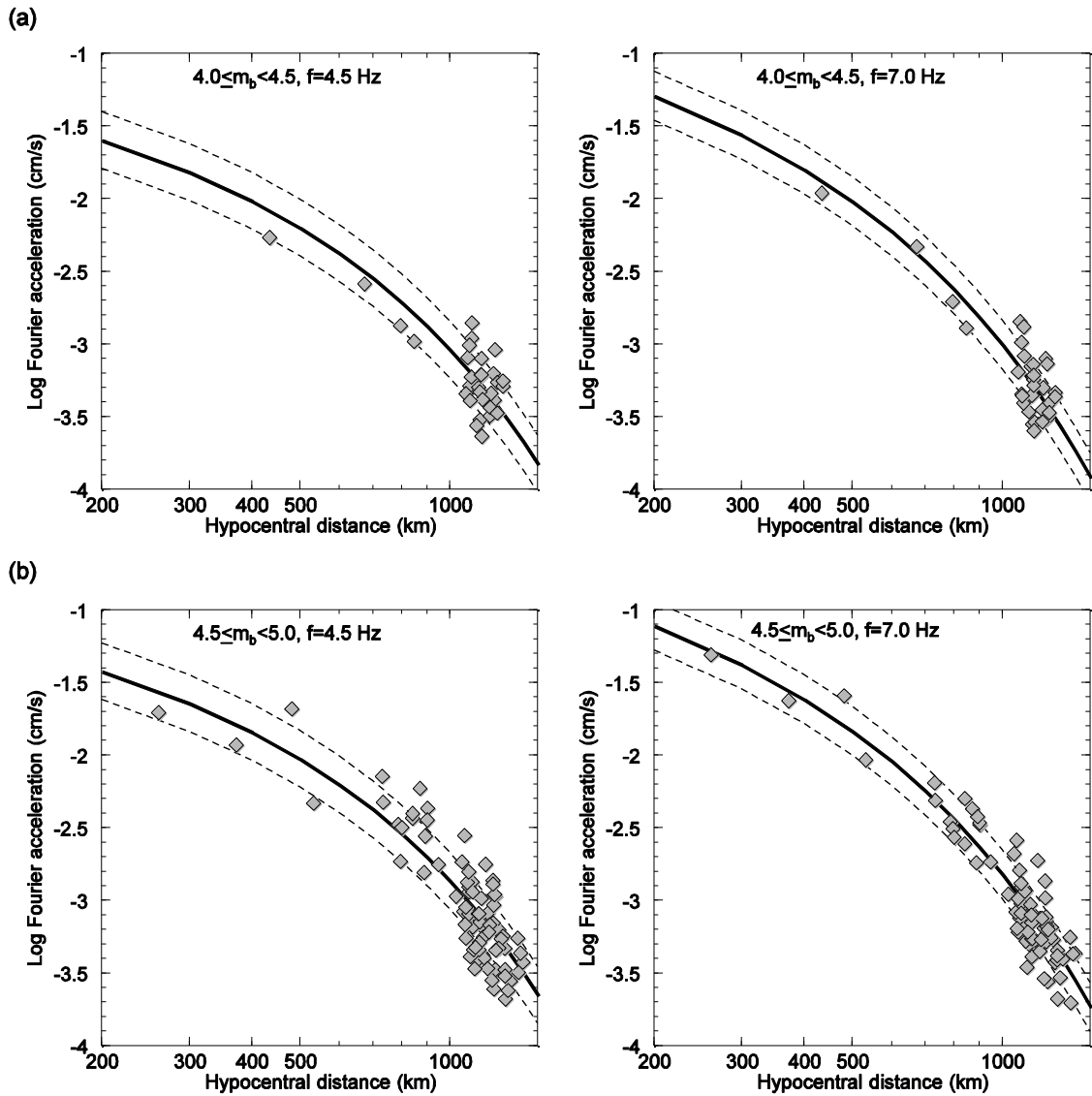


Figure 5.2 Comparison of recorded vertical component acceleration amplitudes with predicted ones from the applied attenuation relationship [equation (5.7)], at two selected frequencies (4.5 and 7.0 Hz), for two magnitude bands m_b 4.0-4.5 and 4.5-5.0. The predicted amplitudes are based on the median magnitude in each selected magnitude band, i.e., m_b 4.25 and 4.75, respectively, for m_b 4.0-4.5 and 4.5-5.0. Solid line represents the mean predicted amplitudes and diamonds represent recorded amplitudes. Dash lines denote standard error on mean. (a) For m_b 4.0-4.5. (b) For m_b 4.5-5.0.

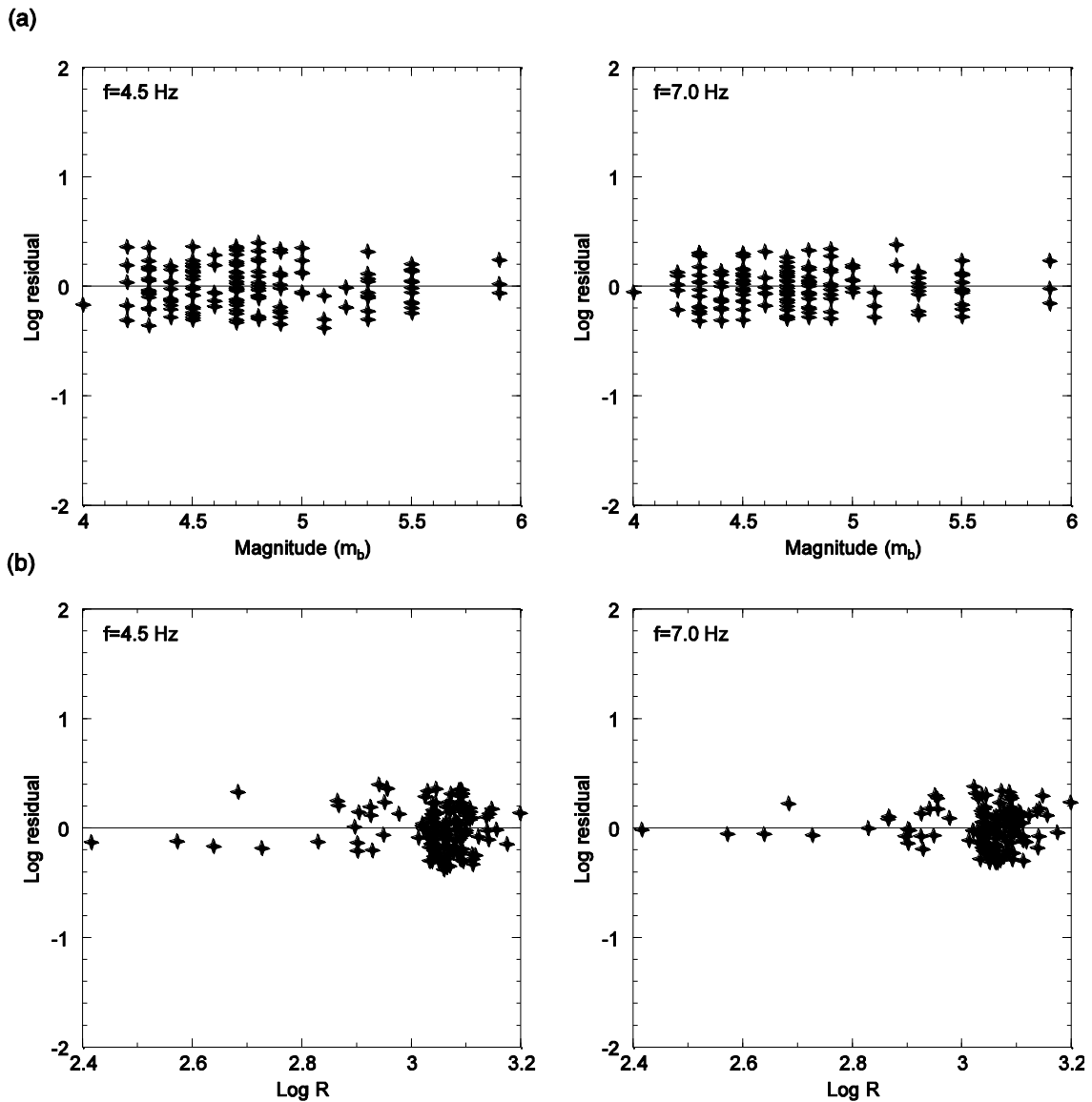


Figure 5.3 Log residual (= log observed amplitude-log predicted amplitude) variation for selected frequencies (4.5 and 7.0 Hz). (a) Log residual vs. magnitude (m_b). (b) Log residual vs. Log hypocentral distance. Figures show no any apparent trend in residuals in respect to the selected variables.

5.3.2 The secondary regression

Individual variations of each regression coefficient, C_1 , C_2 and C_T with the wave frequency are examined (Figure 5.4). Figures 5.4a and 5.4b evidence some random variations in C_1 and C_2 with the frequency, although a meaningful trend is hard to be identified in either case. Nevertheless, Figure 5.4c indicates a clear increasing trend in C_T showing a frequency dependent variation as which alluded in section 5.2.2 (“The secondary regression”). The probable reason for this observation can be related to previously discussed amalgamation of the high frequency cutoff filter (or the near-surface attenuation function). By taking this into account, resulted C_T is fitted with equation (5.8) for decomposing near-surface attenuation, and near- and medium-source

geometric attenuation portions hidden inside C_T . Estimated C_T values given in Table 5.1 (from the main regression) are first modified to the respective displacement spectral amplitude (by adding $-\log[2\pi f]^2$), and then the secondary regression is performed for a preselected 0.5-5.5 Hz frequency range in order to avoid or to minimize effects by frequency dependent magnitude parameter- C_3 (explained in section 5.2.2).

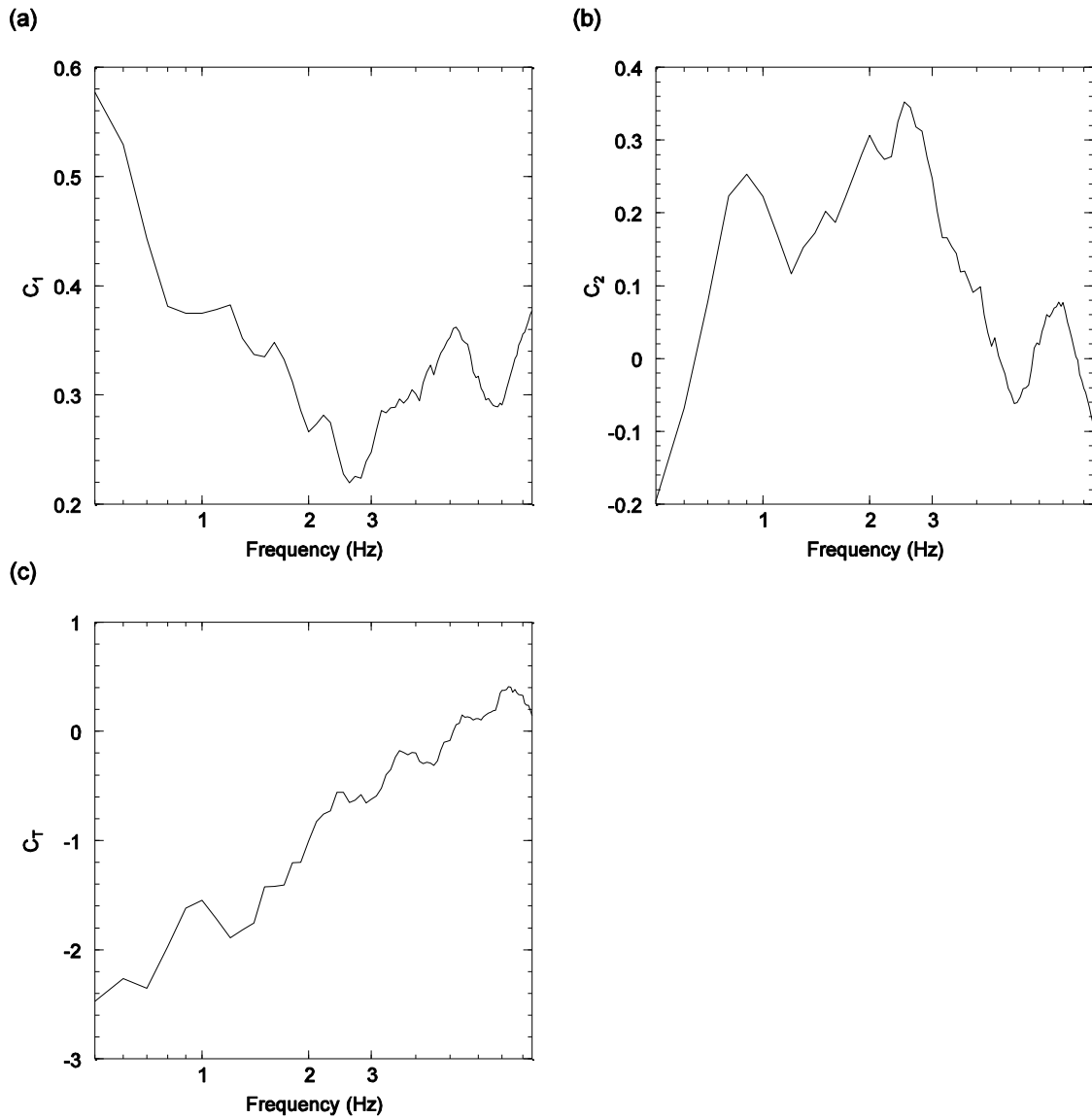


Figure 5.4 Variation of regression coefficients, C_1 , C_2 and C_T with wave frequency. (a) C_1 vs. frequency. (b) C_2 vs. frequency. (c) C_T vs. frequency. C_1 and C_2 show a random variation with wave frequency, though, C_T poses a clear increasing trend as expected, probably due to amalgamation with the high frequency cutoff filter (or near-surface attenuation function) defined in equation (5.6).

This secondary regression results are given in Table 5.2, and are graphically presented in Figure 5.5. A slightly higher Kappa value of 0.041 ± 0.009 s is resulted by the regression. A similar higher Kappa value of 0.04 ± 0.02 s has found based on a spectral analysis of a smaller dataset consisted

with small magnitude local events occurred in the country's continental crust (described in Chapter 6). Two studies are different each other in the senses of the data used and methodology applied; the data in the local study described in Chapter 6 comprise with small magnitude shallow crustal events which occurred at short and medium hypocentral distances (the maximum of about 185 km), whereas the data in the present study are from a number of moderate magnitude oceanic crustal events occurred at distant sources. Again, Kappa in the local study is determined by direct measuring the slope in attenuation corrected displacement source spectra of individual events, yet the calculation of the present study is based on the overall spectral shape featured by the dataset. Regardless of potential discrepancies in source characteristics between two regions (due to smaller events in a continental crust and moderate events in an oceanic crust in the local study described in Chapter 6 and in the present study, respectively), similar Kappa values have resulted in both of the studies. This urges the high frequency cutoff filter is to be more treated as a wave path modification function rather than a derivative of source property as explained by Papageorgiou and Aki (1983). This wave path modification can be mostly related to the localized upper portion of the crust where the seismic wave front ends, since dissimilarities in other path modifications such as differences in Q and geometric attenuation between the two studies, have caused no any major impact on final Kappa values. It is also acknowledged that the small difference between estimated Kappa values in the two studies may be due to differences in the data type and sample size, differences in the applied methodology and respective degree of uncertainty associated with the each method, accuracy of other path modification parameters, etc. A Kappa of 0.041 ± 0.009 s, however, seems reasonable for a typical intraplate crust, given the evidence of findings in other analogous regions; 0.05 and 0.045 s, for central Europe and Northeastern Italy, respectively (Malagnini et al, 2000a; 2002).

Table 5.2 Results of the secondary regression by equation (5.8)

Resulted regression coefficients for equation (5.8); $*C_T = -\pi\kappa \log[exp] f - \log[R_{x2}] b + C_3 + a \log R_{x1}$

$$-\pi\kappa \log[exp] = -0.055279, \text{ Therefore, } \kappa = 0.041 \pm 0.009$$

$$-\log[R_{x2}] = -2.078378, \text{ Therefore, } R_{x2} = 120 \pm 30 \text{ km}$$

$$C_3 + a \log R_{x1} = -3.846155$$

* C_T values from the main regression (Table 5.1) have been modified in order to comply with displacement amplitude by adding $-\log[2\pi f]^2$ prior to the secondary regression

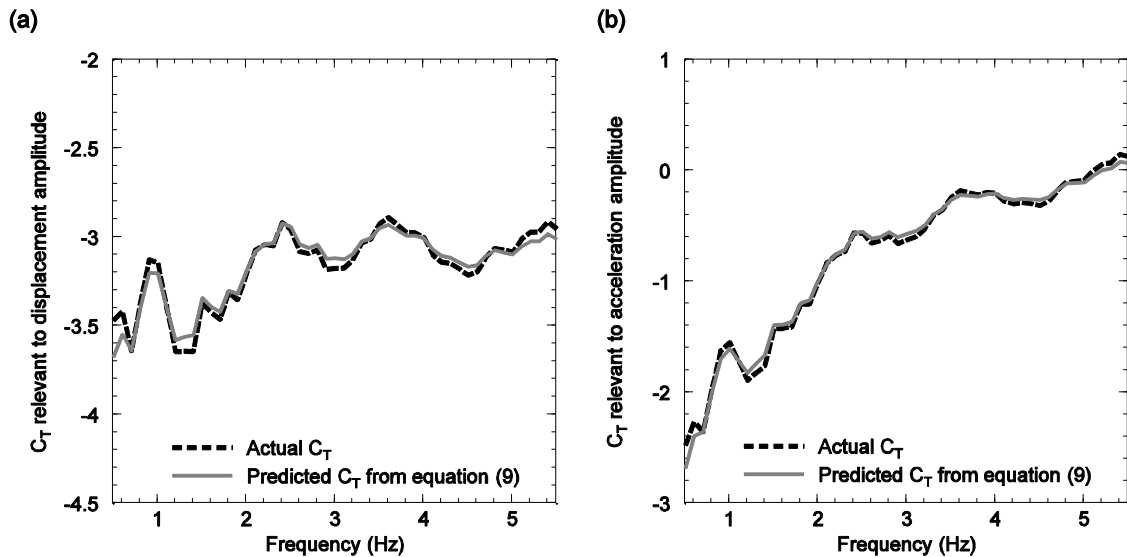


Figure 5.5 Comparison of actual C_T resulted from the main regression with the predicted from equation (5.8). The secondary regression is undertaken for a lower frequency range of 0.5-5.5 Hz as to avoid the effects of frequency dependent magnitude parameter- C_3 . (a) Comparison of C_T relevant to displacement amplitude. (b) Comparison of C_T relevant to acceleration amplitude.

The resulted Kappa value 0.041 ± 0.009 s supports the fact that presence of a poor quality upper crustal layer in the country's underlying bedrock as speculated in section 5.2.2. However, the overall impact on the final wave content due to the presence of a thin sedimentary layer at the upper crustal level, is still required to be clarified. Apart from the attenuation, certain researchers argue about a possible wave amplification taking place also at the shallow rock depths, within about the uppermost 4 km (see section 2.3.5 in Chapter 2). The reason for this wave amplification is the decline of the propagation velocity when the medium becomes weaker by poor physical characteristics (i.e., hardness, rigidity, cavity content) (Boore and Joyner, 1997). The situation is simply analogous to that of vertically propagating shear waves in a typical soil column, in which seismic waves are subject to a "pile-up" as to obey with the law of conservation of energy. The wave amplification is proposed to quantify by a methodology called "the quarter wavelength approximation method", in which the shear wave travel times measured based on a regional shear wave velocity profile, are averaged at quarter wavelengths along the depth of the upper crust to find corresponding amplification expected at each particular depth (Boore and Joyner, 1997). Amplitude ratio between horizontal to vertical, alias "H/V", is used sometimes as "a crude approximation" to represent the upper crustal amplification of the region (Atkinson, 2004b). According to the results of the study in Chapter 4, the H/V ratio for the Sri Lankan upper crust is almost close to unity (see Figure 4.8 in Chapter 4), which indicates virtually a zero upper crustal amplification in effect. Therefore, existence of a thinner sedimentary stratum has no greater impact on the upper crustal amplification, but substantially on the upper crustal attenuation as

evidenced by the resulted higher Kappa. Therefore, the interdependency between the upper crustal attenuation and amplification with respect to a presence of a younger sedimentary layer at the uppermost part, seems unpredictable. Given this context, the high frequency cutoff filter function would be better described as a spectral characteristic that rolls off high frequency waves, than merely identifying as a path specific feature that reflects the quality of the uppermost crust.

Resulted R_{x2} of 120 ± 30 km as the reference distance of the second hinge point in the trilinear geometric attenuation function, is comparable with findings in the literature (e.g., 140 km for ENA and southeastern Canada (Atkinson, 2004b), and 130 km for ENA (Atkinson and Boore, 1995)). The reference distances are sometimes calibrated based on geometric properties of the crust such as thickness. For instance, Lam et al (2000a) propose the two reference distances R_{x1} and R_{x2} of the trilinear form can be equal to $1.5D$ and $2.5D$, respectively, where D represents the regional crustal thickness in kilometers. Herrmann and Kijko (1983), in their bilinear form [in equation (5.1)], consider R_x as about twice as the crustal thickness. However, such a direct assertion between the estimated hinge point (R_{x2}) and the regional crustal thickness, is difficult to be rendered from the study, since 120 km is around 12 times greater than the average crustal thickness of the northern Indian Ocean region (which is about 10 km). Moreover, R_{x2} of about 25 km in accordance with $2.5D$ as proposed by Lam et al (2000a), can sometimes cause an underestimate of the actual geometric attenuation possible in the region. R_{x1} of the first hinge point is approximated to 55 km by a trial and error approach based on a spectral amplitude matching between recorded and simulated ground motions (discussed in section 5.3.4). The value of R_{x1} also follows the consensus of apparent source spectral level with that of the theoretical level as predicted by Brune's model. The near-source attenuation rate is taken as $R^{-1.3}$ based on the results of recent seismological studies undertaken in intraplate regions, in which the attenuation rate at the near-source range has shown clearly diverting from the typical R^{-1} , and has indicated higher rates close to $R^{-1.3}$ (Allen et al, 2007; Atkinson, 2004b). Additionally, a negligible or zero attenuation rate is applied to the medium-source distance range (between R_{x1} and R_{x2} , i.e., 55 and 120 km) in the trilinear form. Note that, the hinge point R_{x1} and the attenuation rates of near- and medium-source distances are not purely based on the data analysis. Hence, a final validation is essential, which is accomplished by a comparison of ground motions as shown in section 5.3.4.

Attenuated amounts in each mode (i.e., geometric, anelastic and upper crustal attenuation) are compared for a typical shallow crustal earthquake occurred in the northern Indian Ocean region. Estimated geometric and upper crustal attenuation parameters in this Chapter and the previously estimated anelastic attenuation form (in Chapter 4), are selected for the comparison. Figure 5.6a, in the frequency domain, compares wave attenuations due to the seismic absorption [or anelastic effects - $A_n(f)$] and high frequency cutoff effects [or upper crustal attenuation - $P(f)$] during the

travel through the oceanic crust to Sri Lanka. Figure 5.6b, in the hypocentral distance domain, shows the comparison of attenuations between $A_n(f)$ and G .

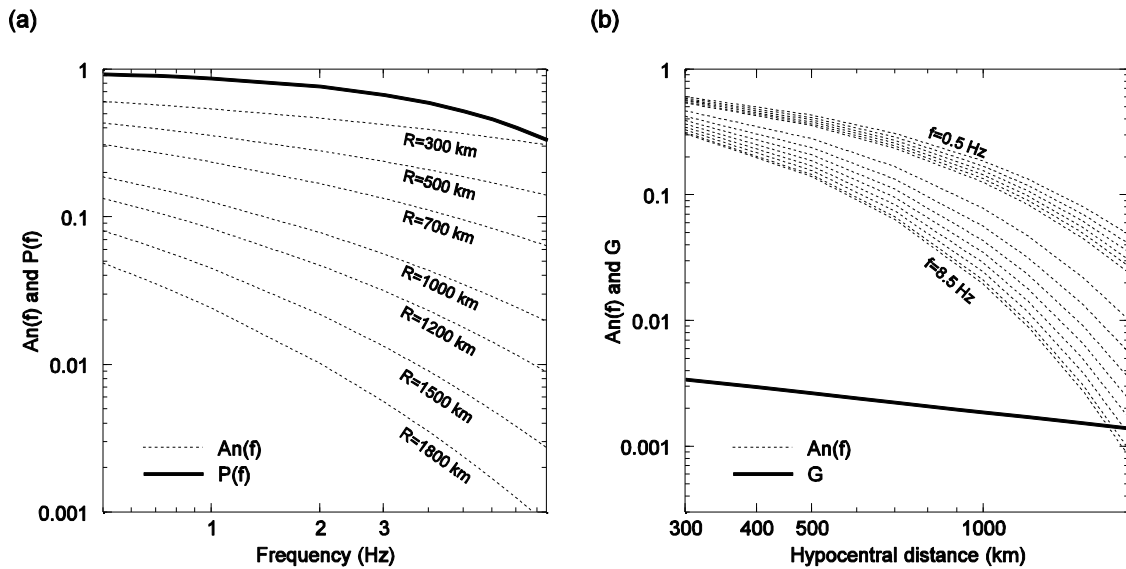


Figure 5.6 Comparison of expected path attenuations for a typical shallow crustal event occurred at a hypocentral distance within a possible range of 300-1800 km in the northern Indian Ocean region. The anelastic attenuation is estimated by equation (4.3) in Chapter 4 with $Q = 389f^{0.70}$; the upper crustal attenuation is found by equation (5.6) with $Kappa$ equals to 0.041 s; the geometric attenuation is obtained using, $G = 1/55^{1.3} \sqrt{120/R}$, $R > 120 km$. (a) Comparison of the anelastic attenuation and upper crustal attenuation in the frequency domain. (b) Comparison of the anelastic attenuation and geometric attenuation in the hypocentral distance domain. Figures show, for the selected frequency range (0.5-8.5 Hz), the geometric attenuation is by far the most dominant attenuation type for a typical earthquake occurred in the northern Indian Ocean at a possible scenario hypocentral distance of 300-1800 km from the country. The high frequency cutoff filter seems the least causative attenuation type on the final spectral level at the selected frequency range, provided the hypocentral distance of the event is relatively large. The anelastic attenuation on final wave modification can be subjective, since it depends on both of the hypocentral distance and frequency.

Figures evidence for the selected frequency range (0.5-8.5 Hz), the geometric attenuation is by far the most dominant attenuation form for a typical moderate magnitude earthquake of the northern Indian Ocean occurred at a possible scenario hypocentral distance of 300-1800 km from the country. The high frequency cutoff filter is the least causative attenuation type on the final spectral level at the selected frequency range, provided that the hypocentral distance of the event is relatively large. The anelastic attenuation on final wave modification can be subjective, since it depends on both the hypocentral distance and frequency. As shown in Figure 5.6b, $A_n(f)$ is possible to be the highest attenuation out of all three forms, only if the earthquake occurs at a very

large distance at least of about 1600 km, and also if the frequency of the wave considered is relatively high (f greater than about 8.0 Hz). In conclusion, “the spectral level” of a distant event in the northern Indian Ocean mostly depends on the geometric attenuation, whilst “the spectral shape” is owned by both the anelastic and upper crustal attenuations depending on the hypocentral distance and wave frequency of interest.

5.3.3 Apparent source parameters

Estimated source parameters by equation (5.11) are given in Table 5.3. Regression results that are based on negative intercepts are eliminated. Two sample plots that compare source amplitudes between actual and predicted are shown in Figure 5.7.

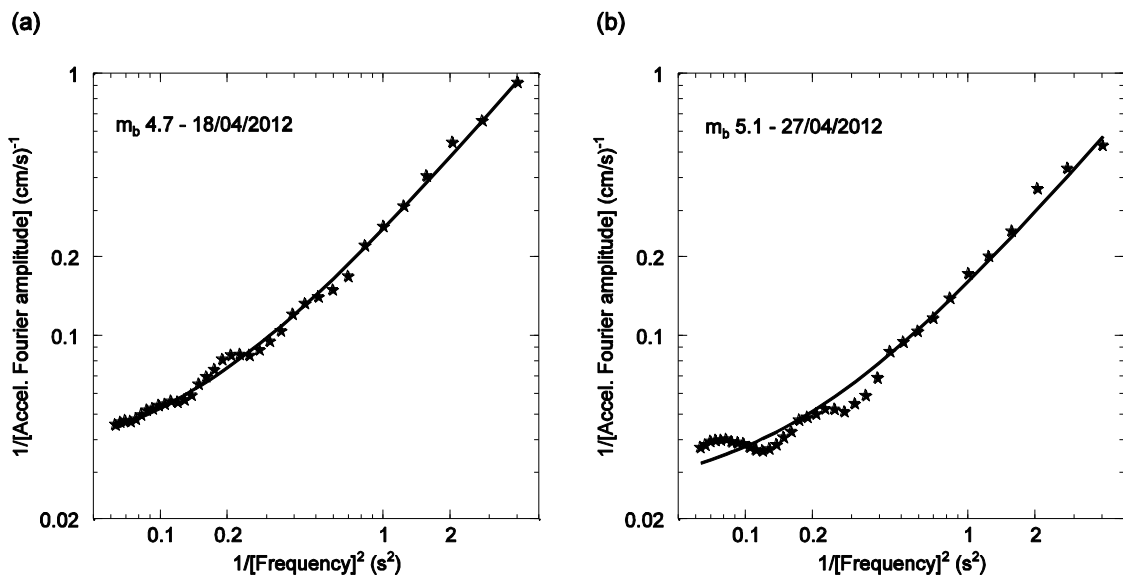


Figure 5.7 Comparison of source amplitudes between observed and predicted (note that the comparison is based on $1/\text{Amplitude}$). Stars represent observed amplitudes averaged over recorded stations and continuous line represents predicted amplitudes from Brune’s model, i.e., equation (5.11). (a) For m_b 4.7 - 18/04/2012. (b) For m_b 5.1 - 27/04/2012.

Table 5.3 Estimated source parameters for the dataset (source parameters are defined at the end of Table)

| Mag. (m _b) | Date and Time (UTC) | Lat. | Lon. | Depth (km) | Dist. R (km) | Regression results of eq. (5.11) | | | Source parameters | | | |
|------------------------|---------------------|--------|---------|------------|--------------|----------------------------------|-----------|-----|-------------------|------------|----------------------|-----|
| | | | | | | Slope | Intercept | R2 | f_0 | M_0 (Nm) | $\Delta\sigma$ (Mpa) | Mw |
| 4 | 25/07/10-09:35:02 | 6.54°N | 76.84°E | 10 | 435 | 0.967 | 0.344 | 0.7 | 1.7 | 7.00E+14 | 0.5 | 3.9 |
| 4.1 | 30/11/02-02:11:09 | 5.92°N | 89.00°E | 10 | 930 | 0.411 | 0.059 | 0.9 | 2.6 | 1.65E+15 | 4.3 | 4.1 |
| 4.2 | 13/04/12-04:36:33 | 1.09°N | 91.58°E | 10 | 1332 | 0.468 | 0.079 | 0.9 | 2.4 | 1.45E+15 | 3.0 | 4.1 |
| 4.2 | 06/05/12-08:08:04 | 2.39°N | 89.65°E | 10 | 1210 | 0.176 | 0.099 | 0.7 | 1.3 | 3.86E+15 | 1.3 | 4.4 |
| 4.2 | 14/04/12-02:49:15 | 2.63°N | 90.04°E | 10 | 1232 | 0.355 | -0.007 | 1.0 | - | - | - | - |
| 4.3 | 13/04/12-22:03:21 | 2.22°N | 89.67°E | 10 | 1223 | 0.441 | 0.126 | 1.0 | 1.9 | 1.53E+15 | 1.4 | 4.1 |
| 4.3 | 12/04/12-23:34:30 | 3.03°N | 89.54°E | 10 | 1040 | 0.617 | 0.324 | 0.7 | 1.4 | 1.10E+15 | 0.4 | 4.0 |
| 4.3 | 14/04/12-02:18:23 | 2.55°N | 89.99°E | 10 | 1232 | 0.371 | -0.004 | 1.0 | - | - | - | - |
| 4.3 | 26/04/12-03:17:42 | 3.59°N | 87.90°E | 10 | 974 | 0.381 | 0.272 | 0.6 | 1.2 | 1.77E+15 | 0.4 | 4.1 |
| 4.3 | 19/05/12-22:29:31 | 2.35°N | 89.80°E | 10 | 1094 | 0.192 | 0.109 | 0.7 | 1.3 | 3.53E+15 | 1.2 | 4.3 |
| 4.3 | 13/04/12-22:58:56 | 1.89°N | 89.69°E | 10 | 1246 | 0.540 | 0.024 | 1.0 | 4.7 | 1.25E+15 | 18.8 | 4.0 |
| 4.3 | 12/04/12-18:00:52 | 1.73°N | 89.55°E | 10 | 1244 | 0.306 | 0.170 | 0.9 | 1.3 | 2.21E+15 | 0.8 | 4.2 |
| 4.4 | 14/05/12-08:40:23 | 4.43°N | 86.53°E | 10 | 796 | 0.144 | 0.108 | 0.9 | 1.2 | 4.71E+15 | 1.0 | 4.4 |
| 4.4 | 18/05/12-15:46:38 | 2.26°N | 89.77°E | 10 | 1230 | 0.125 | 0.060 | 1.0 | 1.4 | 5.40E+15 | 2.4 | 4.5 |
| 4.4 | 14/04/12-04:03:49 | 2.47°N | 90.43°E | 10 | 1279 | 0.312 | 0.028 | 1.0 | 3.3 | 2.17E+15 | 11.4 | 4.2 |
| 4.4 | 12/05/12-10:30:26 | 2.60°N | 90.50°E | 10 | 1278 | 0.154 | 0.047 | 1.0 | 1.8 | 4.38E+15 | 3.7 | 4.4 |
| 4.5 | 30/05/12-17:21:18 | 3.53°N | 88.39°E | 10 | 1024 | 0.208 | 0.055 | 0.7 | 1.9 | 3.26E+15 | 3.5 | 4.3 |
| 4.5 | 15/04/12-10:20:59 | 2.58°N | 89.94°E | 10 | 1226 | 0.237 | 0.182 | 0.8 | 1.1 | 2.85E+15 | 0.6 | 4.3 |
| 4.5 | 23/04/12-00:12:26 | 2.72°N | 89.67°E | 10 | 1192 | 0.184 | 0.092 | 0.8 | 1.4 | 3.68E+15 | 1.5 | 4.3 |
| 4.5 | 13/05/12-12:30:56 | 2.45°N | 90.53°E | 10 | 1289 | 0.173 | 0.082 | 0.9 | 1.5 | 3.91E+15 | 1.7 | 4.4 |
| 4.5 | 13/04/12-19:52:06 | 1.54°N | 91.15°E | 10 | 1402 | 0.318 | 0.046 | 1.0 | 2.6 | 2.13E+15 | 5.6 | 4.2 |
| 4.5 | 18/04/12-17:50:26 | 2.54°N | 90.33°E | 10 | 1190 | 0.147 | 0.079 | 0.9 | 1.4 | 4.61E+15 | 1.7 | 4.4 |
| 4.5 | 07/07/12-09:01:51 | 3.07°N | 86.57°E | 10 | 893 | 0.135 | 0.027 | 1.0 | 2.2 | 5.00E+15 | 8.2 | 4.4 |
| 4.5 | 13/04/12-05:31:44 | 2.71°N | 89.73°E | 10 | 1198 | 0.567 | 0.028 | 1.0 | 4.5 | 1.19E+15 | 15.7 | 4.0 |
| 4.6 | 14/04/12-10:08:44 | 3.85°N | 89.95°E | 10 | 1157 | 0.184 | 0.023 | 1.0 | 2.8 | 3.67E+15 | 11.8 | 4.3 |
| 4.6 | 09/05/12-05:09:13 | 4.92°N | 87.77°E | 10 | 888 | 0.335 | 0.150 | 0.8 | 1.5 | 2.02E+15 | 1.0 | 4.2 |
| 4.6 | 06/07/12-14:18:27 | 4.96°N | 77.19°E | 10 | 533 | 0.402 | 0.145 | 1.0 | 1.7 | 1.68E+15 | 1.1 | 4.1 |
| 4.7 | 19/11/11-10:40:17 | 4.28°N | 79.19°E | 10 | 482 | 0.516 | 0.010 | 1.0 | 7.0 | 1.31E+15 | 64.8 | 4.0 |
| 4.7 | 09/05/12-07:30:39 | 4.99°N | 87.95°E | 10 | 902 | 0.197 | 0.005 | 1.0 | 6.3 | 3.43E+15 | 121.4 | 4.3 |
| 4.7 | 18/04/12-01:15:15 | 2.48°N | 89.76°E | 10 | 1215 | 0.229 | 0.031 | 1.0 | 2.7 | 2.96E+15 | 8.6 | 4.3 |
| 4.7 | 19/04/12-06:30:09 | 1.46°N | 90.79°E | 10 | 1373 | 0.089 | 0.095 | 0.9 | 1.0 | 7.61E+15 | 1.0 | 4.6 |
| 4.7 | 13/04/12-14:29:02 | 2.22°N | 90.26°E | 10 | 1277 | 0.512 | 0.059 | 1.0 | 2.9 | 1.32E+15 | 4.8 | 4.0 |

| | | | | | | | | | | | | |
|-----|-------------------|--------|---------|----|------|-------|--------|-----|-----|----------|------|-----|
| 4.7 | 13/04/12-04:49:49 | 1.67°N | 91.07°E | 10 | 1386 | 0.128 | 0.069 | 0.9 | 1.4 | 5.30E+15 | 1.9 | 4.4 |
| 4.7 | 09/05/12-14:27:16 | 2.33°N | 89.77°E | 10 | 1225 | 0.201 | 0.072 | 0.8 | 1.7 | 3.37E+15 | 2.2 | 4.3 |
| 4.7 | 15/05/12-00:25:36 | 2.09°N | 89.66°E | 10 | 1230 | 0.172 | 0.033 | 0.9 | 2.3 | 3.93E+15 | 6.6 | 4.4 |
| 4.7 | 12/05/12-15:01:26 | 2.47°N | 89.82°E | 10 | 1221 | 0.159 | 0.031 | 1.0 | 2.3 | 4.24E+15 | 7.1 | 4.4 |
| 4.8 | 26/02/02-01:50:43 | 2.97°N | 86.22°E | 10 | 777 | 0.679 | 0.096 | 0.9 | 2.7 | 9.97E+14 | 2.7 | 4.0 |
| 4.8 | 13/04/12-03:38:37 | 2.68°N | 90.07°E | 10 | 1232 | 0.233 | -0.004 | 1.0 | - | - | - | - |
| 4.8 | 05/05/12-03:34:00 | 3.66°N | 86.81°E | 10 | 871 | 0.058 | 0.048 | 0.9 | 1.1 | 1.17E+16 | 2.2 | 4.7 |
| 4.8 | 12/04/12-06:47:36 | 2.98°N | 89.42°E | 10 | 1030 | 0.459 | 0.026 | 1.0 | 4.2 | 1.47E+15 | 15.4 | 4.1 |
| 4.8 | 07/05/12-21:31:36 | 2.43°N | 89.81°E | 10 | 1223 | 0.135 | 0.054 | 0.9 | 1.6 | 5.02E+15 | 2.8 | 4.4 |
| 4.8 | 12/04/12-07:34:49 | 2.70°N | 89.76°E | 10 | 1202 | 0.144 | 0.074 | 0.9 | 1.4 | 4.70E+15 | 1.8 | 4.4 |
| 4.8 | 02/08/12-15:25:20 | 2.20°N | 89.63°E | 10 | 1220 | 0.107 | 0.062 | 0.6 | 1.3 | 6.33E+15 | 2.1 | 4.5 |
| 4.9 | 05/05/12-12:08:43 | 4.88°N | 87.92°E | 10 | 905 | 0.087 | 0.010 | 1.0 | 2.9 | 7.79E+15 | 28.3 | 4.6 |
| 4.9 | 18/04/12-11:59:15 | 1.81°N | 89.74°E | 10 | 1256 | 0.286 | 0.053 | 0.9 | 2.3 | 2.37E+15 | 4.3 | 4.2 |
| 4.9 | 14/06/12-10:58:25 | 2.63°N | 91.37°E | 10 | 1291 | 0.094 | 0.063 | 0.8 | 1.2 | 7.16E+15 | 1.9 | 4.5 |
| 4.9 | 13/04/12-12:48:11 | 3.42°N | 89.95°E | 10 | 1180 | 0.115 | 0.009 | 1.0 | 3.6 | 5.91E+15 | 41.0 | 4.5 |
| 4.9 | 15/04/12-13:57:40 | 1.74°N | 90.93°E | 10 | 1369 | 0.115 | 0.046 | 1.0 | 1.6 | 5.87E+15 | 3.3 | 4.5 |
| 5 | 29/04/12-02:13:55 | 2.39°N | 89.76°E | 10 | 1221 | 0.099 | 0.020 | 1.0 | 2.2 | 6.87E+15 | 11.1 | 4.5 |
| 5 | 25/07/12-06:13:04 | 2.09°N | 89.71°E | 10 | 1235 | 0.108 | 0.027 | 0.9 | 2.0 | 6.24E+15 | 7.4 | 4.5 |
| 5 | 16/09/12-06:07:26 | 3.60°N | 90.16°E | 10 | 1191 | 0.067 | 0.025 | 0.8 | 1.6 | 1.01E+16 | 6.5 | 4.6 |
| 5.1 | 27/04/12-01:40:52 | 2.23°N | 89.70°E | 10 | 1225 | 0.139 | 0.024 | 1.0 | 2.4 | 4.87E+15 | 9.6 | 4.4 |
| 5.2 | 15/05/12-05:19:55 | 2.72°N | 89.53°E | 10 | 1179 | 0.098 | -0.002 | 0.9 | - | - | - | - |
| 5.3 | 04/05/12-16:23:43 | 2.07°N | 89.73°E | 10 | 1238 | 0.049 | 0.004 | 1.0 | 3.4 | 1.38E+16 | 75.0 | 4.7 |
| 5.3 | 14/04/12-12:18:26 | 2.60°N | 90.35°E | 10 | 1263 | 0.039 | 0.012 | 0.9 | 1.8 | 1.72E+16 | 15.1 | 4.8 |
| 5.3 | 23/06/12-21:27:28 | 2.59°N | 90.49°E | 10 | 1277 | 0.020 | 0.008 | 0.9 | 1.6 | 3.34E+16 | 19.3 | 5.0 |
| 5.3 | 11/04/12-13:58:06 | 1.39°N | 90.82°E | 10 | 1381 | 0.048 | 0.031 | 1.0 | 1.3 | 1.42E+16 | 4.0 | 4.7 |
| 5.5 | 30/04/12-08:00:10 | 1.76°N | 89.66°E | 10 | 1252 | 0.025 | 0.012 | 0.9 | 1.4 | 2.76E+16 | 11.3 | 4.9 |
| 5.5 | 11/04/12-23:56:34 | 1.81°N | 89.60°E | 10 | 1243 | 0.013 | 0.012 | 0.8 | 1.1 | 5.12E+16 | 8.9 | 5.1 |
| 5.5 | 21/08/12-17:39:37 | 0.08°S | 91.95°E | 10 | 1578 | 0.030 | 0.018 | 0.8 | 1.3 | 2.29E+16 | 6.8 | 4.9 |
| 5.5 | 11/04/12-22:51:57 | 2.83°N | 89.54°E | 10 | 1173 | 0.022 | 0.012 | 0.9 | 1.4 | 3.10E+16 | 11.5 | 5.0 |
| 5.9 | 11/04/12-11:53:35 | 2.91°N | 89.56°E | 10 | 1171 | 0.005 | 0.004 | 0.9 | 1.0 | 1.47E+17 | 22.3 | 5.4 |

f_0 – Corner frequency

M_0 – Seismic moment

$\Delta\sigma$ – Static stress drop [from $f_0 = 4.9 \times 10^6 \beta (\frac{\Delta\sigma}{M_0})^{1/3}$]

M_w – Moment magnitude

Figure 5.8 presents resulted stress drop and corner frequency values for the dataset. Higher stress drops, averages close to 9.5 MPa (95 bars) and 16.0 MPa (160 bars) for magnitudes between m_b 4-5 and 5-6, respectively, are resulted (Figure 5.8a). While the corner frequency falls roughly within 1.0 to 7.0 Hz, the stress drop varies from 0.4 to a maximum about 140 MPa for the selected events. The corner frequency exhibits an inverse relation with the event magnitude as can be seen from Figure 5.8b. A small magnitude dependency in the stress drop showing a minor increasing trend is also evident from Figure 5.8a, however, this may have a trivial importance in practical situations.

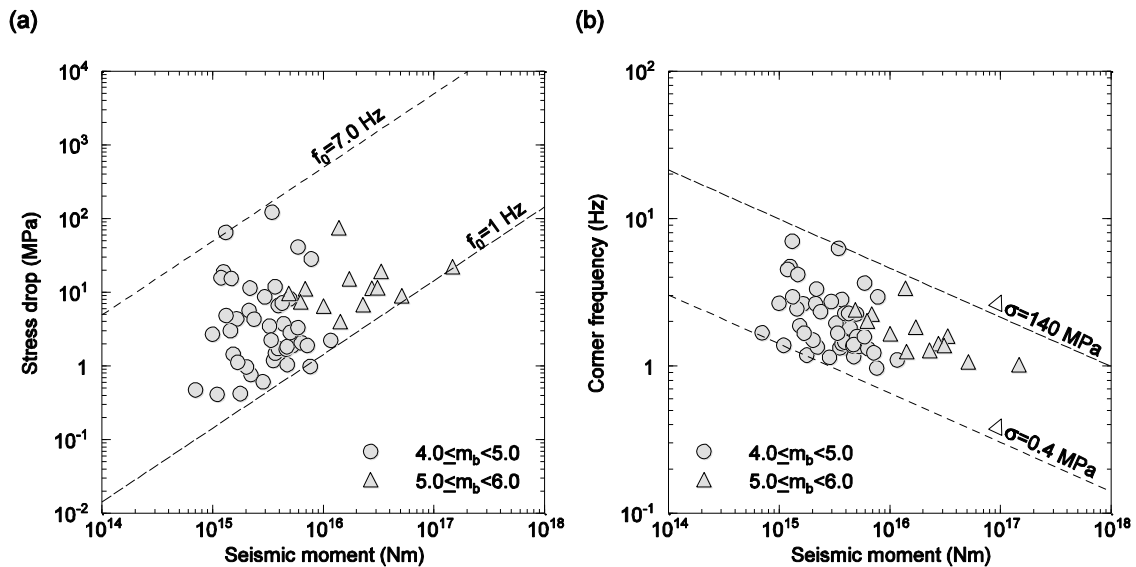


Figure 5.8 Estimated source parameters by the regression of equation (5.11). Circles and triangles are to denote events between m_b 4-5 and 5-6, respectively. (a) Variation of stress drop with the seismic moment. Higher stress drops, averages close to 9.5 MPa (95 bars) and 16.0 MPa (160 bars) for m_b 4-5 and 5-6, respectively, have been resulted. Dash lines represent constant corner frequencies of 1 and 6.5 Hz. (b) Variation of corner frequency with the seismic moment. Dash lines represent constant stress drops of 0.4 and 140 MPa.

Estimated stress drops agree with previous findings, as some studies have shown higher stress drop values for moderate magnitude earthquakes in intraplate oceanic crusts (Abercrombie et al, 2003; Allmann, 2008; Choy and Boatwright, 1995). Allmann (2008)'s comprehensive study specifically indicates higher stress drops of more than 10 MPa (100 bars) for large magnitude events ($5.5 < m_b$) in the northern Indian Ocean region towards the southeastern direction of Sri Lanka. Abercrombie et al (2003) derive higher stress drop levels of 5-10 MPa (50-100 bars) for Wharton basin area based on a study of M_w 7.9 event triggered in June 2000. Robinson et al (2001) have shown that the same event can be associated with a much larger stress drop value of about 20 MPa (200 bars). In Chapter 4, it has established 5 MPa (50 bars) as a reasonably accurate average stress drop value for moderate magnitude events in the subject region, though the value

seems to be inconsistent with the average stress drops found in the present study. The reason for the apparent inconsistency would be associated with the respective method followed in each case; in the previous study, the value was approximated based on a visual comparison of apparent source spectra obtained after correcting for path attenuations with the theoretical source spectra as defined by Brune's model, whereas in the present study, the stress drops are computed using event wise regressions. The difference between the geometric attenuation models applied in each study, would also be possible for the apparent alteration in the source spectral level (explained in section 4.5 in Chapter 4).

Deduced M_0 values are plotted with event magnitude, m_b (Figure 5.9). The best-fit line between M_0 and m_b is also shown in the Figure. Given the uncertainty in estimated and inferred attenuation parameters, the factors are validated following a comparison of ground motions between recorded and artificially simulated events employing estimated parameters in a stochastic model as described below.

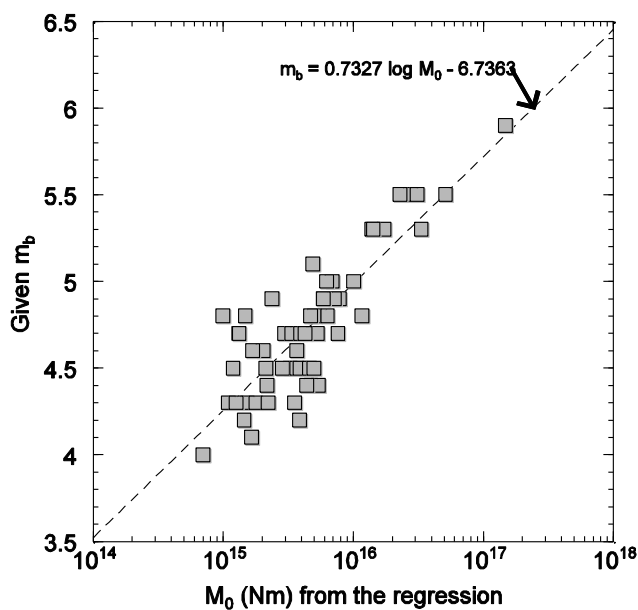


Figure 5.9 Resulted Seismic moment (M_0) vs. event magnitude m_b . The best fit relation between M_0 and m_b is also shown in dash line.

5.3.4 Ground motion comparison

Stochastic methods have successfully been implemented in seismic hazard assessment studies over many years even in stable continental regions, where strong motion records for empirical modeling are generally lacking (Balendra et al, 2002; Lam et al, 2009; 2002). The seismological model or attenuation model that sieves the final frequency content of the target amplitude spectrum to be used in the stochastic process, is similar to the general form given in equation (5.3), noting the high frequency cutoff filter function [defined in equation (5.6)] should also be

included herein. The model encompasses the Fourier spectrum of a given magnitude event at the source and subsequent path modifications (i.e., attenuations and amplifications) predicted to undergo during the propagation (see sections 2.3 and 2.4.2 in Chapter 2). The anelastic attenuation is modeled by equation (4.3) in Chapter 4 with $Q = 389f^{0.70}$. Kappa of the high frequency cutoff filter function is taken as 0.041 s in accordance with results of the secondary regression. The tri-linear hinged shape geometric attenuation function is applied with resulted and collated parameters; the average far-source and near-source attenuation rates are equal to $R^{-0.5}$ and $R^{-1.3}$, respectively. Zero attenuation is taken between the reference distances 55 and 120 km. Atkinson's double corner frequency ENA source model (Atkinson, 1993a; Atkinson and Boore, 1995) is applied to formulate source characteristics in the stochastic simulation. Brune's model has sometimes shown to be incompatible with the actual large magnitude events (see Figure 2.2 in Chapter 2), for which the model has been evident in predicting a bit higher amplitudes for long period waves (Chen and Atkinson, 2002). Therefore, Atkinson's ENA source model is seemingly more reliable for the stochastic simulation of moderate and large magnitude events in the present study. Required magnitude conversion, i.e., m_b to M_w , is done using relationships proposed by Johnston (1996) for intraplate events in stable continental regions. The seismological parameters adopted in the stochastic simulation are summarized in Table 5.4. The comparison that shows simulated events against observed records in terms of the relative displacement for 5% critical damping ratio, is shown in Figure 5.10. The relative displacement is considered to be optimum for the comparison because of major concerns on design aspects of the displacement or drift demand in structures due to distant events. Simulations are carried out using FORTRAN packages GENQKE and ETAMAC (Lam, 1999), and a detailed description of the applied stochastic method is available in Lam et al (2000b).

Interesting consistency between observed and modeled relative displacements can be seen from the plots (Figure 5.10), and this supports the fact that the applied seismological parameters are accurate enough in capturing attenuation characteristics of distant earthquakes in the region. The comparison covers a range of events between M_w 4.1 and 8.2, as well as a long range of hypocentral distance from 542 to 1491 km. The favorable matching at such long distances principally ensures the reliability of applied geometric and anelastic attenuation parameters of the northern Indian Oceanic crust. Conformity in spectral shapes between modeled and recorded events, would attest the accuracy of both the high frequency cutoff filter function (or the upper crustal attenuation parameter) and anelastic attenuation function. In all cases, the selected source model to represent actual source characteristics, and the applied stochastic procedure, are also verified. Given the accuracies of the comparison, these region-specific key attenuation parameters can be accepted for generic application of seismic hazard analysis in the chosen region - Sri Lanka.

Table 5.4 Seismological parameters used in the stochastic simulation

| Seismological parameter | Applied relationship | Remarks |
|---|--|--|
| Source factor [$S(f)$] | Atkinson's (1993a) ENA source model, $S(f) = CM_0 \left[\frac{1 - \varepsilon}{1 + \left[\frac{f}{f_a}\right]^2} + \frac{\varepsilon}{1 + \left[\frac{f}{f_b}\right]^2} \right]$ $C = 0.78/(4\pi\rho\beta^3)$ $\log f_a = 2.41 - 0.533M_w$ $\log f_b = 1.43 - 0.188M_w$ $\log \varepsilon = 2.52 - 0.637M_w$ | C is called "scaling factor". M_0 is the seismic moment, which is related to $\log M_0 = 1.5M_w + 10.7$. Body wave magnitude (m_b) of events is converted to M_w by the relationships proposed in Johnston (1996) for applying in the source factor. ρ (density) and β (shear wave velocity) of the source region are taken as 2800 kg/m ³ and 3.9 km/s, respectively, based on CRUST2.0 information. |
| Geometric attenuation factor [G] | $G = 1/R^{1.3}, \quad R \leq 55 \text{ km}$ $G = 1/55^{1.3}, \quad 55 \text{ km} < R \leq 120 \text{ km}$ $G = \frac{1}{55^{1.3}} \sqrt{\frac{120}{R}}, \quad R > 120 \text{ km}$ | The tri-linear hinged shape model defined in equation (5.2), with estimated and collated parameters. |
| Anelastic whole path attenuation factor [$An(f)$] | $An(f) = e^{-\left[\frac{\pi f R}{Q\beta}\right]}$ | Equation (4.3) in Chapter 4, and $Q = Q_0 f^n$, where $Q_0 = 389$ and $n = 0.70$ (Chapter 4). ρ and β are retained as same as that used in the source factor. |
| Upper crustal attenuation factor [$P(f)$] | $P(f) = e^{-\pi f K}$ | Equation (5.6) in the main text, where Kappa (κ) is taken as 0.041 s based on results of the secondary regression. |

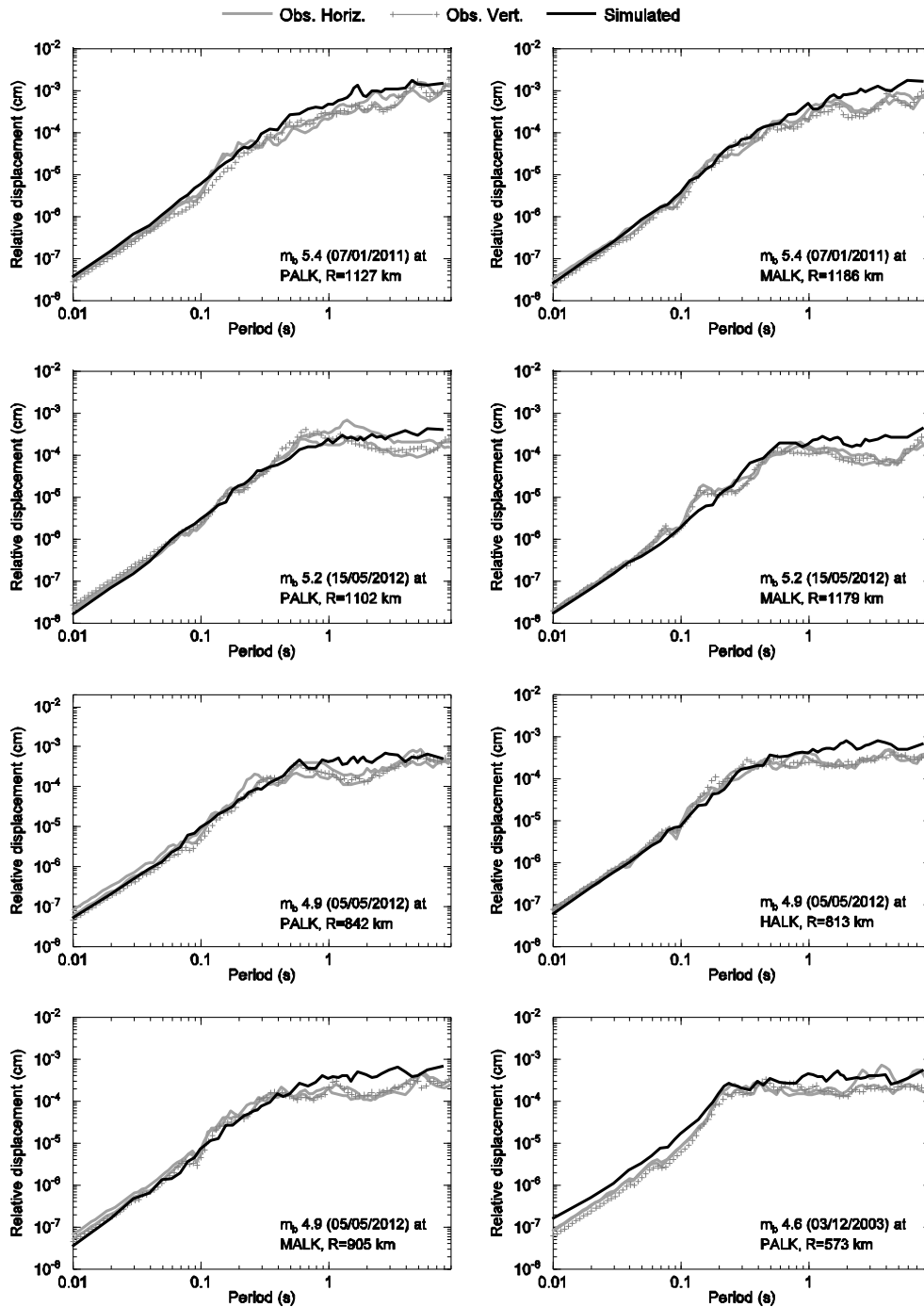


Figure 5.10 Comparison between observed records and stochastically simulated events in terms of relative displacement for 5% critical damping ratio. Stochastic simulations are performed employing seismological parameters given in Table 5.4. Interesting consistency between observed and modeled relative displacements can be seen from the plots, which is supporting the fact that applied seismological parameters are adequately reliable in capturing actual attenuation characteristics of the region. Comparison covers a range of events between about M_w 4.1 and 8.2, as well as a long range of hypocentral distance from 542 to 1491 km.

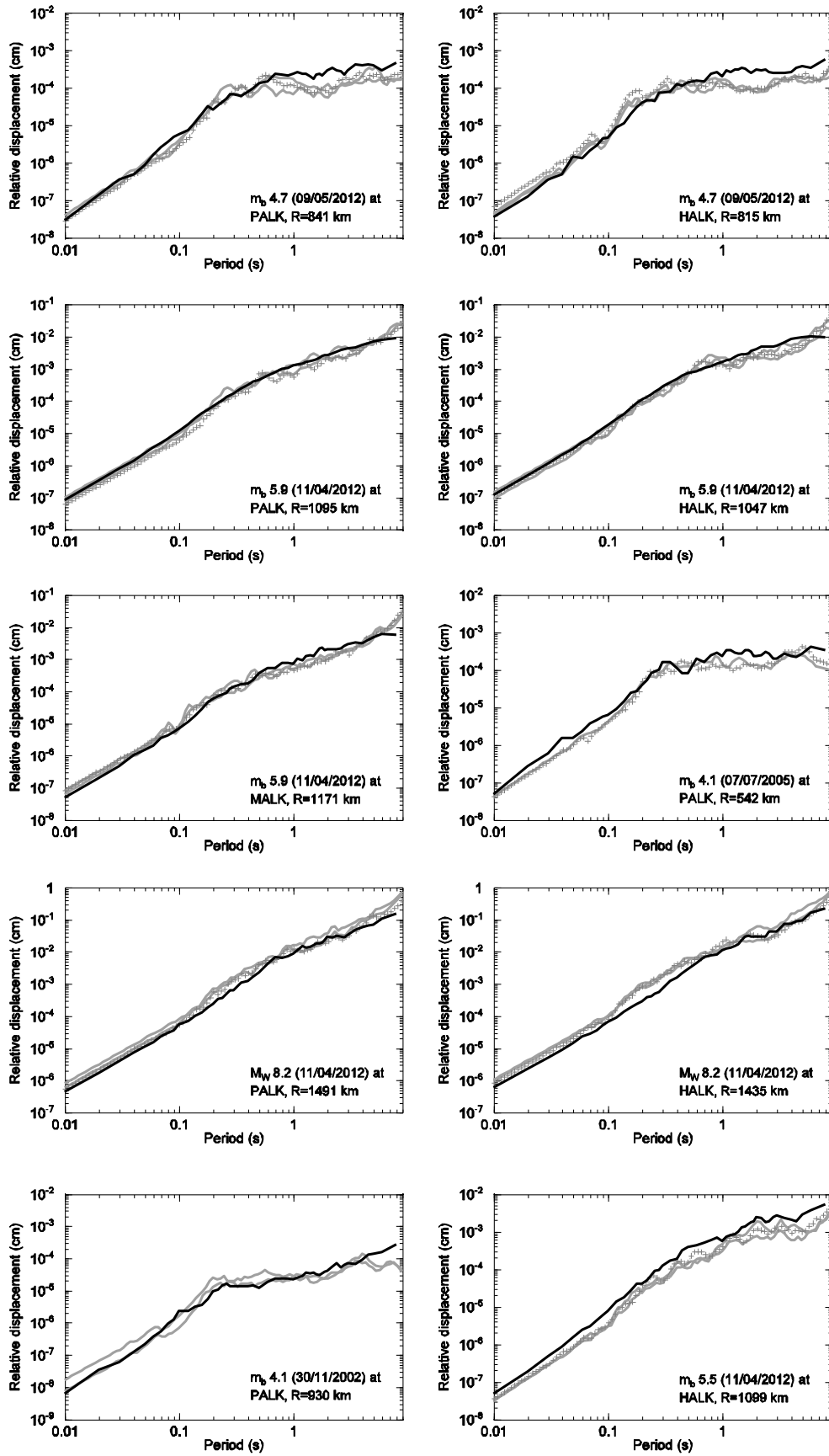


Figure 5.10 (continued)

5.3.5 Ground motions for hypothesized regional events

Spectral amplitudes are simulated for 3 hypothesized large magnitude events M_w 9.0, 8.5 and 8.0 each occurred at scenario distances 300, 400 and 500 km away from the country in the northern Indian Ocean. Simulations are based on the seismological parameters derived for regional events as indicated in Table 5.4. Event magnitudes and respective scenario distances are selected considering the seismic energy releasing potential of the diffuse plate boundary of Royer and Gordon (1997) (shown in Figure 3.7 in Chapter 3), and its proximity to the southeastern coast of the country, respectively. Elastic spectral amplitudes of pseudo acceleration and relative displacement for 5% critical damping ratio, of the simulated events are indicated in Figure 5.11. The figure shows the worst combination M_w 9.0 at 300 km produces the maximum PSA of 0.50 ms^{-2} at around 0.5 s period, while all other combinations except M_w 8.0 at 500 km produce PSAs greater than 0.10 ms^{-2} . Predicted relative displacements seem to be relatively small with a maximum around 20 mm for structures up to the natural period 3 s.

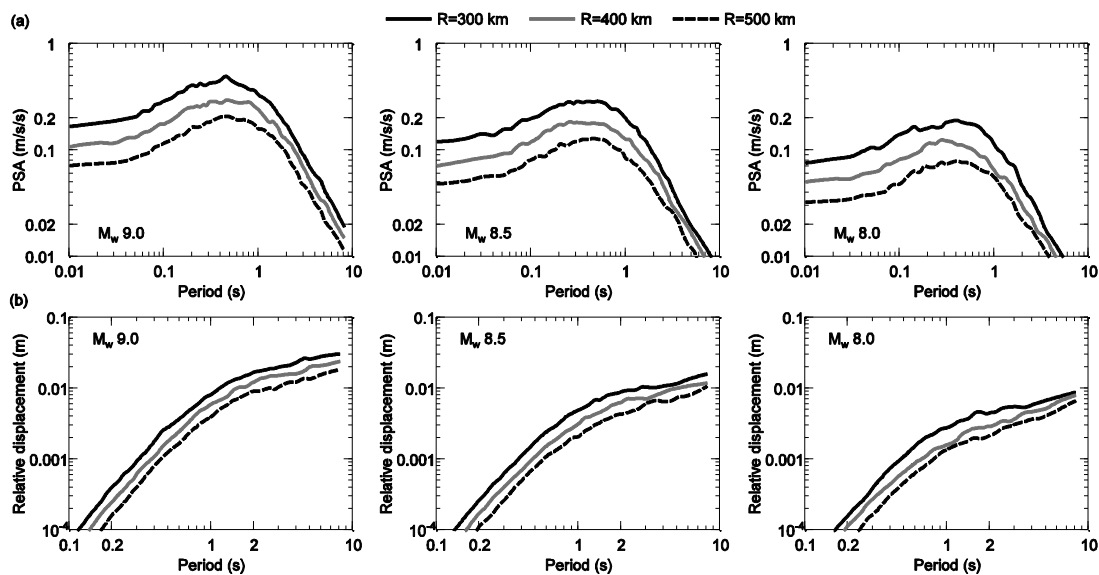


Figure 5.11 Simulated spectral amplitudes of 3 hypothesized large magnitude events M_w 9.0, 8.5 and 8.0 occurred in the northern Indian Ocean. (a) PSA. (b) relative displacement.

5.4 Summary and conclusion

A data analysis of moderate magnitude distant events that occurred in the northern Indian Oceanic crust, reveals a similar far-source geometric attenuation rate of $R^{-0.5}$, as which typically identified in continental crusts where regional phases such as L_g dominates. Despite some obvious differences in the crustal structure and in the regional wave fields between continental and oceanic crusts, a similar average far-source attenuation rate is observed from the analysis. This suggests that the geometric attenuation is more independent of the seismic wave field and the dominant

wave type in the crust. At low frequencies (below about 2 Hz) slightly lower attenuation rates than $R^{-0.5}$, are resulted. The residual analysis shows no apparent trend with the selected independent variables, and thus supports the congeniality of the selected attenuation equation in the main regression. Kappa, in the high frequency cutoff filter function or in the upper crustal attenuation function, is found by a secondary regression undertaken in the frequency domain for constants resulted from the main regression. Resulted Kappa 0.041 ± 0.009 s by this newer technique, has correlated with a separate Kappa estimation for Sri Lanka (described in Chapter 6) which is based on direct measuring of the slope in attenuation corrected displacement source spectra of individual events. Estimated higher Kappa suggests a poor quality upper crustal layer, which may be composed of younger Sedimentary rocks as it is also evidenced in elsewhere (in CRUST2.0 observation), is plausible for the country. Resulting similar Kappa values in two different studies, in viewpoints of the data used and methodology applied, urges Kappa to be considered as an upper crustal attenuation property rather than a source phenomenon as identified in certain studies. The reference distance that defines the second hinge point of the geometric attenuation function is estimated as 120 ± 30 km. The near- and medium-source attenuation rates along with the first hinge point are unable to be estimated from the direct data analysis due to unavailability of near- and medium-field events. Nonetheless, they are collated; the near- and medium-source attenuation rates are from findings in the literature, and the first hinge point by a trial and error approach of spectral matching between the actual and simulated events. The final shape of the trilinear geometric attenuation function for distant earthquakes of the northern Indian Ocean region as found by this study, is suggested in below;

$$G = \frac{1}{55^{1.3}} \sqrt{\frac{120}{R}}, \quad R > 120 \text{ km}$$

Source characteristics in the subject region are simply estimated by the least squares regression of the attenuation corrected spectra to theoretical Brune's point source model. Comparably higher static stress drop averages about 9.5 MPa (95 bars) and 16.0 MPa (160 bars) for m_b 4-5 and 5-6, are observed from regressions, respectively. The estimated stress drops agree with the literature findings for the region (e.g., Allmann, 2008). The corner frequencies vary between 1.0 to 7.0 Hz for the selected events. Observed attenuation characteristics are further validated by a comparison of ground motions between recorded events and stochastically simulated events. The simulated events possess a good match with actual events for a range magnitudes up to M_w 8.2 occurred at large hypocentral distances up to about 1500 km away from the country. Given the accuracy in the stochastic simulation, these region-specific key attenuation parameters can be reliably used in generic applications for seismic load estimation for Sri Lanka, particularly, due to large magnitude events generated at long distances.

6. Seismological parameters for local earthquakes in Sri Lanka

6.1 Introduction

Attenuation characteristics of seismic waves during propagation need to be carefully identified for a hazard study in a given region. These region-specific characteristics are mostly associated with the inherent geotectonic features of the region. Thus, studying attenuation characteristics of a particular region would also be helpful to explore featuring tectonic structures of the region. Attenuation of seismic waves inside a rock crust, in respect to the most dominating phases such as S and L_g , can be generally classified into three categories depending on the mode of attenuation and local characteristics of the uppermost crust (discussed in Chapter 2); (1) Geometric spreading (2) Anelastic whole path attenuation (3) Upper crustal attenuation. These identified wave attenuation types are also case sensitive, i.e., the dominance of one particular mode can be controlled by several other factors such as site source distance, wave frequency, crustal properties, local site characteristics, etc.

In Chapters 4 and 5, efforts were undertaken to determine attenuation and source characteristics for regional earthquakes of the northern Indian Ocean region, by considering Sri Lanka in the regional context. In the present Chapter, attempts are made to characterize attenuations of the continental crust beneath Sri Lanka, and thus the study can be considered in the local context. Attenuation and even source characteristics of events that occur at regional or teleseismic distances can be incomparable with that of local events occurred at short distances. Variation of the crust, in terms of age, composition, geometric properties, etc., along the wave travelling path, and any difference in source features such as stress drop and tectonic environment of the region, can significantly impact the final wave content observed at a rock outcrop. On the basis of this understanding and also with the argument made in Chapter 3 of the requirement of separate consideration of the country in the regional and local contexts for seismic hazard estimation, it has recognized that separate evaluations of seismological characteristics to be applied in those contexts, would be more appropriate. The study in the present Chapter is also a continuation of the same comprehensive effort, yet this time on characterizing seismological properties in the local context.

The country has not experienced major and frequent local seismic activities during recent past. However, according to historical evidence (discussed in Chapter 3) there were few major events reported within the island including a devastating one that occurred near the capital city-Colombo on 14th of April 1615 with an estimated magnitude of the order of M_w 6.4 causing more than 2000

casualties (Wimalaratne, 1993). Apparent sparse seismicity within the country, as evidenced by such events, is likely to be concentrated in areas where active local lineaments and faults are present. In Chapter 3, such active areas are explored within the country, by correlating reported events with local seismo-tectonic structures such as lineaments and shear zones particularly located at geological boundaries. The next step would be a proper examination of seismological characteristics of the underlying crust, which have never been explicitly parameterized before. With the availability of broadband data of some small magnitude shallow crustal events occurred at near- to medium-source distance ranges within the island, it is possible to undertake a study to examine coda Q , Kappa (κ) and H/V ratios for the crustal structure underlain Sri Lanka. A possible geometric attenuation function to characterize attenuation at local distances, is also approximated. Digital high-gain records of 13 small to micro earthquakes, magnitude varying from M_L 3.6 to 1.5 in local magnitude scale, has been processed for the analysis. The standard single scattering model, which demands the decay rates of backscattered coda waves located at the tail part of seismograms, is used to estimate coda Q . The near-surface attenuation parameter Kappa, which is also found in Chapter 5 using regional events, is determined here by measuring the slope of displacement spectral amplitudes at frequencies below the corner frequency. A ground motion comparison between observed and stochastically predicted amplitudes has been performed for the validation of estimated and inferred parameters. Source spectra of the selected events are also derived to compare with Brune's classical point source model. Finally, a scenario investigation is carried out in seismically active Colombo area to evaluate ground motions that can be expected due to a possible major event.

6.2 The coda Q method and Q value

Q value alias “the wave transmission quality factor” is merely regarded as a region-specific property, which may highly depend on regional crustal characteristics such as age and composition of the crust, degree of heterogeneity, amount of asperities and irregularities, etc. There are several well established methods available in determining Q value for a region, out of which coda Q methods and spectral analysis methods are popular in the current seismological practice. However, selection of a method to be applied in a region would depend on fundamental assumptions associated with the specific method. For example, single backscattering coda Q method proposed by Aki (1969), postulates coda waves as a derivative of surface waves which are singly scattered at acute angles in a heterogeneous medium, and the scattering is isotropic. The isotropic scattering means the medium considered itself is isotropic as well as the scattering taking place at a given heterogeneity is uniform in all directions despite the direction of the wave travel prior to the scattering. Furthermore, the method omits station-source distances during the calculation, given the epicentral paths are short enough to neglect. Hence, the method would be best used in a less complex medium which can be hypothesized as isotropic, at short site-source

distances, otherwise due modifications need to be addressed. On the other hand, spectral analysis techniques in which empirical attenuation equations are fitted with observed Fourier spectral amplitudes, have shown to be widely adopting in regional studies that handle large amount of data at teleseismic distances. Although, the method is advantageous to determine the actual shape of Q which directly relates to the strong motion part (shear window) of a seismogram, one must be careful to apply the proper attenuation relationship which encompasses all possible means of attenuation for the subject region.

Aki and Chouet (1975) introduce following formulae to interpret the shape of coda amplitude decay with the lapse time;

$$P(\omega|t) = St^{-1}e^{-\omega t/Q} \quad (\text{Surface waves}) \quad (6.1)$$

$$P(\omega|t) = St^{-2}e^{-\omega t/Q} \quad (\text{Body waves}) \quad (6.2)$$

Here, $P(\omega|t)$ is the power spectral density of coda wave at time t . S is the source factor and ω is the circular frequency which is equal to $2\pi f$, where f is the wave frequency. Q is the frequency dependent wave transmission quality factor. During the derivation, coda waves are assumed to be singly backscattered (scattered at acute angles) at discrete heterogeneities which are uniformly distributed in the isotropic medium. Energy loss in direct waves that are not subjected to scattering and any effect due to downward scattering (into the upper mantle), have been neglected. Furthermore, the above equations are theoretically valid for collocated source-receiver condition, yet modified relationships to account for the distance effect in distant events are also available in the literature (Kopnichev, 1975; Sato, 1977; Pulli, 1984; Woodgold, 1990). Energy contribution from the multiple scattering is considered minimal in effect, and hence ignored for the coda decay rate. Wu and Aki (1988) suggest Q value estimated in this way by coda decay rates represents both attenuation effects, i.e., intrinsic attenuation and scattering effects, however, effect of scattering on the decay rate would depend on amount of scattering taking place within the medium. When the scattering is weak the decay rate depends on both (intrinsic and scattering), while when it is strong (as in a defuse medium) the rate would depend only on intrinsic attenuation. Despite its difficulty in estimating individual contribution in each effect over the decay rate, efforts have been given sometimes to separate intrinsic Q from scattering Q (Zeng et al, 1991; Hoshiba, 1993). Further extensions of the method such as multiple scattering model (Gao et al, 1983) take effects due to multiply scattered phases into account in a heterogeneous medium.

Since the wave amplitude is proportional to square root of energy, writing above equations in terms of amplitude and taking natural logarithm would yield;

$$\ln[A(f, t)t^{0.5}] = \ln S' - \pi ft / Q \quad (\text{Surface waves}) \quad (6.3)$$

$$\ln[A(f, t)t] = \ln S' - \pi ft / Q \quad (\text{Body waves}) \quad (6.4)$$

Where, $A(f, t)$ denotes the coda wave amplitude at time t for a given frequency f and S' represents the modified source term that corresponds to amplitude. In both of equations (6.3) and (6.4), the logarithm of the product of wave amplitude and lapse time (the term in left side) exhibits a linear variation with lapse time (in 2nd term in right side) where the amplitude is multiplied by $t^{0.5}$ and by t , for surface and for body waves, respectively. Equations also indicate the geometric spreading rate for surface waves is about square root of that for body waves. Q value for a given frequency can be found by the slope of the linear fit defined in equation (6.3) or (6.4). The intercept of the linear fit which represents so-called “source term” can be sometimes merged with upper crustal attenuation term parameterized by Kappa, though the slope does not affect such an amalgamation, given Kappa remains constant with the lapse time. Therefore, Q value estimated in this way by fitting envelopes in the time domain can be considered as a reliable measure to represent the crustal quality in regional seismic wave transmission. Amplitude is calculated as the RMS (Root Mean Square) average of a moving time window, for which the window size can typically be of 3 s for short period waves (Havskov and Ottemöller, 2010). Here, the RMS average is found to be optimum since its better representation of total energy absorbed within the window. The starting time of coda envelope in order to employ in the backscattering model, has been commonly taken as twice as S or L_g arrival time (Singh and Herrmann, 1983). Studies have further revealed that after about thrice as the time taken for S or L_g , the coda arrival is permanently established (Rautian and Khalturin, 1978). Early coda available immediately after S or L_g , are often omitted in the decay rate calculation, mainly due to the fact that they are not being susceptible for backscattering. On the contrary, late coda coming after at least not less than twice as S or L_g arrival, show a steady rate of decay which is free from undue instabilities such as sudden spikes and humps in respect to early coda, making the decay rate almost as independent of the travelled distance. A sample seismogram band pass filtered between 1-19 Hz, indicating essential phase arrivals and coda length to be used in a coda Q study, is shown in Figure 6.1. There has been a debate on of what the coda waves are composed, whether from surface waves or from body waves. In early studies, many researches used to adopt coda as superimposed surface waves which are generated by incidence of primary waves at randomly distributed heterogeneities (Aki, 1969; Kopnichev, 1975; Herrmann, 1980). However, soon later, body wave approximation has also been proposed to explain the behaviour of coda (Sato, 1977; Pulli, 1984). During the present study, again it is presumed the coda as singly backscattered body waves suggesting equation (6.4) to be valid in Q estimation. In addition to aforementioned Born assumptions which are bound with the single backscattering method, wave mode conversion at a heterogeneity such as a primary body

wave to a secondary surface wave and vice versa, is assumed not to be incidental for the purpose of applying equation (6.4).

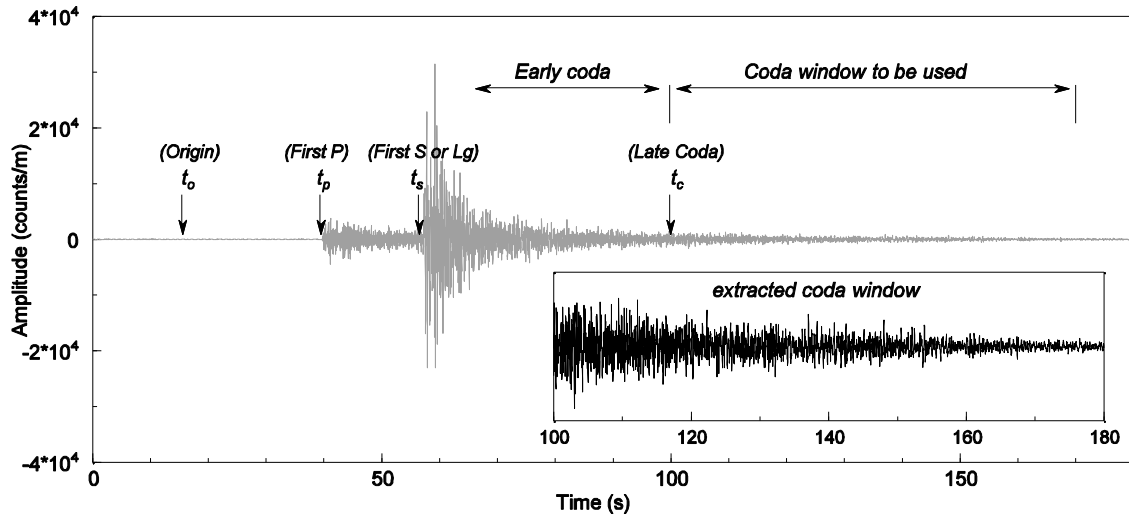


Figure 6.1 A sample seismogram band pass filtered between 1-19 Hz, indicating origin, essential phase arrivals and coda length to be used in a coda Q study. Early coda available immediately after S or L_g are often omitted when determining the decay rate, since they are less likely for being backscattered. However, late coda coming not less than at least twice as S or L_g arrival, show a steady rate of decay in amplitudes with respect to early coda. Extracted coda window to be used is shown as an insert. Event- M_L 3.5 at HALK, Hypocentral distance is 109 km.

Table 6.1 List of events used in the study

| Date | Time (UTC) | Lat. | Lon. | Depth (km) | Local magnitude (M_L) |
|------------|------------|------|-------|------------|---------------------------|
| 19/05/2012 | 20:14:36 | 7.04 | 80.91 | 7 | 3.5 |
| 26/05/2012 | 16:22:06 | 7.54 | 81.20 | 15 | 3.6 |
| 18/06/2012 | 16:37:54 | 7.48 | 81.12 | 4 | 2.1 |
| 28/08/2012 | 10:12:47 | 7.49 | 81.19 | 10 | 2.5 |
| 31/08/2012 | 14:34:46 | 7.13 | 81.49 | 10 | 2.1 |
| 14/09/2012 | 23:41:19 | 7.47 | 81.14 | 10 | 1.9 |
| 28/09/2012 | 23:56:11 | 7.03 | 81.50 | 10 | 2.1 |
| 01/12/2012 | 2:47:46 | 7.15 | 81.50 | 10 | 2.3 |
| 01/12/2012 | 3:31:32 | 7.15 | 81.52 | 10 | 2.3 |
| 01/12/2012 | 11:09:33 | 7.14 | 81.50 | 10 | 2.2 |
| 14/12/2012 | 7:35:05 | 7.14 | 81.51 | 10 | 1.5 |
| 25/01/2013 | 4:04:30 | 7.15 | 81.50 | 10 | 2.0 |
| 25/01/2013 | 5:08:22 | 7.15 | 81.50 | 10 | 2.4 |

Database in the study consist a total of 13 shallow crustal local events with the estimated local magnitude ranging between M_L 1.5-3.6. Hypocentral distance varies from 35 to 185 km, and the level of intensity of events would fall within the range of micro-tremor to small magnitude.

Details of event data are given in Table 6.1, whereas station-source paths to be used in the analysis and magnitude-hypocentral distance variation are shown in Figure 6.2. Location and origin time of events are determined based on “the flat earth layered velocity model”, which has been considered to be reliable for estimations within smaller distance ranges. Local magnitude is determined by the maximum amplitude picked in a filtered (between 1.25-19.75 Hz) standard Wood-Anderson seismogram. All processing steps including coda Q determination have been carried out using tools provided in SEISAN package (Havskov and Ottensmøller, 2012).

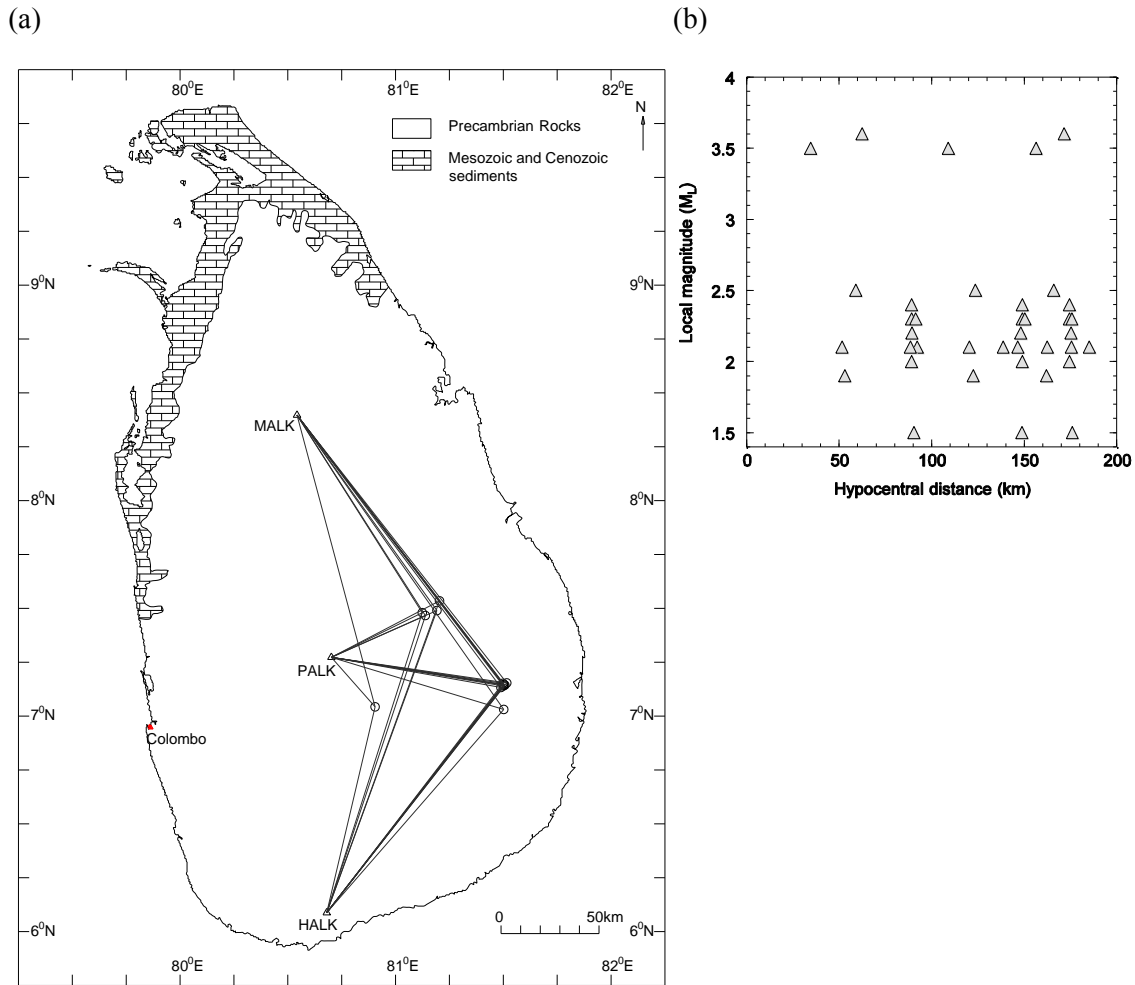


Figure 6.2 Earthquake data used in the study. (a) Station-source paths for the dataset. Circles denote earthquakes while triangles at HALK (Hakmana), PALK (Pallekelle) and MALK (Mahakanadarawa) represent broadband stations. Extent of the Precambrian crust is also indicated. (b) Distribution of the dataset in magnitude and hypocentral distance space. Magnitude ranges from M_L 1.5 to 3.6, whereas hypocentral distance varies between 35 and 185 km.

Seismograms recorded at the country’s national broadband seismic network’s high-gain channels having sample rates of 40 (for PALK) and 50 (for HALK and MALK), are selected for the processing. Both horizontal and vertical components are used in the study in order to enlarge the

size of the original sample. Besides, variation of the horizontal amplitude with respect to the vertical (H/V ratio) has shown to be insignificant in practical situations (based on results of Chapter 4 and this Chapter), which may imply a negligible upper crustal amplification associated with the region's uppermost crust. This permitted both of the components are to consider as identical each other for the study. The main purpose of this is to increase the sample size and thereby to avoid any error that can be arisen due to being a smaller sample. Each seismogram is filtered by a 6-pole Butterworth filter applied at eight different pass-bands with centre frequencies 4, 6, 8,..., 18 Hz. Since low frequency amplitudes (less than about 2 Hz) sometimes have caused low resolution quantisation problems due to poor signal strength, they have been omitted in the calculation. Pass-bands are defined to comply with a constant relative bandwidth of 0.5, which has resulted bandwidths to be in the form 4 ± 1 , 6 ± 1.5 , 8 ± 2 ,..., 18 ± 4.5 for selected centre frequencies. $A(f,t)$ for a given centre frequency is then calculated by the RMS average of a moving 5-cycle ($5f$) window as described in Havskov et al (1989). In the study, coda length starting time is hardwired to two times S or L_g arrival time because of its optimal use in the backscattering model in both viewpoints of having a steady decay rate which is uncontaminated with early coda (discussed previously), and of following the consistency in the method for the purpose of comparison results with other regions. A slightly lower average V_p/V_s ratio of about 1.73 is resulted for the data in arrival time calculation, and is retained as same for selecting the coda length. A fixed coda length is applied at a turn for the dataset, and the entire process is repeated for four different coda window cases as 40, 50, 60 and 70 s. Finally, an average Q representing all windows has been estimated. A parametric study extending beyond a single time window case has been undertaken to investigate the time dependent behaviour of Q , if any. A number of studies evidence on increasing coda Q with time (Pulli, 1984; Kvamme and Havskov, 1989; Gusev, 1995), seemingly, due to magnifying multiple scattering effects as sampling larger volumes at higher crustal depths. Moreover, the effective earthquake duration which depends mainly on magnitude-stress drop parameters, can partly affect the final uniformity in coda windows. Therefore, a parametric study has been implemented to explore the variation of Q with time and to derive a value which would represent the average behaviour. 40 s as the lower limit is considered adequate for stable results, whilst the upper limit, 70 s, is chosen as a compromise of retaining sufficient amount of data that have higher signal strength for the final processing. Signal to Noise (S/N) ratio is calculated by the ratio between RMS amplitude of the last 5 s of the filtered coda window and that of the noise window preceding first P arrival. Q values resulted with S/N ratio below 3 are eliminated from final results. Consequently, linear fits to coda envelopes given in equation (6.4), which are unable to indicate a 50% minimum correlation, have also been omitted.

Two sample plots indicating coda amplitude decay with the lapse time for two randomly selected centre frequencies (4 and 14 Hz) are shown in Figure 6.3. It can be seen that the coda amplitude diminishes (approximately linearly in the log scale) with time due to above discussed attenuation and scattering effects, and the apparent rate of decay denoted by the slope, is higher at 14 Hz than at 4 Hz indicating a more rapid decay in high frequency waves.

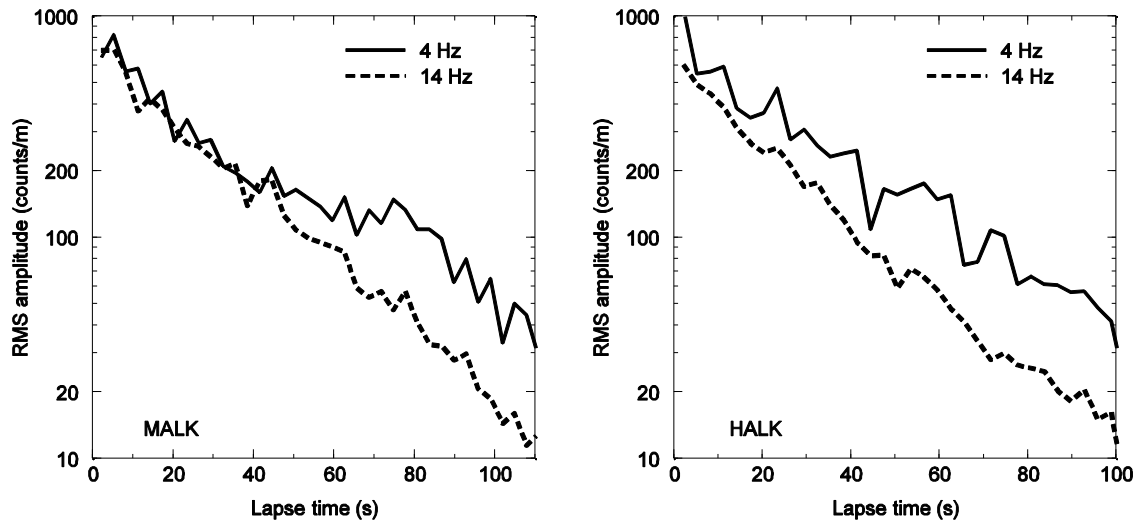


Figure 6.3 Decay of coda amplitude (RMS value) with the lapse time at two random centre frequencies (4 and 14 Hz). The apparent rate of decay denoted by the slope is higher at 14 Hz than at 4 Hz, indicating a rapid decay in high frequency waves. Lapse time “0” is relevant to start of the coda window. Two plots are for the event M_L 3.5 recorded at MALK and at HALK.

6.3 Kappa (κ) value

Kappa parameterizes attenuation effects that undergo at the uppermost crust, at say upper 3-4 km. Although, mode of attenuation follows a similar mechanism as that involved in the anelastic whole path attenuation, the effect is separately considered in the seismological practice due to the key difference in the quality of the uppermost crust from that of other parts. The uppermost rocks are of poor in quality and therefore would lead attenuations to be happened in substantial amounts at the near-surface level than at mid and at deeper levels. The equation does have an exponential form as indicated in Chapters 2 and 5;

$$P(f) = \exp[-\pi f \kappa] \quad (6.5)$$

where, $P(f)$ is the upper crustal attenuation factor. Kappa is generally identified as a frequency independent parameter (Abercrombie, 1998), and typically shows lower values for regions with older and harder upper crustal rocks such as Precambrian. On the other hand, Kappa takes higher values for areas with younger rock formations at the upper crustal level, in which instances sometimes up to about 90% of the total anelastic attenuation can be happened within the topmost

3 km (Abercrombie 1997). Therefore, the upper crustal attenuation can be notable in regions where low quality rock formations are dominating the upper crust. Hence, a proper assessment on Kappa of a region is essential for accurate characterization of ground motions in the region. In Chapter 5, the average Kappa possible for the Sri Lankan upper crust is determined as 0.041 s, based on an analysis of moderate magnitude events that occurred at the teleseismic distance range. In the present study, however, Kappa is re-estimated by the slope of attenuation corrected displacement Fourier spectral amplitudes at frequencies below the corner frequency, using a set of smaller magnitude event data recorded at local distances. The attenuation equation to be fitted with observed displacement amplitudes follows the same basic format as that given in Chapter 2 [equation (2.1)], Chapter 4 [equation (4.1)] and Chapter 5 [equation (5.3)];

$$A_x(f) = S(f).G.A_n(f).P(f) \quad (6.6)$$

$A_x(f)$ and $S(f)$ are displacement Fourier spectral amplitude for a given frequency f at the station and at the source, respectively. G is the geometric attenuation factor and $A_n(f)$ is the anelastic attenuation factor (parameterized by Q) as described in previous Chapters. $A_n(f)$ is modeled by its usual form which is reproduced in the following equation;

$$A_n(f) = \exp[-\pi fR/Q\beta] \quad (6.7)$$

R and β are hypocentral distance and shear wave velocity at the source region, respectively. Substituting equations (6.5) and (6.7) in (6.6) and taking logarithm yield;

$$\log[A_x(f)] = \log[S(f)] + \log[G] - \frac{\pi fR}{Q\beta} \log[\exp] - \pi\kappa \log[\exp]f \quad (6.8)$$

In equation (6.8), frequency dependent site amplification term is left following the H/V estimations carried out in Chapter 4, which clearly intuit a negligible upper crustal amplification associated with the region. However, H/V ratio is re-examined in the present study as well to see how far this inference is consistent with newer data of local events (described in section 6.4). Observed displacement amplitudes are first corrected for anelastic attenuation using estimated coda Q values, and are then regressed by using equation (6.9) in the least squares sense;

$$\log[A_x(f)] + \frac{\pi fR}{Q\beta} \log[\exp] = \log[S(f)] + \log[G] - \pi\kappa \log[\exp]f \quad (6.9)$$

Note that, a correction for geometric spreading is not essential here, since the slope of the linear fit is not affected by G , provided G is frequency independent. Two main assumptions are taken in the process of Kappa estimation; firstly, Fourier displacement spectrum at the source is

compatible with theoretical Brune's model (Brune, 1970; 1971), which would facilitate a nearly constant amplitude level at frequencies below the corner frequency. Secondly, Kappa needs to be frequency independent. Data processing procedure followed in the calculation is fundamentally similar to which adopted in Chapters 4 and 5, and can be exactly summarized as follows; each seismogram of vertical component is 10% tapered at either end, is instrument corrected, is band pass filtered between 1-19 Hz using a 4-pole Butterworth filter, and thereby the respective displacement time history is obtained. Next, Fourier amplitude spectrum of strong or shear part of each time history is found and is smoothed for the selected frequency range at 0.1 log frequency bins by introducing a box (rectangular) weighting function that computes the geometric average of amplitudes within each frequency bin. Logarithms of smoothed displacement amplitudes are tabulated at 0.1 frequency increments and are corrected for anelastic attenuation prior to the regression. Least squares regressions are then undertaken by using equation (6.9) between corrected log displacement amplitudes and frequencies below the corner frequency.

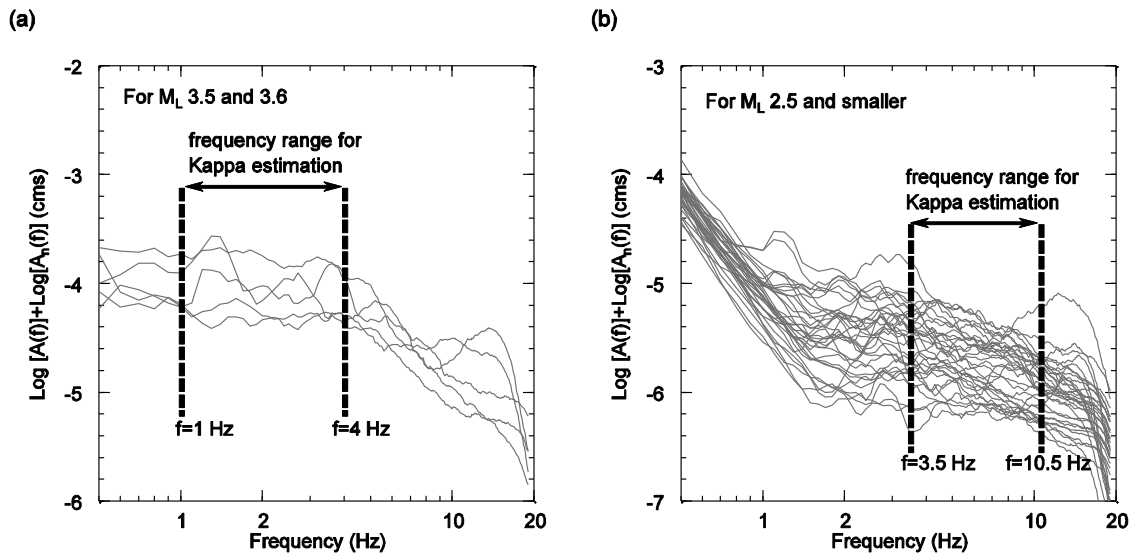


Figure 6.4 Frequency ranges used in the Kappa estimation: (a) For M_L 3.5 and 3.6. (b) For relatively small events ($M_L \leq 2.5$). For M_L 3.5 and 3.6 it is clear that the corner frequency is greater than 4.0 Hz (between around 4.0 and 6.0 Hz), hence frequencies between 1.0-4.0 Hz were adopted for Kappa estimation. For smaller events ($M_L \leq 2.5$), a higher frequency range of 3.5-10.5 Hz was considered to be more stable given both much higher corner frequencies (higher than even about 11.0 Hz) and some observed instabilities in the decay rate at low frequencies ($f < 3$ Hz).

The corner frequency as a cut-off is approximated first by visually examining corrected Fourier spectra (Figure 6.4) and second by further verifying the value using theoretical Brune's source model for about 4 MPa (40 bars) stress drop. A lower average stress drop is presumed because of the selected events were small in magnitude. Both these suggested, for two events M_L 3.5 and 3.6 corner frequencies can be roughly in between 4.0 and 6.0 Hz, whereas for relatively small events

($M_L \leq 2.5$) these can be higher than even about 11.0 Hz. Therefore, for events $M_L \geq 3.5$, amplitudes at frequencies between 1.0 and 4.0 Hz are considered for the linear regression, while for relatively small events ($M_L \leq 2.5$) a higher frequency range of 3.5-10.5 Hz is used. Low frequency amplitudes ($f < 3$ Hz) of relatively small events ($M_L \leq 2.5$) are omitted in the regression due to some observed instabilities in the decay rate (see Figure 6.4), which in turn has resulted lower correlations in the regression fittings. This may be because of low frequency noise contamination in the record and/or because of low amplitude quantization noise problems as indicated by Atkinson (2004b). Consequently, neither lower correlations ($R^2 < 0.5$) nor positive slopes are used for final results. A sample displacement Fourier spectrum before and after correcting for anelastic attenuation is shown in Figure 6.5. The least squares fit that used in the Kappa estimation is also shown.

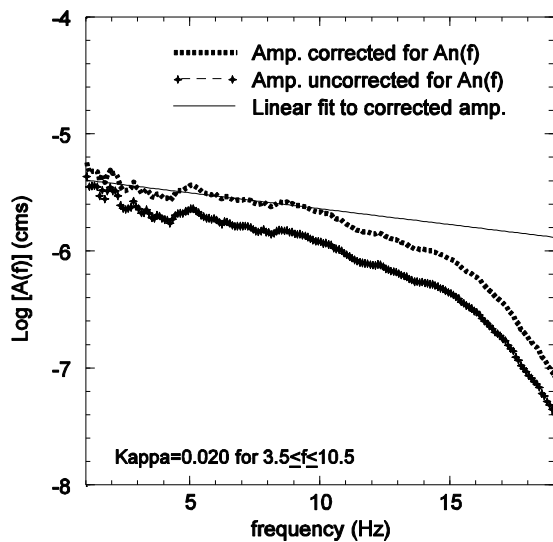


Figure 6.5 Kappa value estimation. Kappa is estimated by using the slope of the displacement Fourier spectrum, which is obtained after correcting for anelastic attenuation, at frequencies below the corner frequency. Uncorrected spectrum has also been shown to indicate the impact of attenuation correction on Kappa calculation. Event- M_L 2.3 at PALK, Hypocentral distance is 91 km.

6.4 H/V ratio

H/V ratio, defined as the ratio of amplitudes between horizontal and vertical component records, is referred to as a crude yet sufficiently accurate estimate of upper crustal amplification (Atkinson, 2004b; Siddiqi and Atkinson, 2002; Lermo and Chavez-Garcia, 1993). In H/V ratio, as per the law of conservation of energy, amplitude of the horizontal component is considered to be subject to continuous amplification as a compensating action against depletion of propagation velocity while traveling in a medium in which the impedance is gradually ascending. On the other hand, amplitude of the vertical component is treated to remain nearly same as which at the source because of counteractions by wave refractions toward the vertical direction (Atkinson, 2004b).

Hence, the net effect of amplitude ratio between the horizontal and vertical would give an overall measure of amplification of seismic waves expected to undergo during propagation through the whole path starting from the origin – source. However, since amplifications at mid and deeper levels of the crust are indiscernible with respect to that at the upper level due to distinguished difference in quality of rock, H/V ratio would characterize amplifications at the upper crustal level, the most. The same equation as which used in Chapter 4 is adopted in the present study (Venkatesan and Gamage, 2013; Chen and Atkinson, 2002);

$$\log[H / V] = \log \left[\frac{\sqrt{H_1 H_2}}{V} \right] \quad (6.10)$$

H_1 and H_2 are orthogonal partitions of amplitude of the horizontal wave component, and V is the vertical component amplitude. For the calculation, two horizontal components of each record are processed again in the same way as that done for the vertical component described in the previous section. Note that, for PALK station, only one horizontal accelerometer has functioned properly during the period which the events were being reported, and hence data were available for one horizontal component. Given this situation, the horizontal component for which data are available is used for both H_1 and H_2 for PALK records.

6.5 Results and discussion

6.5.1 Q , Kappa and H/V ratio

Resulted Q values at selected centre frequencies in each time window case are shown in Table 6.2 and in Figure 6.6. Q at 1 Hz termed as Q_0 , and n (exponent) resulting from weighted linear regression of $Q = Q_0 f^n$ (Mitchell 1981) are given in each case. Comparably higher Q_0 values are resulted except at 40 s time window case, in which a lower value of $Q_0 = 184 \pm 16$ would be attributed to sampling a smaller volume that mainly encircles the younger upper portion of the crust. Besides, multiple scattering effects (although neglected in the single backscattering method), which evolves magnification of “scattering Q ”, might cause observed increments in Q_0 with time. The increasing trend shown is noticeable up to 60 s window case, and then after at 70 s Q_0 has again dropped to 368 ± 35 . Since, the variation of Q_0 with respect to the length of time window is obvious, an average value for all time window cases is considered to represent the overall behaviour of Q_0 in the region. Therefore, average Q values for all four cases are found and by which corresponding Q_0 and n values are obtained, respectively, as 301 ± 17 and 0.67 ± 0.02 from the respective weighted linear fit (Figure 6.6e).

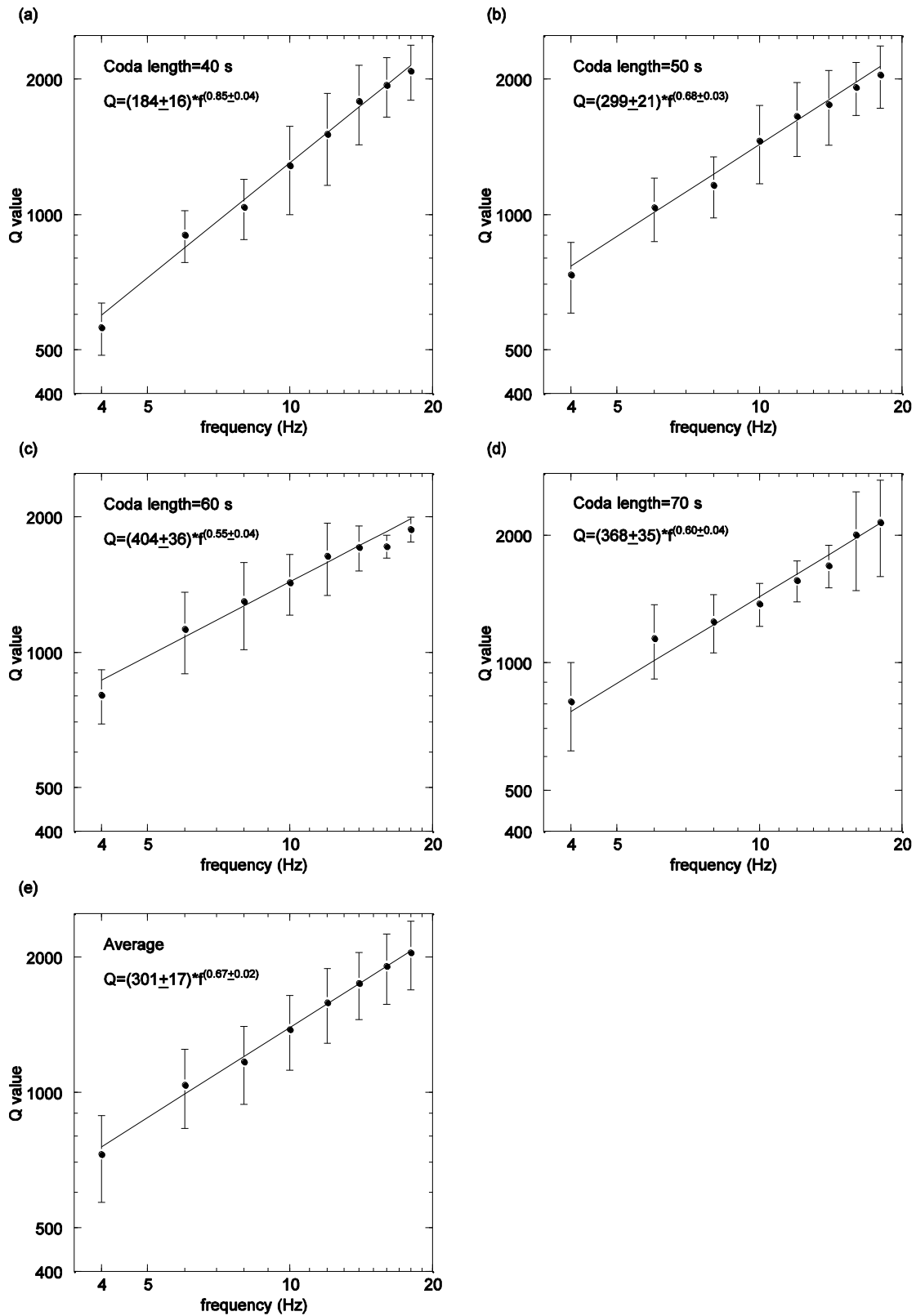


Figure 6.6 Resulted Q values with standard deviations at selected centre frequencies are shown in each coda window length case. Solid lines represent weighted linear least squares fits of $Q = Q_0 f^n$. (a) For 40 s. (b) For 50 s. (c) For 60 s. (d) For 70 s. (e) Average Q values and the respective weighted linear fit for all cases.

Table 6.2 Resulted Q values from the single backscattering method

| Frequency (Hz) | Q values for selected coda time windows (N is number of obs.) | | | | | | | | Ave. for all cases | |
|--|---|----|------------------|----|------------------|----|-----------------|----|--------------------|----|
| | 40 s | N | 50 s | N | 60 s | N | 70 s | N | | N |
| 4 (3-5) | 561±75 | 7 | 735±132 | 10 | 804±111 | 12 | 810±191 | 9 | 729±160 | 38 |
| 6 (4.5-7.5) | 901±119 | 18 | 1037±167 | 21 | 1127±232 | 18 | 1142±227 | 16 | 1040±209 | 73 |
| 8 (6-10) | 1039±159 | 20 | 1163±181 | 17 | 1298±284 | 18 | 1251±197 | 14 | 1171±230 | 69 |
| 10 (7.5-12.5) | 1286±286 | 20 | 1459±288 | 19 | 1430±220 | 14 | 1379±160 | 11 | 1381±260 | 64 |
| 12 (9-15) | 1510±349 | 19 | 1656±310 | 16 | 1638±300 | 13 | 1566±175 | 11 | 1586±301 | 59 |
| 14 (10.5-17.5) | 1787±358 | 20 | 1759±332 | 15 | 1713±197 | 10 | 1697±195 | 9 | 1750±298 | 54 |
| 16 (12-20) | 1941±294 | 11 | 1920±260 | 10 | 1720±102 | 6 | 2007±526 | 9 | 1910±340 | 36 |
| 18 (13.5-22.5) | 2087±292 | 10 | 2046±325 | 8 | 1879±120 | 6 | 2147±550 | 8 | 2049±357 | 32 |
| Q_0 (Q at 1 Hz) | 184±16 | | 299±21 | | 404±36 | | 368±35 | | 301±17 | |
| n (exponent) | 0.85±0.04 | | 0.68±0.03 | | 0.55±0.04 | | 0.6±0.04 | | 0.67±0.02 | |

Variation of Q with the coda time window is more elaborated in Figure 6.7. Figure 6.7b clearly illustrates individual variation of Q with the length of coda window used in each case. The figure evidences on an increasing trend of Q with the window time at low frequencies and a reverse trend at high frequencies. The increase of low frequency Q is more pronounced at frequencies below say 8 Hz (also the trend can be seen at 10 and 12 Hz in 40-50 s window range), while the high frequency Q reduction is apparent at frequencies above 14 Hz. The probable reason behind Q increase with the length of time window would be related to earlier discussed time dependency in scattering Q which is mainly governed by the facts; sampling deeper volumes in much denser crust and enhancing multiple scattering effects. Both of these would reduce the rate of coda amplitude decay resulting higher Q values with time. Moreover, it shows the rate of Q increase over the time window is prominent between 40-60 s window range, and then after at 70 s the rate seems trivial as more like saturated. In contrary, Q reduction at high frequencies is hard to ascertain and appears to be a minor trend due to its limited consistency for the whole range of coda lengths. However, this can be resulted partially as a counter effect of reducing the number of observations when increasing the coda length from 40 to 60 s (see Table 6.2), which may have caused elimination of observations with higher Q values. Reduction in Q with time for a given frequency is less likely to happen as a result of increasing the decay rate, unless any localized trend is there in the seismogram. On the other hand, discernible trade-offs which can sometimes alter final results, may arise due to many other possible reasons; being a smaller data sample recorded at a smaller network, being an inhomogeneous medium with various unrevealed irregularities in the crust, inconsistency due to the combined effect of single and multiple scattering, and any other uncertainty arisen due to not being compatible with basic assumptions of the method set at the outset.

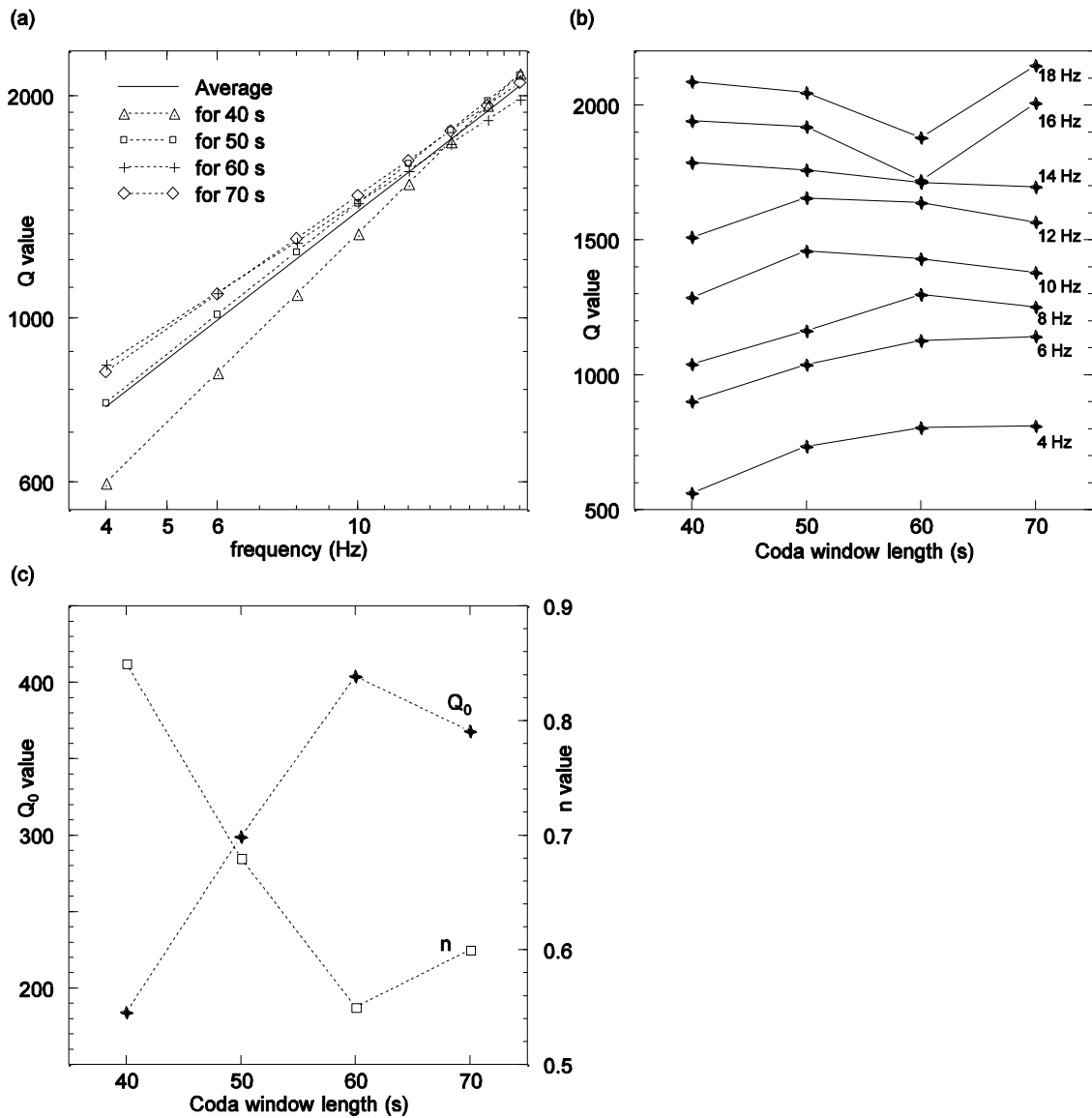


Figure 6.7 Variation of Q with the length of coda window used. (a) Comparison of weighted linear fits, $Q = Q_0 f^n$, with respect to the length of coda window. (b) Individual Q comparison with the length of coda window. An increase of Q with the coda length especially at low frequencies ($f \leq 8$ Hz) and a minor reversing trend at high frequencies ($f \geq 14$ Hz), can be seen for selected centre frequencies. (c) Q at 1 Hz (Q_0) and "exponent", n , variation with the coda window length. A rapid variation in both coefficients is apparent between 40 to 60 s window cases.

Resulted average Q_0 value 301 ± 17 appears to be reasonable for a typical intraplate continental crust. A comparably higher Q_0 yields lesser anelastic attenuation to be undergone during the wave travel through the medium which would contain harder/older rocks. As discussed in Chapter 3, more than 90% of Sri Lanka's crustal rocks is composed with Crystalline rocks of Precambrian whose age can be as old as about 2000 Ma (Cooray, 1994; Kroner and Brown, 2005). Geochronological studies have further confirmed the sedimentation process of the crust in the

central part of the country was completed during the Paleoproterozoic era (Mathavan et al, 1999; Barber, 2000) of the late Precambrian period. By referring to the country's geology, one may argue that the inferred Q_0 does not seem completely reflecting inherent characteristics of a crust of typical Precambrian, since much higher Q_0 values than this are rather more common in such regions; e.g., Canadian shield-893 (Atkinson, 2004b), Indian shield-800 (Singh et al, 2004), Western Australia-457 (Allen et al, 2006). However, it is possible that Q_0 calculation in the present study can be largely affected by local characteristics of the uppermost rocks as well. Such effects can be crucial in situations where a poor quality upper crust, may be as a result of a thin lining of younger Sedimentary stratum resting on top of the older Precambrian crust and/or due to bedrock fractures in the upper crust, is present. A similar case can also be correlated for the Sri Lankan crust, as it is further evidenced by a higher average Kappa value of 0.04 s (discussed later). A rapid increase of Q_0 with the coda window length, starting from 184 ± 16 at 40 s window to 404 ± 36 at 60 s window case, would attest the evolution of crustal characteristics along a vertical profile that corresponds to the sampled volume in which the scattering has taken place, from a younger upper crust to a much older deeper crust underlain (sometimes may extend to the upper mantle), respectively. Hence, the estimated Q_0 that parameterizes attenuation along the whole travel path can immensely depend on the nature of the uppermost part, albeit these attenuation effects of the upper crust are separately parameterized. Malagnini et al (2000a; 2002) based on spectral analysis have also determined relatively higher Q_0 values as 400 ($n=0.42$) and 260 ($n=0.55$), with at the same time higher Kappa values of 0.05 and 0.045 s, for central Europe and for Northeastern Italy, respectively. Other comparable estimations of Q_0 may include northwestern United States, $Q_0=300$, $n=0.3$ (Singh and Herrmann, 1983); Guangdong-China, $Q_0=370$, $n=0.4$ (Jin and Aki, 1988). In Chapter 4, a similar regional Q_0 value of about 389 has found for the northern Indian Oceanic crust surrounding Sri Lanka based on a spectral analysis of moderate magnitude shallow crustal events that occurred at teleseismic distances. However, the estimated regional Q_0 , which is mostly characterized by properties of the northern Indian Oceanic crust that features a diffuse seismicity, would not probe a direct comparison with the local coda Q_0 estimated in the present study, mainly because of the difference in two crustal structures. Studies have shown the regional seismic wavefield in an oceanic crust can be significantly different from that in a continental crust (Knopoff et al, 1979; Kennett, 1985; Campillo, 1990). Hence, the wave traverse pattern and final content of waves guided through a thinner oceanic crust such as the northern Indian Ocean, can be considerably different from that in a typical thicker continental crust like the one of Sri Lanka.

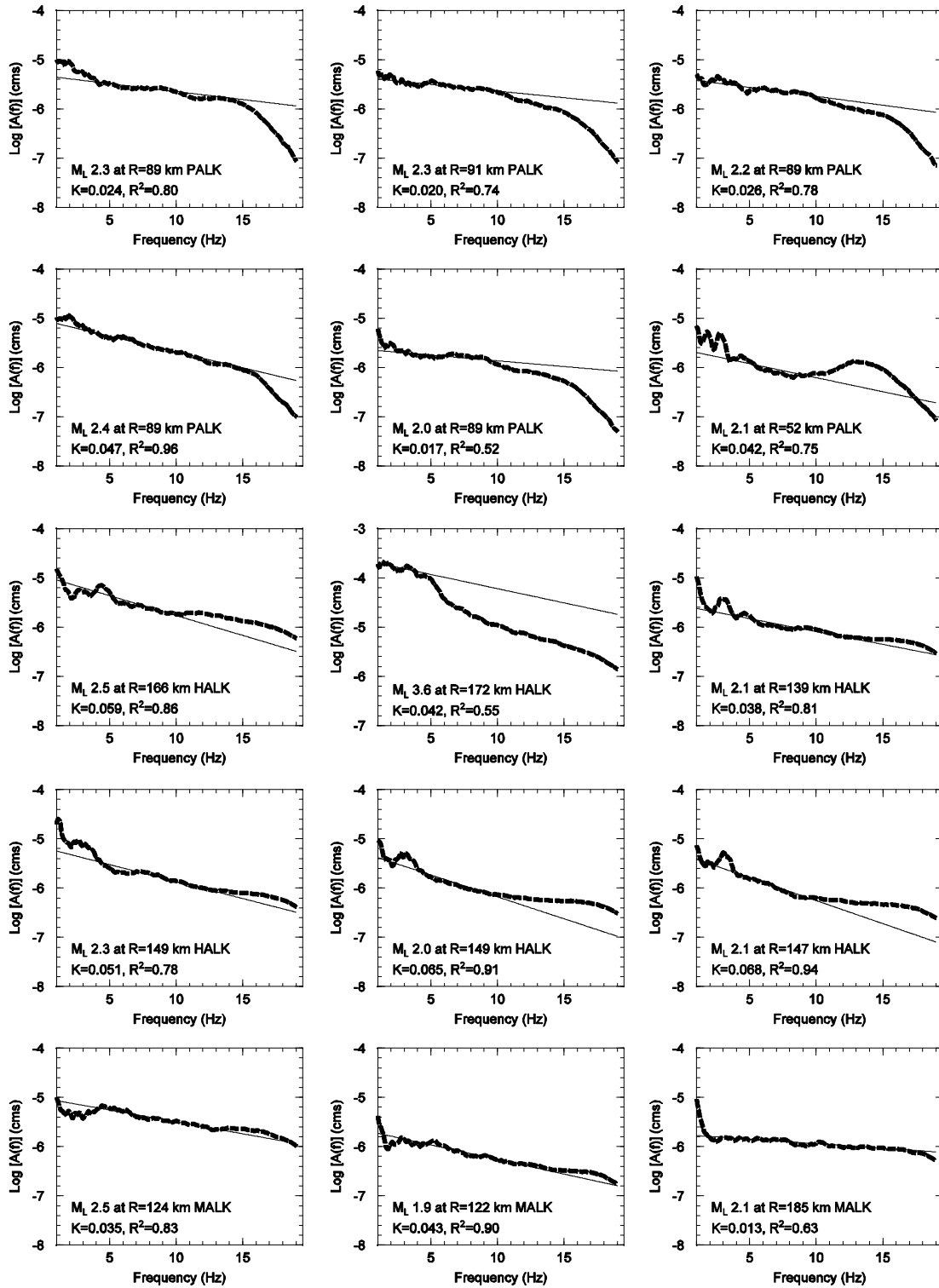


Figure 6.8 Sample estimations of individual Kappa values for the selected stations. Logarithmic displacement amplitude spectrum of the vertical component corrected for anelastic attenuation is indicated in dash line, whereas the line of best-fit given in equation (6.9) to be used in the Kappa estimation at the selected frequency range, is denoted by the continuous straight line. Estimated Kappa and correlation coefficient (R²) for the line of best-fit, are given in each plot.

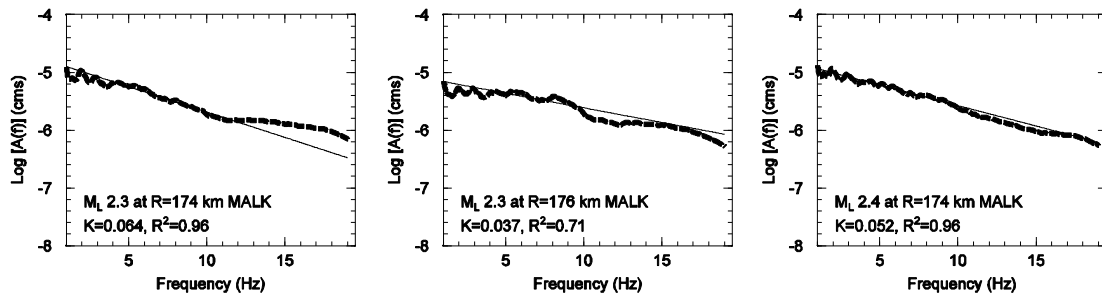


Figure 6.8 (continued)

The average Kappa for selected 3 stations is estimated to be 0.04 ± 0.02 s, whilst that locally varies as 0.03 ± 0.01 , 0.04 ± 0.02 and 0.06 ± 0.02 s at PALK, MALK and HALK, respectively. The average Kappa 0.04 s found in this study is quite well matched with that found in Chapter 5 for distant earthquakes. Figure 6.8 graphically exemplifies sample estimations of individual Kappa values for selected stations. Logarithmic displacement amplitude spectrum of the vertical component corrected for anelastic attenuation along with the line of best-fit [equation (6.9)] used in the Kappa estimation at the selected frequency range, are indicated in each plot. An average Kappa such as around 0.03-0.04 s, as resulted for PALK and MALK, may agree with certain findings in other continental crustal regions; e.g., Central Europe – 0.05 s (Malagnini et al, 2000a), Northeastern Italy – 0.045 s (Malagnini et al, 2002); Greece – 0.035 s (Margaris and Boore, 1998), Northeastern India – 0.025 s (Raghukanth and Somala, 2009). However, a higher average Kappa (0.06 s) at HALK seems a bit unusual for a typical rock site. Information pertaining to site geology, which may be helpful to identify the explanatory reason for apparent higher Kappa at HALK, is not given in the respective data management system (GEOFON). Perhaps, the site may be predominated by younger rock deposits such as Sedimentary. CRUST2.0 also supports this hypothesis in which it shows a 0.5 km thickness soft Sedimentary layer at the uppermost part of the crust in the southern portion of the country. In the overall sense, an average Kappa of about 0.04 s for Sri Lanka would signify the country's upper crust is more close to a form of younger rock as concluded also in Chapter 5, rather to a typical Precambrian crust. Precambrian cratons are mostly associated with lower Kappa values than other crustal forms. For instance, ground motions of ENA are found to be compatible with a Kappa as small as about 0.005 s (Atkinson and Boore, 2006), implying attenuation at the upper crustal level is as negligible. Therefore, the average Kappa estimated in the study sounds more suited to contextualise for a region of younger upper crustal formations, than for a crust formed by older Precambrian rocks. Another explicable reason for resulted higher Kappa values can be linked with the existence of possible bedrock fractures in the crust. There is evidence on younger brittle deformations of the country's lower crustal structure particularly at places where relative uplifts or "exhumations" of the lower crust into the upper crustal level have happened (Kehelpannala et al, 2006; Vitanage, 1985). Brittle

fractures lead by such brittle deformations can significantly depreciate “wave transmission quality” (parameterized by Q) of the medium, and can result in excessive damping of wave energy at the upper crustal level (Anderson and Hough, 1984; Anderson, 1986; 1991). Hence, higher Kappa values, as a consequence of being a fractured upper crust, can be resulted even in regions where older and harder rock forms are well preserved. Atkinson (1996) presents an example of a similar case in which relatively higher Kappa values of 0.02-0.04 s are found for Charlevoix and Sudbury areas of southeastern Canada, those are reportedly located on fractured Precambrian rock within an ancient meteor impact crater. Silva and Darragh (1995) also find a higher Kappa of 0.025 s for a hard rock site comprised by which they called “sheared rock”. In the present study, for the studied area of the country’s upper crust, either both the presence of Sedimentary deposits over hard Precambrian Crystalline strata as evidenced from CRUST2.0 and the existence of bedrock fractures due to brittle deformations as shown by geological investigations, or at least one of these may have strongly contributed toward the higher Kappa estimations. However, neither these reasons can be well justified within the scope of the present study, but may be in a separate study that involves major geo-tectonic investigations of the country. Regardless of the exact reason behind higher Kappa, one thing is quite convinced from Kappa results, which is the presence of a lower quality upper crust beneath the country. It can be noted the average Kappa 0.04 s estimated in here would collate with NEHRP site classes B (rock) and/or C (soft rock and very dense soil) according to the relationship proposed by Silva et al (1999) between Kappa and the shear wave velocity at 30 m depth (V_{s30}). However, care needs to be taken when trying to identify the site class using local Kappa estimated, instead using V_{s30} that the classification is actually based upon, because of the inconsistency of the interdependence between Kappa and V_{s30} , which can sometimes be misleading as discussed by Campbell et al (2014). Figure 6.9 shows individual Kappa estimations in magnitude and hypocentral distance domains. It seems that the figures do not guarantee on any detectable trend in Kappa with either magnitude or hypocentral distance, yet show a sparse behaviour with them. Note that, the average Kappa 0.04 ± 0.02 s found above is not from the average of individual Kappa estimates shown in Figure 6.9, but is the average (arithmetic mean value), rounded to the nearest hundredth, of average Kappa values estimated at each of the sites (i.e., PALK, HALK and MALK).

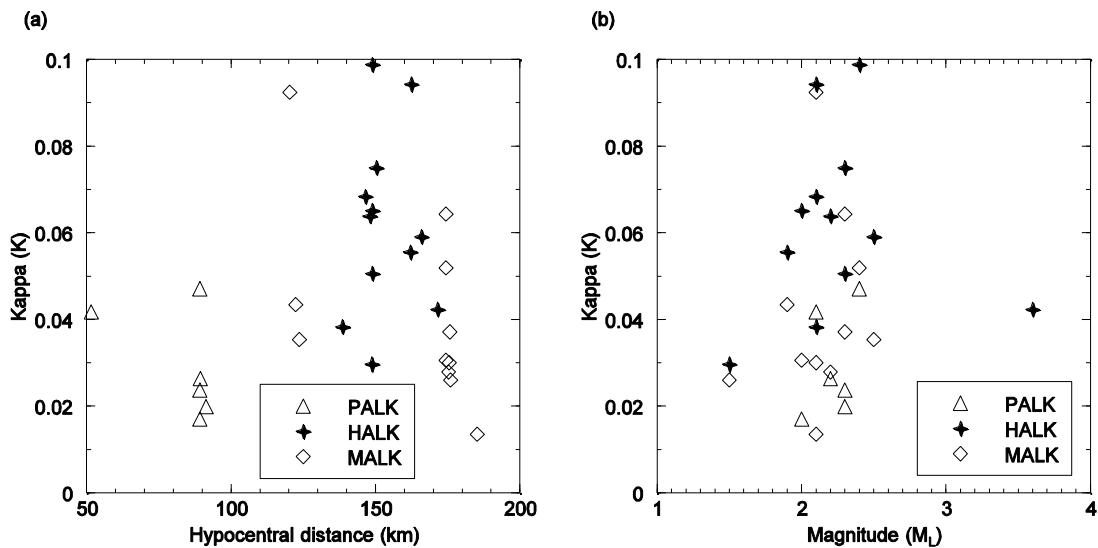


Figure 6.9 Individual Kappa variation with earthquake properties. Variations at each station are separately indicated. No any discernible trend can be found from the plots. (a) Kappa vs hypocentral distance (km). (b) Kappa vs earthquake magnitude (M_L).

The assessment made above on the country's upper crust based on Kappa can be still contradicted with H/V estimations for the selected sites. H/V ratio, which is used as a measure of the upper crustal amplification, is obtained close to unity for the selected sites (Figure 6.10). For average site conditions, the maximum possible amplification taking place at the upper crustal level of the country is about 1.20 and that occurs at a frequency around 11 Hz (Figure 6.10d). Individually, this shows varying as about 1.30 for PALK and MALK (Figures 6.10a and 6.10c, respectively), and about 1.25 for HALK (Figure 6.10b) stations at higher frequencies ($f \geq 4.0$). Estimated H/V ratios are similar to the findings of Chapter 4, in which H/V calculations are made for a set of amplitudes of moderate magnitude distant earthquakes recorded at the same stations. Furthermore, the average maximum amplifications deduced by H/V ratio here, are comparable to findings for ENA hard rock sites for which the maximum H/V is found to be in between 1.2 and 1.5 at a frequency about 10 Hz (Atkinson, 1993b; Siddiqi and Atkinson, 2002). The resulted lower site amplifications would also correspond to NEHRP "site class A" hard rock conditions (Atkinson and Boore, 2006). The average Kappa and its reflective upper crustal characteristics of the region may not agree with H/V ratio findings. H/V estimations close to 1.0 would theoretically justify that virtually there is no wave amplification to be possible at the upper crustal level, and hence would testify that the upper crust is of high quality with much improved wave propagation features. On the other hand, a Kappa of 0.04 s would more suit for a crust of poor quality. The real reason behind these two controversial assertions is difficult to be tracked down. Given lower H/V values, it is possible to conclude the shear wave velocity of the horizontal component has not been largely affected at the upper crustal level of the selected three sites. This may sometimes be related to shear wave polarization effects taking place at fractures of the medium. Winterstein

(1992) discusses the effect of bedrock fractures on the wave polarization and speed of the wave travel for several possible combinations of different fracture orientations and wave traveling directions, in which he shows that some combinations of fracture orientation and direction of wave travel (e.g., both the fracture and direction of wave travel are vertical) can cause no effect on the wave speed. Therefore, the shear wave velocity of a medium may be a lesser dependent to bedrock fractures than to the type of rock (whether older/harder or younger/softer) which the medium is composed of. Following this argument, the idea that the country's upper crust has comprised with fractured hard rock formations, can be put forward, however, it is necessary to acknowledge that there may also be other reasons attributed for concurrent observation of higher K_{appa} and negligible H/V, which are not that clear at this stage.

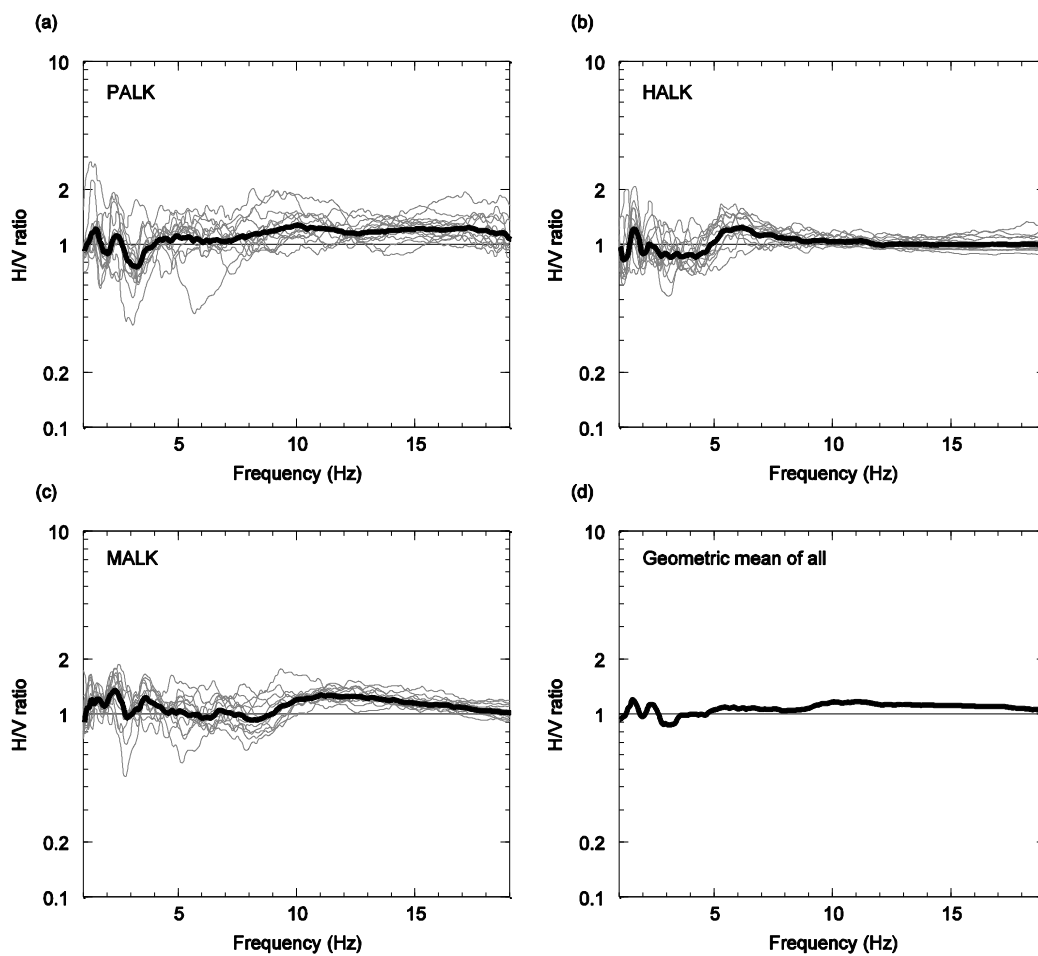


Figure 6.10 H/V estimations for the selected sites in the study. Individual estimations are shown in thin grey lines, while the geometric mean at the respective site is indicated by a thick dark line. (a) For PALK. (b) For HALK. (c) For MALK. (d) Geometric mean of all estimations. H/V has resulted close to unity for each of the selected sites, with a maximum indicating about 1.20 (occurs at a frequency around 11 Hz) for average upper crustal conditions of the country. Individually, this varies as about 1.30 for PALK and MALK, and about 1.25 for HALK stations for higher frequencies ($f \geq 4.0$). Estimated H/V ratios are similar to that of Chapter 4.

Given uncertainties in above estimated local seismological parameters, the factors are validated following a comparison of ground motions between recorded events and stochastically modelled events employing estimated seismological parameters, which is discussed in the next section.

6.5.2 Comparison of ground motions

Ground motion modelling in present day engineering seismology, has become an important aspect in seismic hazard studies. Stochastic methods are becoming increasingly popular in seismic hazard assessments particularly in stable continental regions (Balendra et al, 2002; Lam et al, 2002; 2009). Seismological model that defines the final frequency content of the target amplitude spectrum to be used in stochastic simulation, follows the same form as which given in equation (6.6). Brune's circular point source model known as ω^2 -model (Brune, 1970; 1971), with lower average stress drops of 2-4 MPa (20-40 bars), is adopted as the source factor for the simulation. Brune's model is considered to be sufficiently accurate to represent the selected smaller magnitude events whose source/rupture areas are relatively small enough that they can approximate as point sources. On the other hand, other source models such as Atkinson's double corner frequency intraplate model (Atkinson, 1993a; Atkinson and Boore, 1995) and intraplate earthquake source model proposed by Boatwright and Choy (1992), are limited to apply for smaller events since their derivations are based on comparably higher magnitude ranges, which may finally result in overestimation of apparent source amplitudes of smaller events. Relatively small average stress drop values in a range of 2-4 MPa (20-40 bars) for reported events are selected loosely based on few trials considering the final conformity in both spectral shapes and spectral levels between real records and simulated ones. Generally, intraplate regions can exhibit higher static stress drops than interplate regions. For instance, intraplate ENA is associated with a higher average stress drop value of the order of 15 MPa (150 bars) for moderate to large magnitude events (Atkinson, 1993a) whereas on the other hand, interplate WNA has shown to be associated with an average stress drop value as low as about 5 MPa (50 bars) even for large magnitude events (Atkinson and Silva, 1997). Similar observations are made by Kanamori and Anderson (1975) based on a study of global earthquakes, in which they conclude the stress drops in areas of intraplate events can be about 10 MPa (100 bars) on average, while noting a lower average of about 3 MPa (30 bars) for interplate areas. Surprisingly, relatively small stress drops have also been observed in some intraplate regions; an average of 3 MPa (30 bars) for the Central European continental crust found in an intraplate region (Malagnini et al, 2000a). The average stress drop of a region is generally identified as independent of earthquake magnitude (Lam et al, 2000b). Notwithstanding, Atkinson (2004b) has noticed smaller magnitude events ($4 < M_w$) in ENA and southeastern Canada are allied with much smaller stress drop values than the average found for moderate and large magnitude events in the region. Following this observation of smaller magnitude events, source spectra of the selected events in the present study are modeled

with lower stress drop values as chosen above. However, moderate and large magnitude events of the region are assumed to be related with higher stress drop values with the average being close to 10 MPa (100 bars), in accordance with findings by Kanamori and Anderson (1975) for intraplate earthquakes on global basis. However, it should also be noted that, overall a parameter like stress drop would be uncertain to identify always as a constant value within the region, and variations can be expected even event wise due to trade-offs which may not be quantified in generic terms, i.e., fault geometry, rupture properties, tectonic setting and crustal structure, as an artifact of the modelling method followed, etc. Magnitude measure defined by the seismic moment (M_0) of Brune's model, is taken as the moment magnitude (M_w) determined based on the apparent displacement source spectral level at frequencies below the corner frequency obtained by correcting for attenuations as described in the next section. Estimated Q_0 and n values, 301 and 0.67, respectively, are applied in the anelastic attenuation factor which defined in equation (6.7) with its frequency dependent linear variation, $Q = Q_0 f^n$. Subsequently, resulted Kappa values are applied to parameterize incurred upper crustal attenuations as given in equation (6.5).

Tri-linear hinged shape geometric attenuation function proposed by Atkinson and Boore (1995), with little modifications to hinge points as 65 and 140 km, instead original 70 and 130 km, is used for characterizing geometric damping of the continental crust in Sri Lanka. Original hinge points are a bit "tuned-up" in order to accomplish consistency in the spectral level between recorded and simulated events in the comparison. Nonetheless, decay rates of the proposed geometric attenuation model are retained as same as that of Atkinson and Boore (1995). Changing hinge points 70 and 130 km to 65 and 140 km, respectively, has resulted in slightly lower geometric attenuation for the Sri Lankan crust, preferably at medium and larger distances, than which for ENA, as shown by Figure 6.11a. Perhaps, this reduction in attenuation may correlate with the lesser average crustal thickness of the country (about 30 km from CRUST2.0) according to some theoretical claims by certain scientists (Lam et al, 2000a; 2000b), who relate the average crustal thickness of a region as proportional to the amount of geometric attenuation to be undergone in the region. The proposed model of geometric attenuation is compared with actual attenuations (Figures 6.11b and 6.11c) estimated by first correcting the recorded amplitude for anelastic and upper crustal attenuations with estimated parameters, and by second dividing this corrected amplitude by a theoretical source amplitude obtained using Brune's model for about 3 MPa (30 bars) stress drop. Both scantiness of reported data (in terms of magnitude and distance) as well as scatter, do not permit a sensible comparison that would allow for a more distinguish identification of the validity of the proposed model in representing actual data, however, it shows that the proposed model is generally in a good agreement with actual geometric attenuations.

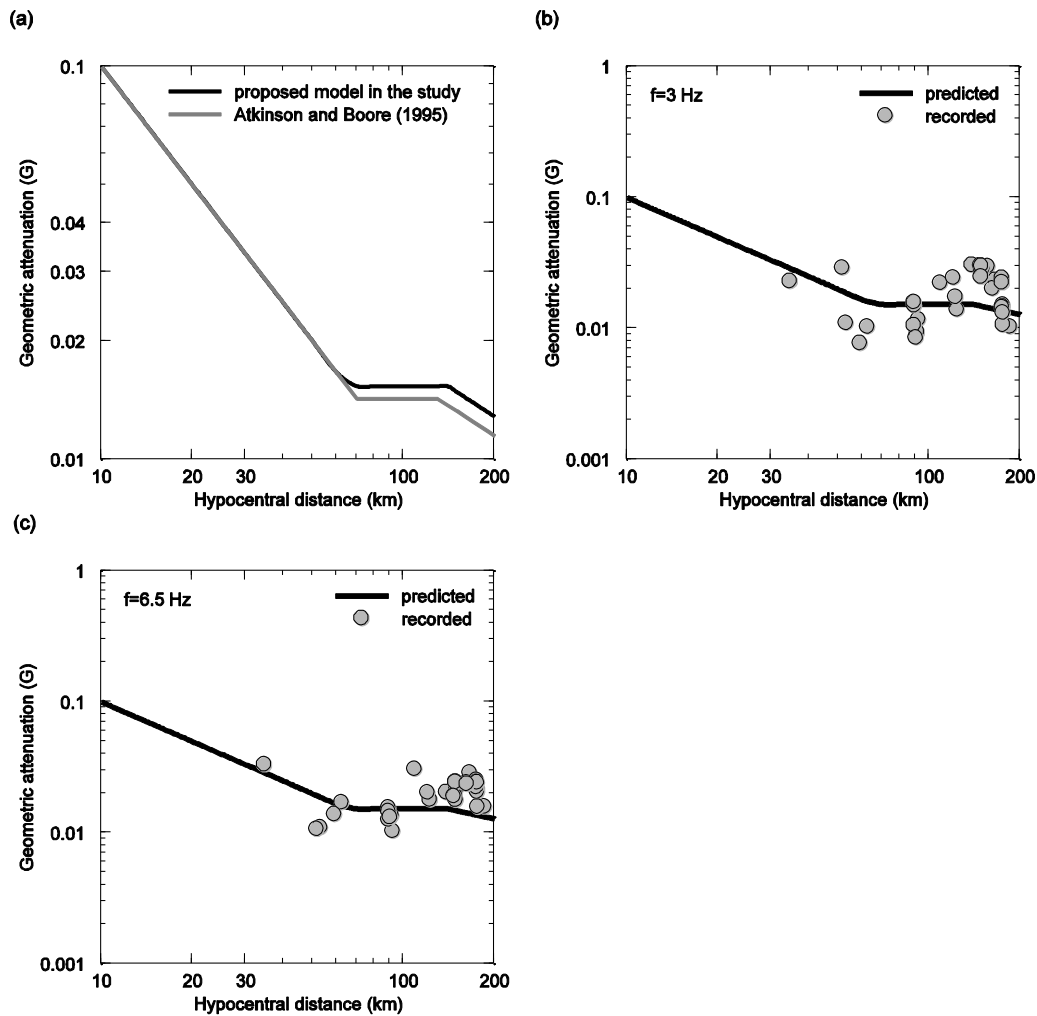


Figure 6.11 Proposed model of geometric attenuation to be used at local distances in the country. (a) Comparison of the proposed model with Atkinson and Boore's (1995) model for ENA regions. (b) and (c) Comparison of the proposed model with actual geometric attenuations estimated for reported events at two sample frequencies. Both scantiness of reported data (in terms of magnitude and distance) as well as scatter, do not offer a clear comparison for the proposed model's validity in representing actual data, however, it shows the proposed model is generally in a good agreement with actual geometric attenuations.

Employed seismological parameters in the stochastic method are summarized in Table 6.3, whereas the comparison of simulated events with observed records in terms of Pseudo Spectral Acceleration (PSA) for 5% critical damping ratio and acceleration time history to account for frequency and time domain comparisons, respectively, are shown in Figure 6.12. PSA is considered in the frequency domain comparison, since other ground motion parameters such as spectral velocity or displacement are not found to be clear enough and producing amplitudes in an unmeasurable range for selected events. Simulations are carried out using FORTRAN packages GENQKE and ETAMAC (Lam, 1999).

Interesting consistency between observed and modelled ground motions can be seen from the plots, supporting the fact that estimated and applied seismological parameters are in an acceptable level of accuracy. Matching the events which recorded at medium and long distances (more than about 80 km) would ensure the reliability of estimated Q_0 to characterize whole path attenuations specific to the continental crust of Sri Lanka, whereas comparisons for near-field events would more convince accuracy of Kappa estimation. In both cases, proposed geometric spreading function and applied stress drop values are also verified.

Table 6.3 Seismological parameters used in the stochastic simulation

| Seismological parameter | Applied relationship | Remarks |
|--|---|---|
| Source factor [$S(f)$] | Brune's model (1970, 1971), $S(f) = \frac{CM_0}{1 + \left[\frac{f}{f_0}\right]^2}$ $C = 0.78/(4\pi\rho\beta^3)$ $f_0 = 4.9 \times 10^6 \beta (\Delta\sigma/M_0)^{1/3}$ | C is called "scaling factor". M_0 is the seismic moment, which is related to $\log M_0 = 1.5M_w + 10.7$. M_w is estimated using the average spectral level of the corrected displacement amplitude spectrum, as described in section 6.5.3. ρ (density) and β (shear wave velocity) of the source region are taken as 2800 kg/m ³ and 3.5 km/s, respectively (CRUST2.0). Average stress drop ($\Delta\sigma$) is taken as 2-4 MPa (20-40 bars) for simulation of smaller events in the ground motion comparison. However, the scenario event M_w 6.5 is modeled with 10 MPa (100 bars) average stress drop, given the evidence of higher stress drops in intraplate regions. Note that the relationship given for corner frequency, f_0 , is valid when β , $\Delta\sigma$ and M_0 are in km/s, bars and dyne centimetres, respectively. |
| Geometric attenuation factor [G] | $G = 1/R, \quad R \leq 65 \text{ km}$ $G = 1/65, \quad 65 \text{ km} < R \leq 140 \text{ km}$ $G = \frac{1}{65} \sqrt{\frac{140}{R}}, \quad R \geq 140 \text{ km}$ | Tri-linear model proposed by Atkinson and Boore (1995) has been used with modified hinge points of 65 and 140 km, instead 70 and 130 km, respectively. |
| Anelastic whole path attenuation factor [$An(f)$] | $An(f) = e^{-\left[\frac{\pi f R}{Q\beta}\right]}$ | Equation (6.7) in the main text, and $Q = Q_0 f^n$, where $Q_0 = 301$ and $n = 0.67$ determined in the study are used. ρ and β are retained as same as that used in source factor. |
| Upper crustal attenuation factor [$P(f)$] | $P(f) = e^{-\pi f K}$ | Equation (6.5) in the main text, where Kappa (K) is taken as 0.03, 0.04 and 0.06 s at PALK, MALK and HALK, respectively. |

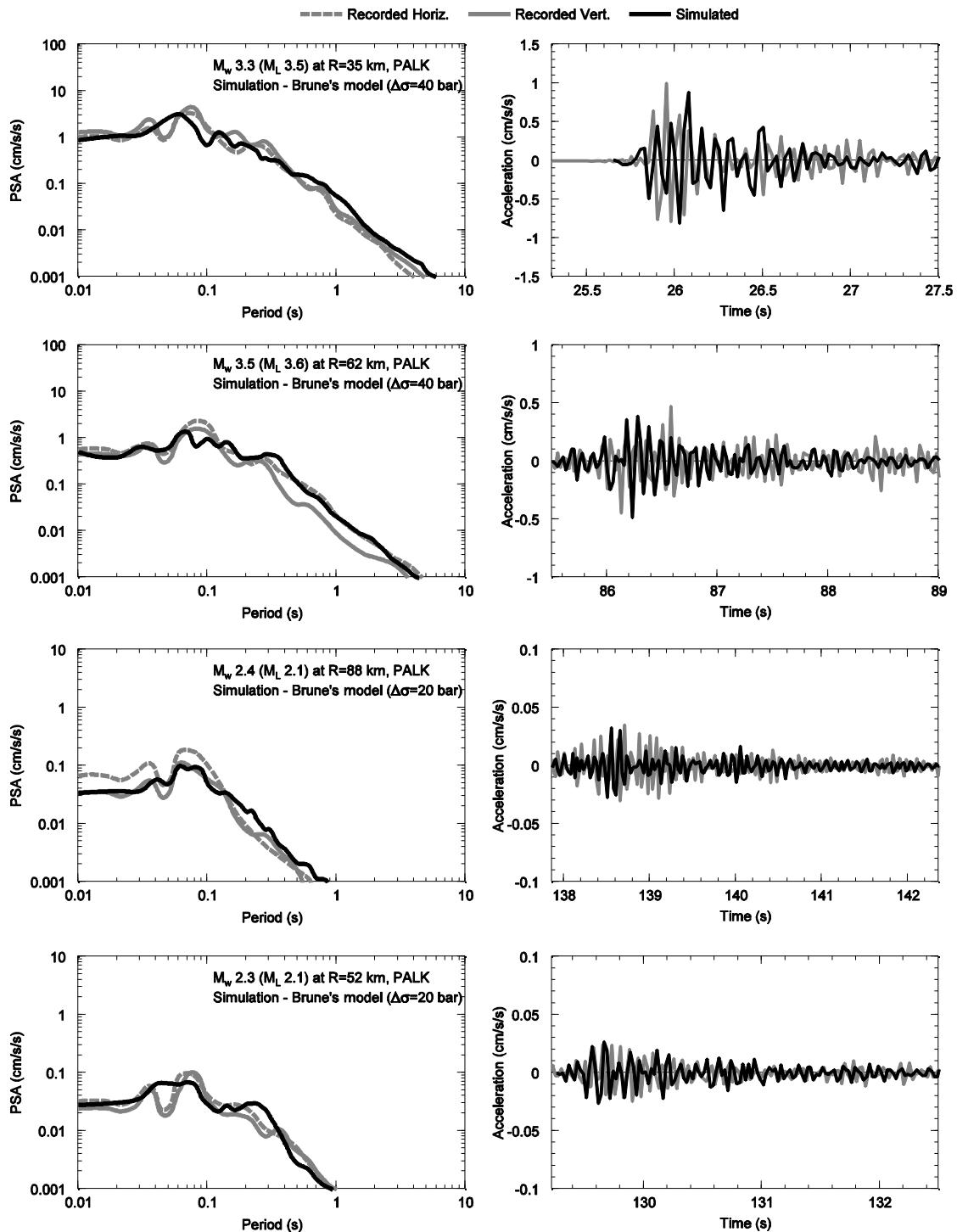


Figure 6.12 Comparison between observed records with stochastically simulated events in terms of Pseudo Spectral Acceleration (PSA) for 5% critical damping ratio and acceleration time history. Stochastic simulations were done employing inferred attenuation parameters with Brune's point source spectra of about 2-4 MPa (20-40 bars) stress drop values. The parameters adapted in the simulation are summarized in Table 6.3. Simulations result in a good match with observed records as indicating similar maximum spectral values even at around same periods, and comparable Peak Ground Accelerations (PGAs).

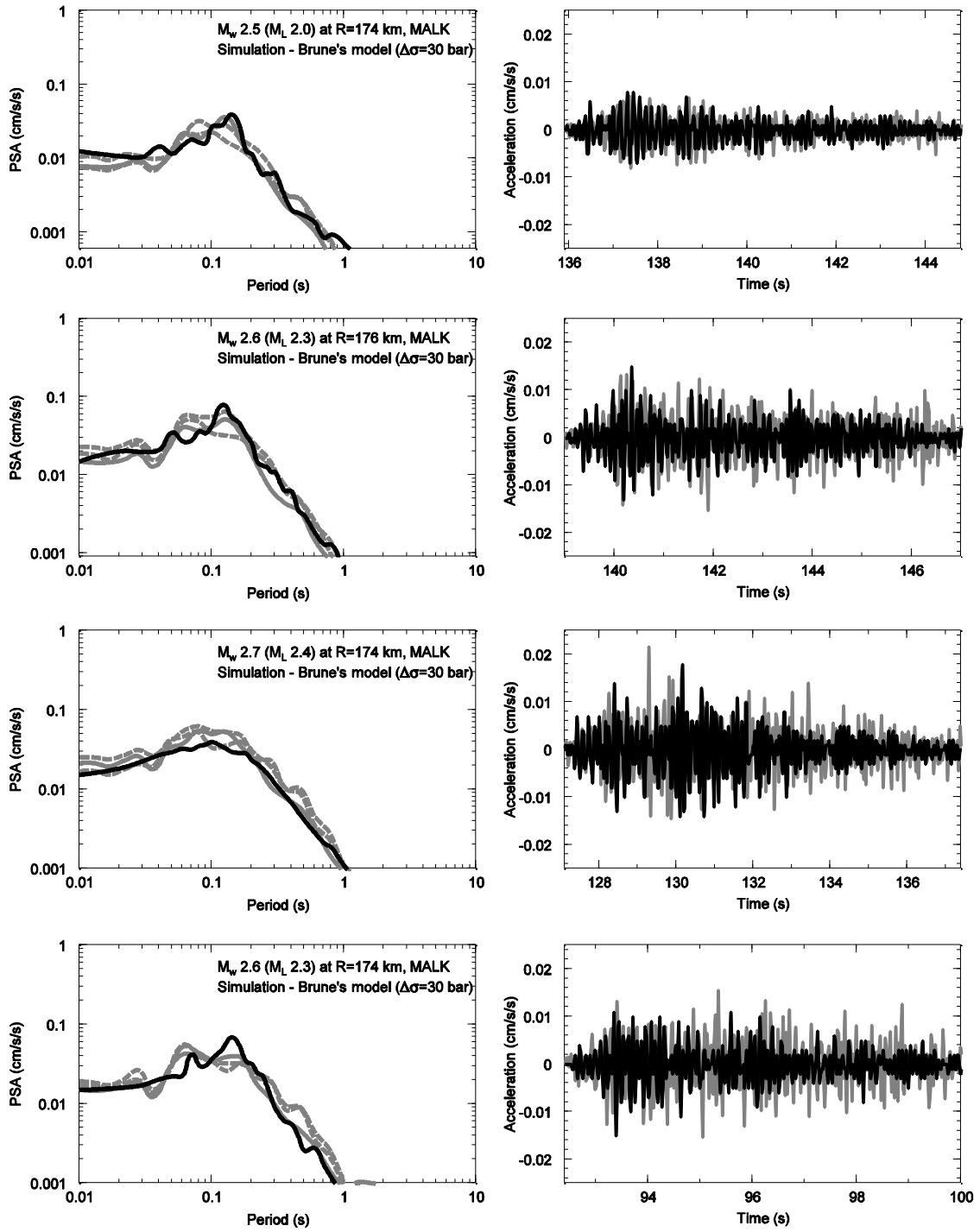


Figure 6.12 (continued)

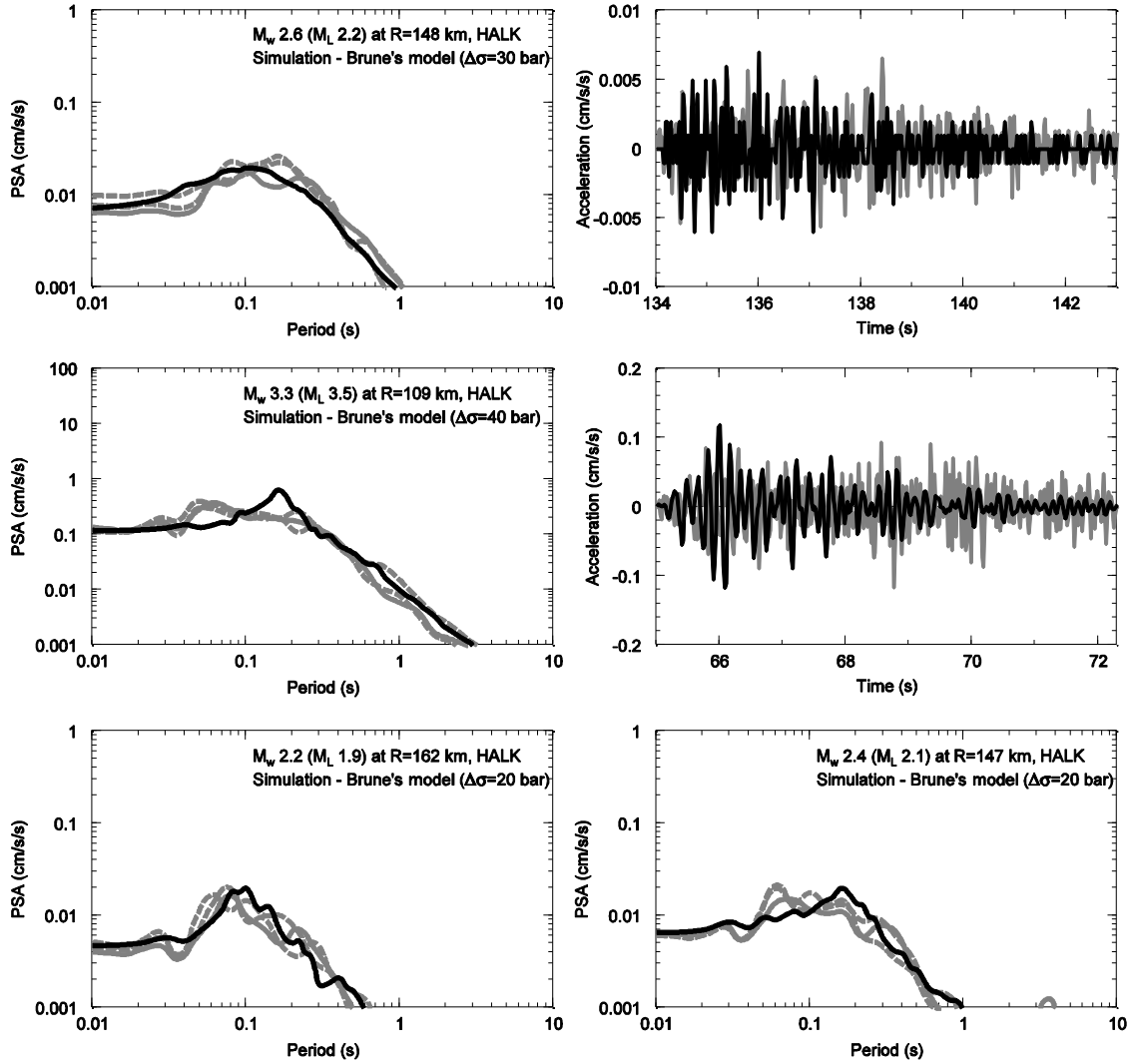


Figure 6.12 (continued)

6.5.3 Source spectra

Source spectra of the events, obtained by correcting for all intended attenuations identified above, have been investigated. Fourier amplitude at the source of an event at a given frequency after averaging for all stations which the event was recorded, can be obtained by applying a rearranged form of equation either (6.8) or (6.9);

$$\log[S(f)]_{Avg.} = \log[A_x(f)] - \log[G] + \frac{\pi f R}{Q\beta} \log[\exp] + \pi\kappa \log[\exp] f \quad (6.11)$$

Here, the terms have their same meanings as defined previously [in equations (6.5)-(6.9)], however, the average log acceleration amplitude, $\log[S(f)]_{Avg.}$, instead individual displacement amplitudes is considered as the source amplitude. Figure 6.13 shows resulted acceleration amplitudes of Fourier spectra at the source along with theoretical Brune's spectra for 3 MPa (30

bars) and 10 MPa (100 bars) stress drops. Figure 6.13a compares source spectra of events between M_w 3-4, while 6.13b compares that of smaller events between M_w 2-3. Observed source spectra of relatively small events (M_w 2-3) are within the limits that are defined by Brune's model even for 3 MPa stress drop level, which explains that the smaller events are characterized by comparably low stress drop levels, may be around 2-4 MPa (20-40 bars) as identified before. Two events between M_w 3-4 also indicate complying with Brune's model of 3 MPa stress drop at lower frequencies, however, the events look to be associated with a higher average stress drop level such as about 10 MPa (100 bars) given their overestimation of the Brune' spectral level for a 3 MPa stress drop at higher frequencies ($f >$ about 10 Hz). It is also worthy of mention that the estimated apparent source spectra of the recorded events can highly depend on uncertainties of the estimated attenuation parameters. High frequency spectral shape as well as the spectral level can be significantly altered by variations of Q and Kappa, since their respective attenuations are frequency dependent in such a way that the higher the frequency the higher the attenuation [see equations (6.5) and (6.7)]. Uncertainty in geometric attenuation can also be influential to change the spectral level in constant amounts at each frequency, though this is not likely to be the case in here, since low frequency source spectral levels of actual events are well matched with those of theoretical models.

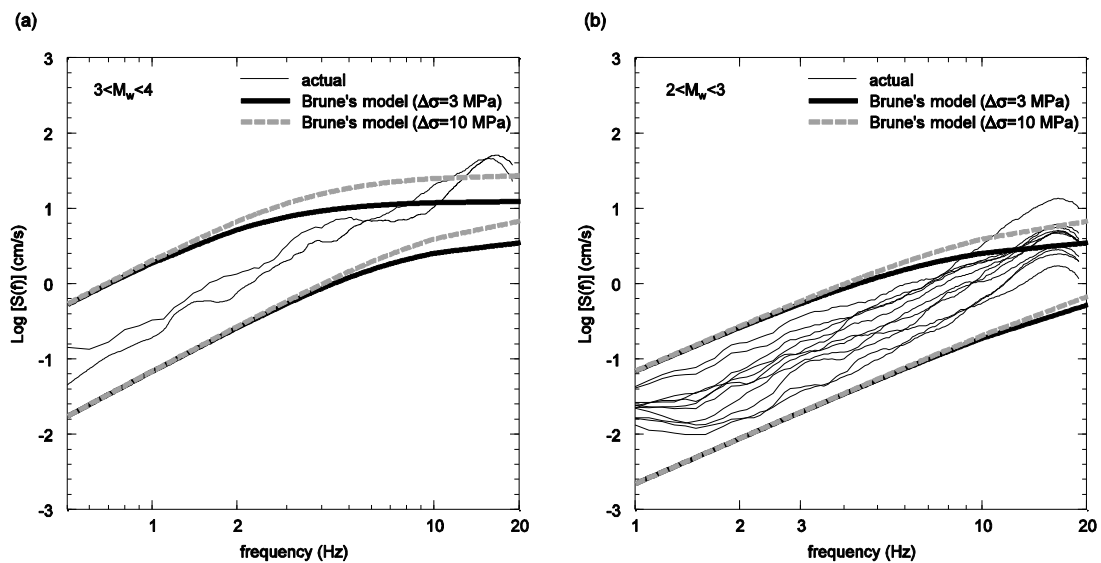


Figure 6.13 Comparison of attenuation corrected source spectra with theoretical Brune's spectra for 3 and 10 MPa (30 and 100 bars) stress drop values. Values are in terms of Fourier acceleration amplitude. Observed source spectra of a given event are averaged over all the stations which the event was recorded. (a) For $3 < M_w < 4$. (b) For $2 < M_w < 3$. Observed source spectra of relatively small events (M_w 2-3) are within the limits that are defined by Brune's model even for 3 MPa stress drop level, however, relatively large two events (between M_w 3-4) indicate complying more with a higher stress drop of about 10 MPa (100 bars) due to their overestimation of the Brune' spectral level for a 3 MPa stress drop at higher frequencies ($f >$ about 10 Hz).

Moment magnitudes of the events are estimated based on the average spectral level of displacement source spectra, at frequencies below the corner frequency. In here, displacement source spectra are obtained by above estimated average acceleration source spectra for each of the events. As given in Brune's model (see the equation in Table 6.3), displacement source spectral amplitude at frequencies below the corner frequency can be approximated into CM_0 by simply taking the denominator as 1.0 (assuming $f/f_0 \approx 0$ for frequencies below the corner frequency). Then, the seismic moment (M_0) of the respective event can be found by using the ratio between the average displacement source spectral amplitude (at below the corner frequency) and C (scaling factor). The corner frequencies are kept as same as that used in the Kappa estimation. Resulted M_0 values are then converted to M_w using the standard relationship by Hanks and Kanamori (1979). Resulted M_w values are plotted in Figure 6.14 against initial M_L estimations for the events. The line of best-fit between M_L and M_w along with some other published relations for smaller events in other regions are also shown.

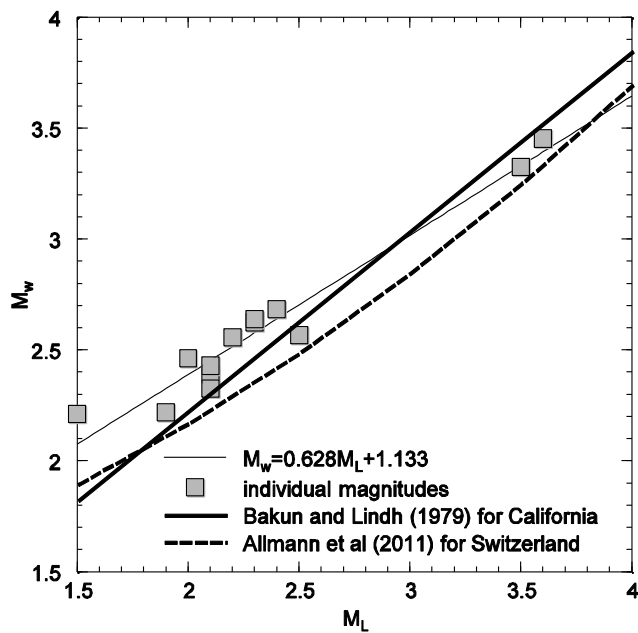


Figure 6.14 Initial M_L vs. estimated M_w values for the selected events. The line of best-fit between M_L and M_w along with some other published relations for smaller events in other regions are also shown.

6.5.4 A scenario investigation

A scenario investigation as a deterministic approach, is implemented to evaluate expected ground motions caused due to a possible major event that is likely to occur within the country. In Chapter 3 section 3.2, two possible seismically unstable zones are identified within the inland based on historical data with giving emphasis on the country's geotectonic setting, area around the capital city-Colombo and Mahawelli shear zone (refer Figure 3.4 in Chapter 3). Here, the former is

considered to be susceptible to more adverse effects owing to its uncertain tectonic structure and higher rate of recurrence with respect to the latter. Accordingly, for the assessment in the present study, based on historical records, an M_w 6.5 shallow crustal event is considered as “the characteristic earthquake” in the area around the capital city-Colombo. Note that, a circular area of about 15 km radius is assumed as the possible source zone. The event is stochastically simulated with above determined and validated seismological parameters. Attenuation characteristics of the region are assumed to be earthquake magnitude independent, and hence those estimated attenuation parameters are considered to be equally applicable for both small as well as strong magnitude events. Nevertheless, the average stress drop level of larger events such as an M_w 6.5 can be necessarily different than that of a smaller event, and therefore an average of 10 MPa (100 bars) is assumed to be appropriate for the scenario event for applying in Brune’s source model. Resulted PGAs at rock sites are mapped in Figure 6.15. A maximum PGA of more than 0.5g (g is 9.81 m/s/s) has resulted in the vicinity of epicentral area in Colombo due to M_w 6.5 event, and this may give rise to a maximum spectral acceleration of more than 1.2g at the short period range if they are related by a factor of 2.5 as in the common codes of practice. This is possible as shown in the response spectral diagram in Figure 6.16 that gives elastic spectral accelerations for 5% damping ratio of M_w 6.5 event at 5, 10, 20 and 30 km distances. These rock ground motions can further be accentuated several times at soil sites due to local site amplification effects and can be severe at places where deep soft soil sediments are found in abundance. Moreover, induced ground motions are likely to produce shakings in considerable levels at distances as far as about 190 km away from the epicentre. Although the expectancy of such a catastrophic event would be little in probability, the possibility cannot be always omitted as it happened in 1615 in Colombo and in Christchurch-New Zealand in 2011.

The vulnerability of the places can be much higher than anticipated since it depends on earthquake properties (magnitude, distance) as well as the preparedness of the location (or city), which particularly includes adherence to the technology and code of practices to cope with the event. Furthermore, this scenario investigation is only in the local context, and has not included other possible scenarios such as a large magnitude long distant event that occurs at surrounding Indian Ocean crust. The procedure is basically a deterministic and hence may not be able to account for effects due to uncertainties. Therefore, the final seismicity of the country would be properly assessed only after a comprehensive study which may be more based on a probabilistic approach.

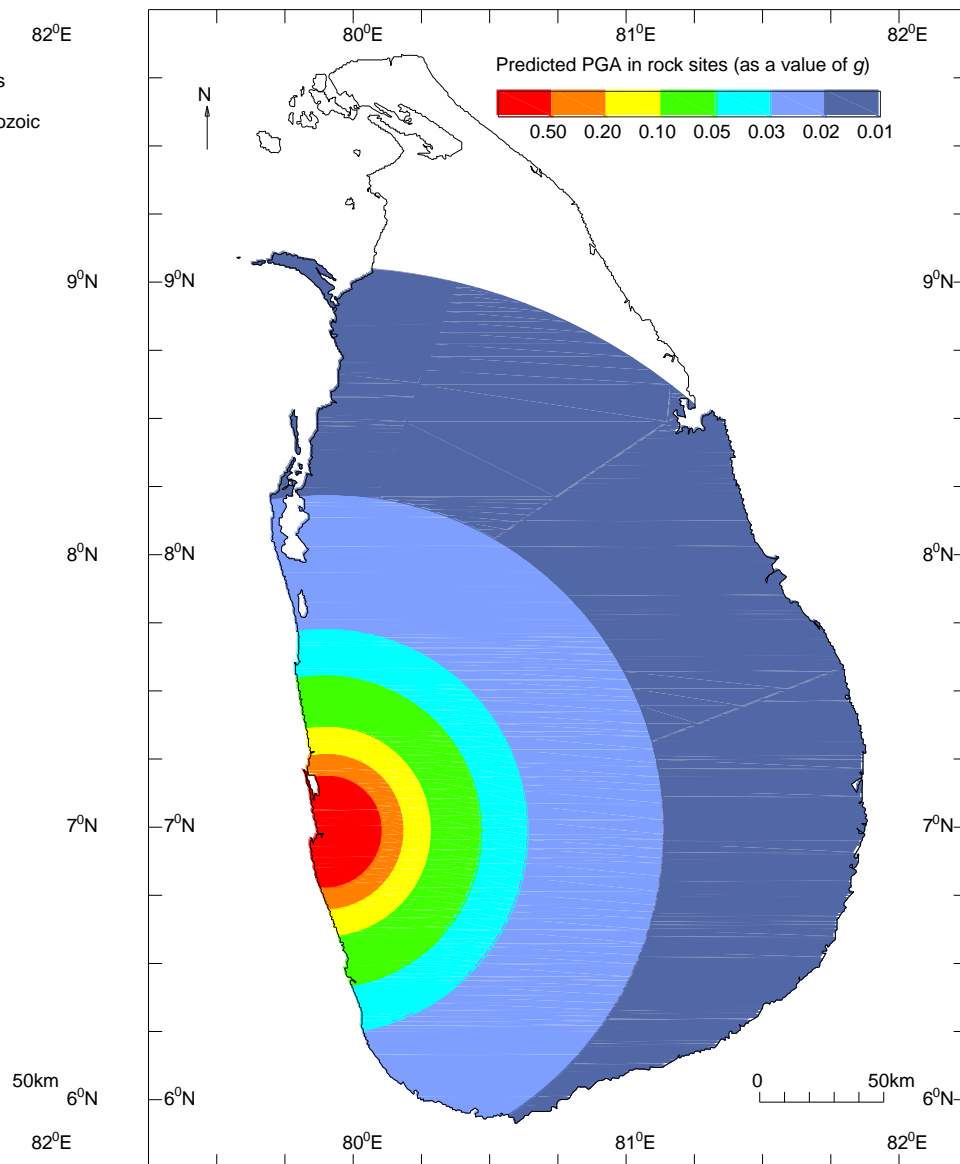


Figure 6.15 A possible scenario investigation for Sri Lanka in the local context. Expected PGAs at rock sites due to “the characteristic earthquakes” M_w 6.5 in the Colombo area, are stochastically simulated employing inferred seismological parameters, with Brune’s model of 10 MPa (100 bars) stress drop.

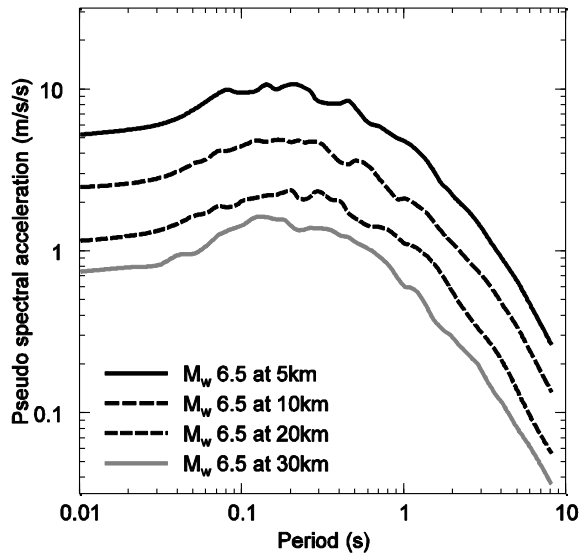


Figure 6.16 Pseudo spectral accelerations for 5% damping ratio of the M_w 6.5 scenario event occurred at 5, 10, 20 and 30 km hypocentral distances.

6.6 Summary and conclusion

Attenuation and apparent source characteristics of the Sri Lankan Precambrian crust have been investigated by analysing digital waveform data of small and micro earthquakes recorded at the country's broadband network. Application of the single backscattering coda wave method with varying coda window length reveals a notable lapse time dependency in estimated Q , which supports previous observations in coda Q studies. An increase of Q with the coda length especially at low frequencies (≤ 8 Hz) and a minor reverse trend at high frequencies (≥ 14 Hz), can be noted at the selected frequency range, which in turn has resulted in higher Q_0 values at longer time windows. Increase of scattering Q due to multiple scattering effects and sampling much larger volumes at the deeper crust can result in higher Q with time. The average coda Q for all time window cases has followed the form, $Q = (301 \pm 17)f^{0.67 \pm 0.02}$. This would agree, to a certain extent, with the type of the crust underneath the country which is of Precambrian, yet a poor quality upper crust as a result of a thinner sedimentary layer on above and/or due to being a fractured bedrock, is susceptible since it is further evidenced by a higher average Kappa of 0.04 ± 0.02 s resulted. The average Kappa found in this study interestingly well coincides with a previous Kappa estimation for the same region yet by a different method (described in Chapter 5). H/V ratios are estimated to be close to unity, and are found to be comparable with results of a previous study undertaken for distant events occurred in the northern Indian Ocean (presented in Chapter 4). H/V results imply that the country's upper crust is composed of higher quality rock formations, though which is contradicted with the average Kappa resulted. Given controverted results of Kappa and H/V estimations, the idea that the upper crust of the region as being fractured yet composed by hard rock formations, can be put forward. However, further evidence of

geological investigations may essential for a proper justification. Estimated Q_0 and Kappa values, along with the proposed geometric attenuation model for the region, have further been validated by a comparison of ground motions. The comparison is done in both frequency and time domains, between original records and stochastically generated events employing those estimated and collated seismological parameters with Brune's point source model for average stress drops of 2-4 MPa (20-40 bars). Attenuation corrected source spectra show a sufficient consistency with the same Brune's model, yet lead toward possible higher stress drop levels for relatively larger events. Deterministic based scenario investigation, undertaken for one of the critical seismic zones within the country, indicates significant ground motions, PSA more than 0.5g near Colombo, emphasizing the vulnerability of the place due to an event of M_w 6.5 can be as such happened in the same place in 1615 and recently in Christchurch, New Zealand in 2011.

7. Ground motion prediction equations for rock sites in Sri Lanka

7.1 Introduction

Ground motion prediction equations (otherwise known as attenuation models) are essentially utilized in the process of seismic hazard assessment when computing “the hazard level” which is commonly expressed as a motion parameter (such as peak ground acceleration/velocity or as an elastic spectral ordinate of a selected natural period) of a certain probability of exceedance, at a site from an identified source. As discussed in Chapter 2, attenuation models are often developed by empirical approaches based on regression or parametric analysis of actual strong motion data recorded in the region. Regions located in the neighbourhood of plate margins (e.g., California, Japan, Indonesia, New Zealand, etc.) are generally rich in strong motion data, and therefore, empirical modelling using actual data for such regions can be easily carried out by various analysis techniques. However, these relationships originally developed in active seismic regions are sometimes limited for direct application in other low to moderate seismicity places owing to the difference in seismo-geological characteristics between the regions. With this in mind, the objectives of the project were set to achieve accurate estimations of region-specific ground motion characteristics of the subject region in the first place. Analysis of recorded data available at the country’s seismic network and stochastic comparisons, were carried out through Chapters 4, 5 and 6, as appropriately, in determining these region-specific attenuation parameters. The study presented in this Chapter is devoted for the next step which is derivation of ground motion (attenuation) models for the region based on those estimated ground motion parameters in previous Chapters. These models are developed using regression analysis of artificial data produced using stochastic simulations employing estimated ground motion parameters. Therefore, rationality between the developed attenuation models and their applicability to the region of interest, is distinguishable.

In this Chapter, twin ground motion attenuation models are developed for prediction of rock ground motions in the subject region. One of the models mainly considers attenuation characteristics of local events at short and medium distance range of the country’s close proximity, whilst the other essentially captures attenuations of regional events occurred at teleseismic distances in the surrounding oceanic crust.

7.2 Methodology

7.2.1 Preparation of the database using stochastic simulation

The attenuation models in the study are derived using regression analysis of an artificial strong motion dataset built by stochastic simulations of possible events. A set of spectral amplitudes of synthetic time histories generated by the stochastic process, is adapted as “raw data” for the regression in the absence of adequate amount of actual strong motion waveform records in the country. There is a certain amount of low amplitude actual recorded data available in Sri Lanka as it was evidenced by the previous Chapters of the thesis. However, these data may not be that accurate to characterize “strong ground motions” of the region as most of them are relatively low amplitudes of either distant moderate magnitude events (as in Chapters 4 and 5) or short distance small magnitude events (as in Chapter 6). Therefore, given the ultimate hazard is governed by strong motions, it would be a vital option to use a strong motion dataset simulated based on estimated seismological characteristics of the region (in previous Chapters), rather than using actual low amplitude data of the region. The stochastic simulation is incorporated in a seismological model which defines the final frequency content of the target Fourier amplitude spectrum to be used in the stochastic process. The seismological model, which parameterizes seismic wave modifications (in terms of attenuations and amplifications) that occur during wave traveling through the rock medium, is in the same format as that used elsewhere in the thesis. The model stipulates Fourier amplitude spectrum of shear waves at the level of rock outcrop, and is typically expressed as a product of factors that represents source properties of the origin and wave modifications (attenuations and amplifications) happening during the propagation through the rock crust [note that the equation is also appeared in Chapter 2 – equation (2.1), however is reproduced here for easy reference]:

$$A_x(f) = S(f) \cdot G \cdot A_n(f) \cdot P(f) \cdot V_a(f) \quad (7.1)$$

Definitions of terms in equation (7.1) and other essential explanations on each of the factors are given in previous Chapters (e.g., section 2.3 in Chapter 2; section 4.3 in Chapter 4; section 5.2 in Chapter 5). In Chapters 4, 5 and 6, efforts are made to investigate above given attenuation and amplification parameters for the subject region, taking the country into the consideration in both local and regional contexts. These studies involve analysis of recorded data at both near-source as well as far-source distances by using standard methods described as appropriately in respective Chapters. Moreover, estimated seismological parameters through these studies are validated following a spectral matching of actual records with stochastic simulations. Relevant seismological parameters including source factors, to be applied in the corresponding stochastic simulation (regional and local), are summarized in Table 5.4 in Chapter 5 and Table 6.3 in Chapter

6, respectively. The dataset for the local attenuation model is based on Brune's (1970; 1971) model with an average stress drop of 100 bars. 100 bars is a reasonable value for source spectra of moderate magnitude events in typical intraplate regions (Kanamori and Anderson, 1975) and also a comparable value with other models for many different tectonic regions including both interplate and intraplate (Chen and Atkinson, 2002). It has not considered lower stress drops for the local database which is mainly comprised with moderate and strong events (M_w between 4.0 and 6.5), though these lower stress drops may be in an agreement with local small magnitude events (M_w less than about 3.5) as shown in Chapter 6.

The frequency content of seismic waves defined by the seismological model given in equation (7.1) is combined with the stochastic process to simulate synthetic accelerograms. The basic assumption in any stochastic process is that the far-field accelerations on an elastic half space can be approximated into band-limited, finite-duration white Gaussian noise (Boore, 1983). Therefore, band limited white noise is generated, which is then followed by an application of a windowing function to "shape" the accelerogram in order to comply with the effective earthquake duration which depends on the properties (magnitude and hypocentral distance) of the selected earthquake. Next, filtering in the frequency domain is done using the frequency content established by the seismological model to create seismograms at randomly selected phase angles (refer section 2.4.2 in Chapter 2). Simulations of stochastic time histories are carried out by FORTRAN based program GENQKE (Lam, 1999). Corresponding elastic response spectra are obtained by ETAMAC (Lam, 1999).

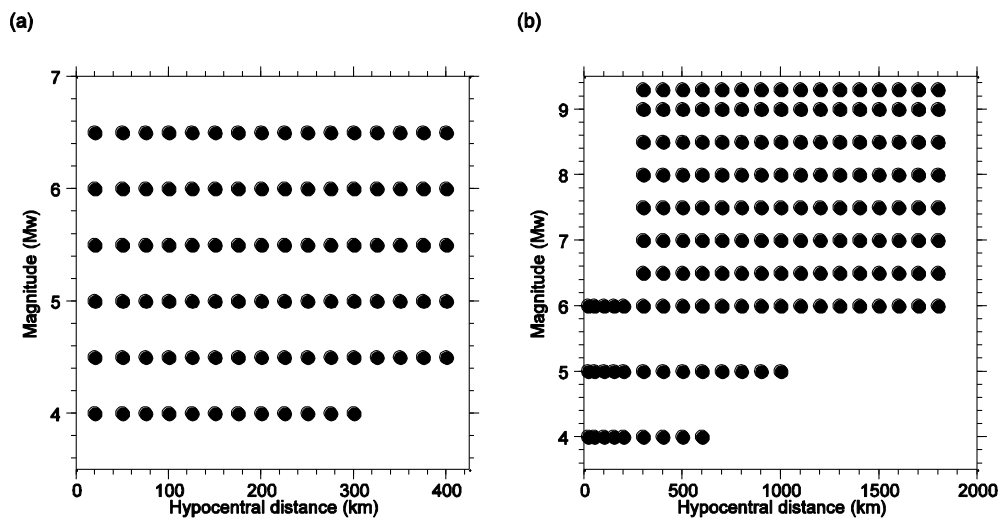


Figure 7.1 Magnitude and hypocentral distance combinations used in the preparation of synthetic databases for deriving ground motion equations. (a) For the local model. (b) For the regional model.

6 equally spaced magnitudes in a range of M_w 4.0 to 6.5, each at 16 different hypocentral distances varying between 20 and 400 km, are used to build the database for the local attenuation model.

The maximum magnitude of M_w 6.5 is chosen considering the historical seismicity in the local context. The synthetic database to be used for the regional attenuation model is prepared using 10 different magnitudes ranging between M_w 4.0 and 9.3, with each again at 16 different hypocentral distances varying from a minimum of 20 km for small and moderate events (M_w 4.0-6.0) to a distance as large as about 1800 km for strong and mega events ($M_w \geq 6.5$). M_w 9.3 as the upper magnitude limit is taken in memory of M_w 9.3 mega event which occurred at the eastern margin of northern Indian oceanic plate on 26th December 2004 which caused a devastating Tsunami in the country. Selected magnitude and hypocentral distance combinations in each case (local and regional) are shown in Figure 7.1. For the regional attenuation model, near-field events in a short range of distances are modelled using seismological parameters corresponding to the local attenuation model, and not by using the database made for the regional attenuation model itself. This is because the assumption that much similar seismo-geological features (geometric properties - thickness, density, age, etc.) between the continental Sri Lanka and adjacent continent-ocean boundary region than that between continent-ocean boundary and Indian oceanic crust. In both of the attenuation models, only shallow crustal events (depth less than may be around 10 km) are considered, and hence any depth dependency on attenuations is omitted. The database in each case consists PGA values at rock sites and pseudo elastic SAs of 5% critical damping ratio (also at rock sites) for 50 different natural periods between 0.01 to 8.00 s.

7.2.2 Regression analysis

The following equation is fitted with simulated data using the multiple linear regression method;

$$\log[Y] = AM^2 + BM + CR + D\log R + E \quad (7.2)$$

Y is the predicted ground motion parameter (i.e., PGA or SA) in m/s/s for average rock conditions in Sri Lanka. M is the magnitude in M_w and R is the hypocentral distance in kilometres. A , B , C , D and E are coefficients to be determined from the regression. Regressions are undertaken using the least squares method by setting line of best-fits between the dependent variable ($\log[Y]$) and independent variables (M and R). One may note that the form of equation (7.2) also follows that of the seismological model given in equation (7.1). Term $AM^2 + BM + E$ would resemble to the source factor identified in equation (7.1), as the term is clearly a dependent of the seismic moment (magnitude) or moment release of the event. CR accounts for the anelastic attenuation effects, while $D\log R$ represents attenuations due to the geometric spreading, since hypocentral distance of these functional forms is, respectively, normally and log normally proportionate to the logarithmic value of the ground motion parameter at a given frequency (refer Tables 5.4 and 6.3, respectively, in Chapters 5 and 6 for functional forms of the attenuation factors). Constant E can

be considered partly contributing for representation of the frequency independent upper crustal attenuation factor as explained in Chapter 5.

7.3 Results and discussion

Regression coefficients of attenuation relationships are given in Tables 7.1 and 7.2. Data are well-described by the selected attenuation model [equation (7.2)] as it is indicated by statistical measures resulted, lower standard error (σ_{est}) and higher coefficient of determination (R^2) values.

Table 7.1 Regression coefficients of the local attenuation model developed for Sri Lanka

| Natural period (s) | Regression coefficients of the local attenuation model, Y in m/s/s | | | | | σ_{est} | SS(Resi) | R^2 |
|--------------------|--|--------|---------|---------|----------|----------------|----------|-------|
| | $\log[Y] = AM^2 + BM + CR + D \log R + E$ | | | | | | | |
| | A | B | C | D | E | | | |
| 0.00 (PGA) | -0.0510 | 1.1411 | -0.0015 | -0.9104 | -3.9319 | 0.069 | 0.417 | 0.990 |
| 0.01 | -0.0613 | 1.2538 | -0.0016 | -0.8955 | -4.2394 | 0.063 | 0.362 | 0.993 |
| 0.02 | -0.0567 | 1.1960 | -0.0016 | -0.9023 | -4.0245 | 0.063 | 0.356 | 0.993 |
| 0.03 | -0.0513 | 1.1282 | -0.0017 | -0.9084 | -3.7711 | 0.061 | 0.341 | 0.993 |
| 0.04 | -0.0445 | 1.0480 | -0.0017 | -0.9248 | -3.4551 | 0.061 | 0.342 | 0.993 |
| 0.05 | -0.0426 | 1.0150 | -0.0019 | -0.8844 | -3.3537 | 0.059 | 0.312 | 0.994 |
| 0.06 | -0.0430 | 1.0094 | -0.0020 | -0.8658 | -3.3001 | 0.056 | 0.284 | 0.994 |
| 0.07 | -0.0387 | 0.9606 | -0.0020 | -0.8742 | -3.1122 | 0.055 | 0.273 | 0.994 |
| 0.08 | -0.0368 | 0.9372 | -0.0020 | -0.8542 | -3.0479 | 0.055 | 0.272 | 0.994 |
| 0.09 | -0.0357 | 0.9259 | -0.0020 | -0.8545 | -3.0031 | 0.054 | 0.261 | 0.994 |
| 0.10 | -0.0376 | 0.9434 | -0.0020 | -0.8358 | -3.0629 | 0.056 | 0.289 | 0.994 |
| 0.12 | -0.0458 | 1.0285 | -0.0020 | -0.8240 | -3.2783 | 0.056 | 0.282 | 0.994 |
| 0.14 | -0.0511 | 1.0907 | -0.0019 | -0.8277 | -3.4390 | 0.055 | 0.271 | 0.994 |
| 0.16 | -0.0510 | 1.0973 | -0.0019 | -0.7981 | -3.5282 | 0.048 | 0.213 | 0.995 |
| 0.18 | -0.0577 | 1.1748 | -0.0018 | -0.8071 | -3.7414 | 0.053 | 0.260 | 0.994 |
| 0.20 | -0.0659 | 1.2698 | -0.0017 | -0.8143 | -4.0112 | 0.053 | 0.252 | 0.994 |
| 0.22 | -0.0735 | 1.3575 | -0.0017 | -0.7926 | -4.2942 | 0.050 | 0.225 | 0.995 |
| 0.24 | -0.0808 | 1.4430 | -0.0017 | -0.7932 | -4.5527 | 0.053 | 0.260 | 0.994 |
| 0.26 | -0.0952 | 1.6030 | -0.0015 | -0.8042 | -4.9963 | 0.055 | 0.279 | 0.994 |
| 0.28 | -0.1036 | 1.7057 | -0.0015 | -0.7955 | -5.3385 | 0.059 | 0.315 | 0.993 |
| 0.30 | -0.1075 | 1.7540 | -0.0015 | -0.7615 | -5.5612 | 0.059 | 0.314 | 0.993 |
| 0.35 | -0.1198 | 1.9113 | -0.0015 | -0.7447 | -6.1094 | 0.054 | 0.264 | 0.994 |
| 0.40 | -0.1351 | 2.0977 | -0.0014 | -0.7395 | -6.7197 | 0.053 | 0.256 | 0.995 |
| 0.45 | -0.1431 | 2.2103 | -0.0013 | -0.7473 | -7.1256 | 0.056 | 0.286 | 0.994 |
| 0.50 | -0.1524 | 2.3307 | -0.0012 | -0.7129 | -7.6022 | 0.062 | 0.344 | 0.993 |
| 0.60 | -0.1759 | 2.6241 | -0.0010 | -0.7631 | -8.4937 | 0.064 | 0.371 | 0.994 |
| 0.70 | -0.1860 | 2.7704 | -0.0010 | -0.7391 | -9.0923 | 0.065 | 0.380 | 0.994 |
| 0.80 | -0.1907 | 2.8526 | -0.0010 | -0.7357 | -9.4669 | 0.061 | 0.338 | 0.995 |
| 0.90 | -0.1963 | 2.9444 | -0.0008 | -0.7525 | -9.8468 | 0.061 | 0.341 | 0.995 |
| 1.00 | -0.1978 | 2.9921 | -0.0008 | -0.7384 | -10.1527 | 0.061 | 0.337 | 0.995 |
| 1.10 | -0.1870 | 2.9039 | -0.0007 | -0.7491 | -10.0489 | 0.060 | 0.331 | 0.996 |
| 1.20 | -0.1952 | 3.0206 | -0.0006 | -0.7643 | -10.4650 | 0.062 | 0.345 | 0.996 |
| 1.30 | -0.1973 | 3.0699 | -0.0006 | -0.7505 | -10.7403 | 0.069 | 0.431 | 0.995 |
| 1.40 | -0.1880 | 2.9900 | -0.0006 | -0.7652 | -10.6099 | 0.065 | 0.383 | 0.995 |
| 1.50 | -0.1890 | 3.0273 | -0.0006 | -0.7608 | -10.8322 | 0.065 | 0.383 | 0.996 |
| 1.60 | -0.1780 | 2.9209 | -0.0006 | -0.7516 | -10.6414 | 0.066 | 0.392 | 0.996 |
| 1.70 | -0.1718 | 2.8688 | -0.0005 | -0.7753 | -10.5520 | 0.063 | 0.363 | 0.996 |

| | | | | | | | | |
|------|---------|--------|---------|---------|----------|-------|-------|-------|
| 1.80 | -0.1640 | 2.7951 | -0.0004 | -0.7909 | -10.4119 | 0.067 | 0.408 | 0.996 |
| 1.90 | -0.1557 | 2.7165 | -0.0003 | -0.8148 | -10.2424 | 0.070 | 0.440 | 0.995 |
| 2.00 | -0.1481 | 2.6443 | -0.0003 | -0.8350 | -10.0908 | 0.071 | 0.463 | 0.995 |
| 2.20 | -0.1348 | 2.5148 | -0.0002 | -0.8321 | -9.8742 | 0.073 | 0.472 | 0.995 |
| 2.40 | -0.1262 | 2.4454 | -0.0002 | -0.8284 | -9.8315 | 0.079 | 0.540 | 0.994 |
| 2.60 | -0.0948 | 2.1151 | -0.0002 | -0.8215 | -9.0521 | 0.081 | 0.564 | 0.993 |
| 2.80 | -0.1039 | 2.2386 | -0.0002 | -0.8125 | -9.5282 | 0.090 | 0.678 | 0.991 |
| 3.00 | -0.0782 | 1.9661 | -0.0004 | -0.7739 | -8.9320 | 0.096 | 0.770 | 0.990 |
| 3.50 | -0.0507 | 1.6967 | -0.0002 | -0.8560 | -8.2877 | 0.093 | 0.695 | 0.990 |
| 4.00 | -0.0395 | 1.5929 | 0.0003 | -0.9642 | -8.0208 | 0.090 | 0.634 | 0.991 |
| 4.50 | -0.0069 | 1.2369 | 0.0002 | -0.9439 | -7.1963 | 0.093 | 0.663 | 0.989 |
| 5.00 | 0.0144 | 0.9993 | 0.0004 | -1.0086 | -6.5269 | 0.095 | 0.661 | 0.988 |
| 6.00 | 0.0498 | 0.6009 | 0.0002 | -0.9561 | -5.6499 | 0.101 | 0.710 | 0.986 |
| 8.00 | 0.1000 | 0.0189 | 0.0004 | -1.0272 | -4.1108 | 0.086 | 0.482 | 0.988 |

σ_{est} – Standard error of estimate

SS(Resi) – Residual sum of squares

R² – Coefficient of determination

Table 7.2 Regression coefficients of the regional attenuation model developed for Sri Lanka

| Natural period (s) | Regression coefficients of the regional attenuation model, Y in m/s/s | | | | | σ_{est} | SS(Resi) | R ² |
|--------------------|---|--------|---------|---------|---------|----------------|----------|----------------|
| | $\log[Y] = AM^2 + BM + CR + D \log R + E$ | | | | | | | |
| | A | B | C | D | E | | | |
| 0.00 (PGA) | -0.0227 | 0.7929 | -0.0006 | -1.4952 | -2.1064 | 0.073 | 0.644 | 0.989 |
| 0.01 | -0.0207 | 0.7963 | -0.0007 | -1.5214 | -2.1118 | 0.071 | 0.726 | 0.994 |
| 0.02 | -0.0183 | 0.7574 | -0.0007 | -1.5005 | -1.9786 | 0.070 | 0.711 | 0.994 |
| 0.03 | -0.0177 | 0.7442 | -0.0007 | -1.5145 | -1.8473 | 0.069 | 0.686 | 0.994 |
| 0.04 | -0.0154 | 0.7100 | -0.0007 | -1.5257 | -1.6627 | 0.071 | 0.727 | 0.994 |
| 0.05 | -0.0160 | 0.7168 | -0.0007 | -1.5414 | -1.6002 | 0.071 | 0.734 | 0.994 |
| 0.06 | -0.0165 | 0.7217 | -0.0008 | -1.5345 | -1.5877 | 0.072 | 0.754 | 0.994 |
| 0.07 | -0.0150 | 0.6939 | -0.0008 | -1.5149 | -1.4801 | 0.066 | 0.637 | 0.995 |
| 0.08 | -0.0149 | 0.6915 | -0.0008 | -1.5133 | -1.4421 | 0.064 | 0.594 | 0.995 |
| 0.09 | -0.0149 | 0.6911 | -0.0008 | -1.4869 | -1.4714 | 0.064 | 0.590 | 0.995 |
| 0.10 | -0.0163 | 0.7110 | -0.0009 | -1.4665 | -1.5625 | 0.066 | 0.640 | 0.995 |
| 0.12 | -0.0184 | 0.7393 | -0.0009 | -1.4597 | -1.6298 | 0.067 | 0.665 | 0.995 |
| 0.14 | -0.0226 | 0.7986 | -0.0009 | -1.4204 | -1.8864 | 0.065 | 0.622 | 0.995 |
| 0.16 | -0.0276 | 0.8728 | -0.0009 | -1.3976 | -2.1823 | 0.063 | 0.574 | 0.995 |
| 0.18 | -0.0290 | 0.8965 | -0.0009 | -1.3615 | -2.3378 | 0.063 | 0.586 | 0.995 |
| 0.20 | -0.0317 | 0.9366 | -0.0009 | -1.3460 | -2.5136 | 0.058 | 0.491 | 0.996 |
| 0.22 | -0.0332 | 0.9627 | -0.0009 | -1.3259 | -2.6587 | 0.061 | 0.535 | 0.996 |
| 0.24 | -0.0338 | 0.9744 | -0.0009 | -1.3088 | -2.7538 | 0.060 | 0.534 | 0.996 |
| 0.26 | -0.0356 | 1.0054 | -0.0009 | -1.3043 | -2.8990 | 0.061 | 0.548 | 0.995 |
| 0.28 | -0.0374 | 1.0341 | -0.0009 | -1.2885 | -3.0522 | 0.062 | 0.557 | 0.995 |
| 0.30 | -0.0382 | 1.0517 | -0.0009 | -1.2655 | -3.1895 | 0.065 | 0.608 | 0.995 |
| 0.35 | -0.0422 | 1.1207 | -0.0009 | -1.2701 | -3.4916 | 0.062 | 0.568 | 0.995 |
| 0.40 | -0.0415 | 1.1215 | -0.0008 | -1.2484 | -3.6171 | 0.063 | 0.574 | 0.995 |
| 0.45 | -0.0436 | 1.1629 | -0.0008 | -1.2492 | -3.8242 | 0.064 | 0.607 | 0.995 |
| 0.50 | -0.0466 | 1.2215 | -0.0008 | -1.2653 | -4.0793 | 0.062 | 0.554 | 0.995 |
| 0.60 | -0.0500 | 1.2895 | -0.0007 | -1.2763 | -4.4269 | 0.072 | 0.755 | 0.993 |
| 0.70 | -0.0493 | 1.2948 | -0.0007 | -1.2773 | -4.5666 | 0.075 | 0.827 | 0.993 |
| 0.80 | -0.0517 | 1.3425 | -0.0006 | -1.2959 | -4.7979 | 0.079 | 0.910 | 0.992 |
| 0.90 | -0.0547 | 1.4007 | -0.0006 | -1.3299 | -5.0417 | 0.081 | 0.947 | 0.992 |
| 1.00 | -0.0519 | 1.3707 | -0.0006 | -1.3129 | -5.0719 | 0.087 | 1.097 | 0.991 |

| | | | | | | | | |
|------|---------|--------|---------|---------|---------|-------|-------|-------|
| 1.10 | -0.0521 | 1.3788 | -0.0005 | -1.3175 | -5.1650 | 0.086 | 1.081 | 0.991 |
| 1.20 | -0.0527 | 1.3939 | -0.0005 | -1.3084 | -5.3148 | 0.094 | 1.293 | 0.989 |
| 1.30 | -0.0550 | 1.4362 | -0.0005 | -1.3208 | -5.5112 | 0.097 | 1.352 | 0.989 |
| 1.40 | -0.0522 | 1.4003 | -0.0005 | -1.3204 | -5.4498 | 0.094 | 1.286 | 0.989 |
| 1.50 | -0.0534 | 1.4222 | -0.0005 | -1.3251 | -5.5769 | 0.090 | 1.154 | 0.990 |
| 1.60 | -0.0531 | 1.4220 | -0.0005 | -1.2958 | -5.6975 | 0.101 | 1.476 | 0.988 |
| 1.70 | -0.0504 | 1.3795 | -0.0005 | -1.2751 | -5.6284 | 0.104 | 1.553 | 0.987 |
| 1.80 | -0.0504 | 1.3804 | -0.0004 | -1.2859 | -5.6548 | 0.103 | 1.529 | 0.987 |
| 1.90 | -0.0480 | 1.3451 | -0.0004 | -1.2742 | -5.5922 | 0.103 | 1.518 | 0.987 |
| 2.00 | -0.0464 | 1.3219 | -0.0004 | -1.2578 | -5.5839 | 0.103 | 1.508 | 0.987 |
| 2.20 | -0.0446 | 1.2991 | -0.0004 | -1.2600 | -5.5767 | 0.099 | 1.387 | 0.987 |
| 2.40 | -0.0477 | 1.3442 | -0.0004 | -1.2627 | -5.7901 | 0.099 | 1.372 | 0.987 |
| 2.60 | -0.0445 | 1.2937 | -0.0004 | -1.2534 | -5.6850 | 0.102 | 1.460 | 0.985 |
| 2.80 | -0.0486 | 1.3490 | -0.0003 | -1.2514 | -5.9289 | 0.104 | 1.487 | 0.984 |
| 3.00 | -0.0489 | 1.3479 | -0.0003 | -1.2463 | -5.9738 | 0.107 | 1.568 | 0.983 |
| 3.50 | -0.0493 | 1.3577 | -0.0003 | -1.2256 | -6.1712 | 0.116 | 1.821 | 0.979 |
| 4.00 | -0.0587 | 1.4924 | -0.0003 | -1.2373 | -6.7087 | 0.111 | 1.658 | 0.979 |
| 4.50 | -0.0605 | 1.5146 | -0.0003 | -1.2044 | -6.9275 | 0.119 | 1.907 | 0.976 |
| 5.00 | -0.0650 | 1.5791 | -0.0002 | -1.2226 | -7.1851 | 0.118 | 1.824 | 0.974 |
| 6.00 | -0.0588 | 1.4714 | -0.0002 | -1.1541 | -7.0230 | 0.112 | 1.626 | 0.975 |
| 8.00 | -0.0540 | 1.3952 | -0.0002 | -1.1399 | -6.9671 | 0.106 | 1.396 | 0.974 |

σ_{est} – Standard error of estimate

SS(Resi) – Residual sum of squares

R^2 – Coefficient of determination

The attenuation models are intended to use only in the specified magnitude and distance combinations of the subject region; for local model M_w 4.0 to 6.5 with hypocentral distance between about 20 and 400 km, and for regional model M_w 4.0 to 9.3 at long distances preferably between about 100 and 1800 km. The main purpose of the regional model is to characterize ground motions of large magnitude events striking at long distances, therefore, moderate magnitude events (between about M_w 4.5 to 6.0) that occur at short distance range (within about 100 km) are discouraged to model from the regional model, but from the local model. Again, both of the models are solely for the use of modeling shallow crustal earthquakes (depths less than about 10 km) of the subject region, and are preferably to predict vertical ground motion. The developed models are incapable of modeling discrepancies of ground motions due to change in the fault type (strike-slip, normal and reverse) of the event. This is primarily due to the fact that the modeling has based on an artificially derived database, which is independent of the type or mechanism of the fault source of the event. The stochastic simulation procedure coded in GENQKE does not specify the simulation with respect to the fault mechanism. However, the equations may be more collated with shallow crustal strike-slip events since those are more common to observe than other fault types (Boore and Atkinson, 2007; 2008). In addition, the equations are not possible of modeling advanced characteristics such as directivity effects, basin effects and asymmetric ground motions (the hanging wall versus the footwall of thrust faults), etc.

A residual analysis is carried out as part of a reevaluation of the validity of the applied regression equation for data modeling. Residuals are defined on the basis as same as that specified in Chapters 4 and 5, which is the difference between log observed (in this case, simulated data) and log predicted (from the equation). Residual plots of PGA and some of sample periods (0.1, 0.5 and 1.0 s) for both cases (for local and regional models) each showing residual variations against both magnitude and hypocentral distance, are given in Figures 7.2 and 7.3. Figures 7.2 and 7.3, respectively, show residual variations for local and regional attenuation models developed in the study, and plots are separately given for each of the selected attenuation parameters (PGA and SAs for 0.1, 0.5 and 1.0 s periods). Neither of Figures 7.2 nor 7.3 shows any detectable trend in residuals with respect to the selected independent variables of the equation. Most of the times, residuals are well within 0.5 and -0.5 log margins and are distributed in parallel with the zero axis. Thus, it is confirmed that the selected regression equation satisfactorily describes the simulated dataset used in the modeling.

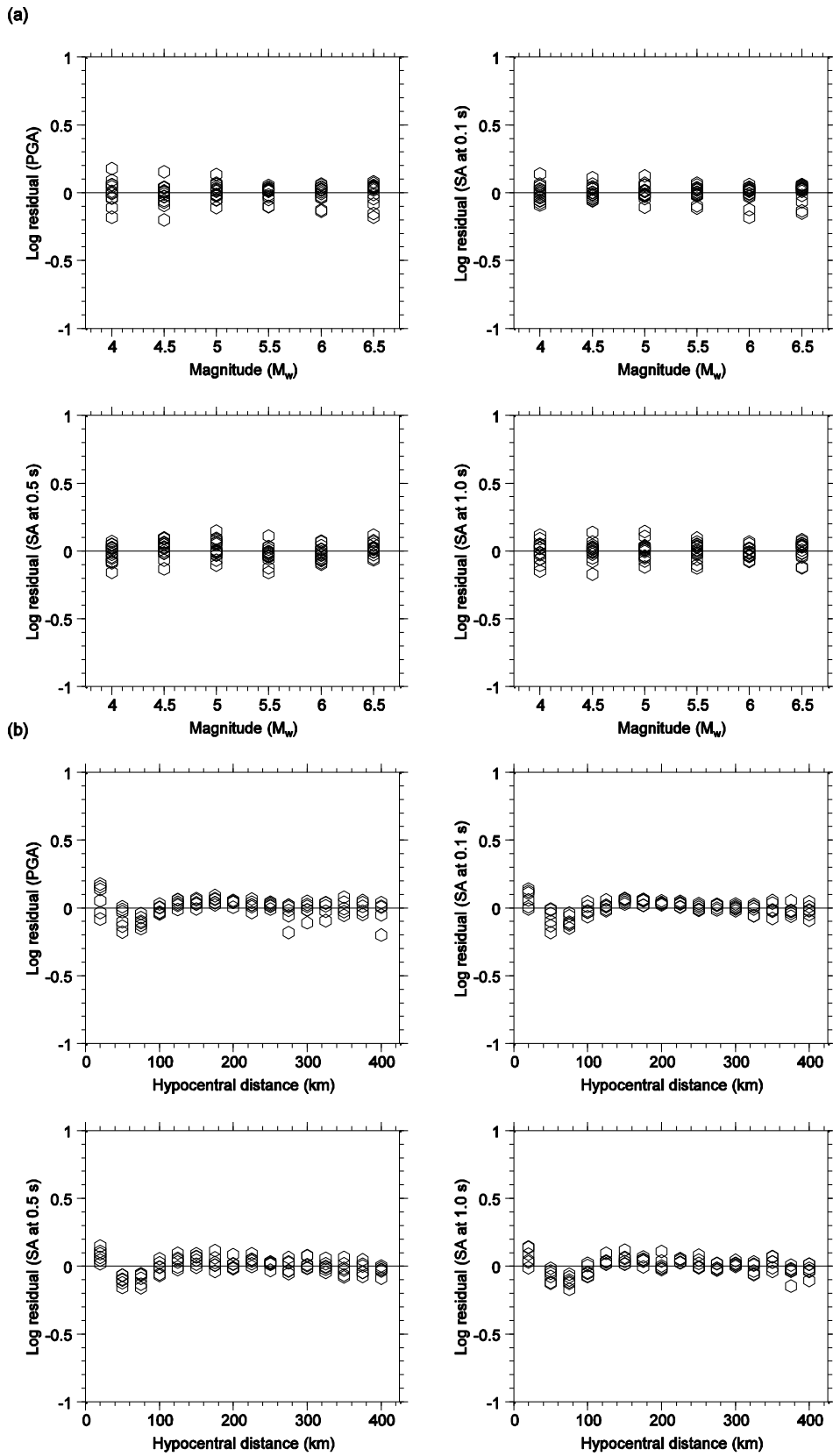


Figure 7.2 Variation of residuals [log observed (in this case, simulated data) - log predicted from the derived model] for the local attenuation model. Variations are given with respect to (a) Magnitude (M_w) and (b) Hypocentral distance (km).

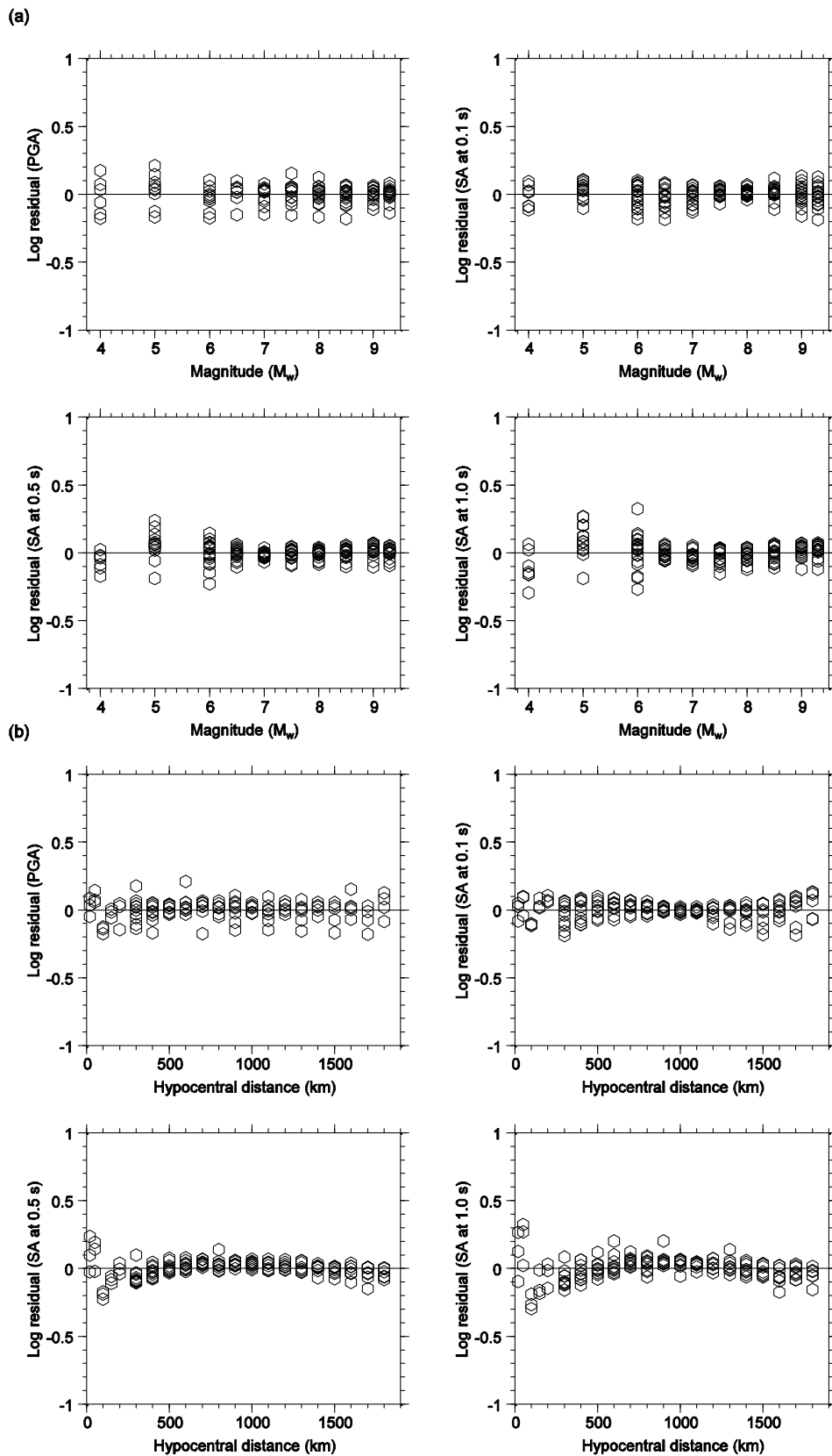


Figure 7.3 Variation of residuals [log observed (in this case, simulated data) - log predicted from the derived model] for the regional attenuation model. Variations are given with respect to (a) Magnitude (M_w) and (b) Hypocentral distance (km).

Figure 7.4 compares the developed local attenuation model with some of published models available in the literature for an M_w 6.0 shallow crustal event. Published models are chosen after considering some overall aspects which may direct toward for a more meaningful comparison; global applicability of the model in other regions for hazard assessment studies, apparent similarities in seismotectonic behavior between Sri Lanka and the region where the attenuation model has originally been developed for, use of high precision data and advanced analysis techniques in the original derivation to significantly improve the accuracy in the prediction, etc. Note also that nowadays there are many more published models being available in the literature, albeit the comparison is limited to only few selected models as shown in Figure 7.4, and this is partly due to the requirement of not making the comparison unnecessarily complicated. Comparisons are made for PGA and for some of sample periods (0.1, 0.5 and 1.0 s) used in the study. For PGA (Figure 7.4a), the local model shows predicting relatively low amplitudes than most of other selected models, however, the model appears to have a close resemblance with Boore and Atkinson (2007) NGA (Next Generation Attenuation) model for WNA region and with Idriss (2008) NGA model for shallow crustal earthquakes. Both of these selected models are developed using thousands of well-recorded strong motion data, compiled from shallow crustal earthquakes in “active tectonic environments” worldwide. Even though, the local model derived in the present study represents a seismically more stable intraplate region, final ground motions predicted by the model show a similitude with those predicted by models derived for active tectonic regions. This inference is further supported by the resulted higher PGAs by models which are developed for more stable intraplate regions [e.g., the model for ENA by Toro et al (1997), the model for western Australian region by Somerville et al (2009)]. These intraplate models attribute attenuations of regions that are associated with older Precambrian shields (ENA and western Australian region) where the anelastic and upper crustal attenuation effects (i.e., intrinsic attenuations) can be considerably low due to the presence of “high quality” crustal rocks (described in Chapter 2). Therefore, ground motions in such older intraplate regions may pose higher amplitudes than in active younger regions due to lesser anelastic attenuations. On the other hand, although Sri Lanka also lies in an intraplate region, the continental crust underlain is characterized by a lower local Q_0 value ($Q_0=301$ - Chapter 6) and a moderate Kappa value (about 0.40 - Chapter 5). This implies that the crust is associated with higher intrinsic attenuation features than of a typical Precambrian shield region (such as exemplified above) regardless of geological assertions (described in Chapter 3) that classify the country’s crust as of Precambrian. Hence, PGAs predicted by the local model derived in the study can be more harmonized with that of younger active regions than of stable older intraplate regions, as evidenced in Figure 7.4a. Two other models, Abrahamson and Silva (1997), and Sadigh et al (1997), developed for active tectonic regions also seem in a comparison with the local model developed in the study for PGA. Comparisons for SAs as shown in Figure 7.4 still agree with the above argument, except the

comparison for SA at 1.0 s period, in which the local model has shown predicting higher amplitudes than other models, yet still being comparable with Idriss (2008) NGA model.

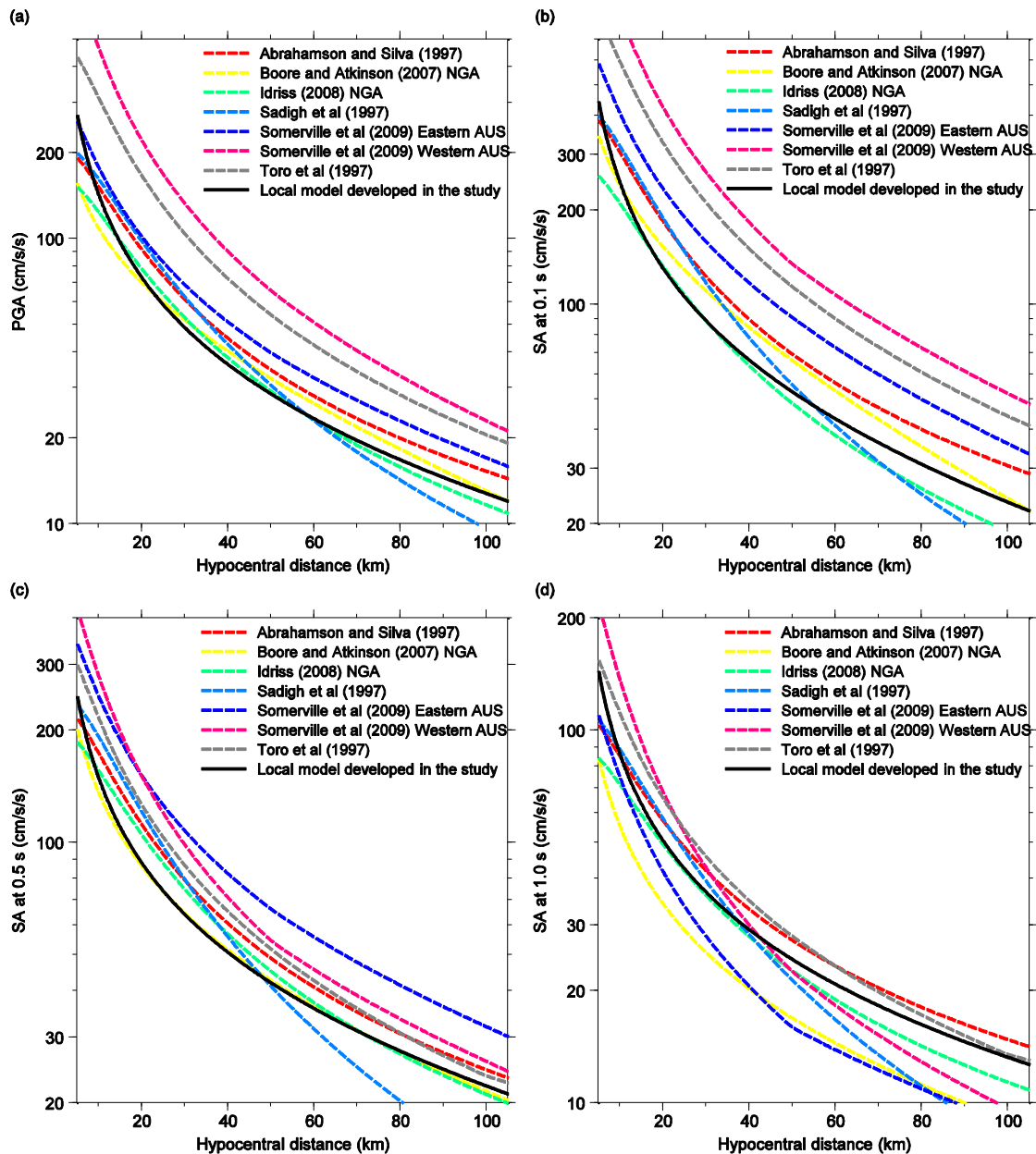


Figure 7.4 Comparison of the derived local attenuation model with some of published models available in the literature. Chosen published models; Abrahamson and Silva (1997), Boore and Atkinson (2007) NGA, Idriss (2008) NGA, Sadigh et al (1997), Somerville et al (2009), Toro et al (1997). Comparisons are for an M_w 6.0 shallow crustal earthquake at an assumed depth of 10 km for a rock crust of V_{s30} equals 650 m/s. Comparisons are given for (a) PGA. (b) SA at 0.1 s. (c) SA at 0.5 s. (d) SA at 1.0 s.

Figure 7.5 shows a comparison for the regional attenuation model developed in the study. The comparison is made with some of published models available in the literature for predicting distant events. Many of models being used in the practice are only for the application at short

distance ranges (probably up to 100 - 200 km of maximum), and thus are unable to be used for a direct comparison for distant events. Besides, in most cases, the rest of few published models that are capable of predicting distant events, are up to a maximum hypocentral distance of about 500 km (Chandler and Lam, 2004). Therefore, the comparison shown in Figure 7.5 is for a maximum curtailed hypocentral distance of 500 km, for a chosen M_w 7.0 shallow crustal event. Given the lack of long distance attenuation models for intraplate seismic regions, some models developed for interplate subduction zones are also used for the comparison. In Figure 7.5a, the developed regional model for PGA predicts lower amplitudes than all other models up to about 220 km, and then after the model gives higher amplitudes than McVerry et al (2006) model for New Zealand and Atkinson and Boore (2003) model for Cascadia intraslab events. Atkinson and Boore (1995) ENA model predicts the highest PGAs at almost all distances out of all the models selected for the comparison. The reason for this is lower intrinsic attenuations of ENA region due to much high quality bedrock, as explained in the previous paragraph. Lower amplitudes predicted by the developed model, in both PGA and SA, can be related with higher geometric and anelastic attenuations forecasted for the northern Indian Ocean region (see Figure 5.6 in Chapter 5). Particularly, effects of the geometric attenuation factor can be significant than other attenuation modes, for apparent reduction in ground motion amplitudes for the region. Youngs et al (1997) subduction zone models (interface and intraslab), developed using worldwide data, give higher amplitudes in all cases (all PGA and selected SAs) than the predictions by the developed regional model, and this coincides with their conclusion as well which is the rate of attenuation of peak motions of subduction zone earthquakes is lower than that of shallow crustal earthquakes in active tectonic areas with the amplitude difference being significant for very large earthquakes. Atkinson and Boore (2003) models for Cascadia region appear to be more comparable with the developed model than Youngs et al (1997) models in each case, however, have shown predicting lower amplitudes than the regional model at larger distances, in most of the cases.

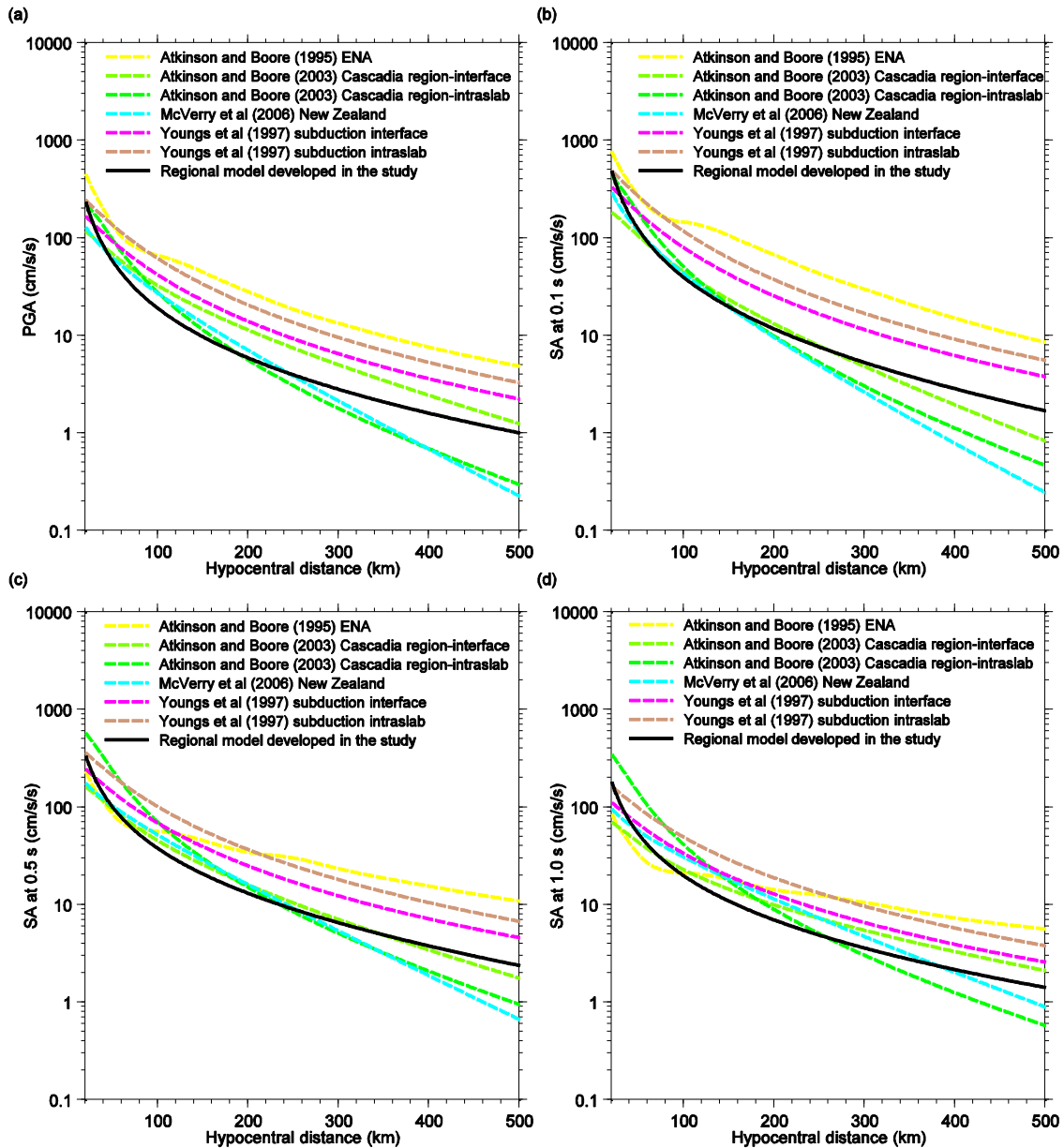


Figure 7.5 Comparison of the derived regional attenuation model with some of published models available in the literature. Chosen published models; Atkinson and Boore (1995), Atkinson and Boore (2003) Cascadia region, McVerry et al (2006), Youngs et al (1997). Comparisons are for an M_w 7.0 shallow crustal earthquake at an assumed depth of 10 km for a rock crust of V_{s30} equals 650 m/s. Comparisons are given for (a) PGA. (b) SA at 0.1 s. (c) SA at 0.5 s. (d) SA at 1.0 s.

Resulted attenuation relationships are further validated by a comparison with data of actual events recorded in the country's national seismic network. Some of such sample comparisons are shown in Figure 7.6. Note that, the vertical component of recorded ground motions is chosen in the comparison, because of the vertical motion is more robust for site-specific wave modification effects than the horizontal motion which on the other hand could easily be subject to alterations by local site effects and thus be deviated from the actual motion. Developed attenuation models

are less sensitive to such deviations including any departure caused by high frequency noise contamination in the signal. Figures 7.6a compares local events arisen within the country, while 7.6b indicates the comparison of ground motions for regional events occurred at teleseismic distances. Figure 7.6a compares ground motions for cluster of smaller events (magnitudes in between about M_w 2.0 and 3.6) recently reported in Sri Lanka. Figure 7.6b shows comparisons for regional events occurred in the surrounding oceanic crust with magnitude varying between M_w 5.0 and 6.3, and M_w 4.0 and 5.0. Note that, fewer comparisons given in Figure 7.6a than in 7.6b reflect the difference in amount of actual data available at the country's local distances than at regional distances. Predicted values of the attenuation models developed in the study show a satisfactory comparison with actual data. Reliability of the regional attenuation model as evidenced by the figures, especially at long distances, is of particular interest since accurate prediction of actual ground motions at such long distances is a novel exercise and is generally beyond the limits of other typical models available in the literature.

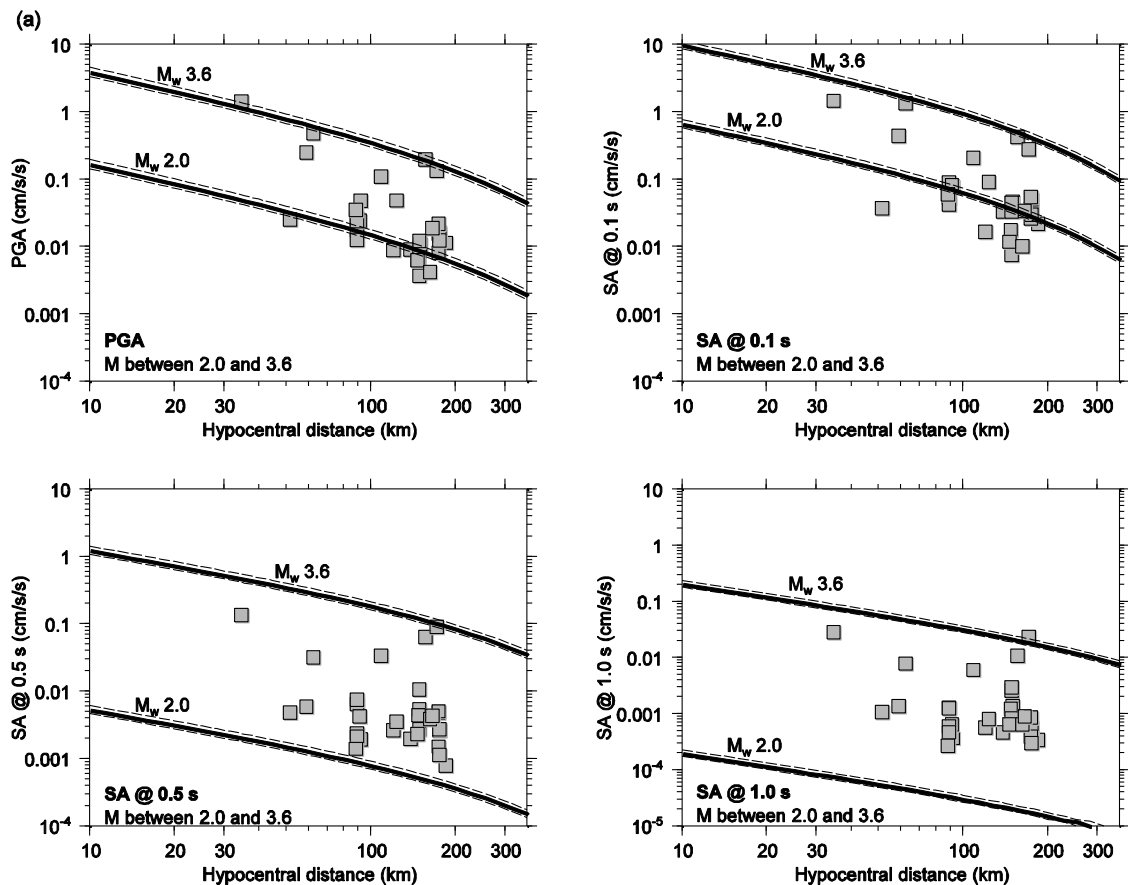


Figure 7.6 Comparison of ground motions between actual values in recorded vertical components of events (denoted by filled squares) and predicted values (denoted by dark continuous lines) by developed attenuation models. Standard error limits of predicted values are shown in light dash lines. (a) For local events. (b) For regional events. Predicted values show a good comparison with actual data for the selected events. Developed attenuation models are given in Tables 7.1 and 7.2.

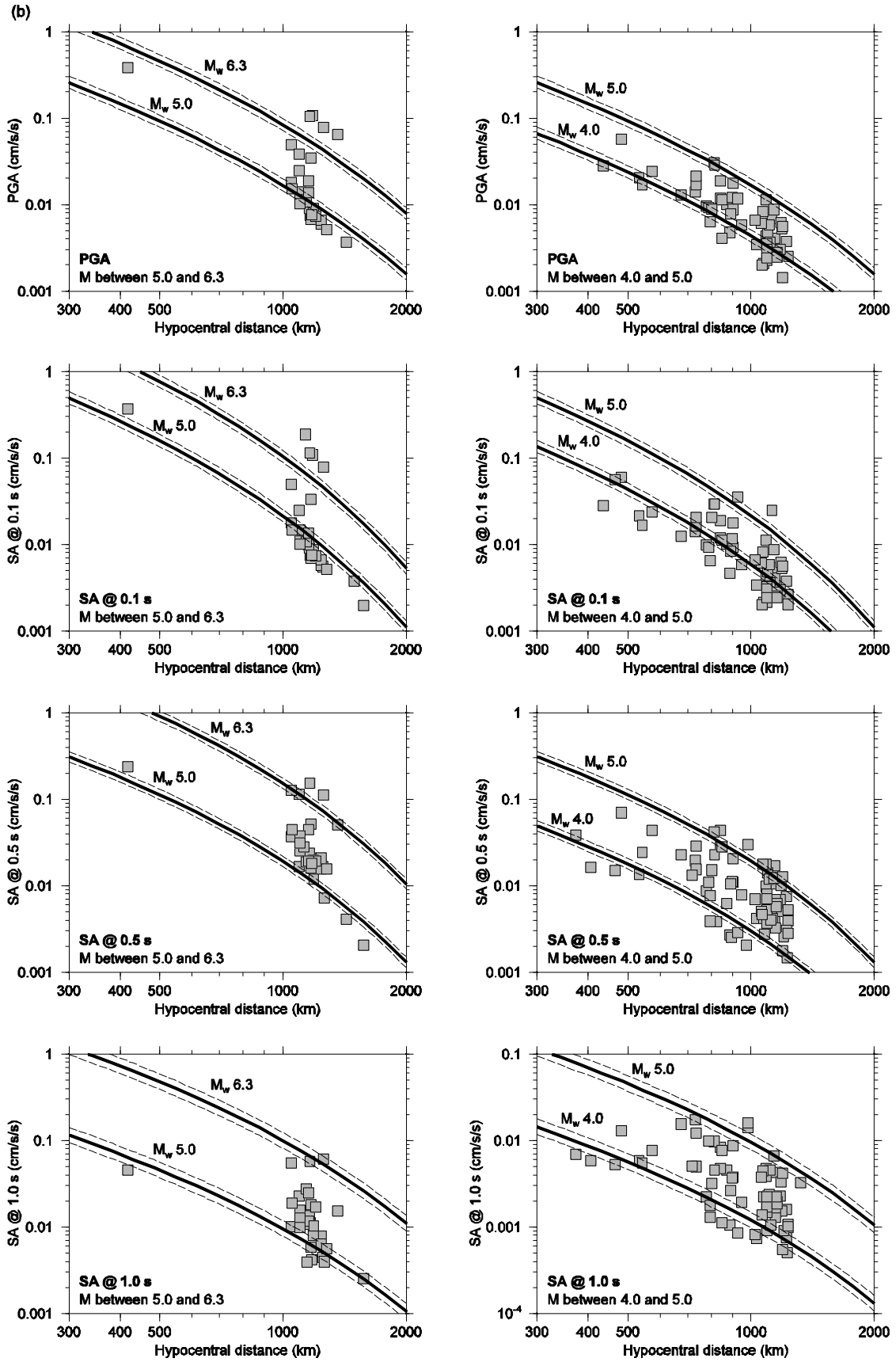


Figure 7.6 (continued)

7.4 Conclusion

The attenuation models developed in the study for a low seismicity intraplate region of Sri Lanka, are proven to be sufficiently precise in predicting ground motions (in terms of PGA and SAs at rock sites) for both local events of the continental crust and regional events of the surrounding oceanic crust. The local attenuation model is comparable with some of published models for active tectonic environments developed recently using worldwide strong motion data. The regional model shows predicting lower amplitudes than that of Youngs et al (1997) models developed for subduction zone earthquakes, however, this observation seems to be reasonable given their conclusion that subduction zone events are more susceptible to produce higher amplitudes than those of active tectonic events.

8. Development of seismic hazard maps for Sri Lanka

8.1 Introduction

Expressing ground motion parameters with an exceeding probability in a given period of time is a widely accepted technique used in risk analysis in the engineering seismology. The methodology has proven to be advantageous in accounting for uncertainties associated with seismological properties (identified as seismic sources and earthquake properties – magnitude and location, earthquake recurrence) and with attenuation models applied in the ground motion estimation, in comparison to other conventional methods such as deterministic analysis.

The study presented in this Chapter is an application of the above introduced “probabilistic seismic hazard analysis” for Sri Lanka, whose seismotectonic location is often claimed to be in a stable continental region. Tectonic location of Sri Lanka guarantees that the country is hardly subjected to interplate or plate-margin earthquakes (discussed in Chapter 3), as the major plate boundaries are located at least 1000-1500 km away from the country (see Figure 3.1 in Chapter 3). Intraplate or mid-plate earthquakes, on the other hand, are abundant in the region and can pose direct threats of striking at the country’s close vicinity. Seismicity and seismogenic features in and around Sri Lanka have rarely drawn the attention of local researchers. Only a few published studies are available in the literature (Abayakoon, 1996; Fernando and Kulasinghe, 1986; Gamage and Venkatesan, 2012a; Gamage et al, 2013; Peiris, 2007; Uduweriya et al, 2013; Vitanage, 1994; 1995). These studies are found to be important in providing certain essential insights to nourish the discourse on seismicity and seismic hazard of the country. Most of these studies involve assessing seismic hazard either in the whole country or just in a particular location which has a significant importance in socio-economic terms (such as the capital city – Colombo) than other places, and these assessments are based on both probabilistic methods (Abayakoon, 1996; Peiris, 2007; Uduweriya et al, 2013) as well as deterministic approaches (Gamage and Venkatesan, 2012a, Gamage et al, 2013). Resulted ground motions and final predicted values in above studies for engineering applications show a little consensus, leaving a debate among engineering professionals on what to choose as “the design basis ground motion” in the seismic design of structures. The situation sometimes turns them to “hire” values from codes of practice developed in other seismically analogous regions (e.g., Australia, India), and/or to select even arbitrary values by “guess works” in the given ambivalence. Historical evidence suggests that the country’s seismicity is at a measurable level well beyond the nullified level (discussed in Chapter 3). Therefore, the requirement should be quantifying the actual level of seismicity based on a proper evaluation of regional seismic characteristics and then working towards for an own seismic code of practice for which everyone in the field can agree. A complete assessment of risk due to any

kind of hazard may require various collaborative works of many professionals such as technical experts in the field (for earthquake hazard – seismologists, geologists, engineers), risk analysts, economists, social scientists, etc., yet the role of “technical experts” among others can be decisive since future forecasts solely rely upon their works.

The seismic hazard analysis method applied in the study basically follows that described in Cornell (1968). Seismic source zonation, earthquake catalog preparation, recurrence rates estimation, attenuation relationships application and hazard values in terms of ground motion parameters computation, are systematically described throughout the Chapter. Computed ground motions in terms of PGA and Spectral Accelerations (SAs) at 0.1, 0.5 and 1.0 s natural periods for 5% critical damping ratio, are represented by raster maps in the results and discussion section.

8.2 Methodology

8.2.1 Seismic source zones

Identifying and/or defining zones that are likely to produce seismic activities in a way that they would impend direct threats to the site of interest, is a preliminary step in the seismic hazard analysis process. Defining these source zones can be based on well identified tectonic features inherited in the region (e.g., faults, lineaments, fractures, shear zones, subduction zones, etc.) and/or can be done by inspecting historical seismic activities reported in the region in which case seismically more dense areas are approximated as source zones by isolating into simple geometric forms – polygons (or volumes). Source zonation would be accurate and effective as long as the tectonic structure underlain is exactly known in detail, but can become complicated and erroneous when the available information is insufficient. Stable continental areas are seldom investigated for seismotectonic characteristics, and thus may have a little or no information available for accurate zonal characterization. Sri Lanka also owns a little information particularly on seismic sources within the country, therefore in the study, seismic zonation in the local context is performed primarily based on historical seismic activities of the country. However, the regional zonation is carried out, to a certain extent, based on identified tectonic structures in the surrounding oceanic crust. All the identified regional zones are characterized as broad area zones, this is because their mild activity rates which allow a uniform seismicity to be safely assumed through the whole area. Source zonation in the study, as it should be, is centered on the relevant target area of sites (i.e., Sri Lanka) for which the hazard to be estimated, therefore, the zones are defined also on the basis that their importance and impact on the final hazard level of target sites of interest. This concedes for use of a set of source zones exclusively identified for Sri Lanka, which can be sometimes different from the source zonation adopted based on different target sites in other neighboring regions, for example Tamil Nadu in India (Menon et al, 2010; Uduweriya et al, 2010). Final source zones defined in the study are shown in Figure 8.1, and are briefly

discussed in the following paragraphs. The source zonation in the present study is principally based upon the discussion of possible seismic sources identified in Chapter 3.

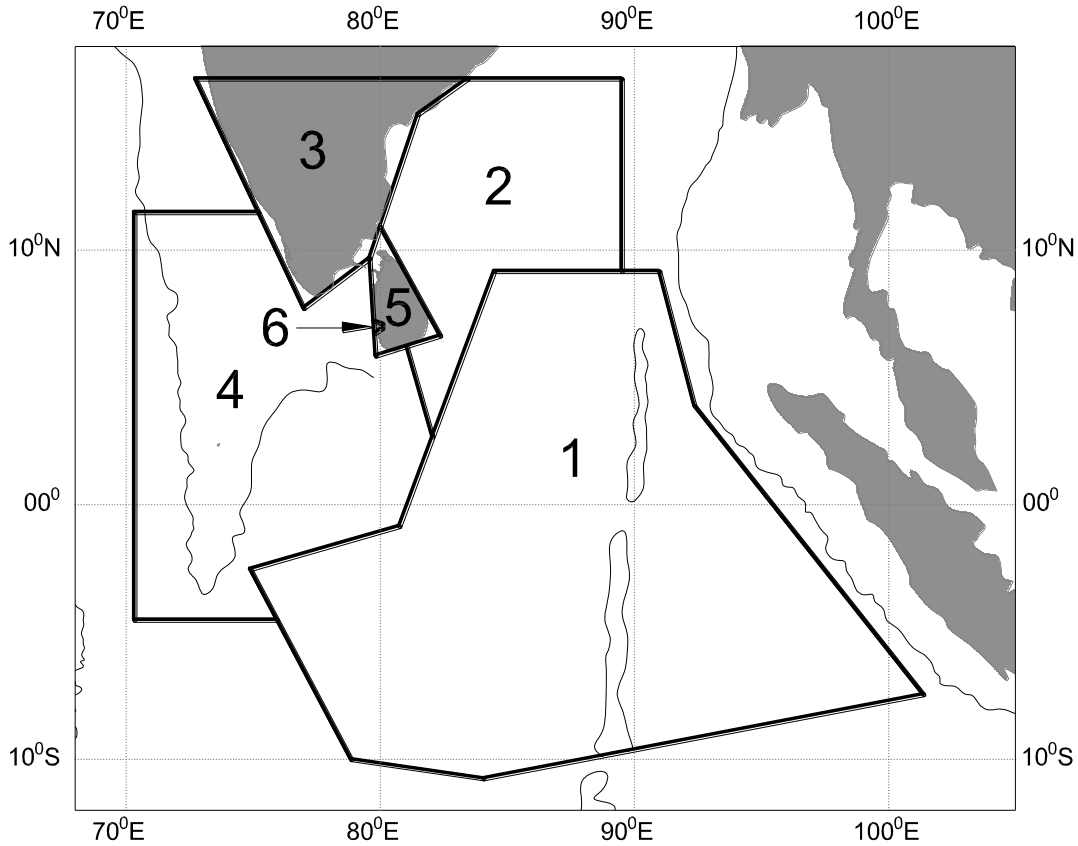


Figure 8.1 Source zones defined in the study. Source zones 1, 2, 3 and 4 characterize regional intraplate seismic activities outside Sri Lanka, while 5 and 6 are based on sparse local seismicity within the country. (Seismic activities in each of the zones are discussed in section 8.2.1)

Source zone 1

Source zone 1 covers the oceanic region located south and southeast of Sri Lanka towards Ninetyeast Ridge, and is to represent the famous northern Indian Oceanic intraplate seismicity created by the so-called intense “diffuse deformation” (refer section 3.3.1 in Chapter 3). In the present study, source zone 1 is defined based on the diffuse boundary area proposed by Royer and Gordon (1997) (Figure 3.7 in Chapter 3). Not the entire “original source” (hatched area shown in Figure 3.7 in Chapter 3), but only the upper portion is considered adequate to represent regional seismicity in the area for the purpose of assessing seismic hazard in Sri Lanka. The lower part, which is more than a 2000-2500 km away from the country, has a trivial impact upon final ground motions computed at target sites because of large site-source distance. Most of the previously reported events are also scattered towards the northern part of the diffuse region close to the northern portion of Ninetyeast Ridge, which implies that higher seismic rates are associated towards the northern part than the southern part (can see clearly in the catalog data – Figure 8.2).

Therefore, sampling events only of the northern part would not result in a distinguished underestimation of actual recurrence rates pertaining to the whole diffuse zone (total hatched area in Figure 3.7 in Chapter 3), yet a plausible change in the probability distribution of hypocentral distance (a more sharper curve when considering only the northern part may be expected as the elimination of large hypocentral distance components) can be expected due to curtailment of site-source distance. Hence, it is acknowledged that mean annual recurrence rates, probability distribution of hypocentral distance and corresponding hazard levels can be affected, each up to a certain limit, due to reduction of the original source area.

Seismicity in the adjacent subduction zone - Sunda Arc, which margins the diffuse region in east, is assumed not to have any “contribution” to the seismicity in the diffuse region. Term “contribution” explicates any miscount of dependent events (aftershocks and foreshocks) in the diffuse zone, but whose main events have actually occurred in the subduction zone. Care is taken when removing such dependent events (discussed in section 8.2.2 “Earthquake catalog processing”) as they can easily be misidentified as random events resulted by the process of diffuse seismicity within the zone. Following the general rule commonly adopted in hazard assessments, a uniform rupture likelihood is assumed over the total source zone irrespective of some obvious variations in tectonic stresses.

Source zone 2

Source zone 2 encapsulates seismic activities in the neighboring oceanic crust located in east and northeast of the country. The zone covers a major portion of Bay of Bengal including the northern half of a low seismic form 85°E Ridge (see Figure 3.6 in Chapter 3). In overall, seismicity within the zone does not seem to be biased to a certain localized area which is tectonically linked with these identified structures, instead a sparse distribution of seismic activities can be seen through the zone. Although, the majority of frequent events fall into small and moderate magnitude category ($M_w < 6.0$), some rare occurrences of strong magnitude events can also be found in the past. Tectonic stresses in the area can easily be “energized” by activities in adjacent source zone 1 identified above. Leaving a little curiosity on some theoretical inferences drawn on aseismic nature of 85°E Ridge (Bergman and Solomon, 1985; Liu et al, 1982), few moderate events can still be found occurred along the ridge close to Sri Lanka, which have made major tremors in southeastern and central parts of the country (e.g., M_L 5.8 in 1973, M_L 6.5 in 1918).

Given “the inert nature” of seismicity of the region, an area that includes the oceanic crust in southern Bay of Bengal juxtaposing with Sri Lankan eastern coast, is assigned as source zone 2.

Source zone 3

Source zone 3 also represents a regional source which encloses seismic activities of the continental crust of southern peninsular India. Seismicity in the southern part of peninsular India is generally featured by shallow-focus small magnitude events (see Figure 3.9 in Chapter 3). Surprisingly, activity rates of those events appear to be higher than that of similar events in other zones defined in the study (see computed seismicity parameters given in Table 8.1). Historical events in the region are rigorously compiled at several times as to produce a reliable catalog to be used in local hazard assessments (Chandra, 1977; Jaiswal and Sinha, 2007; Menon et al, 2010, Rao and Rao, 1984). The closest southern Indian territory – Tamil Nadu, separated by less than 30 km from Sri Lanka, is generally considered aseismic in respect to other neighboring territories. Nevertheless, some densely populated areas within the state such as Chennai and places at the border between Andhra Pradesh, are classified into Zone III in the Indian Standard IS 1893 (Part 1)-2002 to comply with a ground shaking intensity of VII in MSK (Medvedev–Sponheuer–Karnik) scale. Most of other places are categorized under Zone II. Reported events in Tamil Nadu show confining to boundary areas with adjacent territories such as Karnataka and Andhra Pradesh, and most of them are attributed to activities of local faults and lineaments (Gangrade and Arora, 2000). Because of both of the reasons that strong earthquakes are not much common in the southern portion of Indian peninsula and the minimum distance between the zone and Sri Lanka is considered to be “seismically safe” for other smaller events, the entire continental part of southern India is called for as a single source in this study.

Source zone 4

Oceanic crust spanning between the western coastal line of Sri Lanka and the eastern banks of Chagos-Laccadive Ridge including Laccadive Sea and Gulf of Mannar, indicates a moderate level of seismicity (refer section 3.3.2 in Chapter 3). Events of medium size magnitudes exhibit a lower recurrence rate as in a typical stable region. Tectonic features of the region are clearly identified, although most of them govern a less potential risk in generating strong earthquakes. However, some of tectonic structures found around the country’s close vicinity (such as Gulf of Mannar-Palk Strait lineament) are still susceptible for such a threat, as it previously evidenced (e.g., M_s 4.7 in 1993 and M_s 5.8 in 1938).

Source zones 5 and 6

Source zones 5 and 6 aggregate associated seismicity in continental Sri Lanka. Source zone 5 renders apparent local seismicity in the country, except that in the capital city – Colombo, whereas source zone 6 exclusively defines seismicity around Colombo. Past seismic activities reported within Sri Lanka reveal that the country is yet an infrequent source for strong magnitude events. Smaller events (up to M_w 4.0) however seem to be evident occurring in the country’s Precambrian basement, where brittle fractures, lineaments, faults and shear zones are present. In section 3.2.2

of Chapter 3, it has emphasized two such localized areas that either are inhabited with active tectonic features which are capable of producing earthquakes, or have been subject to several strong and medium earthquakes in the past so that a logical risk of striking a similar event in future can also be expected. The area around Colombo is inferred as one of possible seismic sources (probably the most hazardous local source zone) based on the latter observation, while “Mahawelli shear zone” is indicated as the other possible source by mainly referring to its geotectonic layout (see Figure 3.4 in Chapter 3). Colombo is known to be having the most disastrous earthquake ever occurred in the country that was happened on 14th of April 1615 with an estimated magnitude of about M_w 6.4. The event incurred a damage of 200 houses and caused over 2000 casualties (Wimalaratne, 1993). Other structural collapses including a portion of a masonry city wall and complete collapse of a stone bridge would rank the event’s intensity as at least VIII in Modified Mercalli Intensity (MMI) scale. A total of 10 small and strong earthquakes, magnitude ranging from M_w 3.0 to 6.4, have been reported within about a 20 km diameter of Colombo, out of which at least 3 have been greater than M_w 5.0 and about 9 have occurred within last 200 years. Therefore, Colombo is reserved as a separate smaller area source (source zone 6) given the past evidence of seismic activities. This separate zone allocation of Colombo is strengthened by other factors which owe merits rather in “the socio-economical context”; being the capital city of the country and being the most industrialized city in the country, holding the highest population density and having numerous building structures with other infrastructural developments, etc.

Mahawelli shear zone identified in section 3.2.2 in Chapter 3 is not considered as a separate source zone for the hazard assessment in the current study due to its minor seismicity. This and rest of the country except Colombo are zoned to a single source zone (source zone 5) given their slow activity rates.

8.2.2 Earthquake catalog processing

Preparing an earthquake data catalog to include all if not at least a considerable amount of independent seismic activities for an accurate representation of the actual seismicity in a region for a selected period of time, is a key task in the seismic hazard analysis. Collecting previously reported events of the region and refining them to prepare an independent and complete dataset to utilize in the hazard computation, require some standard techniques to be followed in order, which are discussed in the following;

Catalog data

Data are obtained from several sources; online archival databases such as ISC, ANSS, NEIC (National Earthquake Information Centre), GFZ-GEOFON, GCMT (Global Centroid Moment

Tensor catalog), and some previously published data (Abayakoon, 1996; Fernando and Kulasinghe, 1986; Uduweriya et al, 2013) are used. When the same event appeared in several databases (mostly in newer events), priority is given to ANSS information and then to others. Records are compiled over a lengthy timespan, starting since as early as 1507 and spanning till 2014. Nonetheless, not all the events occurred within this period are guaranteed for the count, especially those with smaller magnitude events (M_w less than about 4.0) which occurred during the pre-instrumental era have a higher chance of being unnoticed. The situation can be even worse for zones lying on remote oceanic crusts which are located in “isolated areas” with hundreds if not thousands of kilometers away from mainlands where people live. Therefore, not only less perceivable smaller events, but powerful moderate magnitude events would have also been undetected due to obscurity (or isolation) in such areas.

The original catalog of all source zones contained a total of 2421 events (including dependent events) for the selected period. Only events, of which either magnitude or intensity is known, are chosen for the catalog, whilst those with unknown magnitudes/intensities are safely omitted due to the reason that many of such events fell below the minimum threshold magnitudes used in the study. Variation of hypocentral depth of selected events is assumed to have no any relation with recurrence rates, and therefore, effects due to “depth” and any uncertainty in depth are negated for the study. Data are originally in various magnitude types such as M_L and M_S for most of the older events and M_w , m_B and m_b for newer events reported within the instrumental period. These different magnitude types, other than M_w , are converted to a unified scale M_w , using relationships developed for mid-plate and stable continental regions based on global data (Johnston, 1996; Nuttli, 1983). M_w is considered optimum for the final catalog as it is the same magnitude type used in the ground motion attenuation models applied in the study. Note that, if M_w of an event has already been available in GCMT catalog, then that value, rather any converted value from different magnitudes, is directly selected for the catalog. Few of local events available in the form of felt reports as intensity values are converted to M_w using relationships developed by Greenhalgh et al (1988) for Australian continent. The continental Australia, which also lies in a low to moderate seismic intraplate region as Sri Lanka, is assumed correlating with the Sri Lankan conditions in the sense of intensity parameters such as induced ground shaking, incurred damage, nature of seismic activities, etc.

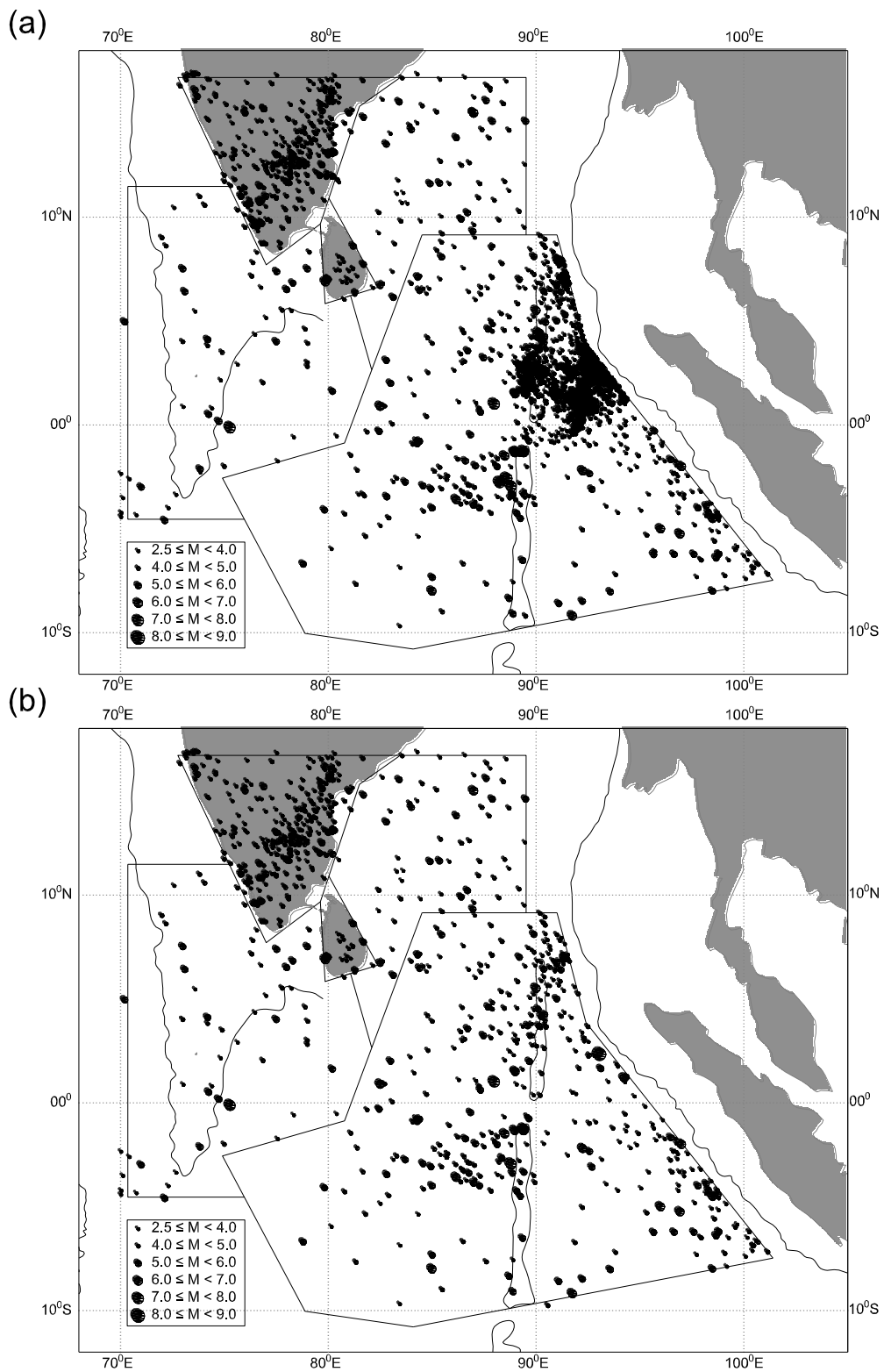


Figure 8.2 Epicentral locations of earthquake catalog data used in the hazard computation in the study. (a) Before declustering (2421 events). (b) After declustering (870 events). The largest dependent event contribution is from source zone 1.

Epical locations of earthquake catalog data in assigned source zones are shown in Figure 8.2, in which 8.2a and 8.2b, respectively, show data before and after removing dependent events. It is evident that source zone 1 is carrying the highest number of dependent events out of all zones for the selected time period. Continuous plate convergence driven by the earlier discussed diffuse deformation has been a clear reason for the active seismicity evidenced in the Figure 8.2. Figure 8.3 demonstrates magnitude (Figure 8.3a) and hypocentral depth (Figure 8.3b) distributions of selected events before and after the declustering. It is clear by the figures that most of the events in the region are shallow crustal earthquakes (depth less than 15 km) with small to moderate magnitude sizes (M_w up to 6.0). Declustering procedure is described in the next section.

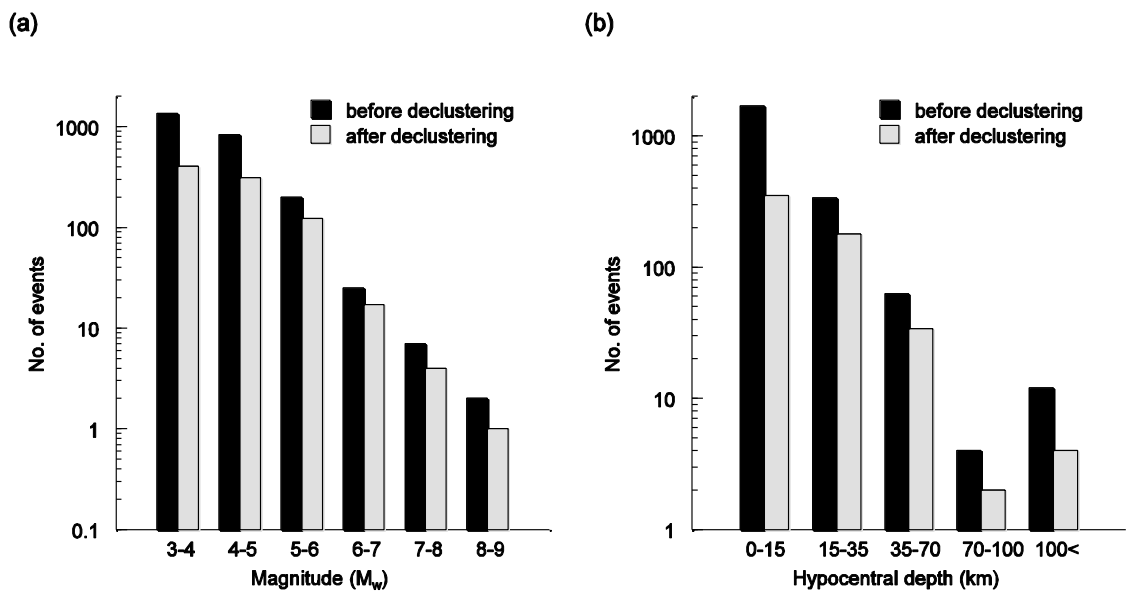


Figure 8.3 Magnitude and hypocentral depth distributions of the selected events. Figures evidence that most of the events in the region are shallow crustal earthquakes (depth less than 15 km) with small to moderate magnitude sizes (M_w up to 6.0). (a) Magnitude distribution. (b) Hypocentral depth distribution.

Declustering

In reality, generation of an earthquake involves a chain of key actions happening in a logical fashion; accumulating elastic stresses at the fault/source as a result of plate motion, slip between contact surfaces once this accumulated stress exceeded the maximum shear (or frictional) stress available between two surfaces, and subsequent start of rupture through the plate initiating from the point hypocenter. Accordingly, earthquake generation is a rational process with a sound theoretical basis, and is significantly appertained with tectonic stresses accumulated within the medium. This stress level is closely correlated with the next “scheduled” earthquake in the region, in which the date and properties of the event (size and location) are largely predefined by this

stress level. Magnitude of a main event would also depend on that of the predecessor since both of these events are interrelated by the final residual stress level of the source.

On the contrary, occurrence of an earthquake is considered yet as a random and independent process (in time) in most of the probabilistic approaches. “Main events”, which are relatively large in size, are generally not frequent, but follow a kind of “idle/slow” sequence in space and time domains. Therefore, these larger events can be ideally treated as mutually exclusive in spatial and temporal distributions. However, relatively small events congested (in both time and space) around main events are not as mutually exclusive as main events, and are thus defined as “dependent events” of main events in the probabilistic risk analysis terminology. The common practice is to remove these dependent events from the raw catalog, and then preparing an independent dataset for easier handling in a probabilistic framework. A number of models are proposed to “clean” a catalog for dependent events, out of which most are based on magnitude dependent windowing functions defined in time and space (Gardner and Knopoff, 1974; Grünthal, 1985; Musson, 1999; Reasenber, 1985). The temporal shape of a catalog which has already been cleaned for dependent events is satisfactorily described by the homogeneous Poisson distribution (Cornell and Winterstein, 1986). When a declustered catalog is actually following a Poissonian event occurrence, then the temporal distribution of recurrences of the region can be effectively modeled by using a Poisson model in the hazard computation. Gardner and Knopoff (1974) show even for seismically active regions like southern California, independent earthquake arrivals follow a Poisson distribution.

In the study, dependent events are initially eliminated by applying the same time and space windows as which proposed by Gardner and Knopoff (1974). However, some dependent events, mainly the aftershocks that resulted due to large magnitude main events (events with magnitude greater than about M_w 8.0) showed arising at farther away from the main event than the respective distance windows for the same magnitude assigned in their study. In other words, Gardner and Knopoff's (1974) spatial windows for dependent events of a large magnitude main event appeared to be underestimating actual likelihood areas of aftershocks of major earthquakes occurred in the region. The total area of rupture of such larger events can be up to thousands of kilometers in size, and therefore, the area where possible aftershocks are arisen can also be expanded over a similar widespread area. Two of such mega events are noteworthy in the subject region; M_w 8.6 on 11th April 2012 and M_w 9.3 on 26th December 2004. The former was an intraplate event located within source zone 1 near Ninetyeast Ridge, while the latter was identified as an interplate event occurred at the subduction zone outside source zone 1. Dependent events of the second event are identified based on rupture areas given in Ammon et al (2005) and US Geological Survey's earthquake summary maps (2005). The rupture areas given in these studies are larger than the possible aftershock area of a typical M_w 9.3 event as extrapolated from Gardner and Knopoff's (1974)

spatial windows [Since Gardner and Knopoff's (1974) algorithm is up to M_w 8.0, an extrapolation is necessary]. Hence, the rupture areas determined in above studies are considered as the possible area for dependent shocks of M_w 9.3 Boxing-day event with the subsequent assumption that the total area subjected to the rupture has an equal possibility of generating dependent events. Note however, the aftershock period is obtained based on an extrapolation of the original algorithm by Gardner and Knopoff (1974). Classification based on these modified aftershock areas resulted in to recognize a new set of other events triggered within source zone 1 as dependent events of the main event M_w 9.3, but their epicentral locations are still far away by up to thousands of kilometers from the main event and Sunda subduction zone. M_w 8.6 earthquake has so far generated hundreds of dependent events since April 2012, and probably would represent the largest known aftershock sequence in the selected dataset (see Figure 8.2b). Many of dependent shocks of the event (in this case mostly aftershocks), those remained after the initial sieving by the method of Gardner and Knopoff (1974), are carefully removed through a manual process based on some intuitive observations; small time gaps with the main event, significant increase of the activity rate in the area after the main event, etc. Although, these removals are not by using any identified aftershock area for the event (research is yet to be undertaken, since the event is fairly a new one), they are found to be in agreement with certain other declustering models such as the one recently developed for the continental Australia (Leonard, 2008), which also specifies larger areas for possible dependent shocks of strong/large magnitude events.

The final catalog after the declustering included 870 events, and is just about 36% of the original catalog size. This is not a surprise, since many of small and moderate magnitude events, particularly in source zone 1, are aftershocks of major earthquakes. Temporal distribution of final "independent" earthquake data of the total region which covers all the source zones is compared with the Poisson distribution. Events with medium and higher sizes ($M_w \geq 4.0$) generated only after 1965 are considered for the comparison, in which 1965 is kept as a cutoff in parallel with the World-Wide Standard Seismograph Network (WWSSN) program launched in 1964. The possibility of not detecting a moderate and large magnitude earthquake after the WWSSN program is very low or can be ideally considered as null with respect to the situation prior to the WWSSN. Therefore, earthquake data available after the WWSSN project would be a more accurate reflection of actual earthquake recurrence pattern of the region. Figure 8.4 compares the actual earthquake distribution with the theoretical Poisson distribution for events greater than M_w 4.0 (Figure 8.4a) and 4.5 (Figure 8.4b). Distributions for each of the respective raw catalogs (before declustering) are also included. The figures attest that the declustered catalogs "visually agree" with a Poissonian event arrival, although, the actual arrivals found to be having a little way off with chi-square goodness values. Actual form of the recurrence for so-called "independent events" may or may not be Poissonian, but be bound by other complexities which need to be

addressed in separate contexts; independent data may still be contaminated by dependent events, the dataset may not be “complete” enough (still missing some data), the period considered may not be lengthy enough for reflecting recurrence characteristics of much larger events; actual data may have a variation from the Poisson distribution, etc. Despite these probable uncertainties, actual independent events are assumed following a Poissonian variation in the time domain given the sufficient consistency as evidenced from the figures.

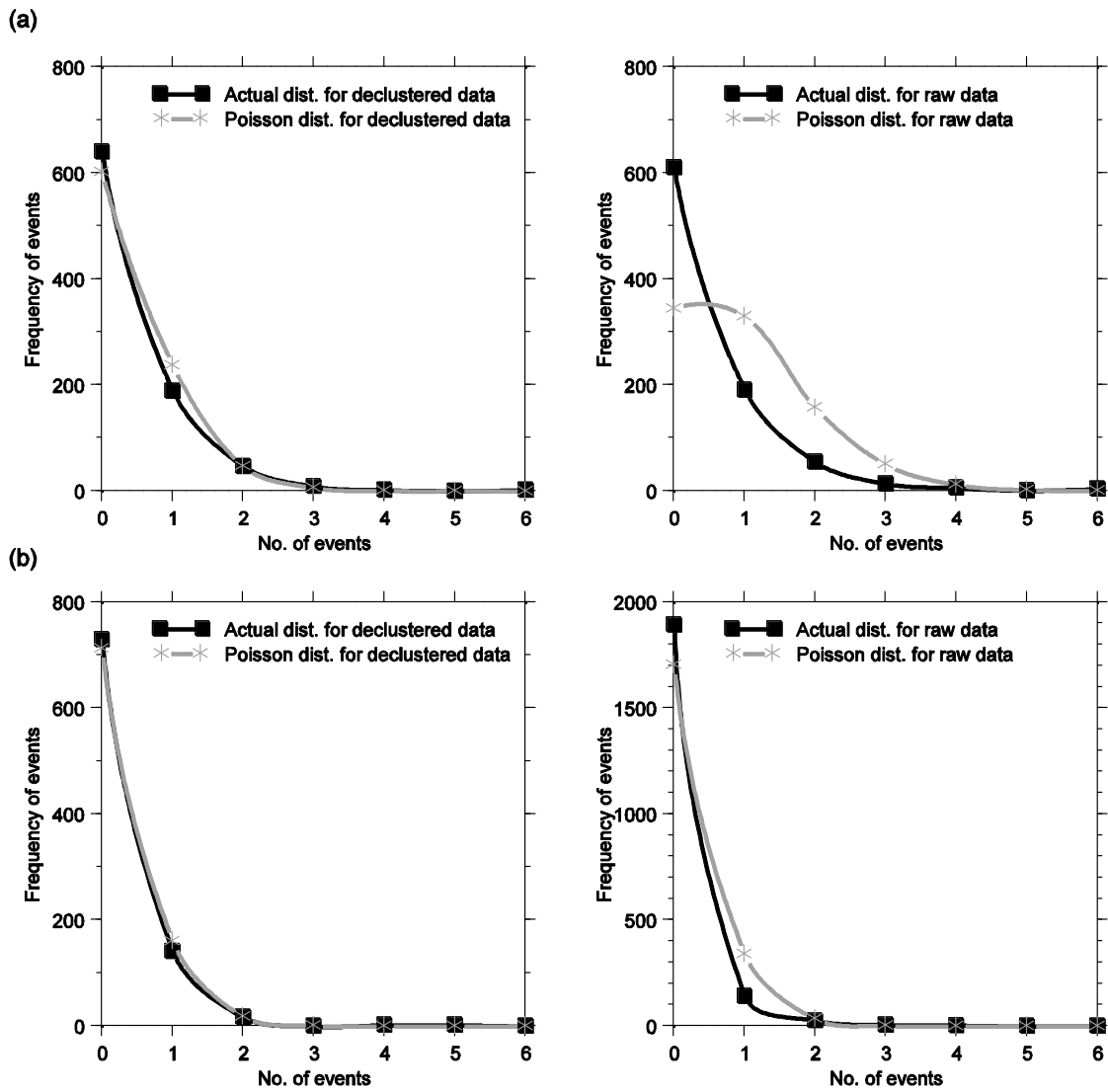


Figure 8.4 Comparison of the actual earthquake distribution with the theoretical Poisson distribution. Distributions for each of the respective raw catalogs (before declustering) are also included. Declassified catalogs of independent events “visually agree” with a Poissonian event arrival. However, the actual arrivals have shown a little way off by chi-square goodness values. (a) For events greater than M_w 4.0. (b) For events greater than M_w 4.5.

Completeness analysis and recurrence rates

Earthquake catalog completeness is performed to find whether the data of a given catalog are “a complete representation” of the actual seismicity in the region. A complete representation delineates that all the events (excluding smaller events, which are of no significance) occurred in the region during a particular period of time are taken into account without leaving any event. Therefore, completeness of a catalog is always assessed for a selected time period, usually counted backward from the latest date of the catalog, and for a selected magnitude range. The longer the period considered the lesser the possibility that the catalog is being complete for the selected magnitude range. Another common observation is that higher magnitude events can be complete for longer periods in time than smaller magnitude events do, which is due to the major awareness always on large magnitude events. Unlike stronger or larger events, smaller events are less reliable to be ascertained during an occurrence because of comparably low energy releases. Even detected, during the pre-instrumental era, such events are easily omitted for reporting due to their insignificant influence upon mankind. This omission of smaller magnitude events can result in a flatter recurrence curve for the region, which can eventually lead to underestimate and overestimate of smaller and larger event recurrences, respectively. Thus, completeness check has become a mandatory part in the probabilistic hazard analysis methods to characterize the actual seismic recurrent nature in a region.

Stapp’s method (1972; 1971) is adopted to estimate completeness periods in the present study. The method assumes that earthquake occurrence in a particular magnitude class as a point process in time, following a Poisson event arrival. For a selected time period (T), the mean rate of recurrence (λ) of a given magnitude class can be expressed as;

$$\lambda = \frac{\sum_{i=1}^T n_i}{T} \quad (8.1)$$

n_i is the number of earthquakes in a unit year. The standard deviation $[\sigma(\lambda)]$ of the mean rate of recurrence, can be then taken as;

$$[\sigma(\lambda)] = \sqrt{\frac{\lambda}{T}} \quad (8.2)$$

T counts backward, preferably in 3-5 year laps, starting from the most recent date of the catalog. If the mean annual rate of recurrence of a region is hypothesized to be at a constant for a given magnitude class, $\sigma(\lambda)$ would follow a linear variation (in logarithmic scale) with $1/\sqrt{T}$. Following this norm, the point at which the slope of $\sigma(\lambda)$ starts changing from its initial $1/\sqrt{T}$ is identified as the upper margin of the time period that the catalog is considered to be complete for the selected magnitude class. The test of completeness is essential for smaller magnitude events due to their

recording uncertainty in comparison to larger/stronger events which are generally unlikely to be undetected. Consequently, in the study, more attention is given on completeness periods of “smaller magnitude events” which are yet so capable of producing ground shakings at sufficient levels for the selected sites of interest. This minimum magnitude varied from M_w 3.0 to 5.0 for identified source zones depending on availability of smaller magnitude events in each of the source zones, and site-source distance which “calibrates” the size of magnitude needed for a lower bound shaking level. For instance, for source zone 1, M_w 5.0 is considered as the minimum magnitude for the completeness check, given the scantiness of smaller event data ($M_w < 5.0$) in the zone and large site-source distance between the country and source. For source zones 5 and 6, however, fairly a small magnitude M_w 3.0 is chosen mainly because of the inadequacy or sometimes the complete absence of other moderate and strong events ($M_w > 4.0$) reported within the country (the situation especially prevails in source zone 5). Any such absence of events within a certain magnitude class would produce no data in the respective Stepp’s plot (for that magnitude class). Stepp’s plots for selected minimum magnitudes are shown in Figure 8.5, and resulted completeness periods are given in Table 8.1.

Table 8.1 Seismicity parameters of defined source zones (see end of the table for definitions of terms)

| Source zone | Stepp’s test for the completeness | | Input parameters for hazard computation | | | | |
|-------------|---|----------------------------|---|---------|---------------|-----------------|---------------------|
| | Min magn. considered for the test (M_w) | Completeness periods (yrs) | α | β | CV of β | m_0 (M_w) | m_{max} (M_w) |
| 1 | 5.0 | 50 | 9.239 | 1.799 | 0.018 | 4.5 | 9.0 |
| 2 | 4.5 | 30 | 7.229 | 1.669 | 0.004 | 3.5 | 6.7 |
| 3 | 4.0 | 75 | 10.619 | 2.522 | 0.017 | 4.0 | 6.0 |
| 4 | 4.0 | 40 | 6.251 | 1.657 | 0.017 | 3.5 | 7.5 |
| 5 | 3.0 | Incomplete | 4.955 | 1.629 | 0.026 | 3.0 | 6.0 |
| 6 | 3.0 | Incomplete | 2.629 | 1.386 | 0.000 | 3.0 | 6.5 |

α and β - a and b values, respectively, in natural logarithms in the standard Gutenberg-Richter law [$\lambda_m = \exp(\alpha - \beta m)$]

CV of β - Coefficient of variation of β

m_0 - Minimum threshold magnitude used in the hazard computation

m_{max} - Maximum expected magnitude for the source zone

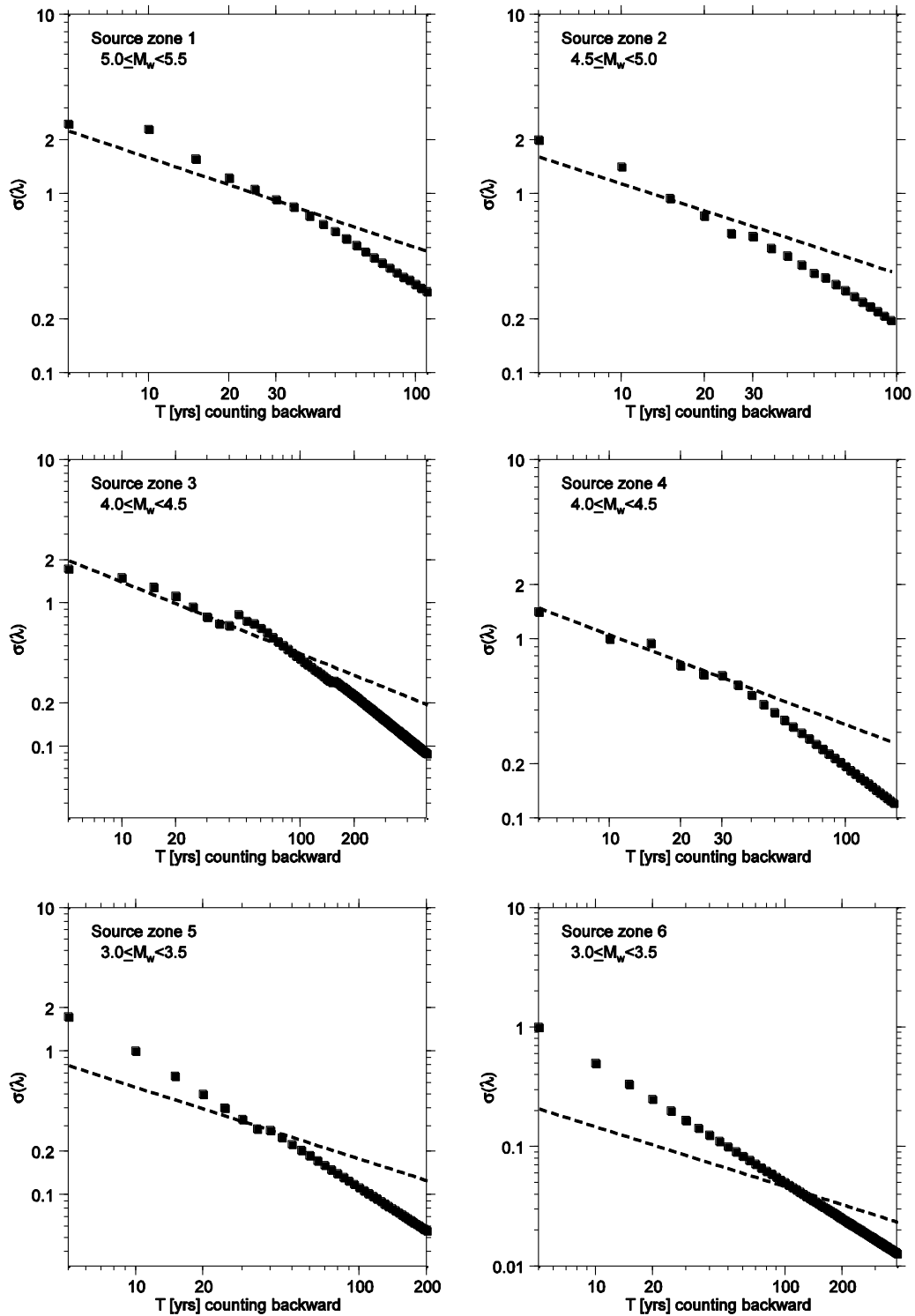


Figure 8.5 Stepp's plots of the completeness check. Selected minimum magnitude bands in each source zone are given inside the figure. Source zones 1-4 are complete for at least part of their total catalog durations in the selected magnitude ranges, as evidenced by the variation of $\sigma(\lambda)$ which follows $1/\sqrt{T}$ slope before diverting to a much steeper slope. Source zones 5 and 6, however, are not as complete as other regional sources, since the slope of $\sigma(\lambda)$ clearly deviates from $1/\sqrt{T}$ for the total period of catalog in either case. Resulted completeness periods are given in Table 1. Squares denote the actual variation, while dashed lines represent $1/\sqrt{T}$ variation.

The minimum magnitude applied in the Gutenberg-Richter bounded equation (see Table 8.1) basically followed the criteria of assigning a limiting magnitude which is able in producing a “threshold level of risk” at the site of interest. This “threshold magnitude” ranged from a minimum of M_w 3.0 for source zones 5 and 6 to a maximum of M_w 4.5 for the distant source - source zone 1. A lower magnitude of M_w 3.0 for local source zones 5 and 6 is selected in perspective of higher “vulnerability” expected during even a small ground shaking induced at local sites in Sri Lanka, which are not yet “well-prepared” against earthquake shakings as places in other countries where design codes of practice have been properly adopted. Level of impact even by a such a smaller event occurred at a site in Sri Lanka can be higher than that of a similar shaking at a place of where all the structural/infrastructural elements have been designed to a certain nominal ground motion level derived based on the seismicity of that place. The selection of M_w 3.5 for source zones 2 and 4 that are juxtaposed with the country, is also partly encouraged by the same reason. During the selection of minimum magnitude for hazard computation, concerns on the absence of smaller events in some magnitude classes as that done in the completeness check, are not considered, and only a magnitude which is posing a minimal risk is selected for each zone. The maximum magnitude as a cut-off is generally chosen based on historical evidence of the largest event occurred in the zone. However, a bit higher magnitudes than those are sometimes selected on the basis of conservatism.

As evidenced by Figure 8.5, source zones 1-4 are complete at least for part of the total catalog duration for the selected minimum magnitude classes. In all these regional source zones, the variation of $\sigma(\lambda)$ for selected magnitude classes shows approximately following $1/\sqrt{T}$ slope before deviating into much steeper slopes. Source zones 5 and 6, however, are not as complete as other regional sources, since the slope of $\sigma(\lambda)$ is clearly diverting from $1/\sqrt{T}$ for the total period of catalog in either case. Lack of event data, may be due to negligence of previous events, in local catalogs for representing the actual seismicity of the country, can be the principal reason for this incompleteness. Many of smaller and moderate magnitude events previously occurred in the country were left unreported due to inattention. Lack of awareness by the public on earthquake activities, insufficient research works towards assessing the local seismicity and absence of a permanent and sophisticated local seismic network, have overall resulted in the shortening of the data in local earthquake catalogs. Given this situation, source zone 5, which covers most of the country’s inland area, is assumed to be complete for smaller events that occurred only after installing the local seismic network in 2000. Therefore, the period after 2000 is considered for derivation of earthquake recurrence parameters in the continental Sri Lanka (except Colombo). Recurrence parameters of source zone 5 derived based on such a short period showed a little higher recurrence rate for moderate and large magnitude earthquakes than the rates given by the historical seismicity. Nevertheless, derived parameters are accepted for the hazard analysis given

the additional emphasis on hazard due to moderate and large magnitude events. For source zone 6, recurrence parameters are obtained only based on the activity rates of strong magnitude events occurred during the total period of the catalog starting from 1615. Number of smaller magnitude events is not that sufficient to represent “the complete seismicity” of the zone, and would have caused a bias when predicting recurrence rates of moderate and large magnitude events in the zone (particularly, due to change in a value in Guttenberg-Richter curve). Strong magnitude event occurrences in Colombo and its surroundings were noticeable in the past in comparison to other areas of the country (discussed in section 8.2.1 “Seismic source zones”). These strong magnitude events are assumed to be safely reported during the catalog period, in which case the catalog can be treated complete for strong events. Therefore, the recurrence relationship for source zone 6 is inferred merely based on activities of strong events reported in the zone, albeit the relationship is a little conservative for smaller events. Guttenberg-Richter curves for each source zone, in both of the original and bounded form, are presented in Figure 8.6.

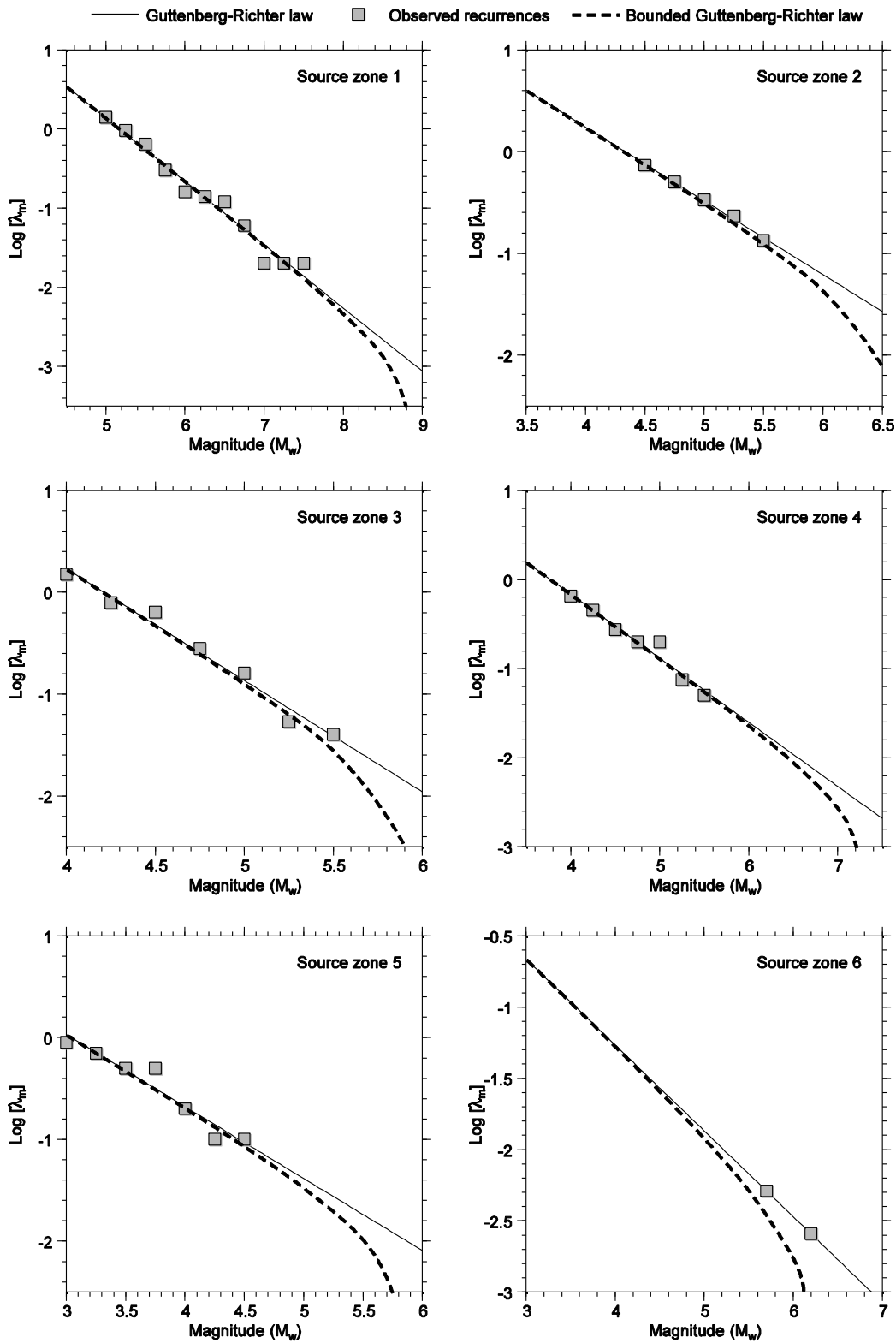


Figure 8.6 Earthquake recurrences of the defined source zones. Actual recurrences and Gutenberg-Richter fitted curves in both of the original and its bounded form are presented for each defined source zone. Estimated recurrence parameters are given in Table 8.1.

8.2.3 Ground motion prediction equations

The attenuation models derived in Chapter 7 are primarily applied for the present hazard study. The local attenuation model indicated in Table 7.1 in Chapter 7 is employed in computing the seismic hazard for source zones 5 and 6. The regional attenuation model (Table 7.2 in Chapter 7) is applied in source zones 1, 2 and 4 where the surrounding oceanic crust is present. Source zone 3 which virtually covers the total continent of southern peninsular India, is assigned with a regional model already developed by event data reported within Indian continent (Raghu Kanth and Iyengar, 2007). Raghu Kanth and Iyengar's (2007) model is applied with the assumption that seismological properties characterized by their model, are similar in nature to that found in the adjacent northern most continental and continental-oceanic boundary area in Sri Lanka (hopefully, the only area of Sri Lanka possible for major shakings due to seismic activities in Indian peninsula). The assumption leaves the permission for considering expected wave path modifications to be the same through the whole propagating path from southern India to northern Sri Lanka. Raghu Kanth and Iyengar's (2007) model is given in Table 8.2.

Table 8.2 Raghu Kanth and Iyengar's (2007) attenuation model for Peninsular India

| Parameter in g [$\ln(y_{br})$] | $\ln(y_{br}) = c_1 + c_2(M - 6) + c_3(M - 6)^2 - \ln(r) - c_4r + \ln(\epsilon_{br})$ | | | | |
|---------------------------------------|--|--------|---------|--------|-----------------------------|
| | c_1 | c_2 | c_3 | c_4 | $\sigma(\ln \epsilon_{br})$ |
| PGA | 1.6858 | 0.9241 | -0.0760 | 0.0057 | 0.4648 |
| SA at 0.1 s | 2.3890 | 0.9548 | -0.0791 | 0.0044 | 0.4503 |
| SA at 0.5 s | 1.1638 | 1.3615 | -0.2546 | 0.0021 | 0.3817 |
| SA at 1.0 s | 0.3604 | 1.6791 | -0.3248 | 0.0014 | 0.3531 |

8.2.4 Hazard computation

Hazard computation is a process that combines; (1) mean rate of recurrence of a selected magnitude (which is bound by a minimum and maximum limits) of a defined source, (2) with probability of occurrence of an event with the same magnitude at a point within the source, (3) and with probability of exceeding a certain ground motion level at the selected site due to the event. Since the computation involves estimating "probability" that the action/incident is taking place, the process naturally accounts for possible uncertainties expected in each action. Therefore, the process of a probabilistic hazard assessment is generally considered unbiased with the each step/action well defined by its own uncertainty. The probability which a selected ground motion parameter (Y) exceeds a certain value (y) due to an M magnitude event occurred at an independent R distance from the targeting site is given by;

$$P[Y > y] = \iint P[Y > y | M, R].f(M).f(R).dM.dR \quad (8.3)$$

$f(M)$ and $f(R)$ are probability density functions for magnitude and distance parameters, respectively. These probability density functions quantify the uncertainty associated with the each parameter (magnitude and location). Uncertainty of the predicted ground motion value is ascertained by the standard error (standard deviation) of the estimate. If the site of interest is located in a region of N number of potential sources each of which has a mean recurrence rate of v_i (where $i=1,2,3,..,N$), then the aggregate result of rate of exceedance (λ_y) of y at the site due to M magnitude events at R possible distances is (Kramer, 1996);

$$\lambda_y = \sum_{i=1}^N v_i \iint P[Y > y | M, R] \cdot f(M) \cdot f(R) \cdot dM \cdot dR \quad (8.4)$$

Equation (8.4) simply outlines the computational procedure that has to be used in estimating seismic hazard of a given region. Although, ideally the equation has double integral terms corresponding to the independent variables magnitude and distance, in normal practice a subdivision of ranges of these variables into smaller segments can be done, so that a simple summation of individual segments instead of the integration is possible. However, the computational process can still be onerous as the calculation may require to be repeated at a number of times depending on other factors, e.g., number of seismic sources available and their sizes, magnitude and distance ranges considered in each source, number of sites to compute seismic hazard, etc. Therefore, the computation would be rather easy if that is handled by any software package specifically developed for the purpose. Estimated hazard values by using such a software package would be still comparable with the theoretical ones given by equation (8.4), as long as the selected segments are smaller in size that the size of an individual segment can be negated when compared with the original composite size. Hence, by choosing a proper segment size in source areas and magnitude ranges, equation (8.4) in the above explained simplified form can be easily applied to estimate mean annual rates of exceedance of the selected ground motion parameter in a region. These estimations are then used in developing “hazard curves” for the site of interest, by which the maximum expected ground motions likely to be exceeded in any given return period can be found. Expected ground motions in the return periods such as 475, 975 and 2475 years are the most of engineering interest.

In the study, hazard computations are done by using an open-source package called CRISIS2007 (Ordaz et al, 2007). Input data naming earthquake catalog information, source zones’ geometries, location data of target sites, recurrence rates and seismicity data in the source zones, and the applied attenuation models are gradually fed into the software in the first place. Then, necessary outputs of the hazard computation (mean annual rates of exceedance of PGA and SAs at 0.1, 0.5 and 1.0 s periods for 5% critical damping ratio at the selected sites), are processed by executing a sample run of the software.

Note that, some optional techniques like a logic tree (Kulkarni et al, 1984; McGuire and Shedlock, 1981) for capturing epistemic uncertainties in the ground motion prediction are not included in the study. The reason for this avoidance is that there is no major requirement to evaluate such “knowledge-based uncertainties” expected in the ground motion attenuation models applied in the study. The attenuation models applied in the study are originally developed based on seismological characteristics specific to the same subject region, and are also validated adequately following a comparison with actual data recorded in the country (refer Chapter 7). Therefore, there are no substantial prerequisites to import another model which may have been initially developed in elsewhere, and then to incorporate biases coming from various uncertainties arising due to the use of different attenuation models.

Results of the hazard computation are discussed in the next section.

8.3 Results and discussion

Computed hazard in the form of expected ground motions (PGA and SAs at 0.1, 0.5 and 1.0 s natural periods for 5% critical damping ratio) at rock sites in Sri Lanka having 10% (475 year return period), 5% (975 year return period) and 2% (2475 year return period) probability of exceedance in 50 years of time, are mapped in separate raster layouts (Figure 8.7). Individual values for some selected major cities in the country are given in Table 8.3. Resulted design spectra, in terms of PSA, for selected cities are shown in Figure 8.8.

Results show that the area around Colombo is by far the most vulnerable place in the country for seismic activities. Colombo possesses nearly 0.043g (g is gravitational acceleration) of a maximum expected PGA to exceed in a 475 year return period. This increases to about 0.053g and 0.065g for 975 and 2475 year return periods, respectively. The rest of the country envisages relatively small ground motions dispersing in a uniform nature through the whole area, and this ultimately warrants the region to be easily classified under the low seismicity category. Predicted PGAs for Colombo area are roughly of the order of one tenth of predicted PGA obtained in the deterministic based scenario prediction carryout in Chapter 6. Lower PGAs resulted in the present probabilistic approach would mainly reflect uncertainties taken into the consideration through the process of hazard computation, which may include uncertainties of earthquake properties (magnitude and hypocentral distance), predictive attenuation models, earthquake recurrence, etc.

Table 8.3 Estimated hazard values in terms of PGA and SAs (at 0.1, 0.5 and 1.0 s natural periods) with exceeding probabilities 10%, 5% and 2% in 50 years for selected major cities in Sri Lanka

| City | Lon. (°E) | Lat. (°N) | Expected ground motion value (in g) having a probability of exceedance | | | | | | | | | | | |
|-------------|--------------|--------------|--|---------------|---------------|-------|----------------------------------|---------------|---------------|-------|-----------------------------------|---------------|---------------|-------|
| | | | 10% in 50 yrs (475 return period) | | | | 5% in 50 yrs (975 return period) | | | | 2% in 50 yrs (2475 return period) | | | |
| | | | PGA (0.1 s) | SA (0.5 s) | SA (1.0 s) | SA | PGA (0.1 s) | SA (0.5 s) | SA (1.0 s) | SA | PGA (0.1 s) | SA (0.5 s) | SA (1.0 s) | SA |
| Colombo | 79.84 | 6.93 | 0.043 | 0.079 | 0.058 | 0.034 | 0.053 | 0.095 | 0.070 | 0.041 | 0.065 | 0.113 | 0.083 | 0.050 |
| Galle | 80.22 | 6.04 | 0.015 | 0.023 | 0.024 | 0.014 | 0.019 | 0.032 | 0.029 | 0.017 | 0.025 | 0.045 | 0.037 | 0.022 |
| Matara | 80.53 | 5.95 | 0.012 | 0.023 | 0.020 | 0.012 | 0.016 | 0.029 | 0.025 | 0.015 | 0.021 | 0.040 | 0.032 | 0.019 |
| Hambantota | 81.12 | 6.12 | 0.012 | 0.024 | 0.020 | 0.011 | 0.016 | 0.032 | 0.025 | 0.014 | 0.023 | 0.045 | 0.033 | 0.018 |
| Batticaloa | 81.70 | 7.72 | 0.013 | 0.026 | 0.020 | 0.011 | 0.018 | 0.035 | 0.026 | 0.014 | 0.025 | 0.048 | 0.035 | 0.019 |
| Trincomalee | 81.23 | 8.57 | 0.013 | 0.026 | 0.020 | 0.011 | 0.018 | 0.035 | 0.026 | 0.014 | 0.025 | 0.048 | 0.035 | 0.018 |
| Jaffna | 80.00 | 9.67 | 0.022 | 0.045 | 0.021 | 0.011 | 0.027 | 0.057 | 0.028 | 0.014 | 0.036 | 0.075 | 0.036 | 0.019 |
| Mannar | 80.07 | 8.87 | 0.015 | 0.031 | 0.021 | 0.011 | 0.020 | 0.040 | 0.027 | 0.014 | 0.026 | 0.051 | 0.035 | 0.019 |
| Chilaw | 79.80 | 7.58 | 0.021 | 0.039 | 0.032 | 0.019 | 0.026 | 0.048 | 0.039 | 0.023 | 0.032 | 0.058 | 0.047 | 0.029 |
| Kandy | 80.64 | 7.30 | 0.019 | 0.035 | 0.029 | 0.017 | 0.023 | 0.042 | 0.034 | 0.020 | 0.028 | 0.051 | 0.041 | 0.025 |

Estimated values may be sometimes suggesting for a comparison of the seismicity in Sri Lanka with that in Tasmania in Australia, since some of the major cities in Tasmania are also provided similar hazard factors (e.g., Hobart-0.03g, Launceston-0.04g, Devonport-0.05g from AS 1170.4-2007). By referring to the pattern of variation of estimated ground motions across the country, it is clear that the maximum ground motion values are associated with source zone 6 that defines the local seismicity in the area around Colombo. Although, the seismicity characterized by source zone 6 is not as much intense as that in regional sources surrounding the country such as source zones 1, 2, 3 and 4, expected ground motions due to an event in source zone 6 appear be still dominant in the country. The key reasons for the apparent dominance of source zone 6 over others are; 1) lower site-source distance for respective sites from Colombo than from other zones (particularly, when compared with regional zones) 2) a bit higher recurrence rates for moderate and strong events than that in the other local source - source zone 5 3) any difference in the attenuation models applied (discussed later in the section). Influence by source zone 1 on final predicted hazard levels, seems to be less effective regardless the zone's active seismic nature (discussed in section 8.2.1). Such an observation would sometimes result in the motive of a little curiosity in one's mind, especially in a context where a number of shakings due to large magnitude distant events in source zone 1 have been reported in the recent past. However, estimated predictions in the study are obtained through a scientifically valid process, within which the degree of uncertainty in each step is assessed as a measure of probability. Predicted ground motions, therefore, by a probabilistic hazard analysis method are always bound by the uncertainty of the respective action being taken place in the process, and are not just predictions solely relating

to a certain magnitude and site-source distance as which do in a deterministic analysis procedure. Other than the area around Colombo, northern most and even northwestern parts of the country, specially the area towards Jaffna peninsula, have shown subjecting to higher risks (higher PGAs and SAs at 0.1 s) than other areas (see Table 8.3). This is because the subject area's (northern part of the country including Jaffna peninsula) location contiguity and direct exposure to southern peninsular India (source zone 3) which has higher activity rates for smaller and medium events than those of other source zones. Another reason for higher ground motions shown in the subject area can be possible to link with the attenuation model applied in source zone 3, which has originally been developed using event data recorded within peninsular India (Raghu Kanth and Iyengar, 2007). The model shows predicting higher ground motions (especially in PGA and SA at 0.1 s) than predictions for similar events by the attenuation models derived in Chapter 7 for the Sri Lankan region (see Figure 8.9), and if that is the case, the deaggregated portion of hazard coming from seismic activities in source zone 3 for the final aggregated hazard expressing as ground motions at target rock sites in the northern part of Sri Lanka, can be higher than contributions by other source zones which use the newly derived attenuation models. Above explanations help to unfold any core-reason for apparent higher hazard levels expected in the northern part of the country, however, these hazard levels can be justified to a certain extent by turning into characteristics of the underlain bedrock in the area. The bedrock of the northern and northeastern parts of Sri Lanka, which represents about 10% of the country's total continental crust, is made up of much younger Mesozoic and Cenozoic sediments (Cooray, 1994). Seismic waves travelling through younger mediums such as these sediments can be amplified due to upper crustal amplification effects (discussed in section 2.3.4 in Chapter 2), which can result in an escalation of the final ground motion values at high frequencies. Hence, any "conservativeness" observed in predicted ground motions of the northern and northeastern region, is "compensated" with upper crustal amplification effects possible in the region. Note that, any such amplification effect in the region is unable to be investigated at this stage owing to unavailability of recording stations in the area.

Analyzing seismic hazard in Sri Lanka based on probabilistic approaches has been previously conducted by couple of scholars (Abayakoon, 1996; Peiris, 2007; Uduweriya et al, 2013). Abeykoon (1996), for the first time, based on a limited number of earthquake records estimates the maximum expected horizontal PGA (at rock sites) in the country, which is again around Colombo, is about 35 gal (0.036g) for a 300 year return period. The value interestingly shows a resemblance with findings in the present study in which an extrapolated value of about 0.031g can be obtained for a 300 year return period. However, the two studies are different in senses of the amount of data used, basic steps followed and the applied attenuation models in the hazard computation. In Peiris's (2007) study, the design basis PGA having a 10% probability of

exceedance in 50 year return period for Colombo rock sites is recommended as 0.026g. The study defines only a single source area bound by latitudes 0°N to 15°N and longitudes 75°E to 85°E, and considers about 152 moderate magnitude event data (before declustering) since 1819. Uduweriya et al (2013) have estimated the design PGA at Colombo rock sites for a 475 year return period as 0.1g, in which the study compiles a comprehensive event catalog consisting both instrumental and historical data since from 1063. Source zones defined in the study are basically followed the same as in Menon et al (2010), which have originally been defined for assessing the seismic hazard in Tamil Nadu in southern India, and no attempts are given to characterize local and regional seismic sources prevalent in Sri Lanka and the surroundings. Findings of all these studies would generally suggest that Sri Lanka is lying in a low seismic area, technically termed as a stable continental area. In a broad sense, the present study too agrees with this ensemble idea, yet, the final hazard values computed may still narrate some variations in the actual risk level in the country with respect to other studies. These individual tradeoffs are obvious and are dependent on numerous factors associated with each step in the process (earthquake catalog data, quality of data and size, source zonation, completeness periods and recurrence rates calculation, applied attenuation models, etc.). Therefore, comparisons in the final numbers should be done carefully, once after a consideration all the steps followed in the study, since each may have its own merits.

(a)

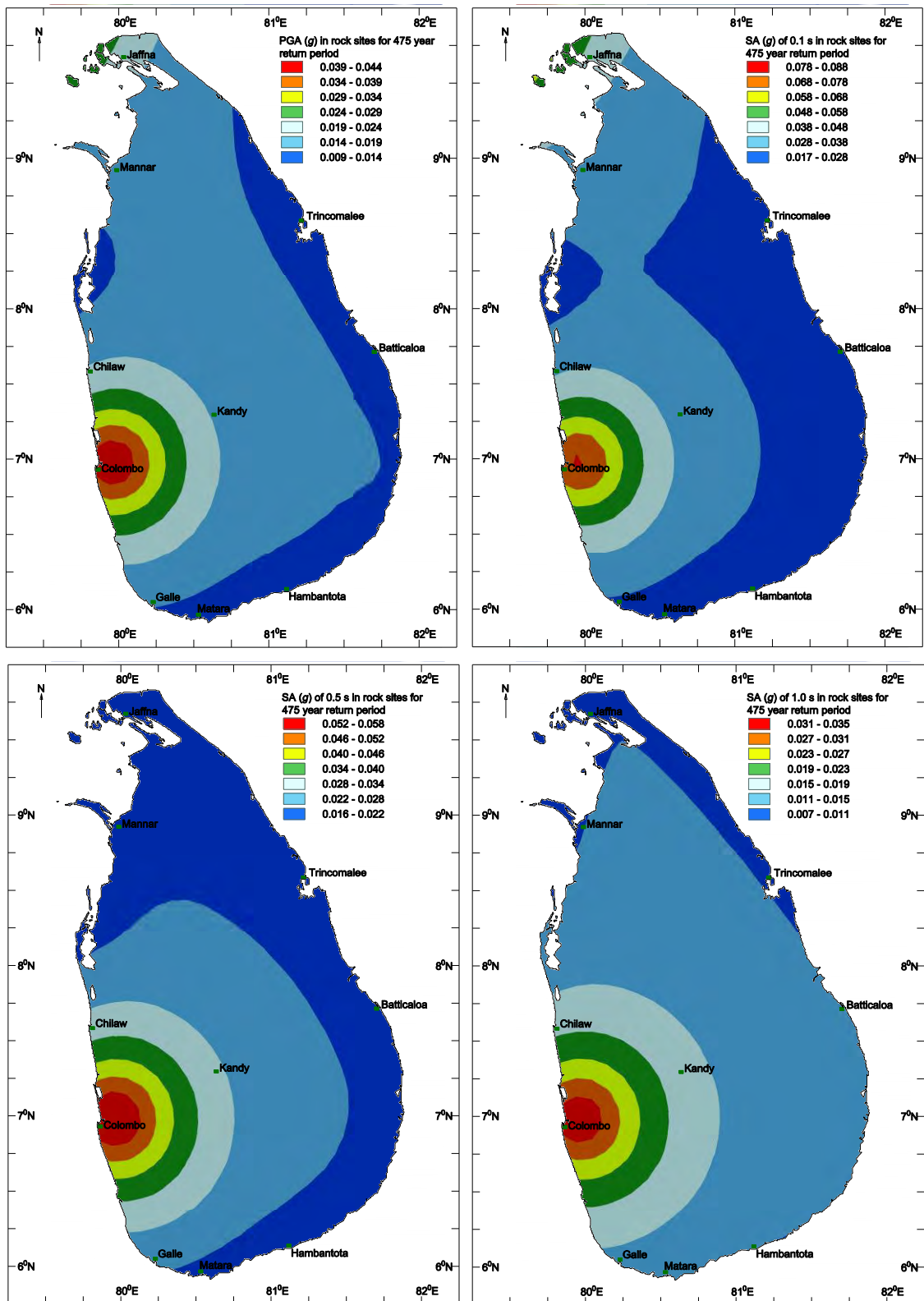


Figure 8.7 Computed hazard values in terms of expected ground motions (PGA and SAs at 0.1, 0.5 and 1.0 s natural periods for 5% critical damping ratio) at rock sites in Sri Lanka for probability of exceedance (a) 10% in 50 years (475 year return period). (b) 5% in 50 years (975 year return period). (c) 2% in 50 years (2475 year return period).

(b)

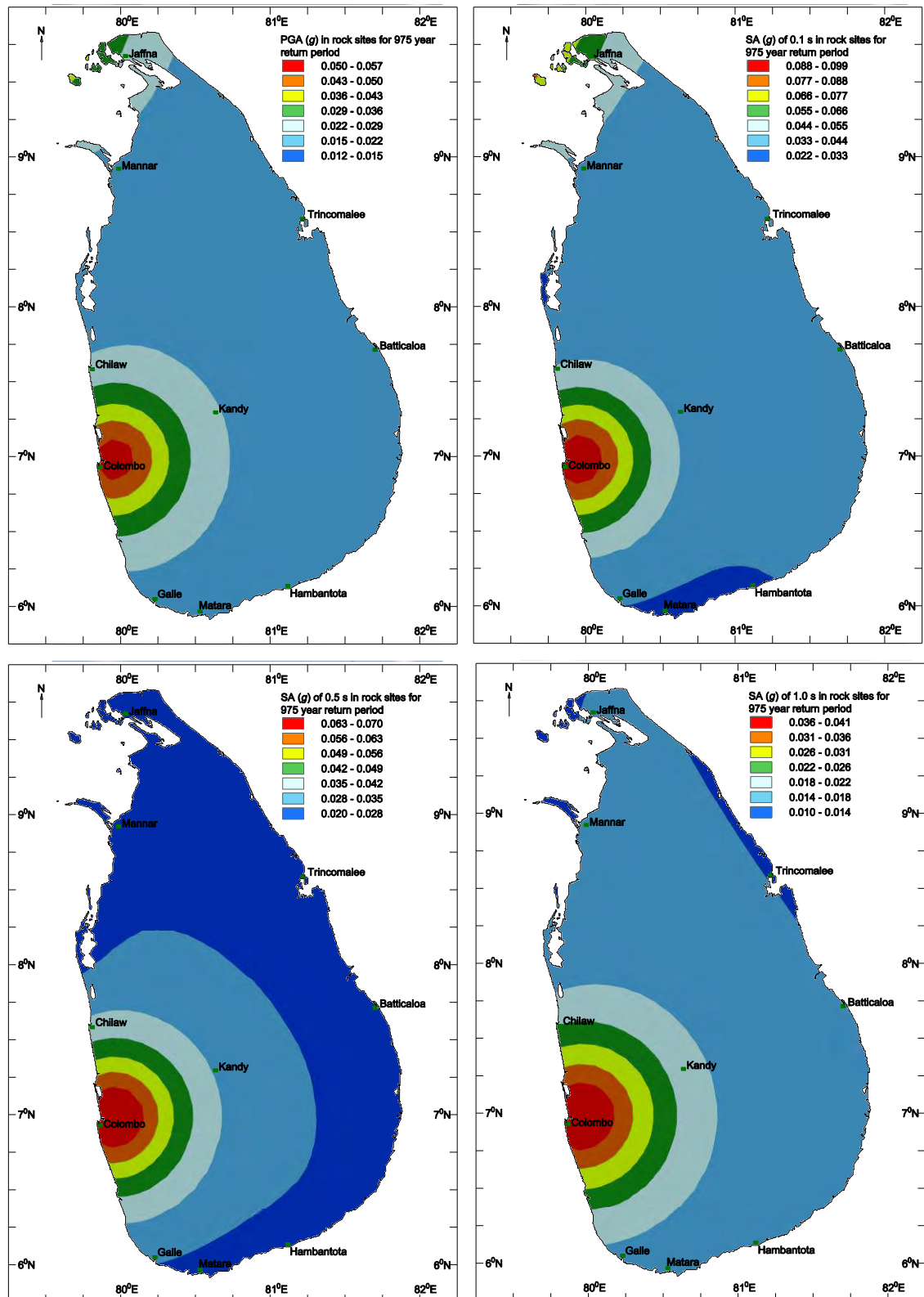


Figure 8.7 (continued)

(c)

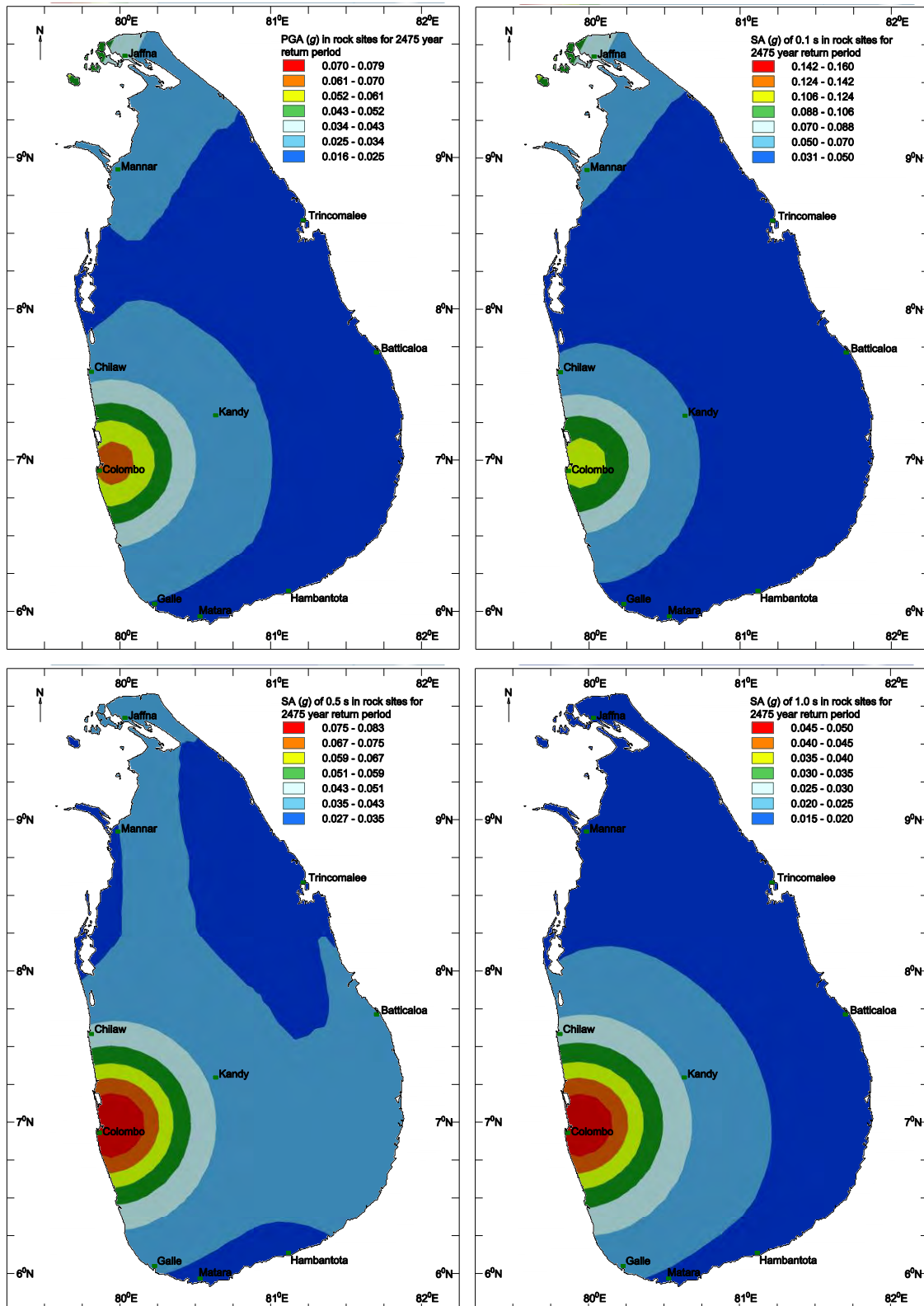


Figure 8.7 (continued)

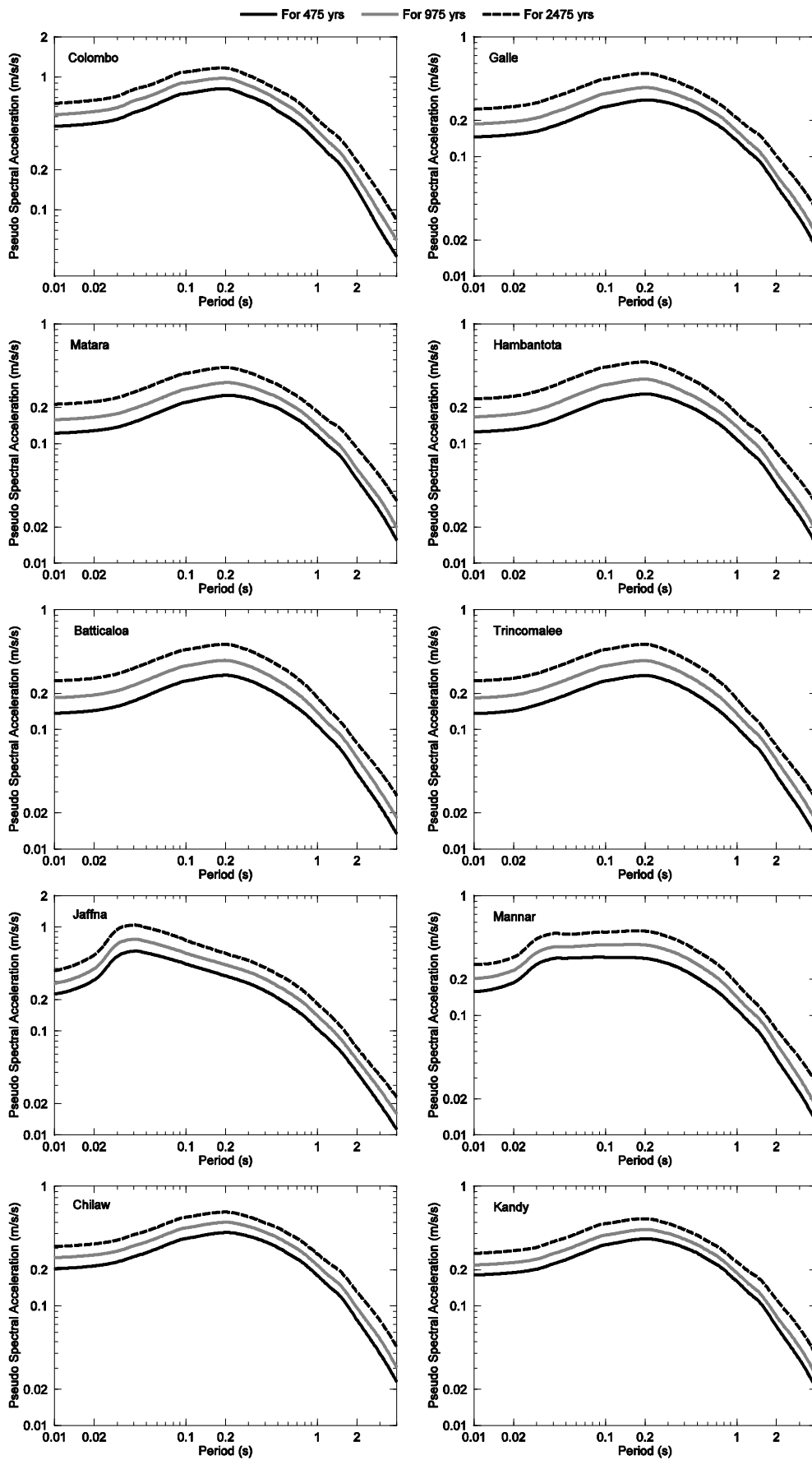


Figure 8.8 Resulted design spectra, in terms of PSA, for selected cities in the country.

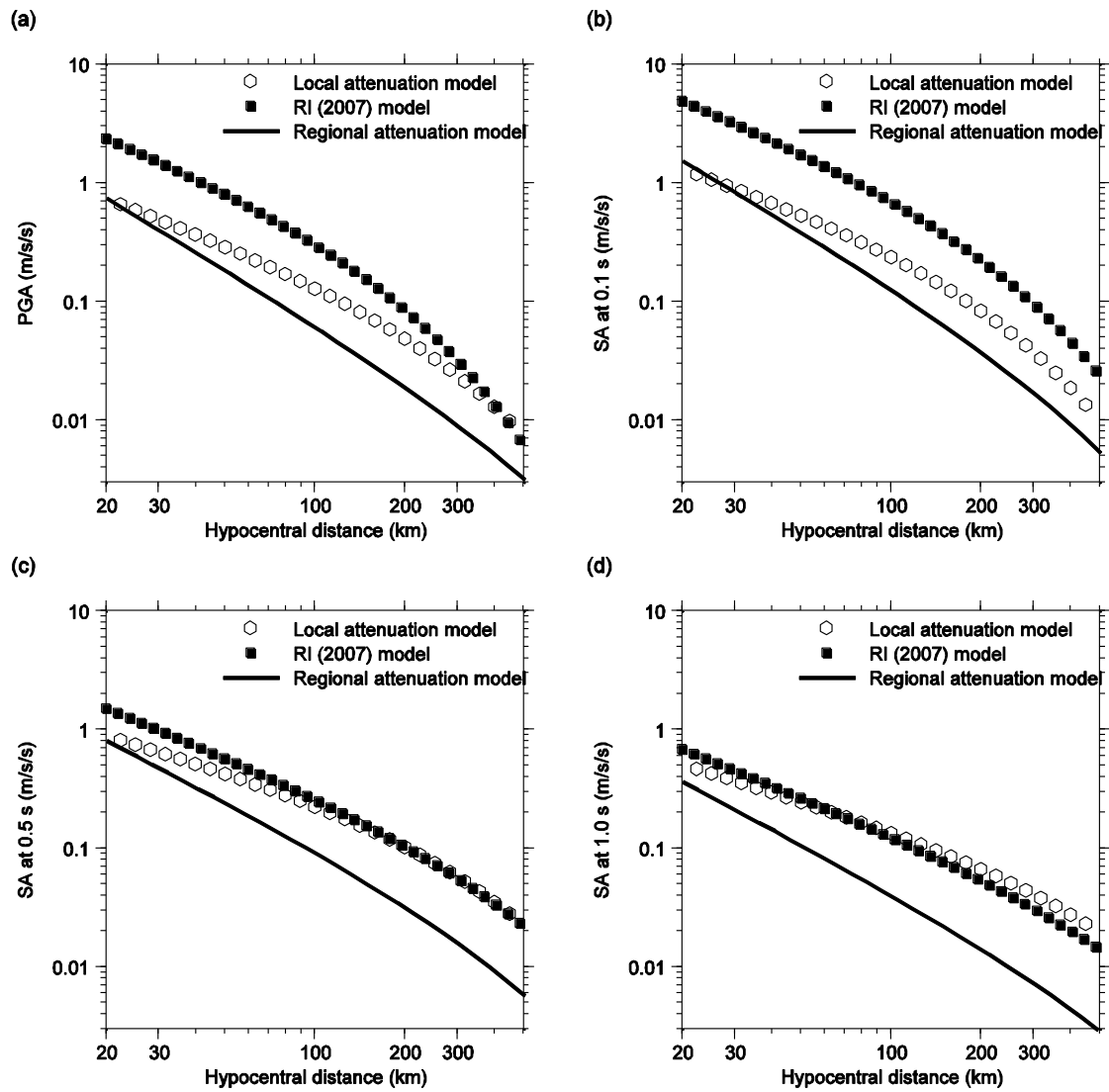


Figure 8.9 Comparison of attenuation models used in the study. Raghu Kanth and Iyengar's (2007) model shows predicting higher ground motions (especially for PGA and SA at 0.1 s) than predictions by the attenuation models derived in Chapter 7 for the Sri Lankan region. Predictions are for an M_w 6.0 shallow crustal earthquake. (a) PGA. (b) SA at 0.1 s. (c) SA at 0.5 s. (d) SA at 1.0 s.

8.4 Summary and conclusion

An assessment of seismic hazard based on a probabilistic approach is carried out for Sri Lanka which is located in an intraplate region of northern Indian Ocean. A catalog of events spanning since 1507 is prepared in a comprehensive manner using several available data sources of both historical and instrumental data. The catalog is sufficiently cleaned for dependent events and is unified into a single magnitude scale using available relationships in the literature. Seismic source zones in the study are defined giving emphasis on potential seismogenic features and attenuation characteristics identified in the subject region. A large area of active seismicity undergoing diffuse deformation located in the northern Indian Ocean towards south southeast of Sri Lanka, impelled

to define into a single large area source (source zone 1), whereas other neighboring oceanic crusts of both of the eastern and western sides of the country are assigned as separate area sources given the mild seismicity of these regions (source zones 2 and 4). Southern part of peninsular India located northward and northeastward from the country is categorized into a single area source (source zone 3) and is found to be richer in small and medium size earthquake activities than the other source zones. In the local context (within Sri Lanka), the area around Colombo is formulated as a small area source (source zone 6) considering both the historical seismicity and socio-economic prominence of the place due to being the capital city, whilst the rest of other area in the country is taken as a low seismic area source - source zone 5. Earthquake recurrence parameters of the source zones are obtained for pre-estimated periods of completeness unless otherwise data of a given source zone are lacking due to insufficient earthquake records, in which case the recurrence parameters are found based on a subjective evaluation. Hazard values are estimated by appropriate application of previously developed twin attenuation models for the Sri Lankan region (local and regional) and using a regional model developed for Peninsular India region. Computed hazard values show that the area around Colombo possesses the maximum expected PGA (in rock sites) which is about 0.043g for a 475 year return period. Most of other areas indicate relatively small ground motion levels. The area towards the northern part of the country around Jaffna peninsula has also shown higher ground motions than in other areas, and this may be either due to the area's close location to southern peninsular India (source zone 3) or due to the attenuation model adopted in ground motion estimation for events in source zone 3, which gives higher predictions than the other models used in the study. The final level of seismic hazard of Sri Lanka implied by the present study's results would "generally agree" with conclusions of the previous studies, although some variations between values remain preserved.

9. Results, conclusions and further research

The work described in the dissertation aims to characterize the seismic-induced ground motion of Sri Lanka, which is considered to be essential for the ultimate purpose of developing a seismic code of practice for the country. The work contributes towards a state-of-the-art hazard study for the region by identification and classification of possible seismogenic sources in and around Sri Lanka, estimation of region-specific seismological properties of the subject area, development of ground motion attenuation models for the region, and seismic hazard computation for engineering applications. The project also manifests the successful use of the stochastic simulation technique for characterizing the expected ground motion in the absence of actual records sufficiently. Developed ground motion attenuation models are of significant importance, especially in the estimation of an accurate hazard level for Sri Lanka, and will also be greatly beneficial for future seismological and engineering studies that would require application of own attenuation models exclusively developed for the region. Seismological parameters derived for the region and certain new techniques developed (e.g., regression technique developed in the estimation of Kappa value) in deriving these parameters, would cater a newer research contribution to the field of seismology and earthquake engineering in both the local-Sri Lankan and international contexts. Developed hazard maps and design spectra would serve as a set of engineering guidelines to be adapted in seismic design criteria for the country. Estimated hazard values (PGA and SAs) are recommended to apply as “hazard factors” acquired based on “the design basis ground motion”, in estimating “the design base shear” for intended structures to be designed. Response spectra developed in the study, either as direct design spectra based on the probabilistic approach for some selected major cities or as stochastic predictions of hypothesized and historically prominent events, can be used as “the site-specific elastic design response spectrum” for relevant sites in the dynamic analysis procedures. These findings are also encouraged to devise in seismic vulnerability assessments of existing structures in the country, in which assessment parameters such as the base shear demand and drift demand can be determined using hazard values and response spectra derived in the thesis to compare with the limiting criteria assigned in codes of practice. Seismological parameters estimated for the northern Indian Oceanic crust and the subsequent data analysis would be helpful to enrich the ongoing scholarly discourse in the region in the global context. Therefore, the outcome of the study is a vital knowledge contribution in the seismology and earthquake engineering field of Sri Lanka as well as of other analogous intraplate regions with similar seismotectonic features.

9.1 Main results

The main results from the study are summarized as follows;

- Historical seismic activities reported within Sri Lanka clearly indicate the area around the Capital city – Colombo is capable of producing strong magnitude events. The rest of the country appears to be associated with low/mild seismic activities which are however correlated with certain tectonic features such as lineaments and faults, thrust/shear zones (e.g., Mahawelli shear zone) and tectonic movements of individual mini-plates.
- In the regional context, a large area of diffuse seismicity located south and southeast of Sri Lanka enclosing Ninetyeast ridge, has shown to be a dominant force among the regional sources in producing large magnitude shallow crustal earthquakes, and this area may render direct threats of strong events at the country's close proximity.
- Multiple linear regression analysis of recorded vertical component Fourier acceleration amplitudes yields the wave transmission quality factor Q for the northern Indian Ocean region surrounding Sri Lanka takes the form $Q = (389 \pm 2.35)f^{0.70 \pm 0.004}$. The average far-source geometric attenuation rate of the region is found to be $R^{-0.5}$, except at low frequencies (below about 2 Hz) for which slightly lower rates than the average are obtained. After considering the final compliance with actual records, the regional geometric attenuation factor to be applied at far-source distances can be collated as;

$$G = \frac{1}{55^{1.3}} \sqrt{\frac{120}{R}}, \quad R > 120 \text{ km}$$

- The average static stress drop values of regional earthquakes that occur in the northern Indian Ocean, are found to be 9.5 MPa (95 bars) and 16.0 MPa (160 bars) for m_b 4-5 and 5-6 magnitude bands, respectively. This indicates the region is associated with relatively high stress drop levels, as also shown in previous studies. The corner frequency approximately fall within 1.0 and 7.0 Hz for the selected dataset.
- Application of the standard single scattering model, which demands the decay rate of backscattered coda waves found at the tail part of seismograms, results the average local coda Q for the Sri Lankan continental crust to be in the form $Q = (301 \pm 17)f^{0.67 \pm 0.02}$. Resulted Q_0 of 301 seems to be somewhat a low value for a typical Precambrian crust which is composed of older and harder rock formations. However, a poor quality upper crustal layer seating on top of the older Precambrian crust, is susceptible for Sri Lanka as it is also evidenced from the resulted higher Kappa values and from CRUST2.0 information.
- The average Kappa, which parameterizes upper crustal attenuation, for the Sri Lankan region is found to be 0.041 ± 0.009 s based on analysis of moderate magnitude regional earthquake data reported in the surrounding oceanic crust, and the value is well comparable with findings

of the local study in which the average Kappa for the region is estimated as 0.04 ± 0.02 s based on analysis of local small magnitude events. The resulted higher Kappa values indicate the upper crust of the country is of poor quality in terms of wave transmission, and this may be due to presence of younger Sedimentary formations at the upper level of the crust (as supported by CRUST2.0 information) and/or due to abundance of bedrock fractures of the upper crust (from geological investigations). Nevertheless, average H/V ratio for the region observed close to unity in both of the local and regional studies, does not agree with Kappa estimations, and implies a negligible upper crustal amplification in effect.

- Source spectra of smaller magnitude events that occurred within Sri Lanka are compatible with Brune's model for lower average stress drop levels about 2-4 MPa (20-40 bars). However, source spectra of relatively higher magnitude events appear to be more comparable with higher average stress drops may be 10 MPa (100 bars) or more.
- The local attenuation model developed for the country predicts lower ground motion parameters than predictions by models developed for intraplate older crustal regions such as ENA and western Australian regions. Instead, the model exhibits close resemblance with ground motion models derived for active tectonic regions [e.g., Boore and Atkinson (2007) NGA model for WNA region and Idriss (2008) NGA model for shallow crustal earthquakes]. The developed regional attenuation model for the application at teleseismic distances in the northern Indian Ocean region, shows predicting lower amplitudes than that of models developed for subduction zone earthquakes (e.g., Youngs et al, 1997), however, this observation seems to be reasonable given the fact that subduction zone events are more susceptible to produce higher amplitudes than those of active tectonic events.
- The assessment of seismic hazard of Sri Lanka undertaken based on a probabilistic approach shows the area around Colombo possesses the maximum expected PGA (in rock sites) which is about $0.043g$ for a 475 year return period. Most of other areas indicate relatively small ground motion levels. Subsequent design spectra in terms of PSA for some of the selected major cities are also obtained. The maximum resulted PGA for Colombo is about one tenth of PGA resulted in a scenario modeling of the M_w 6.5 historical event by using a deterministic approach.

9.2 Future research

The present study of earthquake ground motion modeling for Sri Lanka is related to investigations of ground motion characteristics up to the bedrock level. However, it is a well-established idea that ground motions within subsoil which is resting on the bedrock, are also equally important to investigate for a complete hazard estimate. The effect of subsoil on the ground motion, estimated

as a “site amplification factor”, is commonly attributed by analyzing subsoil profile data using any appropriate method such as the equivalent linear method. Such analysis leading to a possible site classification to be used in ground motion estimations at soil sites in the region of interest, needs to be separately conducted using many soil profile data collected at various places in the region. Therefore, final ground motions expected at a soil site in the country, is required to be obtained based on both ground motions at rock sites as may be determined from the present study and the appropriate site amplification factor estimated using such a method.

It has given thoughts that the country’s national seismic network should be expanded. The present network, which consists only 3 broadband stations, may not be that sufficient for a complete characterization of seismological properties in the region. Particularly, some distinctive variations of the country’s bedrock characteristics are limited to be investigated using the present smaller network. For example, ground motion characteristics in northern and northwestern parts of the country that are composed of younger Mesozoic and Cenozoic sediments are not possible to examine with the present seismic network. Therefore, a much larger network to cover most parts of the country, or any relevant experimental field work that is useful for accurate characterization of ground motions in such areas would be worthwhile for future research.

References

- Abayakoon, S. B. S. (1996). "Seismic Risk Analysis of Sri Lanka." *Journal of the Geological Society of Sri Lanka*, 6, 65-72.
- Abercrombie, R. E. (1997). "Near-surface attenuation and site effects from comparison of surface and deep borehole recordings." *Bulletin of the Seismological Society of America*, 87(3), 731-744.
- Abercrombie, R. E. (1998). "A Summary of Attenuation Measurements from Borehole Recordings of Earthquakes: The 10 Hz Transition Problem." *Pure and Applied Geophysics*, 153(2-4), 475-487.
- Abercrombie, R. E., Antolik, M., and Ekström, G. (2003). "The June 2000 Mw 7.9 earthquakes south of Sumatra: Deformation in the India–Australia Plate." *Journal of Geophysical Research: Solid Earth*, 108(B1), 2003.
- Abrahamson, N., and Silva, W. (2008). "Summary of the Abrahamson & Silva NGA Ground-Motion Relations." *Earthquake Spectra*, 24(1), 67-97.
- Abrahamson, N. A., and Silva, W. J. (1997). "Empirical Response Spectral Attenuation Relations for Shallow Crustal Earthquakes." *Seismological Research Letters*, 68(1), 94-127.
- Aki, K. (1967). "Scaling law of seismic spectrum." *Journal of Geophysical Research*, 72(4), 1217-1231.
- Aki, K. (1968). "Seismic displacements near a fault." *Journal of Geophysical Research*, 73(16), 5359-5376.
- Aki, K. (1969). "Analysis of the seismic coda of local earthquakes as scattered waves." *Journal of Geophysical Research*, 74(2), 615-631.
- Aki, K. (1987). "Magnitude-frequency relation for small earthquakes: A clue to the origin of f_{max} of large earthquakes." *Journal of Geophysical Research: Solid Earth*, 92(B2), 1349-1355.
- Aki, K., and Chouet, B. (1975). "Origin of coda waves: Source, attenuation, and scattering effects." *Journal of Geophysical Research*, 80(23), 3322-3342.
- Allen, T. I., Cummins, P. R., Dhu, T., and Schneider, J. F. (2007). "Attenuation of Ground-Motion Spectral Amplitudes in Southeastern Australia." *Bulletin of the Seismological Society of America*, 97(4), 1279-1292.
- Allen, T. I., Dhu, T., Cummins, P. R., and Schneider, J. F. (2006). "Empirical Attenuation of Ground-Motion Spectral Amplitudes in Southwestern Western Australia." *Bulletin of the Seismological Society of America*, 96(2), 572-585.
- Allmann, B. P. (2008). "Earthquake rupture imaging and multiscale stress drop estimation." *PhD thesis*, University of California, San Diego.
- Ammon, C. J., Ji, C., Thio, H.-K., Robinson, D., Ni, S., Hjorleifsdottir, V., Kanamori, H., Lay, T., Das, S., Helmberger, D., Ichinose, G., Polet, J., and Wald, D. (2005). "Rupture Process of the 2004 Sumatra-Andaman Earthquake." *SCIENCE*, 308(5725), 1133-1139.
- Anderson, J. G. (1986). "Implication of attenuation for studies of the earthquake source." *Earthquake Source Mechanics*, 311-318.
- Anderson, J. G. (1991). "A preliminary descriptive model for the distance dependence of the spectral decay parameter in southern California." *Bulletin of the Seismological Society of America*, 81(6), 2186-2193.

- Anderson, J. G., and Hough, S. E. (1984). "A model for the shape of the fourier amplitude spectrum of acceleration at high frequencies." *Bulletin of the Seismological Society of America*, 74(5), 1969-1993.
- AS 1170.4: 2007 Structural design actions Part 4: Earthquake actions in Australia. Standards Australia, Australia.
- Atkinson, G. M. (1993a). "Earthquake source spectra in eastern North America." *Bulletin of the Seismological Society of America*, 83(6), 1778-1798.
- Atkinson, G. M. (1993b). "Notes on ground motion parameters for eastern north America: Duration and H/V ratio." *Bulletin of the Seismological Society of America*, 83(2), 587-596.
- Atkinson, G. M. (1996). "The high-frequency shape of the source spectrum for earthquakes in eastern and western Canada." *Bulletin of the Seismological Society of America*, 86(1A), 106-112.
- Atkinson, G. M. (2004a). "An overview of developments in seismic hazard analysis." *13th World Conference on Earthquake Engineering*, Vancouver, B.C., Canada.
- Atkinson, G. M. (2004b). "Empirical Attenuation of Ground-Motion Spectral Amplitudes in Southeastern Canada and the Northeastern United States." *Bulletin of the Seismological Society of America*, 94(6), 2419-2423.
- Atkinson, G. M. (2005). "Ground Motions for Earthquakes in Southwestern British Columbia and Northwestern Washington: Crustal, In-Slab, and Offshore Events." *Bulletin of the Seismological Society of America*, 95(3), 1027-1044.
- Atkinson, G. M., and Boore, D. M. (1995). "Ground-motion relations for eastern North America." *Bulletin of the Seismological Society of America*, 85(1), 17-30.
- Atkinson, G. M., and Boore, D. M. (1998). "Evaluation of models for earthquake source spectra in eastern North America." *Bulletin of the Seismological Society of America*, 88(4), 917-934.
- Atkinson, G. M., and Boore, D. M. (2003). "Empirical Ground-Motion Relations for Subduction-Zone Earthquakes and Their Application to Cascadia and Other Regions." *Bulletin of the Seismological Society of America*, 93(4), 1703-1729.
- Atkinson, G. M., and Boore, D. M. (2006). "Earthquake Ground-Motion Prediction Equations for Eastern North America." *Bulletin of the Seismological Society of America*, 96(6), 2181-2205.
- Atkinson, G. M., and Cassidy, J. F. (2000). "Integrated Use of Seismograph and Strong-Motion Data to Determine Soil Amplification: Response of the Fraser River Delta to the Duvall and Georgia Strait Earthquakes." *Bulletin of the Seismological Society of America*, 90(4), 1028-1040.
- Atkinson, G. M., and Mereu, R. F. (1992). "The shape of ground motion attenuation curves in southeastern Canada." *Bulletin of the Seismological Society of America*, 82(5), 2014-2031.
- Atkinson, G. M., and Silva, W. (1997). "An empirical study of earthquake source spectra for California earthquakes." *Bulletin of the Seismological Society of America*, 87(1), 97-113.
- Atkinson, G. M., and Silva, W. (2000). "Stochastic Modeling of California Ground Motions." *Bulletin of the Seismological Society of America*, 90(2), 255-274.
- Atkinson, G. M., and Somerville, P. G. (1994). "Calibration of time history simulation methods." *Bulletin of the Seismological Society of America*, 84(2), 400-414.

- Balendra, T., Lam, N. T. K., Wilson, J. L., and Kong, K. H. (2002). "Analysis of long-distance earthquake tremors and base shear demand for buildings in Singapore." *Engineering Structures*, 24(1), 99-108.
- Barber, A. J. (2000). "Geological Map of Central and Western Sri Lanka: Provisional Series 1997 — scale 1:250,000, and seven 1:100,000 map sheets. Geological Survey and Mines Bureau, Sri Lanka, and the British Geological Survey. US\$10.00+postage." *Journal of Asian Earth Sciences*, 18(4), 509-512.
- Baur, N., Kröner, A., Liew, T. C., Todt, W., Williams, I. S., and Hofmann, A. W. (1991). "U-Pb Isotopic Systematics of Zircons from Prograde and Retrograde Transition Zones in High-Grade Orthogneisses, Sri Lanka." *Journal of Geology*, 99(4), 527-545.
- Ben-Menahem, A. (1961). "Radiation of seismic surface-waves from finite moving sources." *Bulletin of the Seismological Society of America*, 51(3), 401-435.
- Ben-Menahem, A. (1962). "Radiation of seismic body waves from a finite moving source in the Earth." *Journal of Geophysical Research*, 67(1), 345-350.
- Beresnev, I. A., and Atkinson, G. M. (1997). "Modeling finite-fault radiation from the ω spectrum." *Bulletin of the Seismological Society of America*, 87(1), 67-84.
- Beresnev, I. A., and Atkinson, G. M. (1998). "Stochastic finite-fault modeling of ground motions from the 1994 Northridge, California, earthquake. I. Validation on rock sites." *Bulletin of the Seismological Society of America*, 88(6), 1392-1401.
- Beresnev, I. A., and Atkinson, G. M. (2002). "Source Parameters of Earthquakes in Eastern and Western North America Based on Finite-Fault Modeling." *Bulletin of the Seismological Society of America*, 92(2), 695-710.
- Bergman, E. A., and Solomon, S. C. (1985). "Earthquake source mechanisms from body-waveform inversion and intraplate tectonics in the northern Indian Ocean." *Physics of the Earth and Planetary Interiors*, 40(1), 1-23.
- Boatwright, J. (1980). "A spectral theory for circular seismic sources; simple estimates of source dimension, dynamic stress drop, and radiated seismic energy." *Bulletin of the Seismological Society of America*, 70(1), 1-27.
- Boatwright, J., and Choy, G. L. (1992). "Acceleration source spectra anticipated for large earthquakes in northeastern North America." *Bulletin of the Seismological Society of America*, 82(2), 660-682.
- Boore, D. M. (1983). "Stochastic simulation of high-frequency ground motions based on seismological models of the radiated spectra." *Bulletin of the Seismological Society of America*, 73(6A), 1865-1894.
- Boore, D. M. (1986). "Short-period P- and S-wave radiation from large earthquakes: Implications for spectral scaling relations." *Bulletin of the Seismological Society of America*, 76(1), 43-64.
- Boore, D. M. (2003). "Simulation of Ground Motion Using the Stochastic Method." *Pure and Applied Geophysics*, 160(3-4), 635-676.
- Boore, D. M. (2008, revised 2012). "TSPP; a collection of FORTRAN programs for processing and manipulating time series." *Open-File Report 2008-1111*, U.S. Geological Survey.
- Boore, D. M. (2009). "Comparing Stochastic Point-Source and Finite-Source Ground-Motion Simulations: SMSIM and EXSIM." *Bulletin of the Seismological Society of America*, 99(6), 3202-3216.

- Boore, D. M., and Atkinson, G. M. (1987). "Stochastic prediction of ground motion and spectral response parameters at hard-rock sites in eastern North America." *Bulletin of the Seismological Society of America*, 77(2), 440-467.
- Boore, D. M., and Atkinson, G. M. (2007). "Boore-Atkinson NGA Ground Motion Relations for the Geometric Mean Horizontal Component of Peak and Spectral Ground Motion Parameters." Pacific Earthquake Engineering Research Center.
- Boore, D. M., and Atkinson, G. M. (2008). "Ground-Motion Prediction Equations for the Average Horizontal Component of PGA, PGV, and 5%-Damped PSA at Spectral Periods between 0.01 s and 10.0 s." *Earthquake Spectra*, 24(1), 99-138.
- Boore, D. M., and Joyner, W. B. (1997). "Site amplifications for generic rock sites." *Bulletin of the Seismological Society of America*, 87(2), 327-341.
- Boore, D. M., Joyner, W. B., and Fumal, T. E. (1997). "Equations for Estimating Horizontal Response Spectra and Peak Acceleration from Western North American Earthquakes: A Summary of Recent Work." *Seismological Research Letters*, 68(1), 128-153.
- Brillinger, D. R., and Preisler, H. K. (1984). "An exploratory analysis of the Joyner-Boore attenuation data." *Bulletin of the Seismological Society of America*, 74(4), 1441-1450.
- Brillinger, D. R., and Preisler, H. K. (1985). "Further analysis of the Joyner-Boore attenuation data." *Bulletin of the Seismological Society of America*, 75(2), 611-614.
- Brune, J. N. (1970). "Tectonic stress and the spectra of seismic shear waves from earthquakes." *Journal of Geophysical Research*, 75(26), 4997-5009.
- Brune, J. N. (1971). "Correction." *Journal of Geophysical Research*, 76, 5002.
- Büchel, G. (1994). "Gravity, magnetic and structural patterns at the deep-crustal plate boundary zone between West- and East-Gondwana in Sri Lanka." *Precambrian Research*, 66(1-4), 77-91.
- Burridge, R., and Knopoff, L. (1964). "Body force equivalents for seismic dislocations." *Bulletin of the Seismological Society of America*, 54(6A), 1875-1888.
- Campbell, K. W. (2003). "Prediction of Strong Ground Motion Using the Hybrid Empirical Method and Its Use in the Development of Ground-Motion (Attenuation) Relations in Eastern North America." *Bulletin of the Seismological Society of America*, 93(3), 1012-1033.
- Campbell, K. W., and Bozorgnia, Y. (2008). "NGA Ground Motion Model for the Geometric Mean Horizontal Component of PGA, PGV, PGD and 5% Damped Linear Elastic Response Spectra for Periods Ranging from 0.01 to 10 s." *Earthquake Spectra*, 24(1), 139-171.
- Campbell, K. W., and Bozorgnia, Y. (2012). "2012 Update of the Campbell-Bozorgnia NGA Ground Motion Prediction Equations: A Progress Report" *the 15th World Conference on Earthquake Engineering*, Lisbon, Portugal.
- Campbell, K. W., Hashash, Y. M. A., Kim, B., Kottke, A. R., Rathje, E. M., Silva, W., and Stewart, J. P. (2014). "Reference-Rock Site Conditions for Central and Eastern North America: Part II-Attenuation (Kappa) Definition." Pacific Earthquake Engineering Research Center, University of California, Berkeley.
- Campillo, M. (1990). "Propagation and attenuation characteristics of the crustal phase L_g ." *Pure and applied geophysics*, 132(1-2), 1-19.
- Castro, R. R., Anderson, J. G., and Singh, S. K. (1990). "Site response, attenuation and source spectra of S waves along the Guerrero, Mexico, subduction zone." *Bulletin of the Seismological Society of America*, 80(6A), 1481-1503.

- Chandler, A., and Lam, N. (2004). "An attenuation model for distant earthquakes." *Earthquake Engineering & Structural Dynamics*, 33(2), 183-210.
- Chandler, A., Lam, N., Wilson, J., and Hutchinson, G. (2001). "Response spectrum modelling for regions lacking earthquake records." *Electronic Journal of Structural Engineering*, 1(1), 2-14.
- Chandler, A. M., Lam, N. T. K., and Tsang, H. H. (2005). "Shear wave velocity modelling in crustal rock for seismic hazard analysis." *Soil Dynamics and Earthquake Engineering*, 25(2), 167-185.
- Chandler, A. M., Lam, N. T. K., and Tsang, H. H. (2006). "Near-surface attenuation modelling based on rock shear-wave velocity profile." *Soil Dynamics and Earthquake Engineering*, 26, 1004-1014.
- Chandra, U. (1977). "Earthquakes of peninsular India—a seismotectonic study." *Bulletin of the Seismological Society of America*, 67(5), 1387-1413.
- Chen, S.-z., and Atkinson, G. M. (2002). "Global Comparisons of Earthquake Source Spectra." *Bulletin of the Seismological Society of America*, 92(3), 885-895.
- Choy, G. L., and Boatwright, J. L. (1995). "Global patterns of radiated seismic energy and apparent stress." *Journal of Geophysical Research: Solid Earth*, 100(B9), 18205-18228.
- Choy, G. L., and McGarr, A. (2002). "Strike-slip earthquakes in the oceanic lithosphere: observations of exceptionally high apparent stress." *Geophysical Journal International*, 150(2), 506-523.
- Cloetingh, S., and Wortel, R. (1986). "Stress in the Indo-Australian plate." *Tectonophysics*, 132(1-3), 49-67.
- Cooray, P. G. (1994). "The Precambrian of Sri Lanka: a historical review." *Precambrian Research*, 66, 3-20.
- Coppersmith, K. J. (1981). "Probabilities of earthquake occurrence on the San Andreas Fault based on geologic risk." *EOS* 62
- Cornell, C. A. (1968). "Engineering seismic risk analysis." *Bulletin of the Seismological Society of America*, 58(5), 1583-1606.
- Cornell, C. A., and Winterstein, S. (1986). "Applicability of the Poisson earthquake-occurrence model." Electric Power Research Institute.
- Desa, M., Ramana, M. V., and Ramprasad, T. (2006). "Seafloor spreading magnetic anomalies south off Sri Lanka." *Marine Geology*, 229(3-4), 227-240.
- Dissanayake, C. B. (2005). "A new plate boundary near Sri Lanka: Implications for future geohazards." *Journal of National Science Foundation Sri Lanka*, 33(1), 5-8.
- Dissanayake, C. B., and Munasinghe, T. (1984). "Reconstruction of the Precambrian sedimentary basin in the granulite belt of Sri Lanka." *Chemical Geology*, 47(3-4), 221-247.
- Esteva, L. (1970a). "Seismic risk and seismic design", in R. J. Hansen, (ed.), *Seismic Design for Nuclear Power Plants*. The M.I.T. Press.
- Esteva, L. (1970b). "Seismic risk and seismic design decisions." Massachusetts Institute of Technology, Cambridge. University of Mexico, Mexico City.
- Eurocode 8—Design of Structures for earthquake resistance—Part 1: General rules, seismic actions and rules for buildings (1998). de Normalisation, Comité Européen. European Standard NF EN, 1.

- Faust, L. (1951). "Seismic velocity as a function of depth and geologic time." *Geophysics*, 16(2), 192-206.
- Fernando, M. J., and Kulasinghe, A. N. S. (1986). "Seismicity of Sri Lanka." *Physics of the Earth and Planetary Interiors*, 44(2), 99-106.
- Frankel, A. (1995). "Simulating strong motions of large earthquakes using recordings of small earthquakes: the Loma Prieta mainshock as a test case." *Bulletin of the Seismological Society of America*, 85(4), 1144-1160.
- Gamage, P., and Venkatesan, S. "Seismic risk analysis based on historical events reported in Sri Lanka." *Presented at 22nd Australasian Conference on the Mechanics of Structures and Materials, ACMSM22*, Sydney, Australia.
- Gamage, P., and Venkatesan, S. (2012b). "Estimation of Lg-coda Q value for the Northern Indian Ocean region based on spectral analysis." *Australian Earthquake Engineering Society Conference*, Gold Coast, Australia.
- Gamage, P., Venkatesan, S., and Dissanayake, P. B. R. (2013). "Local seismicity and possible ground motion parameters for Sri Lanka." *4th International Conference on Structural Engineering & Construction Management (ICSECM - 2013)*, Kandy, Sri Lanka.
- Gamage, P., Venkatesan, S., and Dissanayake, R. "Seismic drift demand on multi-storey buildings in Sri Lanka due to long-distant earthquakes." *Presented at International Conference on Structural Engineering, Construction and Management, ICSECM 2011*, Kandy, Sri Lanka.
- Gangrade, B. K., and Arora, S. K. (2000). "Seismicity of the Indian Peninsular Shield from Regional Earthquake Data." *Pure and applied geophysics*, 157(10), 1683-1705.
- Gao, L. S., Lee, L. C., Biswas, N. N., and Aki, K. (1983). "Comparison of the effects between single and multiple scattering on coda waves for local earthquakes." *Bulletin of the Seismological Society of America*, 73(2), 377-389.
- Gardner, J. K., and Knopoff, L. (1974). "Is the sequence of earthquakes in Southern California, with aftershocks removed, Poissonian?" *Bulletin of the Seismological Society of America*, 64(5), 1363-1367.
- Grünthal, G. "The up-dated earthquake catalogue for the German Democratic Republic and adjacent areas - statistical data characteristics and conclusions for hazard assessment." *Presented at 3rd Int. Symp. on the Analysis of Seismicity and Seismic Risk*, Liblice Castle, Czechoslovakia.
- Graves, R., and Pitarka, A. (2004). "Broadband time history simulation using a hybrid approach." *13th World Conference on Earthquake Engineering*. Vancouver, B.C., Canada.
- Greenhalgh, S. A., Denham, D., McDougall, R., and Rynn, J. M. W. (1988). "Magnitude-intensity relations for Australian earthquakes." *Bulletin of the Seismological Society of America*, 78(1), 374-379.
- Gusev, A. A. (1995). "Vertical profile of turbidity and coda Q." *Geophysical Journal International*, 123(3), 665-672.
- Gutenberg, B. (1936). "Periods of the Ground in Southern California Earthquakes." U.S.C.&G.S.
- Gutenberg, B., and Richter, C. F. (1954). "Seismicity of the Earth and Associated Phenomena." First edition. Princeton University Press, New Jersey.
- Gutenberg, B., and Richter, C. F. (1956). "Earthquake magnitude, intensity, energy, and acceleration: (Second paper)." *Bulletin of the Seismological Society of America*, 46(2), 105-145.

- Haddon, R. A. W. (1996). "Earthquake source spectra in eastern North America." *Bulletin of the Seismological Society of America*, 86(5), 1300-1313.
- Hanks, T. C. (1979). "b values and $\omega - \gamma$ seismic source models: Implications for tectonic stress variations along active crustal fault zones and the estimation of high-frequency strong ground motion." *Journal of Geophysical Research: Solid Earth (1978–2012)*, 84(B5), 2235-2242.
- Hanks, T. C. (1982). "fmax." *Bulletin of the Seismological Society of America*, 72(6A), 1867-1879.
- Hanks, T. C., and Kanamori, H. (1979). "A moment magnitude scale." *Journal of Geophysical Research: Solid Earth*, 84(B5), 2348-2350.
- Hanks, T. C., and McGuire, R. K. (1981). "The character of high-frequency strong ground motion." *Bulletin of the Seismological Society of America*, 71(6), 2071-2095.
- Hartzell, S., Harmsen, S., Frankel, A., and Larsen, S. (1999). "Calculation of broadband time histories of ground motion: Comparison of methods and validation using strong-ground motion from the 1994 Northridge earthquake." *Bulletin of the Seismological Society of America*, 89(6), 1484-1504.
- Hartzell, S. H. (1978). "Earthquake aftershocks as Green's functions." *Geophysical Research Letters*, 5(1), 1-4.
- Hartzell, S. H., and Heaton, T. H. (1985). "Teleseismic time functions for large, shallow subduction zone earthquakes." *Bulletin of the Seismological Society of America*, 75(4), 965-1004.
- Haskell, N. A. (1964). "Total energy and energy spectral density of elastic wave radiation from propagating faults." *Bulletin of the Seismological Society of America*, 54(6A), 1811-1841.
- Haskell, N. A. (1966). "Total energy and energy spectral density of elastic wave radiation from propagating faults. Part II. A statistical source model." *Bulletin of the Seismological Society of America*, 56(1), 125-140.
- Haskell, N. A. (1969). "Elastic displacements in the near-field of a propagating fault." *Bulletin of the Seismological Society of America*, 59(2), 865-908.
- Hatherton, T., Pattiaratchi, D. B., and Ranasinghe, V. V. C. (1975). "Gravity Map of Sri Lanka 1 : 1,000,000." *Professional Paper No. 3*, Geological Survey Dept. and Govt. New Zealand. pp. 1-37.
- Havskov, J., Malone, S., McClurg, D., and Crosson, R. (1989). "Coda Q for the state of Washington." *Bulletin of the Seismological Society of America*, 79(4), 1024-1038.
- Havskov, J., and Ottemøller, L. (2012). "SEISAN: The Earthquake Analysis Software for Windows, Solaris and Linux, Version 8.0", U. o. B. Institute of Solid Earth Physics, Norway.
- Havskov, J., and Ottemøller, L. (2010). "Routine Data Processing in Earthquake Seismology With Sample Data, Exercises and Software." Springer.
- Herrmann, R. B. (1980). "Q estimates using the coda of local earthquake." *Bulletin of the Seismological Society of America*, 70(2), 447-468.
- Herrmann, R. B., and Kijko, A. (1983). "Modeling some empirical vertical component Lg relations." *Bulletin of the Seismological Society of America*, 73(1), 157-171.
- Hong, T.-K. (2010). "Lg Attenuation in a Region with Both Continental and Oceanic Environments." *Bulletin of the Seismological Society of America*, 100(2), 851-858.
- Hoshiya, M. (1993). "Separation of scattering attenuation and intrinsic absorption in Japan using the multiple lapse time window analysis of full seismogram envelope." *Journal of Geophysical Research: Solid Earth*, 98(B9), 15809-15824.

- Hudson, M., Idriss, I. M., and Beikae, M. (1994). "User's manual for QUAD4M-A computer program to evaluate the seismic response of soil structures using finite element procedures and incorporating a compliant base." Centre for Geotechnical Modelling, Department of Civil and Environmental Engineering, University of California, Davis, California.
- Idriss, I., and Sun, J. (1992). "SHAKE91-A computer program for conducting equivalent linear seismic response analyses of horizontally layered soil deposits". Centre for Geotechnical Modelling, Department of Civil and Environmental Engineering, University of California, Davis, California.
- Idriss, I. M. (2008). "An NGA Empirical Model for Estimating the Horizontal Spectral Values Generated By Shallow Crustal Earthquakes." *Earthquake Spectra*, 24(1), 217-242.
- International Building Code (2006 edition). International Code Council, USA.
- IS: 1893 Part 1 (2002). "Indian standard, criteria for earthquake resistance design of structures." Fifth Revision, Bureau of Indian Standards, New Delhi.
- Irikura, K. (1983). "Semi-empirical estimation of strong ground motions during large earthquakes." *Bulletin of the Disaster Prevention Research Institute*, 33(Part 2, No 298), 63-104.
- Irikura, K. (1986). "Prediction of strong acceleration motions using empirical Green's function." *Proceedings of the 7th Japan Earthquake Engineering Symposium*, Tokyo, Japan. pp. 151-156.
- Irikura, K., Kagawa, T., and Sekiguchi, H. (1997). "Revision of the empirical Green's function method." *PROGRAMME and ABSTRACTS*, Seismological Society of Japan, 2, B25 (in Japanese).
- Irikura, K., and Kamae, K. (1994). "Simulation of strong ground motion based on fractal composite faulting model and empirical Green's function." *Proceedings of the 9th Japan Earthquake Engineering Symposium*, Tokyo, Japan.
- Jaiswal, K., and Sinha, R. (2007). "Probabilistic Seismic-Hazard Estimation for Peninsular India." *Bulletin of the Seismological Society of America*, 97(1B), 318-330.
- Jayawardena, U. d. S. (2001). "A Study of the Engineering Properties of Sri Lankan Rocks." *Engineer, Journal of Institution of Engineers*, XXXIV(2), 7-20.
- Jin, A., and Aki, K. (1988). "Spatial and temporal correlation between coda Q and seismicity in China." *Bulletin of the Seismological Society of America*, 78(2), 741-769.
- Jin, A., Cao, T., and Aki, K. (1985). "Regional change of coda Q in the oceanic lithosphere." *Journal of Geophysical Research: Solid Earth*, 90(B10), 8651-8659.
- Johnson, R. A. (1973). "An earthquake spectrum prediction technique." *Bulletin of the Seismological Society of America*, 63(4), 1255-1274.
- Johnston, A. C. (1996). "Seismic moment assessment of earthquakes in stable continental regions—I. Instrumental seismicity." *Geophysical Journal International*, 124(2), 381-414.
- Joyner, W. B. (1984). "A scaling law for the spectra of large earthquakes." *Bulletin of the Seismological Society of America*, 74(4), 1167-1188.
- Joyner, W. B. (1997). "Ground motion estimates for the northeastern U.S. or southeastern Canada." *U.S. Nuclear Reg. Comm. Rept. NUREG/CR-6372*, Washington, D.C.
- Joyner, W. B. (2000). "Strong Motion from Surface Waves in Deep Sedimentary Basins." *Bulletin of the Seismological Society of America*, 90(6B), S95-S112.

- Joyner, W. B., and Boore, D. M. (1981). "Peak horizontal acceleration and velocity from strong-motion records including records from the 1979 imperial valley, California, earthquake." *Bulletin of the Seismological Society of America*, 71(6), 2011-2038.
- Joyner, W. B., and Boore, D. M. (1993). "Methods for regression analysis of strong-motion data." *Bulletin of the Seismological Society of America*, 83(2), 469-487.
- Joyner, W. B., Warrick, R. E., and Fumal, T. E. (1981). "The effect of quaternary alluvium on strong ground motion in the Coyote Lake, California, earthquake of 1979." *Bulletin of the Seismological Society of America*, 71(4), 1333-1349.
- Kanai, K. (1957). "Semi-empirical Formula for the Seismic Characteristics of the Ground." *Bulletin of the Earthquake Research Institute, University of Tokyo*, 35, 309-324.
- Kanamori, H., and Anderson, D. L. (1975). "Theoretical basis of some empirical relations in seismology." *Bulletin of the Seismological Society of America*, 65(5), 1073-1095.
- Kehelpannala, K. (2004). "Arc accretion around Sri Lanka during the assembly of Gondwana." *Gondwana Research*, 7(4S), 41-46.
- Kehelpannala, K. V. W. (1987). "The structure, tectonics and hydrogeology of lineaments of Sri Lanka with special reference to the Central Highland." *M. Phil. Thesis*, University of Peradeniya, Peradeniya, Sri Lanka.
- Kehelpannala, K. V. W. "Structural evolution of high-grade terrain in Sri Lanka with special reference to the Arenas around Dodangaslanda and Kandy." *Presented at The crystalline crust of Sri Lanka, Part I, Summary of Research of the German-Sri Lankan Consortium*, Geological Survey Dept. Sri Lanka.
- Kehelpannala, K. V. W. (2007). "Seismicity and Earthquakes (of Sri Lanka)", *National Atlas of Sri Lanka*. Survey Department of Sri Lanka, pp. 20-23.
- Kehelpannala, K. V. W., and Ranaweera, L. (2007). "Structural and kinematic evolution of a possible Pan-African suture zone in Sri Lanka", N. Osanai, T. Miyamoto, and M. Santosh, (eds.), *4th International Symposium on Gondwana to Asia and IAGR Annual Convention*, International Association for Gondwana Research Conference Series, pp. 83-88.
- Kehelpannala, K. V. W., Wada, H., Hamana, N., and Ranaweera, L. (2006). "Cataclastic rocks from the granulite terrain of Sri Lanka: evidence for younger brittle deformation of the exhumed lower crust." *Geoscience reports of Shizuoka University*, 33, 9-19.
- Kennett, B. L. N. (1985). "On regional S." *Bulletin of the Seismological Society of America*, 75(4), 1077-1086.
- Kennett, B. L. N. (1986). "Lg waves and structural boundaries." *Bulletin of the Seismological Society of America*, 76(4), 1133-1141.
- Kiremidjian, A. S., and Anagnos, T. (1984). "Stochastic slip-predictable model for earthquake occurrences." *Bulletin of the Seismological Society of America*, 74(2), 739-755.
- Kleinschrodt, R. (1994). "Large-scale thrusting in the lower crustal basement of Sri Lanka." *Precambrian Research*, 66(1-4), 39-57.
- Kleinschrodt, R. (1996). "Strain localization and large-scale block rotation in the lower continental crust, Kataragama area, Sri Lanka." *Terra Nova*, 8(3), 236-244.
- Knopoff, L., Mitchel, R. G., Kausel, E. G., and Schwab, F. (1979). "A search for the oceanic Lg phase." *Geophysical Journal International*, 56(1), 211-218.
- Kopnichev, Y. F. (1975). "A model of generation of the tail of the seismogram." *Doklady Earth Science Sections*, 222, 13-15.

- Kostrov, B. V. (1964). "Selfsimilar problems of propagation of shear cracks." *Journal of Applied Mathematics and Mechanics*, 28(5), 1077-1087.
- Krahn, J. (2004). "Dynamic Modeling with QUAKE/W an Engineering Methodology." GEO-SLOPE International Ltd, Canada.
- Kramer, S. L. (1996). "Geotechnical Earthquake Engineering" Prentice Hall.
- Kröner, A. (1986). "Composition, structure, and evolution of the early Precambrian lower continental crust: constraints from geological observations and age relationships." *American Geophysical Union, Geodynamics Series*, 14, 107-119.
- Kroner, A., and Brown, L. (2005). "Structure, Composition and Evolution of the South Indian and Sri Lankan Granulite Terrains from Deep Seismic Profiling and Other eophysical and Geological Investigations: A LEGENDS Initiative." *Gondwana Research*, 8(3), 317-335.
- Kröner, A., Rojas-Agramonte, Y., Kehelpannala, K. V. W., Zack, T., Hegner, E., Geng, H. Y., Wong, J., and Barth, M. (2013). "Age, Nd-Hf isotopes, and geochemistry of the Vijayan Complex of eastern and southern Sri Lanka: A Grenville-age magmatic arc of unknown derivation." *Precambrian Research*, 234(0), 288-321.
- Kröner, A., and Williams, I. S. (1993). "Age of Metamorphism in the High-Grade Rocks of Sri Lanka." *Journal of Geology*, 101(4), 513-521.
- Kulkarni, R. B., Youngs, R. R., and Coppersmith, K. J. "Assessment of confidence intervals for results of seismic hazard analysis." *Presented at the 8th World Conference on Earthquake Engineering*, San Francisco.
- Kvamme, L. B., Hansen, R. A., and Bungum, H. (1995). "Seismic-source and wave-propagation effects of Lg waves in Scandinavia." *Geophysical Journal International*, 120(3), 525-536.
- Kvamme, L. B., and Havskov, J. (1989). "Q in southern Norway." *Bulletin of the Seismological Society of America*, 79(5), 1575-1588.
- Lam, N., Wilson, J., Chandler, A., and Hutchinson, G. (2000a). "Response spectral relationships for rock sites derived from the component attenuation model." *Earthquake Engineering & Structural Dynamics*, 29(10), 1457-1489.
- Lam, N., Wilson, J., Chandler, A., and Hutchinson, G. (2000c). "Response spectrum modelling for rock sites in low and moderate seismicity regions combining velocity, displacement and acceleration predictions." *Earthquake Engineering & Structural Dynamics*, 29(10), 1491-1525.
- Lam, N., Wilson, J., and Hutchinson, G. (2000b). "Generation of synthetic earthquake accelerograms using seismological modelling: A review." *Journal of Earthquake Engineering*, 4(3), 321-354.
- Lam, N. T. K. (1999). "Program "GENQKE" User's Guide-Program for generating synthetic earthquake accelerograms based on stochastic simulations of seismological models". Department of Civil and Environmental Engineering, The University of Melbourne, Australia.
- Lam, N. T. K., Balendra, T., Wilson, J. L., and Venkatesan, S. (2009). "Seismic load estimates of distant subduction earthquakes affecting Singapore." *Engineering Structures*, 31(5), 1230-1240.
- Lam, N. T. K., Chandler, A. M., and Tsang, H. H. (2006). "Regional and local factors in attenuation modelling: Hong Kong case study." *Journal of Asian Earth Sciences*, 27, 892-906.
- Lam, N. T. K., Chandler, A. M., Wilson, J. L., and Hutchinson, G. L. (2002). "Response spectrum predictions for potential near-field and far-field earthquakes affecting Hong Kong: rock sites." *Soil Dynamics and Earthquake Engineering*, 22(1), 47-72.

- Leonard, M. (2008). "One Hundred Years of Earthquake Recording in Australia." *Bulletin of the Seismological Society of America*, 98(3), 1458-1470.
- Lermo, J., and Chávez-García, F. J. (1993). "Site effect evaluation using spectral ratios with only one station." *Bulletin of the Seismological Society of America*, 83(5), 1574-1594.
- Liu, C.-S., Sandwell, D. T., and Curray, J. R. (1982). "The negative gravity field over the 85°E ridge." *Journal of Geophysical Research: Solid Earth*, 87(B9), 7673-7686.
- Lomnitz-Adler, J., and Lomnitz, C. (1979). "A modified form of the Gutenberg-Richter magnitude-frequency relation." *Bulletin of the Seismological Society of America*, 69, 1209-1214.
- Madariaga, R. (1976). "Dynamics of an expanding circular fault." *Bulletin of the Seismological Society of America*, 66(3), 639-666.
- Madariaga, R. (1978). "The dynamic field of Haskell's rectangular dislocation fault model." *Bulletin of the Seismological Society of America*, 68(4), 869-887.
- Madariaga, R. (2007). "Seismic source theory", in H. Kanamori, (ed.), *Earthquake seismology*. Treatise of Geophysics, Academic Press.
- Magistrale, H., McLaughlin, K., and Day, S. (1996). "A geology-based 3D velocity model of the Los Angeles basin sediments." *Bulletin of the Seismological Society of America*, 86(4), 1161-1166.
- Mak, S., Chan, L. S., Chandler, A. M., and Koo, R. C. H. (2004). "Coda Q estimates in the Hong Kong Region." *Journal of Asian Earth Sciences*, 24(1), 127-136.
- Malagnini, L., Akinci, A., Herrmann, R. B., Pino, N. A., and Scognamiglio, L. (2002). "Characteristics of the Ground Motion in Northeastern Italy." *Bulletin of the Seismological Society of America*, 92, 2186–2204.
- Malagnini, L., Herrmann, R. B., and Di Bona, M. (2000b). "Ground-Motion Scaling in the Apennines (Italy)." *Bulletin of the Seismological Society of America*, 90(4), 1062-1081.
- Malagnini, L., Herrmann, R. B., and Koch, K. (2000a). "Regional Ground-Motion Scaling in Central Europe." *Bulletin of the Seismological Society of America*, 90(4), 1052-1061.
- Margaris, B. N., and Boore, D. M. (1998). "Determination of $\Delta\sigma$ and κ_0 from response spectra of large earthquakes in Greece." *Bulletin of the Seismological Society of America*, 88(1), 170-182.
- Martin, S., and Szeliga, W. (2010). "A Catalog of Felt Intensity Data for 570 Earthquakes in India from 1636 to 2009." *Bulletin of the Seismological Society of America*, 100(2), 562-569.
- Mathavan, V., Prame, W. K. B. N., and Cooray, P. G. (1999). "Geology of the High Grade Proterozoic Terrains of Sri Lanka, and the Assembly of Gondwana: an Update on Recent Developments." *Gondwana Research*, 2(2), 237-250.
- McGuire, R., and Arabasz, W. (1990). "An introduction to probabilistic seismic hazard analysis." *Geotechnical and Environmental Geophysics*, 1, 333-353.
- McGuire, R. K. (1976). "FORTRAN Computer program for seismic risk analysis." *USGS Open-File Report (76-67)*
- McGuire, R. K. (2001). "Deterministic vs. probabilistic earthquake hazards and risks." *Soil Dynamics and Earthquake Engineering*, 21(5), 377-384.
- McGuire, R. K., and Hanks, T. C. (1980). "RMS accelerations and spectral amplitudes of strong ground motion during the San Fernando, California earthquake." *Bulletin of the Seismological Society of America*, 70(5), 1907-1919.

- McGuire, R. K., and Shedlock, K. M. (1981). "Statistical uncertainties in seismic hazard evaluations in the United States." *Bulletin of the Seismological Society of America*, 71(4), 1287-1308.
- McNamara, D., Meremonte, M., Maharrey, J. Z., Mildore, S. L., Altidore, J. R., Anglade, D., Hough, S. E., Given, D., Benz, H., Gee, L., and Frankel, A. (2012). "Frequency-Dependent Seismic Attenuation within the Hispaniola Island Region of the Caribbean Sea." *Bulletin of the Seismological Society of America*, 102(2), 773-782.
- McVerry, G. H., Zhao, J. X., Abrahamson, N. A., and Somerville, P. G. (2006). "New Zealand acceleration response spectrum attenuation relations for crustal and subduction zone earthquakes." *Bulletin of the New Zealand Society for Earthquake Engineering*, 39(1), 1-58.
- Menon, A., Ornthammarath, T., Corigliano, M., and Lai, C. G. (2010). "Probabilistic Seismic Hazard Macrozonation of Tamil Nadu in Southern India." *Bulletin of the Seismological Society of America*, 100(3), 1320-1341.
- Merz, H. A., and Cornell, C. A. (1973). "Seismic risk analysis based on a quadratic magnitude-frequency law." *Bulletin of the Seismological Society of America*, 63(6-1), 1999-2006.
- Milisenda, C. "Compositional characteristics of the Vijayan Complex." *Presented at The crystalline crust of Sri Lanka. Part. I. Summary of research of the German-Sri Lanka consortium*, Geological Survey Dept. Sri Lanka.
- Milne, W. G., and Davenport, A. G. (1969). "Distribution of earthquake risk in Canada." *Bulletin of the Seismological Society of America*, 59(2), 729-754.
- Minster, J. B., and Jordan, T. H. (1978). "Present-day plate motions." *Journal of Geophysical Research: Solid Earth*, 83(B11), 5331-5354.
- Mitchell, B. J. (1981). "Regional variation and frequency dependence of $Q\beta$ in the crust of the United States." *Bulletin of the Seismological Society of America*, 71(5), 1531-1538.
- Motazedian, D. (2006). "Region-Specific Key Seismic Parameters for Earthquakes in Northern Iran." *Bulletin of the Seismological Society of America*, 96(4A), 1383-1395.
- Motazedian, D., and Atkinson, G. M. (2005). "Stochastic Finite-Fault Modeling Based on a Dynamic Corner Frequency." *Bulletin of the Seismological Society of America*, 95(3), 995-1010.
- Munson, C. G., and Thurber, C. H. (1997). "Analysis of the attenuation of strong ground motion on the island of Hawaii." *Bulletin of the Seismological Society of America*, 87(4), 945-960.
- Musson, R. M. W. (1999). "Probabilistic seismic hazard maps for the North Balkan region." *Annals of Geophysics*, 42(6), 1109-1138.
- Nakamura, Y. (1989). "A method for dynamic characteristics estimation of subsurface using microtremor on the ground surface." Railway Technology Research Institute.
- Nakano, H. (1923). "Notes on the nature of the forces which give rise to the earthquake motions." *Seismological Bulletin of Central Metrological Observatory of Japan*, 1, 92-120.
- Nuttli, O. W. (1973). "Seismic Wave Attenuation and Magnitude Relations for Eastern North America." *Journal of Geophysical Research*, 78(5), 876-885.
- Nuttli, O. W. (1983). "Average seismic source-parameter relations for mid-plate earthquakes." *Bulletin of the Seismological Society of America*, 73(2), 519-535.
- Ordaz, M., Aguilar, A., and Arboleda, J. (2007). "CRISIS2007-Ver. 1.1: Program for Computing Seismic Hazard." Instituto de Ingenieria, UNAM, Mexico.

- Pacheco, J. F., Scholz, C. H., and Sykes, L. R. (1992). "Changes in frequency-size relationship from small to large earthquakes." *Nature*, 355(6355), 71-73.
- Papageorgiou, A. S., and Aki, K. (1983). "A specific barrier model for the quantitative description of inhomogeneous faulting and the prediction of strong ground motion. Part II. Applications of the model." *Bulletin of the Seismological Society of America*, 73(4), 953-978.
- Pathirana, H. D. N. C. (1980). "Geology of Sri Lanka in relation to plate tectonics." *Journal of National Science Council Sri Lanka*, 8(1), 75-85.
- Peiris, N. (2007). "Seismic hazard assessment of Sri Lanka and seismic risk in Colombo." *8th Pacific Conference on Earthquake Engineering*, Singapore.
- Pieris, P. E. (1920). "Ceylon and the Portuguese, 1505-1658." Asian Educational Services.
- Pitarka, A., Somerville, P., Fukushima, Y., Uetake, T., and Irikura, K. (2000). "Simulation of Near-Fault Strong-Ground Motion Using Hybrid Green's Functions." *Bulletin of the Seismological Society of America*, 90(3), 566-586.
- Pitarka, A., Somerville, P. G., Fukushima, Y., and Uetake, T. (2002). "Ground-Motion Attenuation from the 1995 Kobe Earthquake Based on Simulations Using the Hybrid Green's Function Method." *Bulletin of the Seismological Society of America*, 92(3), 1025-1031.
- Pulli, J. J. (1984). "Attenuation of coda waves in New England." *Bulletin of the Seismological Society of America*, 74(4), 1149-1166.
- Raghukanth, S. T. G., and Iyengar, R. N. (2007). "Estimation of seismic spectral acceleration in Peninsular India." *Journal of Earth System Science*, 116(3), 199-214.
- Raghukanth, S. T. G., and Nadh Somala, S. (2009). "Modeling of Strong-Motion Data in Northeastern India: Q, Stress Drop, and Site Amplification." *Bulletin of the Seismological Society of America*, 99(2A), 705-725.
- Rana, M. S., Chakraborty, C., Sharma, R., and Giridhar, M. (2008). "Mannar Volcanics - Implications for Madagascar Breakup." *7th International Conference and Exposition on Petroleum Geophysics*, Hyderabad, India.
- Ranaweera, L. (2008). "The Wannai-Highland boundary shear zone of Sri Lanka: Field and structural evidence." *M.Phil. Thesis*, University of Peradeniya, Sri Lanka.
- Rao, B. R., and Rao, P. S. (1984). "Historical seismicity of Peninsular India." *Bulletin of the Seismological Society of America*, 74(6), 2519-2533.
- Rautian, T. G., and Khalturin, V. I. (1978). "The use of the coda for determination of the earthquake source spectrum." *Bulletin of the Seismological Society of America*, 68(4), 923-948.
- Reasenber, P. (1985). "Second-order moment of central California seismicity, 1969-1982." *Journal of Geophysical Research: Solid Earth*, 90(B7), 5479-5495.
- Reiter, L. (1990). "Earthquake hazard analysis: issues and insights." Columbia University Press. New York.
- Richter, C. F. (1935). "An instrumental earthquake magnitude scale." *Bulletin of the Seismological Society of America*, 25(1), 1-32.
- Robinson, D., Henry, C., Das, S., and Woodhouse, J. (2001). "Simultaneous rupture along two conjugate planes of the Wharton Basin earthquake." *SCIENCE*, 292(5519), 1145-1148.
- Rodolfo Saragoni, G., and Hart, G. C. (1973). "Simulation of artificial earthquakes." *Earthquake Engineering & Structural Dynamics*, 2(3), 249-267.

- Royer, J. Y., and Gordon, R. G. (1997). "The motion and boundary between the Capricorn and Australian plates." *SCIENCE*, 277, 1268-1274.
- Sadigh, K., Chang, C.-Y., Egan, J. A., Makdisi, F., and Youngs, R. R. (1997). "Attenuation Relationships for Shallow Crustal Earthquakes Based on California Strong Motion Data." *Seismological Research Letters*, 68(1), 180-189.
- Safak, E., and Boore, D. M. (1988). "On low-frequency errors of uniformly modulated filtered white-noise models for ground motions." *Earthquake Engineering & Structural Dynamics*, 16(3), 381-388.
- Sato, H. (1977). "Energy propagation including scattering effects: Single isotropic scattering approximation." *Physics of the Earth and Planetary Interiors*, 25, 27-41.
- Sato, H., and Hirasawa, T. (1973). "Body wave spectra from propagating shear cracks." *Journal of the Physics of the Earth*, 21(4), 415-431.
- Schnabel, P. B., Lysmer, J., and Seed, H. B. (1972). "A computer program for earthquake response analysis of horizontally layered sites." *Report EERC 72-12*, Earthquake Engineering Research Center, University of California at Berkeley, USA.
- Schwartz, D. P., and Coppersmith, K. J. (1984). "Fault behavior and characteristic earthquakes: Examples from the Wasatch and San Andreas Fault Zones." *Journal of Geophysical Research: Solid Earth*, 89(B7), 5681-5698.
- Shah, H., Huang, M., Kremidjian, A., and Zstutty, T. (1975). "A study of seismic risk for Nicaragua-part I," *Report 11*, The John A. Blume Earthquake Engineering Center, Stanford University, Stanford, California.
- Shin, T.-C., and Herrmann, R. B. (1987). "Lg attenuation and source studies using 1982 Miramichi data." *Bulletin of the Seismological Society of America*, 77(2), 384-397.
- Siddiqi, J., and Atkinson, G. M. (2002). "Ground-Motion Amplification at Rock Sites across Canada as Determined from the Horizontal-to-Vertical Component Ratio." *Bulletin of the Seismological Society of America*, 92(2), 877-884.
- Silva, W., and Darragh, R. B. (1995). "Engineering Characterization of Earthquake Strong Ground Motion Recorded at Rock Sites." Electric Power Research Institute, Palo Alto, CA.
- Silva, W., Darragh, R. B., G., M., Abrahamson, N. A., and C., K. (1999). "Reassessment of Site Coefficients and Near-Fault Factors for Building Code Provisions." Pacific Engineering & Analysis, El Cerrito, CA.
- Silva, W. J., Gregor, N. J., and Darragh, R. B. (2003). "Development of regional hard rock attenuation relations for central and eastern North America, mid-continent and gulf coast." Pacific Engineering Inc.
- Singh, S., and Herrmann, R. B. (1983). "Regionalization of crustal coda Q in the continental United States." *Journal of Geophysical Research: Solid Earth*, 88(B1), 527-538.
- Singh, S. K., García, D., Pacheco, J. F., Valenzuela, R., Bansal, B. K., and Dattatrayam, R. S. (2004). "Q of the Indian Shield." *Bulletin of the Seismological Society of America*, 94(4), 1564-1570.
- Somerville, P., Graves, R., Collins, N., Song, S. G., Ni, S., and Cummins, P. "Source and ground motion models for Australian earthquakes." *Presented at Australian Earthquake Engineering Society Conference*, Newcastle, AUS.
- Sonley, E. (2004). "Investigation of earthquake attenuation in the Charlevoix, Quebec, seismic zone." *PhD Thesis*, Carleton University, Ottawa, Canada.

- Sonley, E., and Atkinson, G. M. (2006). "Path-Specific Attenuation in Eastern Canada." *Bulletin of the Seismological Society of America*, 96(4A), 1375-1382.
- Speidel, D. H., and Mattson, P. H. (1998). "Problems for Probabilistic Seismic Hazard Analysis", in M. I. El-Sabh, S. Venkatesh, C. Lomnitz, and T. S. Murty, (eds.), *Earthquake and Atmospheric Hazards*. Springer Netherlands, pp. 165-179.
- Spudich, P., Fletcher, J. B., Hellweg, M., Boatwright, J., Sullivan, C., Joyner, W. B., Hanks, T. C., Boore, D. M., McGarr, A., Baker, L. M., and Lindh, A. G. (1997). "SEA96—A New Predictive Relation for Earthquake Ground Motions in Extensional Tectonic Regimes." *Seismological Research Letters*, 68(1), 190-198.
- Sreejith, K. M., Krishna, K. S., and Bansal, A. R. (2008). "Structure and isostatic compensation of the Comorin Ridge, north central Indian Ocean." *Geophysical Journal International*, 175(2), 729-741.
- Stein, S., and Okal, E. A. (1978). "Seismicity and tectonics of the Ninetyeast Ridge Area: Evidence for internal deformation of the Indian Plate." *Journal of Geophysical Research: Solid Earth*, 83(B5), 2233-2245.
- Stepp, J. C. (1971). "An investigation of earthquake risk in the Puget Sound area by use of the type 1 distribution of largest extremes," *Ph D Thesis*, State University of Pennsylvania.
- Stepp, J. C. "Analysis of completeness of the earthquake sample in the Puget Sound area and its effect on statistical estimates of earthquake hazard." *Presented at First microzonation Conference*, Seattle, WA.
- Sykes, L. R. (1970). "Seismicity of the Indian Ocean and a possible nascent island arc between Ceylon and Australia." *Journal of Geophysical Research*, 75(26), 5041-5055.
- Tani, Y. (1997). "A preliminary study of the deformational structures and evolution of the high-grade gneisses around Kegalla in central Sri Lanka." *Journal of geosciences Osaka City University*, 40(4), 51-67.
- Toro, G. R., Abrahamson, N. A., and Schneider, J. F. (1997). "Model of Strong Ground Motions from Earthquakes in Central and Eastern North America: Best Estimates and Uncertainties." *Seismological Research Letters*, 68(1), 41-57.
- Uduweriya, S. B., Wijesundara, K. K., and Dissanayake, P. B. R. (2013). " Seismic risk in Colombo – probabilistic approach." *SAITM Research Symposium on Engineering Advancements 2013*. Colombo, Sri Lanka.
- Uniform Building Code (1997 edition). Council of Building Officials, California, USA.
- USGS Earthquake summary maps (2005). "M9.0 Sumatra-Andaman Islands Earthquake of 26 December 2004." US Geological Survey.
- Vanmarcke, E. H. (1977). "Chapter 8", in C. Lomnitz and E. Rosenblueth, (eds.), *Seismic Risk and Engineering Decisions*. Elsevier Publishing Co.
- Venkatesan, S., and Gamage, P. (2013). "Spectral Analysis of Seismic Waves in the Northern Indian Ocean Region." *Bulletin of the Seismological Society of America*, 103(6), 3305-3320.
- Vere-Jones, D., and Ozaki, T. (1982). "Some examples of statistical estimation applied to earthquake data." *Annals of the Institute of Statistical Mathematics*, 34(1), 189-207.
- Vestal, W., and Lowrie, A. (1982). "Large-scale slumps off southern India and Sri Lanka." *Geo-Marine Letters*, 2(3-4), 171-177.
- Vitanage, P. W. (1983). "A regional study of lineaments in Sri Lanka and possible movements of the Sri Lankan Mini-Plate." *Symposium on the geology of Sri Lanka*. Dept. Geol. Univ. Peradeniya, Sri Lanka.

- Vitanage, P. W. (1985). "Tectonics and mineralisation in Sri Lanka." *Bulletin of the Geological Society of Finland*, 57, 157-168.
- Vitanage, P. W. "Seismicity-Neglected aspects of Sri Lankan Landslide studies." *Presented at National Symposium on Landslides in Sri Lanka*, Colombo, Sri Lanka.
- Vitanage, P. W. "Seismicity in lineaments – impact on engineering structures." *Presented at Handbook on Geology and Mineral Resources of Sri Lanka, Second South Asia Geological Congress, GEOSAS – II*, Colombo, Sri Lanka.
- Walker, D. A. (1977). "High-frequency Pn and Sn phases recorded in the western Pacific." *Journal of Geophysical Research*, 82(23), 3350-3360.
- Wiens, D. A. (1986). "Historical seismicity near Chagos: a complex deformation zone in the equatorial Indian Ocean." *Earth and Planetary Science Letters*, 76(3–4), 350-360.
- Wiens, D. A., Stein, S., DeMets, C., Gordon, R. G., and Stein, C. (1986). "Plate tectonic models for Indian Ocean. "intraplate" deformation." *Tectonophysics*, 132, 37-48.
- Wilkie, J., and Gibson, G. (1995). "Estimation of seismic quality factor Q for Victoria, Australia." *AGSO Journal of Australian Geology and Geophysics*, 15(4), 511-517.
- Wilson, J., and Lam, N. T. K. (2003). "A recommended earthquake response spectrum model for Australia." *Australian Journal of Structural Engineering*, 5(1), 17-27.
- Wimalaratne, K. D. (1993). "The First Earthquake Recorded in Sri Lanka." *Daily News*.
- Winterstein, D. (1992). "How shear-wave properties relate to rock fractures: Simple cases." *The Leading Edge*, 11(9), 21-28.
- Wong, Y. L., Zheng, S., Liu, J., Kang, Y., Tam, C. M., Leung, Y. K., and Zhao, X. (2002). "Attenuation function of ground motions and source parameters for Guangdong region of Southern China." *International Conference on Advances and New Challenges in Earthquake Engineering Research*. Hong Kong, pp. 19–20.
- Woo, G. (1996). "Kernel estimation methods for seismic hazard area source modeling." *Bulletin of the Seismological Society of America*, 86(2), 353-362.
- Woodgold, C. R. D. (1990). "Estimation of Q in eastern Canada using coda waves." *Bulletin of the Seismological Society of America*, 80(2), 411-429.
- Wu, R.-S., and Aki, K. (1988). "Multiple scattering and energy transfer of seismic waves— Separation of scattering effect from intrinsic attenuation II. Application of the theory to Hindu Kush region." *Pure and Applied Geophysics*, 128(1), 49-80.
- Yaghmaei-Sabegh, S., and Lam, N. T. K. (2010). "Ground motion modelling in Tehran based on the stochastic method." *Soil Dynamics and Earthquake Engineering*, 30(7), 525-535.
- Youngs, R. R., Chiou, S.-J., Silva, W. J., and Humphrey, J. R. (1997). "Strong Ground Motion Attenuation Relationships for Subduction Zone Earthquakes." *Seismological Research Letters*, 68(1), 58-73.
- Zeng, Y., Anderson, J. G., and Yu, G. (1994). "A composite source model for computing realistic synthetic strong ground motions." *Geophysical Research Letters*, 21(8), 725-728.
- Zeng, Y., Su, F., and Aki, K. (1991). "Scattering wave energy propagation in a random isotropic scattering medium: 1. Theory." *Journal of Geophysical Research: Solid Earth*, 96(B1), 607-619.
- Zhang, T.-R., and Lay, T. (1995). "Why the Lg phase does not traverse oceanic crust." *Bulletin of the Seismological Society of America*, 85(6), 1665-1678.

Web references

- ANSS (Advanced National Seismic System) data archive, USGS. <http://www.ncedc.org/anss/> (last accessed November 2013).
- Global Crustal Model CRUST2.0, Institute of Geophysics and Planetary Physics, The University of California, San Diego. <http://igppweb.ucsd.edu/~gabi/crust2.html> (last accessed November 2013).
- GEOFON Data Centre (1993): GEOFON Seismic Network, Deutsches GeoForschungsZentrum GFZ. <http://geofon.gfz-potsdam.de/> (last accessed November 2013).
- ISC (International Seismological Centre) On-line Bulletin, Thatcham, United Kingdom. <http://www.isc.ac.uk> (last accessed November 2013).
- IRIS (Incorporated Research Institutions for Seismology) Data Management Centre. <http://www.iris.edu/ds/nodes/dmc/> (last accessed November 2013)
- NEIC (National Earthquake Information Center) data archive, USGS. <http://earthquake.usgs.gov/regional/neic/> (last accessed November 2013)

Appendix A

Table A.1 Some of published attenuation models

| Attenuation model | Definitions and Remarks |
|---|--|
| Milne & Davenport (1969); $A = \frac{a_1 e^{a_2 M}}{a_3 e^{a_4 M} + \Delta^2}$ | A is PGA in percentage of g , $a_1 = 0.69$, $a_2 = 1.64$, $a_3 = 1.1$ and $a_4 = 1.10$, Δ is hypocentral distance and M is magnitude. |
| Esteva (1970); $a = c_1 e^{c_2 M} (R + c_3)^{-c_4}$ | a is PGA in cms^{-2} , $c_1 = 1230$, $c_2 = 0.8$, $c_3 = 25$, $c_4 = 2$ and $\sigma = 1.02$ (in terms of natural logarithm). R and M are hypocentral distance and magnitude, respectively. Records from soils comparable to stiff clay or compact conglomerate. Earthquakes of moderate duration are considered. |
| Ambraseys (1975); $\log Y = b_1 + b_2 M_L + b_3 \log R$ | Y is PGA in cms^{-2} , $b_1 = 0.46$, $b_2 = 0.63$, $b_3 = -1.10$ and $\sigma = 0.32$. R (km) and M_L (Richter magnitude) are hypocentral distance and magnitude, respectively. Earthquakes with maximum focal depth of 15 km are used. |
| Trifunac & Brady (1975), Trifunac (1976) & Trifunac & Brady (1976); $\log a_{\max} = M + \log A_0(R) - \log a_0(M, p, s, v)$ | a_{\max} is the maximum PGA in cms^{-2} , $\log A_0(R)$ is an empirically determined attenuation function from Richter (1958) used for calculation of M_L , p is confidence level and v is component direction ($v = 0$ for horizontal and 1 for vertical). Coefficients are: $a = -0.898$, $b = -1.789$, $c = 6.217$, $d = 0.060$, $e = 0.331$, $f = 0.186$, $M_{\min} = 4.80$ and $M_{\max} = 7.50$. R and M are hypocentral distance and magnitude, respectively. $s = 0$ for Alluvium or other low velocity soft deposits, $s = 1$ for intermediate type rock and $s = 2$ for solid |

| | |
|--|---|
| $\log a_0(M, p, s, v) = \begin{cases} ap + bM + c + ds + ev + fM^2 - f(M - M_{\max})^2 \\ , M \geq M_{\max} \\ ap + bM + c + ds + ev + fM^2 \\ , M_{\max} \geq M \geq M_{\min} \\ ap + bM_{\min} + c + ds + ev + fM_{\min}^2 \\ , M \leq M_{\min} \end{cases}$ | <p>hard basement rock. Note that, for large earthquakes, i.e. long faults, $\log A_0(R)$ would have a tendency to flatten out for small epicentral distances and for low magnitude shocks curve would probably have a large negative slope.</p> |
| <p>McGuire (1978);</p> $\ln x = b_1 + b_2 M + b_3 \ln R + b_4 Y_s$ | <p>x is PGA in cms^{-2}, $b_1 = 3.40$, $b_2 = 0.89$, $b_3 = -1.17$, $b_4 = -0.20$ and $\sigma = 0.62$. $Y_s = 0$ Rock (sedimentary or basement rock or soil less than 10m thick) and $Y_s = 1$ Soil (alluvium or other soft material greater than 10m thick). R and M are hypocentral distance and magnitude, respectively.</p> |
| <p>Iwasaki et al. (1980);</p> $PGA = a_1 10^{a_2 M} (\Delta + 10)^{a_3}$ | <p>PGA is in gal. Four types of sites are considered; Type 1 - Tertiary or older rock (defined as bedrock) or diluvium with depth to bedrock $H < 10$ m, Type 2 - Diluvium with $H \geq 10$ m or alluvium with $H < 10$ m, Type 3 - Alluvium with $H < 25$ m including soft layer (sand layer vulnerable to liquefaction or extremely soft cohesive soil layer) with thickness < 5 m, Type 4 - Other than above, usually soft alluvium or reclaimed land. For type 1 sites $a_1 = 46.0$, $a_2 = 0.208$ and $a_3 = -0.686$, for type 2 sites $a_1 = 24.5$, $a_2 = 0.333$ and $a_3 = -0.924$, for type 3 sites $a_1 = 59.0$, $a_2 = 0.261$ and $a_3 = -0.886$, for type 4 sites $a_1 = 12.8$, $a_2 = 0.432$, $a_3 = -1.125$ and for all sites $a_1 = 34.1$, $a_2 = 0.308$ and $a_3 = -0.925$. R and M are hypocentral distance and magnitude, respectively.</p> |

| | |
|---|--|
| <p>Joyner & Boore (1981);</p> $\log y = \alpha + \beta M - \log r + br$ $r = (d^2 + h^2)^{1/2}$ | <p>y is PGA in g, $\alpha = -1.02$, $\beta = 0.249$, $b = -0.00255$, $h = 7.3$ and $\sigma = 0.26$. Model can be used for two types of sites; soil and rock. Derivations were based on shallow crustal events (depths less than 20 km) with magnitude greater than M_w 5.0. r (km) and M (Moment magnitude) are hypocentral distance and magnitude, respectively.</p> |
| <p>Bolt & Abrahamson (1982);</p> $y = a \left\{ (x+d)^2 + 1 \right\}^c e^{-b(x+d)}$ | <p>y is PGA in g, for $5 \leq M < 6$ $a = 1.2$, $b = 0.066$, $c = 0.033$, $d = 23$ and standard error 0.06 g, for $6 \leq M < 7$ $a = 1.2$, $b = 0.044$, $c = 0.042$, $d = 25$ and standard error 0.10 g, for $7 \leq M \leq 7.7$ $a = 0.24$ $b = 0.022$, $c = 0.10$, $d = 15$ and standard error 0.05 g and for $6 \leq M \leq 7.7$ $a = 1.6$, $b = 0.026$, $c = -0.19$, $d = 8.5$ and standard error 0.09 g. The data are from Joyner and Boore (1981). The form of equation and the regression method are considered in a manner to give more emphasis on near-field events.</p> |
| <p>Joyner & Fumal (1984);</p> $\log y = c_0 + c_1(M-6) + c_2(M-6)^2 + c_3 \log r + c_4 + S$ $r = (d^2 + h^2)^{1/2}$ | <p>y is PGA in g, coefficients c_0 to c_4, h and σ are from Joyner & Boore (1981). S is 0 for rock sites and $c_6 \log \frac{V}{V_0}$ for soil sites. d is focal depth. Site classification is done based on the ratio between shear wave velocity and quarter wave length of the depth. r (km) and M (Moment magnitude) are hypocentral distance and magnitude, respectively.</p> |
| <p>Youngs et al. (1988);</p> $\ln(a_{\max}) = C_1 + C_2 M_w - C_3 \ln[R + C_4 \exp(C_5 M_w)] + B Z_t$ | <p>a_{\max} is the maximum PGA in g, $C_1 = 19.16$, $C_2 = 1.045$, $C_3 = -4.738$, $C_4 = 205.5$, $C_5 = 0.0968$, $B = 0.54$ and $\sigma = 1.55 - 0.125 M_w$. Data from subduction zones of Alaska, Chile, Peru, Japan, Mexico and Solomon Islands. Z_t is 0 for interface earthquakes and equals 1 for intra-slab earthquakes. R (km) and M_w (Moment magnitude) are hypocentral distance and magnitude, respectively.</p> |

| | |
|---|---|
| <p>Ambraseys (1990);</p> $\log y = \alpha + \beta M_w - \log r + br$ $r = (d^2 + h^2)^{1/2}$ | <p>y is PGA in g, $\alpha = -1.101$, $\beta = 0.2615$, $b = -0.00255$, $h = 7.2$ and $\sigma = 0.25$. The data and method are similar to that of Joyner & Boore (1981) but M_w is reevaluated for all earthquakes. r (km) and M_w (Moment magnitude) are hypocentral distance and magnitude, respectively.</p> |
| <p>Campbell (1990);</p> $\ln Y = a + bM + d \ln[R + c_1 \exp(c_2 M)] + eF$ $+ f_1 \tanh[f_2(M + f_3)] + g_1 \tanh(g_2 D)$ $+ h_1 K_1 + h_2 K_2 + h_3 K_3$ | <p>Y is PGA in g, $a = -2.245$, $b = 1.09$, $c_1 = 0.361$, $c_2 = 0.576$, $d = -1.89$, $e = 0.218$, $f_1 = 0$, $f_2 = 0$, $f_3 = 0$, $g_1 = 0$, $g_2 = 0$, $h_1 = -0.137$, $h_2 = -0.403$ and $h_3 = 0$. $\sigma = 0.517$ for $M \leq 6.1$ and $\sigma = 0.387$ for $M \geq 6.2$. Also given is $\sigma = 0.450$ for $M \geq 4.7$. $K_1 = 1$ for embedded buildings 3–11 storeys, $K_2 = 1$ for embedded buildings with >11 storeys and $K_3 = 1$ for non-embedded buildings >2 storeys in height. $K_1 = K_2 = K_3 = 0$ otherwise. F is 0 for strike-slip faults and 1 for reverse faults. R (km) and M_w (Moment magnitude) are hypocentral distance and magnitude, respectively.</p> |
| <p>Boore et al. (1997);</p> $\ln Y = b_1 + b_2(M - 6) + b_3(M - 6)^2 + b_5 \ln r +$ $b_v \ln \frac{V_s}{V_A}$ $r = (r_{jb}^2 + h^2)^{1/2}$ | <p>Y is horizontal PGA in g, r_{jb} is distance (km), V_s is average shear wave velocity (m/s) to 30 m. $b_1 = -0.242$ (for unclassified fault mechanism), $b_2 = 0.527$, $b_3 = 0$, $b_5 = -0.778$, $b_v = -0.371$, $V_A = 1396$, $h = 5.57$ and $\sigma = 0.495$ (for overall variance of the regression) and derivations are for five different site categories (Rock, soil, NEHRP – B, C and D). r (km) and M_w (Moment magnitude) are hypocentral distance and magnitude, respectively.</p> |
| <p>Sadigh et al. (1993) & Sadigh et al. (1997);</p> $\ln PGA = C_1 + C_2 M + C_3 \ln(r_{rup} + C_4 e^{C_5 M}) + C_6 Z_T$ | <p>PGA is in g, for horizontal PGA, rock sites and strike-slip faulting $C_3 = 0$ and $C_4 = -2.100$, for $M \leq 6.5$ $C_1 = -0.624$, $C_2 = 1.0$, $C_5 = 1.29649$ and $C_6 = 0.250$ and for $M > 6.5$, $C_1 = -1.274$, $C_2 = 1.1$, $C_5 = -0.48451$ and $C_6 = 0.524$. For reverse and thrust earthquakes multiply strike-slip prediction by</p> |

| | |
|------------------------------|--|
| | <p>1.2. $\sigma = 1.39 - 0.14M$ for $M < 7.21$ and $\sigma = 0.38$ for $M \geq 7.21$. For horizontal PGA</p> <p>and deep soil $C_2 = 1.0$, $C_3 = 1.70$ and $C_6 = 0$, for strike-slip faulting $C_1 = -2.17$ and for reverse or thrust faulting $C_1 = -1.92$, for $M \leq 6.5$ $C_4 = 2.1863$ and $C_5 = 0.32$ and for $M > 6.5$ $C_4 = 0.3825$ and $C_5 = 0.5882$. $\sigma = 1.52 - 0.16M$ for $M \leq 7$ and $\sigma = 0.40$ for $M = 7$. For vertical PGA, rock sites and strike-slip faulting $C_3 = 0$ and $C_4 = -2.300$, for $M \leq 6.5$ $C_1 = -0.430$, $C_2 = 1.0$, $C_5 = 1.2726$ and $C_6 = 0.228$ and for $M > 6.5$, $C_1 = -1.080$, $C_2 = 1.1$, $C_5 = -0.3524$ and $C_6 = 0.478$. For reverse and thrust earthquakes multiply strike-slip prediction by 1.1 and for oblique faulting multiply by 1.048. $\sigma = 0.48$ for $M \geq 6.5$, $\sigma = 3.08 - 0.40M$ for $6 < M < 6.5$ and $\sigma = 0.68$ for $M \leq 6$. Data are from both rock and soil sites. r (km) and M_w (Moment magnitude) are hypocentral distance and magnitude, respectively. Z_T is 1 for reverse faults and 0 for strike-slip faults.</p> |
| Abrahamson and Silva (1997); | <p>Sa is spectral acceleration (or PGA) in g. M is moment magnitude and r_{rup} is the closest distance to the rupture plane (km). F for fault type (1 if reverse, 0.5 if oblique/reverse, 0 otherwise). HW and S are dummy variables for hanging wall effects (1 if hanging wall, 0 otherwise) and site conditions (1 if deep soil, 0 otherwise), respectively. PGA_{rock} is expected PGA on rock sites in g. Magnitude dependent standard error values are given for both horizontal and vertical components. All a_1 to a_{13}, c_1 to c_5 and n are derived from regressions. The model is important in the aspect that its capability for inclusion of a factor to distinguish between ground motions on the hanging wall and footwall on dipping faults. The attenuation model is developed for worldwide applications.</p> |

$$\ln Sa(g) = f_1(M, r_{rup}) + Ff_3(M) + HWf_4(M, r_{rup})$$

$$+ Sf_5(PGA_{rock})$$

$$\text{for } M \leq c_1,$$

$$f_1(M, r_{rup}) = a_1 + a_2(M - c_1) + a_{12}(8.5 - M)^n$$

$$+ [a_3 + a_{13}(M - c_1)] \ln R$$

$$\text{for } M > c_1,$$

$$f_1(M, r_{rup}) = a_1 + a_4(M - c_1) + a_{12}(8.5 - M)^n$$

$$+ [a_3 + a_{13}(M - c_1)] \ln R$$

$$R = \sqrt{r_{rup}^2 + c_4^2}$$

$$f_3(M) = \begin{cases} a_5 & \text{for } M \leq 5.8 \\ a_5 + (a_6 - a_5)/(c_1 - 5.8) & \text{for } 5.8 < M < c_1 \\ a_6 & \text{for } M \geq c_1 \end{cases}$$

$$f_4(M, r_{rup}) = f_{HW}(M) f_{HW}(r_{rup})$$

$$f_{HW}(M) = \begin{cases} 0 & \text{for } M \leq 5.5 \\ M - 5.5 & \text{for } 5.5 < M < 6.5 \\ 1 & \text{for } M \geq 6.5 \end{cases}$$

$$f_{HW}(r_{rup}) = \begin{cases} 0 & \text{for } r_{rup} < 4 \\ a_9 \frac{r_{rup} - 4}{4} & \text{for } 4 < r_{rup} < 8 \\ a_9 & \text{for } 8 < r_{rup} < 18 \\ a_9 \left(1 - \frac{r_{rup} - 18}{7} \right) & \text{for } 18 < r_{rup} < 25 \\ 0 & \text{for } r_{rup} > 25 \end{cases}$$

$$f_5(PGA_{rock}) = a_{10} + a_{11} \ln(PGA_{rock} + c_5)$$

Abrahamson and Silva (2008) NGA;

S_a is spectral acceleration (or PGA) in g. M is moment magnitude and R_{rup} is rupture distance (km). F_{RV} and F_{NM} are dummy variables for type of fault depending on the rake angle; F_{RV} is 1 if reverse and the rake angle between 30 and 150 degrees and 0 otherwise, F_{NM} is 1 if normal fault and the rake angle between -60 and -120 degrees and 0 otherwise. F_{AS} and F_{HW} are dummies for aftershocks (1 for aftershocks, 0 otherwise) and hanging wall sites (1 for hanging wall, 0 otherwise), respectively. R_{jb} is Joyner-Boore distance and R_x is horizontal distance from top edge of rupture in km. Z_{TOR} is depth to top of rupture (km). δ and W are dip angle (degrees) and down-dip rupture width (km). V_{s30} is average shear wave velocity at 30 m depth. $Z_{1.0}$ is depth to shear wave velocity 1 km/s. $PGA_{1000median}$ is medium peak acceleration for $V_{s30}=1000$ m/s. The prediction equations are originally developed for the application in California and other active regions for magnitudes between 5 and 8.5 up to 200 km distances. Regression coefficients are obtained for PGA and spectral accelerations at different periods. Note that, all of the sub-terms defined in the original equation are not provided here, due to space limitation. The reader may refer to original paper for elaborated description.

$$\begin{aligned}
\ln Sa(g) &= f_1(M, R_{rup}) + a_{12}F_{RV} + a_{13}F_{NM} + a_{15}F_{AS} \\
&+ f_5(PGA_{100}, V_{s30}) \\
&+ F_{HW} f_4(R_{jb}, R_{rup}, R_x, W, \delta, Z_{TOR}, M) \\
&+ f_6(Z_{TOR}) + f_8(R_{rup}, M) + f_{10}(Z_{1.0}, V_{s30}) \\
f_1(M, R_{rup}) &= \begin{cases} \text{for } M \leq c_1, & a_1 + a_4(M - c_1) \\ & + a_8(8.5 - M)^2 + [a_2 + a_3(M - c_1)] \ln R \\ \text{for } M > c_1, & a_1 + a_5(M - c_1) \\ & + a_8(8.5 - M)^2 + [a_2 + a_3(M - c_1)] \ln R \end{cases} \\
R &= \sqrt{R_{rup}^2 + c_4^2} \\
f_5(PGA_{100}, V_{s30}) &= \begin{cases} \text{for } V_{s30} < V_{LIN}, & a_{10} \ln \left(\frac{V_{s30}^*}{V_{LIN}} \right) - \\ & b \ln(PGA_{100} + c) + \\ & b \ln \left(PGA_{100} + c \left(\frac{V_{s30}}{V_{LIN}} \right)^n \right) \\ \text{for } V_{s30} \geq V_{LIN}, & (a_{10} + bn) \ln \left(\frac{V_{s30}^*}{V_{LIN}} \right) \end{cases} \\
V_{s30}^* &= \begin{cases} V_{s30} & \text{for } V_{s30} < V_1 \\ V_1 & \text{for } V_{s30} \geq V_1 \end{cases} \\
f_4(R_{jb}, R_{rup}, R_x, W, \delta, Z_{TOR}, M) &= a_{14} T_1(R_{jb}) T_2(R_x, W, \delta) \\
&T_3(R_x, Z_{TOR}) T_4(M) T_5(\delta) \\
f_6(Z_{TOR}) &= \begin{cases} \frac{a_{16} Z_{TOR}}{10} & \text{for } Z_{TOR} < 10 \text{ km} \\ a_{16} & \text{for } Z_{TOR} \geq 10 \text{ km} \end{cases} \\
f_8(R_{rup}, M) &= \begin{cases} 0 & \text{for } R_{rup} < 100 \text{ km} \\ a_{18}(R_{rup} - 100) T_6(M) & \text{for } R_{rup} \geq 100 \text{ km} \end{cases} \\
f_{10}(Z_{1.0}, V_{s30}) &= a_{21} \ln \left(\frac{Z_{1.0} + c_2}{Z_{1.0(\text{median})} V_{s30} + c_2} \right) \\
&+ \begin{cases} a_{22} \ln(Z_{1.0}/200) & \text{for } Z_{1.0} \geq 200 \\ 0 & \text{otherwise} \end{cases}
\end{aligned}$$

| | |
|--|---|
| <p>Atkinson and Boore (1995);</p> $PSA = c_1 + c_2(M - 6) + c_3(M - 6)^2 - \log R - c_4R$ | <p>PSA can be PGA or spectral accelerations in cm/s/s. R (km) and M (M_w) are hypocentral distance and magnitude. The model is to be applied in eastern north American earthquakes with magnitude and distance ranging M_w 4.0 to 7.25 and 10 to 500 km, respectively. c_1 to c_4 are determined from regression analysis.</p> |
| <p>Atkinson and Boore (2006);</p> $\log PSA = c_1 + c_2M + c_3M^2 + (c_4 + c_5M)f_1 + (c_6 + c_7M)f_2 + (c_8 + c_9M)f_0 + c_{10}R_{cd} + S$ $f_0 = \max(\log(R_0 / R_{cd}), 0)$ $f_1 = \min(\log R_{cd}, \log R_1)$ $f_2 = \max(\log(R_{cd} / R_2), 0)$ $S = \begin{cases} \log \{ \exp [b_{lin} \ln (V_{30} / V_{ref}) + b_{nl} \ln (60 / 100)] \} \\ \text{for } pgaBC \leq 60 \text{ cm / sec}^2 \\ \log \{ \exp [b_{lin} \ln (V_{30} / V_{ref}) + b_{nl} \ln (pgaBC 60 / 100)] \} \\ \text{for } pgaBC > 60 \text{ cm / sec}^2 \end{cases}$ $b_{nl} = \begin{cases} \text{for } V_{30} \leq v_1, b_{nl} = b_1 \\ \text{for } v_1 < V_{30} \leq v_2, b_{nl} = (b_1 - b_2) \ln (V_{30} / v_2) \\ \quad / \ln (v_1 / v_2) + b_2 \\ \text{for } v_2 < V_{30} \leq v_{ref}, b_{nl} = b_2 \ln (V_{30} / V_{ref}) \\ \quad / \ln (v_2 / V_{ref}) \\ \text{for } V_{30} > V_{ref}, b_{nl} = 0.0 \end{cases}$ | <p>PSA is pseudo spectral acceleration (it can also be PGA) in cm/s/s. M is magnitude in M_w. R_0, R_1 and R_2 are 10, 70 and 140 km, respectively. S is 0 for hard rock sites. R_{cd} is the closest distance to the fault. V_{30} is shear wave velocity in the upper 30 m. V_{ref}, V_1 and V_2 are 760, 180 and 300 m/s, respectively. C_1 to C_{10} and b_{lin}, b_1 and b_2 factors are determined from regressions. Development of the attenuation model to apply in eastern north American regions, was done using a stochastic finite-fault model.</p> |
| <p>Atkinson and Silva (2000);</p> | <p>PSA can be PGA or spectral accelerations in cm/s/s. R (km) and M (M_w) are hypocentral distance and magnitude. d is the closest distance to the fault.</p> |

| | |
|--|---|
| $\log PSA = c_1 + c_2(M - 6) + c_3(M - 6)^2 - \log R - c_4R$ $R = \sqrt{d^2 + h^2}$ $\log h = -0.05 + 0.15M$ | <p>Application of the equation is for WNA regions. Development of the attenuation model is based on stochastic simulation with region specific seismological characteristics. The model can be applied to events in a range of M_w 4.0-8.0 at distances between 1 and 200 km. c_1 to c_4 are determined from the regression. The soil amplification factor at each selected frequency has also found to predict ground motions at soil sites.</p> |
| <p>Boore and Atkinson (2008) NGA;</p> | <p>Y is the response variable F_M, F_D and F_S represent the magnitude scaling, distance function, and site amplification, respectively. M is moment magnitude, R_{JB} is the Joyner-Boore distance (defined as the closest distance to the surface projection of the fault, which is approximately equal to the epicentral distance for events of $M < 6$), and V_{S30} is the time-averaged shear-wave velocity over the top 30 m of the site. σ is the intra-event aleatory uncertainty and τ is the inter-event aleatory uncertainty. b_{lin}, b_1 and b_2; c_1-c_3 and h; e_1-e_7 are determined by regressions. The equations are applicable for $M=5-8$, R_{JB} 200 km, and $V_{S30}=180-1300$ m/s for shallow crustal WNA events.</p> |

$$\ln Y = F_M(M) + F_D(R_{JB}, M) + F_S(V_{S30}, R_{JB}, M) + \varepsilon\sigma_T,$$

$$\sigma_T = \sqrt{\sigma^2 + \tau^2}$$

$$F_D(R_{JB}, M) = [c_1 + c_2(M - M_{ref})] \ln(R / R_{ref})$$

$$+ c_3(R - R_{ref}),$$

$$R = \sqrt{R_{JB}^2 + h^2}$$

$$F_M(M) = \begin{cases} M \leq M_h, & e_1 U + e_2 SS + e_3 NS + e_4 RS \\ & + e_5 (M - M_h) + e_6 (M - M_h)^2 \\ M > M_h, & e_1 U + e_2 SS + e_3 NS + e_4 RS \\ & + e_7 (M - M_h) \end{cases}$$

$$F_S = F_{LIN} + F_{NL},$$

$$F_{LIN} = b_{lin} \ln(V_{S30} / V_{ref})$$

$$F_{NL} = \begin{cases} pga4nl \leq a_1, & b_{nl} \ln(pga_low / 0.1) \\ a_1 < pga4nl \leq a_2, & b_{nl} \ln pga_low / 0.1 \\ & + c[\ln(pga4nl / a_1)]^2 + d[\ln(pga4nl / a_1)]^3 \\ & b_{nl} \ln(pga4nl / 0.1) \end{cases}$$

$$c = (3\Delta y - b_{nl}\Delta x) / \Delta x^2$$

$$d = -(2\Delta y - b_{nl}\Delta x) / \Delta x^3,$$

$$\Delta x = \ln(a_2 / a_1)$$

$$\Delta y = b_{nl} \ln(a_2 / pga_low)$$

$$b_{nl} = \begin{cases} V_{S30} \leq V_1, & b_1 \\ V_1 < V_{S30} \leq V_2, & (b_1 - b_2) \ln(V_{S30} / V_2) / \ln(V_1 / V_2) \\ & + b_2 \\ V_2 < V_{S30} \leq V_{ref}, & b_2 \ln(V_{S30} / V_{ref}) / \ln(V_2 / V_{ref}) \\ V_{ref} \leq V_{S30}, & 0 \end{cases}$$

| | |
|---|---|
| <p>Campbell (2003);</p> $\ln Y = c_1 + f_1(M_w) + f_2(M_w, r_{rup}) + f_3(r_{rup})$ $f_1(M_w) = c_2 M_w + c_3 (8.5 - M_w)^2$ $f_2(M_w, r_{rup}) = c_4 \ln R + (c_5 + c_6 M_w) r_{rup}$ $R = \sqrt{r_{rup}^2 + [c_7 \exp(c_8 M_w)]^2}$ $f_3(r_{rup}) = \begin{cases} 0 & \text{for } r_{rup} \leq r_1 \\ c_7 (\ln r_{rup} - \ln r_1) & \text{for } r_1 < r_{rup} \leq r_2 \\ c_7 (\ln r_{rup} - \ln r_1) + c_8 (\ln r_{rup} - \ln r_2) & \text{for } r_1 < r_{rup} \leq r_2 \end{cases}$ | <p>Y is geometric mean of the two horizontal components of PGA of 5% damped spectral acceleration in g. r_{rup} is the closest distance to the fault rupture in km. r_1 and r_2 are 70 and 130 km, respectively. c_1 to c_8 are found from regressions. The model is developed from a hybrid method that combines both stochastic theoretical method with empirical ground motion relations developed for WNA. Application of the model is for ENA earthquakes.</p> |
| <p>Campbell and Bozorgnia (2008) NGA;</p> | <p>Y is the median estimate of the geometric mean horizontal component (GMRotI50) of PGA (g), PGV (cm/s), PGD (cm) or PSA (g); M is moment magnitude; R_{RUP} is the closest distance to the coseismic rupture plane (km); R_{JB} is the closest distance to the surface projection of the coseismic rupture plane (km); F_{RV} is an indicator variable representing reverse and reverse-oblique faulting, where $F_{RV}=1$ for $30^\circ < \lambda < 150^\circ$, $F_{RV}=0$ otherwise, and λ is rake defined as the average angle of slip measured in the plane of rupture between the strike direction and the slip vector; F_{NM} is an indicator variable representing normal and normal-oblique faulting, where $F_{NM}=1$ for $-150^\circ < \lambda < -30^\circ$ and $F_{NM}=0$ otherwise; Z_{TOR} is the depth to the top of the coseismic rupture plane (km); δ is the dip of the rupture plane ($^\circ$); V_{S30} is the time-averaged shear-wave velocity in the top 30 m of the site profile (m/s); A_{1100} is the median estimate of PGA on a reference rock outcrop ($V_{S30}=1100$ m/s); and $Z_{2.5}$ is the depth to the 2.5 km/s shear-wave velocity horizon, typically referred to as basin or sediment depth (km). c_0 to c_{12} are</p> |

$$\ln Y = f_{mag} + f_{dis} + f_{fl} + f_{hng} + f_{site} + f_{sed}$$

$$f_{mag} = \begin{cases} c_0 + c_1 M; & M \leq 5.5 \\ c_0 + c_1 M + c_2 (M - 5.5); & 5.5 < M \leq 6.5 \\ c_0 + c_1 M + c_2 (M - 5.5) + c_3 (M - 6.5); & 6.5 < M \end{cases}$$

$$f_{dis} = (c_4 + c_5 M) \ln \sqrt{R_{rup}^2 + c_6^2}$$

$$f_{fl} = c_7 F_{RV} f_{fl.z} + c_8 F_{NM}$$

$$f_{fl.z} = \begin{cases} Z_{TOR}; & Z_{TOR} < 1 \\ 1; & Z_{TOR} \geq 1 \end{cases}$$

$$f_{hng} = c_9 f_{hng.R} f_{hng.M} f_{hng.Z} f_{hng.\delta}$$

$$f_{hng.R} = \begin{cases} 1; & R_{JB} = 0 \\ \frac{\max(R_{RUP}, \sqrt{R_{JB}^2 + 1}) - R_{JB}}{\max(R_{RUP}, \sqrt{R_{JB}^2 + 1})}; & R_{JB} > 0, Z_{TOR} < 1 \\ (R_{RUP} - R_{JB}) / R_{RUP}; & R_{JB} > 0, Z_{TOR} \geq 1 \end{cases}$$

$$f_{hng.M} = \begin{cases} 0; & M \leq 6.0 \\ 2(M - 6.0); & 6.0 < M < 6.5 \\ 1; & M \geq 6.5 \end{cases}$$

$$f_{hng.Z} = \begin{cases} 0; & Z_{TOR} \geq 20 \\ (20 - Z_{TOR}) / 20; & 0 \leq Z_{TOR} < 20 \end{cases}$$

$$f_{hng.\delta} = \begin{cases} 1; & \delta \leq 70 \\ (90 - \delta) / 20; & \delta > 70 \end{cases}$$

$$f_{site} = \begin{cases} c_{10} \ln \left(\frac{V_{S30}}{k_1} \right) + k_2 \left\{ \frac{\ln \left[A_{1100} + c \left(\frac{V_{S30}}{k_1} \right)^n \right]}{\ln [A_{1100} + c]} \right\}; & V_{S30} < k_1 \\ (c_{10} + k_2 n) \ln \left(\frac{V_{S30}}{k_1} \right); & V_{S30} \geq k_1 \end{cases}$$

$$f_{sed} = \begin{cases} c_{11} (Z_{2.5} - 1); & Z_{2.5} < 1 \\ 0; & 1 \leq Z_{2.5} \leq 3 \\ c_{12} k_3 e^{-0.75 Z_{2.5}} [1 - e^{-0.25 (Z_{2.5} - 3)}]; & Z_{2.5} > 3 \end{cases}$$

determined from the regression analysis. Application of the model is for shallow crustal events in WNA.

| | |
|--|---|
| <p>Idriss (2008) NGA;</p> $\ln[PSA(T)] = \alpha_1(T) + \alpha_2(T)M$ $-[\beta_1(T) + \beta_2(T)M]\ln(R_{rup} + 10)$ $+ \gamma(T)R_{rup} + \varphi(T)F$ | <p>PSA(T) in g's is the pseudo-absolute acceleration for period, T, at a spectral damping ratio of 5%; M is moment magnitude; R_{rup} is the closest distance to the rupture surface in km; $\gamma(T)$ is a "distance" adjustment factor (partially accounts for anelastic attenuation); $\psi(T)$ is a source mechanism (or style of faulting) factor; F refers to source mechanism designator with $F=0$ for "strike slip" events and $F=1$ for "reverse" events; and $\alpha_1(T)$, $\alpha_2(T)$, $\beta_1(T)$ and $\beta_2(T)$ are parameters obtained from the regression process. Application of the model is for shallow crustal events with V_{S30} greater than or equal to 450 m/s.</p> |
| <p>Spudich et al (1997);</p> $\log Y = b_1 + b_2(M - 6) + b_3(M - 6)^2 + b_4R + b_5 \log R$ $+ b_6\Gamma$ $R = \sqrt{r_{jb}^2 + h^2}$ | <p>Y is peak horizontal acceleration in g or pseudo velocity response in cm/s. M is moment magnitude and r_{jb} is Joyner-Boore distance in km. Γ is 0 for rock and 1 for soil. b_1 to b_6 are determined from the regression. Application for events with magnitude M_w 5.0-7.5 and with distances up to 100 km.</p> |
| <p>Toro et al (1997);</p> $\ln Y = C_1 + C_2(M - 6) + C_3(M - 6)^2 - C_4 \ln R_M$ $-(C_5 - C_4) \max \left[\ln \left(\frac{R_M}{100} \right), 0 \right] - C_6 R_M + \varepsilon_e + \varepsilon_a$ $R_M = \sqrt{R_{jb}^2 + C_7^2}$ | <p>Y is spectral acceleration or PGA in g. M is either Lg magnitude (m_{Lg}) or Moment magnitude (M_w). R_{jb} is the closest horizontal distance to rupture in km. ε_e and ε_a are epistemic and aleatory uncertainties, respectively. C_1 to C_7 are determined from the regression analysis. Application of the model is for Central and ENA regions.</p> |

Appendix B

Table B.1 List of earthquakes used in the study. Event data are obtained from GFZ-GEOFON (German Research Centre for Geosciences), ISC (International Seismological Centre) and ANSS (International Seismological Centre).

| Data source | Magnitude (m_b) | Date and Time (UTC) | Lat. | Lon. | Depth (km) |
|--------------------|---|--------------------------------|-------------|-------------|-----------------------|
| GFZ- GEOFON | | | | | |
| | 4.2 | 14/04/2012 - 02:49:15 | 2.63°N | 90.04°E | 10 |
| | 4.3 | 12/04/2012 - 18:00:52 | 1.73°N | 89.55°E | 10 |
| | 4.4 | 12/05/2012 - 10:30:26 | 2.60°N | 90.50°E | 10 |
| | 4.4 | 14/05/2012 - 08:40:23 | 4.43°N | 86.53°E | 10 |
| | 4.4 | 18/05/2012 - 15:46:38 | 2.26°N | 89.77°E | 10 |
| | 4.5 | 30/05/2012 - 17:21:18 | 3.53°N | 88.39°E | 10 |
| | 4.5 | 23/04/2012 - 00:12:26 | 2.72°N | 89.67°E | 10 |
| | 4.5 | 13/05/2012 - 12:30:56 | 2.45°N | 90.53°E | 10 |
| | 4.5 | 13/04/2012 - 19:52:06 | 1.54°N | 91.15°E | 10 |
| | 4.5 | 18/04/2012 - 17:50:26 | 2.54°N | 90.33°E | 10 |
| | 4.5 | 07/07/2012 - 09:01:51 | 3.07°N | 86.57°E | 10 |
| | 4.5 | 13/04/2012 - 05:31:44 | 2.71°N | 89.73°E | 10 |
| | 4.6 | 14/04/2012 - 10:08:44 | 3.85°N | 89.95°E | 10 |
| | 4.6 | 09/05/2012 - 05:09:13 | 4.92°N | 87.77°E | 10 |
| | 4.6 | 06/07/2012 - 14:18:27 | 4.96°N | 77.19°E | 10 |
| | 4.7 | 19/11/2011 - 10:40:17 | 4.28°N | 79.19°E | 10 |
| | 4.7 | 09/05/2012 - 07:30:39 | 4.99°N | 87.95°E | 10 |
| | 4.7 | 18/04/2012 - 01:15:15 | 2.48°N | 89.76°E | 10 |
| | 4.7 | 19/04/2012 - 06:30:09 | 1.46°N | 90.79°E | 10 |
| | 4.7 | 13/04/2012 - 04:49:49 | 1.67°N | 91.07°E | 10 |
| | 4.7 | 09/05/2012 - 14:27:16 | 2.33°N | 89.77°E | 10 |
| | 4.7 | 15/05/2012 - 00:25:36 | 2.09°N | 89.66°E | 10 |
| | 4.7 | 12/05/2012 - 15:01:26 | 2.47°N | 89.82°E | 10 |
| | 4.8 | 13/04/2012 - 03:38:37 | 2.68°N | 90.07°E | 10 |
| | 4.8 | 05/05/2012 - 03:34:00 | 3.66°N | 86.81°E | 10 |
| | 4.8 | 12/04/2012 - 06:47:36 | 2.98°N | 89.42°E | 10 |
| | 4.8 | 07/05/2012 - 21:31:36 | 2.43°N | 89.81°E | 10 |
| | 4.8 | 12/04/2012 - 07:34:49 | 2.70°N | 89.76°E | 10 |
| | 4.8 | 02/08/2012 - 15:25:20 | 2.20°N | 89.63°E | 10 |
| | 4.9 | 05/05/2012 - 12:08:43 | 4.88°N | 87.92°E | 10 |
| | 4.9 | 18/04/2012 - 11:59:15 | 1.81°N | 89.74°E | 10 |
| | 4.9 | 14/06/2012 - 10:58:25 | 2.63°N | 91.37°E | 10 |
| | 4.9 | 13/04/2012 - 12:48:11 | 3.42°N | 89.95°E | 10 |
| | 4.9 | 15/04/2012 - 13:57:40 | 1.74°N | 90.93°E | 10 |
| | 5 | 29/04/2012 - 02:13:55 | 2.39°N | 89.76°E | 10 |
| | 5 | 25/07/2012 - 06:13:04 | 2.09°N | 89.71°E | 10 |

| | | | | | |
|------|------------------|-----------------------|---------------------|----------------------|----|
| | 5 | 16/09/2012 - 06:07:26 | 3.60°N | 90.16°E | 10 |
| | 5.1 | 27/04/2012 - 01:40:52 | 2.23°N | 89.70°E | 10 |
| | 5.2 | 15/05/2012 - 05:19:55 | 2.72°N | 89.53°E | 10 |
| | 5.3 | 04/05/2012 - 16:23:43 | 2.07°N | 89.73°E | 10 |
| | 5.3 | 14/04/2012 - 12:18:26 | 2.60°N | 90.35°E | 10 |
| | 5.3 | 11/04/2012 - 13:58:06 | 1.39°N | 90.82°E | 10 |
| | 5.3 | 23/06/2012 - 21:27:28 | 2.59°N | 90.49°E | 10 |
| | 5.5 | 11/04/2012 - 22:51:57 | 2.83°N | 89.54°E | 10 |
| | 5.5 | 11/04/2012 - 23:56:34 | 1.81°N | 89.60°E | 10 |
| | 5.5 ^a | 21/08/2012 - 17:39:37 | 0.08°S | 91.95°E | 10 |
| | 5.5 ^b | 30/04/2012 - 08:00:10 | 1.76°N | 89.66°E | 10 |
| | 5.9 | 11/04/2012 - 11:53:35 | 2.91°N | 89.56°E | 10 |
| ISC | | | | | |
| | 4 | 25/07/2010 - 09:35:02 | 6.54°N | 76.84°E | 10 |
| | 4.1 | 07/07/2005 - 13:13:22 | 4.32°N | 84.59°E | 10 |
| | 4.1 | 30/11/2002 - 02:11:09 | 5.92°N | 89.00°E | 10 |
| | 4.5 | 28/01/2007 - 00:18:52 | 7.77°N | 88.39°E | 10 |
| | 4.6 | 03/12/2003 - 17:43:08 | 9.25°N | 85.51°E | 10 |
| | 4.6 | 23/04/2004 - 02:21:30 | 0.92°S | 83.99°E | 10 |
| | 4.7 | 31/12/2001 - 04:44:39 | 2.61°S | 83.30°E | 10 |
| | 4.7 | 16/10/2008 - 04:28:45 | 3.41°S | 81.61°E | 8 |
| | 4.7 | 13/07/2009 - 15:09:35 | 0.78°S | 84.31°E | 10 |
| | 4.8 | 26/02/2002 - 01:50:43 | 2.97°N | 86.22°E | 10 |
| | 4.8 | 12/10/2008 - 17:27:20 | 3.32°S | 81.63°E | 10 |
| | 5 | 21/12/2005 - 22:35:17 | 2.02°S | 88.12°E | 10 |
| ANSS | | | | | |
| | 4.2 | 13/04/2012 - 04:36:33 | 1.09°N | 91.58°E | 10 |
| | 4.2 | 06/05/2012 - 08:08:04 | 2.39°N | 89.65°E | 10 |
| | 4.3 | 13/04/2012 - 22:03:21 | 2.22°N | 89.67°E | 10 |
| | 4.3 | 12/04/2012 - 23:34:30 | 3.03°N | 89.54°E | 10 |
| | 4.3 | 14/04/2012 - 02:18:23 | 2.55°N | 89.99°E | 10 |
| | 4.3 | 26/04/2012 - 03:17:42 | 3.59°N | 87.90°E | 10 |
| | 4.3 | 19/05/2012 - 22:29:31 | 2.35°N | 89.80°E | 10 |
| | 4.3 | 13/04/2012 - 22:58:55 | 1.89°N | 89.69°E | 10 |
| | 4.4 | 14/04/2012 - 04:03:49 | 2.47°N | 90.43°E | 10 |
| | 4.5 | 15/04/2012 - 10:20:58 | 2.58 ⁰ N | 89.94 ⁰ E | 10 |
| | 4.7 | 13/04/2012 - 14:29:02 | 2.22 ⁰ N | 90.26 ⁰ E | 10 |

^a magnitude was taken from ISC

^b magnitude was taken from ANSS